NUMERICAL MODELING OF THE COOKING EXTRUSION OF A BIO-POLYMER

by

Lori Luxenburg Wagner

Dissertation submitted to the Faculty of the

Virginia Polytechnic Institute and State University

in partial fulfillment of the requirements for the degree of

Doctor of Philosophy

in

Chemical Engineering

APPROVED:

Donald G. Baird, Chairman

Garth L. Wilkes

Junathula N. Reddy

William L. Conger

David R. Bevan

March 6, 1987

Blacksburg, Virginia

NUMERICAL MODELING OF THE COOKING EXTRUSION OF A BIO-POLYMER

by

Lori Luxenburg Wagner

Donald G. Baird, Chairman

Chemical Engineering

(ABSTRACT)

Cooking extrusion is becoming an essential processing step in a number of food processes. Modeling of extruder performance is the first step towards the ultimate goal of prediction of product properties and quality based on governing extruder characteristics and operation. The purpose of this study was to develop a numerical model of the cooking extrusion process. This involved many facets of investigation. A 50% added moisture soy flour dough was selected as the material of study. The material properties for this 50% added moisture dough were then determined. The viscosity of this material was found to be both shear and temperature dependent in addition to exhibiting a yield stress. Both thermal conductivity and heat capacity were determined to be constant over the temperature range of investigation. Finally, although it was discovered that a reaction associated with cooking was present in the system, it was determined that it did not occur under the extrusion processes tested which were to be modelled and hence would not have to be accounted for in the model. These material properties were then incorporated in the three-dimensional finite element program, FIDAP, to model the flow of the 50% added moisture soy flour dough through an extruder and die assembly. These numerical simulations yielded limited results. Only one case out

of the multiple conditions which were attempted converged to a viable solution. As more success was found with a two-dimensional model, it is suggested that the problems of convergence could be due to mesh size and discretization of the three dimensional model as well as the difficult power law index of the material. Suggestions as to methods to overcome these problems are included.

ACKNOWLEDGEMENTS

The author wishes to acknowledge the assistance and support of Dr. Donald G. Baird whose unending guidance enabled completion of this work. The author would also like to thank Drs. Bevan, Conger, Reddy, and Wilkes for serving as an advisory committee and for their patient and beneficial review of this work.

Thanks are also due to the secretaries of the Chemical Engineering Department, , for their overlycompetant help in administrative matters.

Sincere appreciation is expressed to Dr. Georg Viola for his patience in tolerating numerous hours discussing food dough results. The author would like to extend her deepest appreciation to her mother, who lent undying support and love throughout the pursuit of this degree. Also, the author wishes to express much gratitude to her husband, whose patience and love was present in unending supply.

TABLE OF CONTENTS

LIST OF ILLUSTRATIONS

LIST OF TABLES

1.0 CHAPTER ONE: INTRODUCTION

1.1 INTRODUCTION

Cooking extrusion has been a significant development in food preparation. Complete pre-cooking of protein-enriched food mixes into ready-to-eat type products can be accomplished by the cooking extrusion technique which is a continuous, high temperature, short time cooking process. The first part of this introduction is concerned with the cooking extrusion process. Included is a short history of the use of extrusion in food processing, the advantages of cooking extrusion, and a simplified description of the cooking extrusion process. Soy flour is one of the principal raw products used in cooking extrusion. For this reason, soy flour has been chosen as the material for study. The next section, then, discusses soy protein flour. A brief outline of soybean products and their functionality is included. The structure of the soy protein, native, as well as a function of known environmental factors, is presented.

1.2 COOKING EXTRUSION

Extrusion is the process whereby plastic or soft materials are shaped through use of an extruder and appropriate die. Food extrusion is a process in which a food material is forced to flow under one or more of a variety of conditions of mixing, heating, and shear, through a die which is designated to form and/or puff-dry the extrudate[27]. Cooking

extrusion specifies the condition of heating as the definition of cooking is to prepare food for consumption by applying heat. In cooking extrusion, there are many different designs of equipment used to force the food to flow and simultaneously be cooked. A description of this process in a single screw extruder, one of the more popular cooking extruder designs, will be described in a future section.

Cooking extrusion has become of increasing use in the last few years. To follow its development, a short history of food extrusion and its application is included in this section. A list of the advantages which promoted its use as a major processing tool follows. Finally, the flow of a food material is followed through an extruder and a description of processes which occur in the extruder are described.

1.2.1 HISTORY

In 1935, extrusion processing became important to the food industry with the application of the single screw extruder as a pasta press [18]. Pasta extruders do not cook but simply mix and work the dough, delivering a uniform mixture at elevated pressure to the die where it is formed into a variety of pasta shapes. In the late 1930's, General Mills Inc. was the first to use extruders in the manufacture of ready-to-eat cereals. Initially, however, these extruders were used only for shaping of a pre-cooked cereal dough.

In the 1940's, the introduction of the cooking extruder came through the desire to pre-cook animal feed to improve digestibility and palatability. Since that time, the use of cooking extruders has greatly expanded in the food field. Dry, expanded, extrusion cooked pet foods

developed in the 1950's which replaced the baking process previously employed. In the 1960's, ready-to-eat cereals were developed which were cooked and formed continuously with a one-step process in the cooking extruder.

Many of the cooking extruders currently in use were first designed to expel oil from oil seeds. In the 1960's, application of basic cooking extrusion technology of cereal grains to the oil seed protein by-product resulted in a texturized product having meat-like structure and a fibrous texture. This product is particularly of interest for meat supplements and replacements. Hence, much research has been directed in the area of extrusion of these oil seed proteins, soy protein being of principal interest.

1.2.2 ADVANTAGES

Extrusion cooking has been a significant development in food extrusion. There are many reasons for the expanded use of extruders in the food industry. The principal advantages of the modern food extruder were given by Smith [5] and are presented below.

1. VERSATILITY -- A wide variety of foods can be produced on the same basic extrusion system using numerous ingredients and processing conditions.

2. HIGH PRODUCTIVITY -- An extruder provides a continuous processing system having greater production capability than other cooking/forming systems.

3. LOW COST -- Labor and floor space requirements per unit of production are smaller than for other cooking/forming systems enhancing cost effectiveness.

4. PRODUCT SHAPES -- Extruders can produce shapes not easily formed using other production methods.

5. HIGH PRODUCT QUALITY -- The high temperature short time heating process minimizes degradation of food nutrients while improving digestibility by gelatinizing starch and denaturing protein. The short, high-temperature treatment also destroys most undesirable factors in food. Some of these heat denaturable factors are antinutritional compounds such as trypsin inhibitors, hemagglutinins, and gossypol, and undesirable enzymes such a lipases or lipoxidases, microorganisms and other food-borne pests.

6. ENERGY EFFICIENT --Extrusion processing systems operate at relatively low moistures while cooking food products. Lower moisture reduces the quantity of heat required for cooking and redrying the product after cooking.

7. PRODUCTION OF NEW FOODS -- Extruders can modify vegetable proteins, starches, and other food materials to produce

a variety of new food products.

8. NO EFFLUENTS -- The lack of process effluents is an important advantage since stringent controls are being placed upon food processors to prevent their releasing pollutants to the environment.

1.2.3 PROCESS

Cooking extrusion combines the heating of food products with the act of extrusion to form a cooked and shaped food product. Some cooking extrusion processes are called high-temperature, short-time (abbreviated HTST) processes. The reason for this is the temperatures reached by the food during cooking extrusion can be quite high (200°C) but the residence time at these elevated temperatures is short (5 to 10 sec) [27]. Once cooked, the material is forced through the die for the shaping of the final product. Most cooking extruders use a single screw to feed, cook, and meter the food, though twin screw extruders are becoming of increasing importance in processing. A schematic of a generalized cooking extruder is given in Figure 1. A short description of each section follows.

The first section is the feed hopper. In most processing cases, the feed is granular in consistency. The feed hopper holds a quantity of feed material which is gravity fed to the screw. This is also referred to, in some instances, as the preconditioning chamber. This is because the meal or flour to be extruded is sometimes treated with water and/or steam to provide the proper moisture content for extrusion. The preconditioned material then drops down into the feed section of the screw. The feed

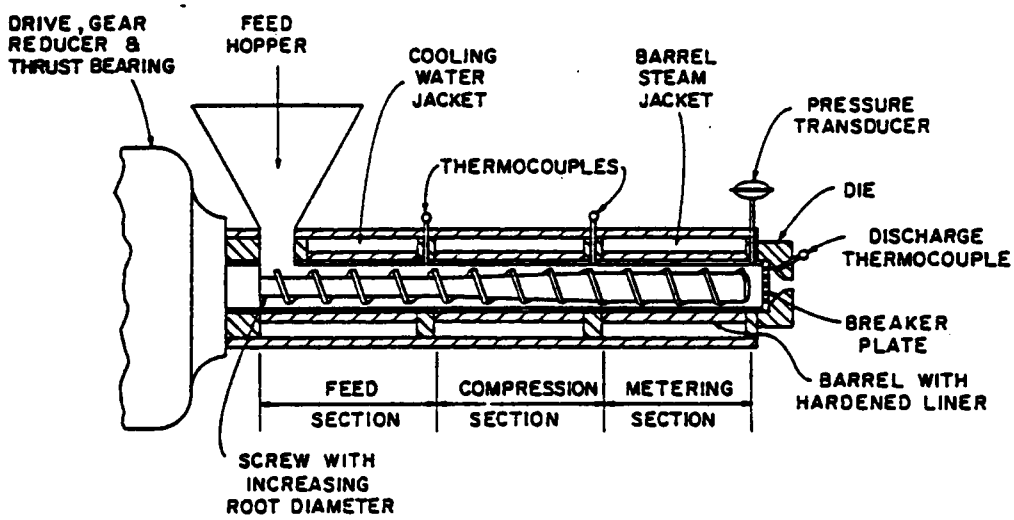

Figure 1. Schematic of a Food Extruder [15].

section is characterized by deep flights or flights with greater than normal pitch which facilitates feeding and prevents starve feeding in the later sections of the screw. The material then is conveyed down the screw to the transition section. Here the material is thoroughly worked into a dough, partially cooked, and elevated in temperature (120°C - 200°C) and pressure ($20x10^5$ - $50x10^5$ Pa) [27]. In the final section of the screw, the metering zone, the dough is further cooked, experiencing high shear rates in the shallow flights. The high shear rates can cause large temperature increases due to viscous dissipation A uniform pressure at the breaker plate to the die is also developed in the metering section. As the dough passes through the die, the pressure is rapidly released which allows a large fraction of the superheated vapor to flash off. This release of vapor as the dough passes out of the die puffs the product. Cooling results in a permanent hardening or solidifying and slight decrease in size of the puffed dough. The extruded product may then pass through a dryer to further reduce its moisture content.

The preceding description of the extrusion operation illustrates its complexity. However, the advantages and products of cooking extrusion far outweigh the problems in handling the actual operation. Although a great amount of literature exists pertaining to the application of extruders to a variety of products, very little of it provides any specific information which explains the exact process and reactions occurring in the material. Even less of the information could be extrapolated for use in developing models for yet untried areas. Results are published in terms of trends or broad generalities. Today, most food extruders are developed by cut and try methods.

1.3 SOY PROTEIN FLOUR

In the past 50 years, soybeans have become a major source of edible oil with the meal by-product an important source of protein for animal feed. The use of soybean protein in the form of defatted flours for human consumption also began in the 1930's but has developed slowly. Employed as an additive or supplement, its present usage is to provide desirable functional properties in standard food products. Availability of a greater variety and more refined forms of soy protein [3] plus rising prices of animal proteins have generated increased interest in soy proteins as substitutes for milk and meat proteins.

As mentioned, soy proteins are the major sources of plant protein used in texturization processes. Soy flour, one of the many forms of soy protein, was chosen for use in this research problem. However, previous research performed by others has not concentrated on any one form of soy protein. Therefore, the forms of soy protein products as well as their associated functionality are discussed. Included is a short description of the method of production of the various forms which may influence their functionality. Also, in its investigation of the gelation process, much of the research performed has been with isolated proteins or has been concentrated simply on the protein fraction reactions. Hence, the structure of a protein and the bonds crucial to that structure are addressed. Finally, a short discussion of denaturation is included as this change in protein structure is thought to be integral in the gelation

process. Consequently, an understanding of the denaturation process is necessary for interpretation of the literature.

1.3.1 SOY PROTEIN PRODUCTS

The processing of soybeans to obtain the various protein products has been described in detail by Smith and Circle [4]. Basically, the cleaned beans are cracked, dehulled, milled, and flaked. The lipids in the flakes are extracted with hexane, and this is further processed to produce oil and lecithin. The defatted flakes are then steam treated with temperatures up to 85°C. Soy flakes, after desolventization and heat treatment, are milled and classified according to particle size. It is from this intermediate product that the various forms of soy protein products are made.

As stated, soy protein products are available in many forms. Consequently, not all studies have used the same form of soy protein. Therefore, a short summary of the forms of soy protein is now provided.

SOY FLOUR-- There are basically three types of soy flour produced: white flour, cooked flour, and toasted flour. This is the least refined form having varying fat contents, particle sizes, textures, and degrees of heat treatment. Flours are prepared by grinding soybean flakes to 100 mesh or finer. Minimum protein contents of these materials range from 40 to 50 % depending on the fat content.

SOY GRITS-- Soy grits are identical in composition to soy flour. The only difference is particle size, being 100 mesh or coarser. Soy grits are normally manufactured with at least two different heat treatments and two mesh sizes.

SOY PROTEIN CONCENTRATE--Soy protein concentrate is manufactured from the flour simply by removing soluble carbohydrates. The resulting product is a 70% or more protein on a dry basis. There exists more than one method of preparing soy concentrate and, depending on the method used, the concentrate can differ in physical properties.

SOY PROTEIN ISOLATE--Isolated soy protein is the most refined form consisting of 90% or more protein. They are made by acid precipitation of the protein from an alkali dispersion of soy flour.

A more detailed breakdown of the components of each of these forms is given in Table 1. Although protein is the major constituent of all forms, notice carbohydrates are present in large amounts in the cruder forms. Due to the large variance of protein and carbohydrate composition in the forms, the functional properties each form provides differs. The functional properties are important in determining the potential uses of the proteins for development of food properties. Typical functional properties include solubility, thermal stability, gelation, and emulsifying capacity. Correlation of the functional properties provided and the protein forms used are presented in Table 2. Although these functional properties are attributed to the proteins, when the cruder soy protein forms are used, the other constituents may also contribute to the overall effect observed. Successful supplementation of existing foods, replacement or simulation of traditional proteinaceous foods, and the fabrication of new foods will depend on the availability of proteins with the critical functional characteristics.

TABLE 1

AVERAGE COMPOSITION OF
SOY FLOUR, CONCENTRATE, AND ISOLATE (%)

Component	Soy Flour	Concentrate	Isolate
Protein	56.0	72.0	96.0
Fat	1.0	1.0	0.1
Fiber	3.5	4.5	0.1
Ash	6.0	5.0	3.5
Carbohydrates (soluble)	14.0	2.5	0.0
Carbohydrates (insoluble)	19.5	15.0	0.3

TABLE 2
FUNCTIONAL PROPERTIES OF VARIOUS PROTEIN FORMS

Functional Property	Protein Form Used*	Food System	References
Emulsification			
Formation	F, C, I	Frankfurters, bologna, sausages	Rock *et al.* (1966); Pearson *et al.* (1965); Inklaar and Fortuin (1969)
		Breads, cakes, soups	Wood (1967); Tremple and Meader (1958)
		Whipped toppings, frozen deserts	Circle and Johnson (1958)
Stabilization	F, C, I	Frankfurters, bologna, sausages	Rock *et al.* (1966); Pearson *et al.* (1965); Inklaar and Fortuin (1969)
		Soups	Wood (1967)
Fat absorption			
Promotion	F, C, I	Frankfurters, bologna, sausages, meat patties	Rock *et al.* (1966); Wood (1967)
Prevention	F, I	Doughnuts, pancakes	Ziemba (1966); Eley (1968); Johnson (1970)
Water absorption			
Uptake	F, C	Breads, cakes	Wood (1967); Tremple and Meader (1958); Turre and Spoo (1968)
		Macaroni	Paulsen (1961)
		Confections	Ziemba (1966)
Retention	F, C	Breads, cakes	Wood (1967); Tremple and Meader (1958)
Texture			
Viscosity	F, C, I	Soups, gravies, chili	Wood (1967); Ziemba (1966)
Gelation	I	Simulated ground meats	Anson and Pader (1958); Circle *et al.* (1963); Frank and Circle (1959)
Chip and chunk formation	F	Simulated meats	Ziemba (1966, 1969)
Shred formation	F, I	Simulated meats	Rusoff *et al.* (1962)
Fiber formation	I	Simulated meats	Ziemba (1966, 1969); Thulin and Kuramoto (1967)
Dough formation	F, C, I	Baked goods	Circle and Johnson (1958)
Film formation	I	Frankfurters, bologna	Circle and Johnson (1958); Ziemba (1966)
Adhesion	C, I	Sausages, lunch meats, meat patties, meat loaves and rolls, baked hams	Rock *et al.* (1966); Ziemba (1966)
		Dehydrated meats	Coleman and Creswick (1966)
Cohesion	F, I	Baked goods	Circle and Johnson (1958)
		Macaroni	Paulsen (1961)
		Simulated meats	Rusoff *et al.* (1962)
Elasticity	I	Baked goods	Circle and Johnson (1958)
		Simulated meats	Rusoff *et al.* (1962)
Color control			
Bleaching	F	Breads	Wood (1967)
Browning	F	Breads, pancakes, waffles	Wood (1967); Eley (1968)
Aeration	I	Whipped toppings, chiffon mixes, confections	Ziemba (1966); Eldridge *et al.* (1963); Circle and Johnson (1958)

* F, C, and I represent flours, concentrates, and isolates, respectively.

1.3.2 PROTEIN STRUCTURE

Although soybean protein products impart functional properties to foods such as texture, elasticity, and cohesion, the physical and chemical aspects involved in functionality are not fully understood. Proteins are organized into three-dimensional structures on four structural levels. Each level is stabilized by bonds of some type. For long peptide chains there exists a three-dimensional organization; many of the otherwise active groups of the constituent amino acids are modified in their activity by virtue of the three-dimensional structure. To better comprehend the literature, an understanding of the structural organization of a protein is needed. The four levels and the nature of the bonds which stabilize their structure will now be discussed.

Proteins are formed from their constituent amino acids by condensation of one amino acid residue via an α-carboxyl group with the α-amino group of another amino acid. These peptide bonds form a backbone joining the amino acid residue in a long chain. The first level of organization, the primary structure, is the sequential arrangement of these residues in the chain. Thus, the amino acid composition, the number and sequence of residues in the chain, and the molecular weight of the chain are properties of the primary structure. Consequently, the stabilizing bond in the primary structure is the covalent peptide bond as shown in Figure 2 with a heat of formation of about 100 kcal/mol (Table 3) [7].

The second level of organization, the secondary structure, are structures that are formed and stabilized through hydrogen bonding. Rotation about the peptide bond is restricted because of the appreciable

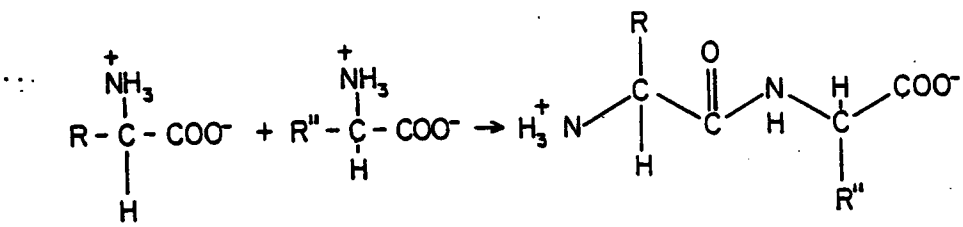

Figure 2. Primary Structure - Covalent Peptide Bond [7].

TABLE 3

ENERGIES AND BOND DISTANCES OF SEVERAL TYPES OF BONDS FOUND IN PROTEINS [20]

Type	Energy (kcal/mol)	Distance of Interaction (A)
Covalent bond	30 - 100	1 - 2
Electrostatic bond	10 - 20	2 - 3
Hydrogen bond	1 - 5	2 - 3
Van der Waals attractive forces	1 - 3	3 - 5

double bond character in the peptide bond. However, free rotation about all other single bonds of the chain can occur if there are no hydrogen bonds, disulfide bonds, or other interactions among the side groups. This state of a protein chain is the random coil. Formation of hydrogen bonds restrict this rotational freedom. The secondary structures, α-helix (Figure 3) and β-pleated sheet (Figure 4), two of the most commonly found structures, are the result of an optimum degree of hydrogen bonding. The single stranded α-helix is stabilized by approximately 3.6 hydrogen bonds per turn [7]. Although each hydrogen bond is weak (Table 3), the multiple hydrogen bonds found in a helical region gives stability to the helix. A point to note is that while hydrogen bonds are readily disrupted by water competing for binding, the hydrogen bonds are not in contact with water in the α-helix. In the β-pleated sheet, the hydrogen bonds are between adjacent chains (interchain), or between parts of a folded chain (intrachain). This structure may also be stabilized to a lesser extent by hydrophobic and electrostatic bonds between side chains of the amino acid residues (Table 3). Individual hydrophobic bonds are quite weak but collectively the numerous hydrophibic bonds are an important stabilizing factor in maintaining not only the secondary but also the tertiary and quaternary structures of a protein.

The third level of organization, the tertiary structure , is the three-dimensional arrangement of these secondary structures within a given chain. The types of bonds involved in maintaining the tertiary structures of proteins are shown in Figure 5. The covalent disulfide bond is the strongest of these with a heat of formation of ~ 50 kcal/mol. However, not all proteins contain disulfide bonds. Most proteins have

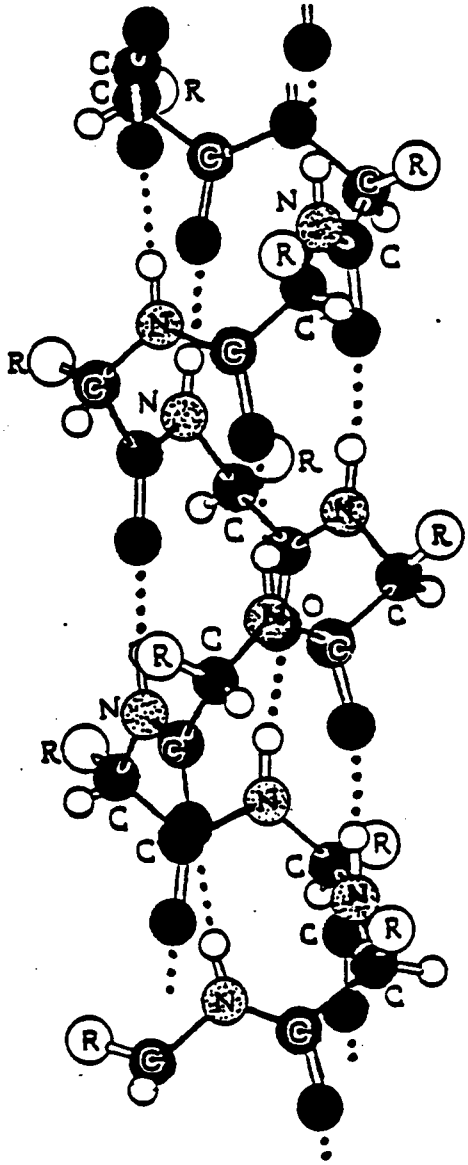

Figure 3. Ball and stick model of a right-handed α-helix [6].

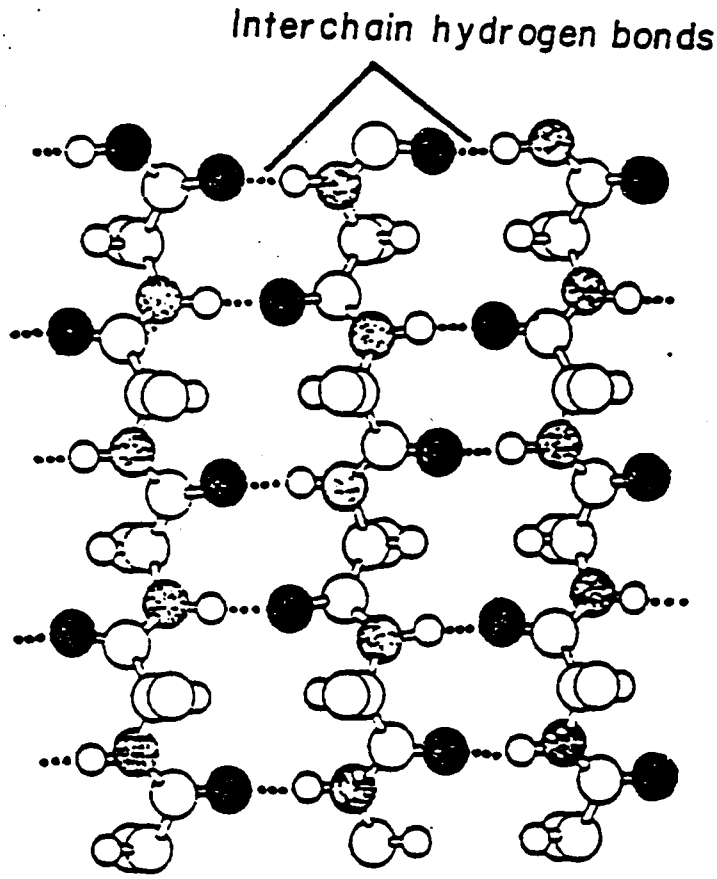

Figure 4. Ball and stick model of an anti-parallel β-pleated sheet [6].

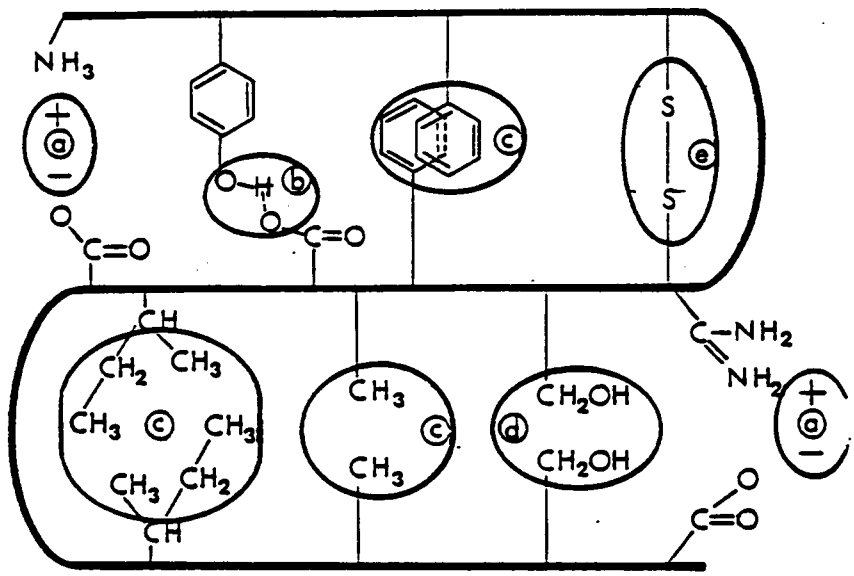

a Electrostatic interaction

b Hydrogen bonding

c Hydrophobic interaction

d Dipole-dipole interaction

e Disulfide bonding

Figure 5. Stabilizing bonds of the tertiary structure [7].

either spherical or rodlike shapes for their tertiary structure. Proteins having spherical or nearly spherical shape are called globular (Figure 6). A globular structure may contain areas of random coil, α-helix, and β-pleated sheet. For example, the globular 11S soy protein contains approximately 60% random coil, 5% α-helix, and 35% β-pleated sheet [8,9].

The fourth level of organization, the quaternary structure, is the three-dimensional arrangement of the single chains as shown in Figure 6. Single chains are referred to as subunits which compose the final structure of the multichain unit. This is differentiated from random aggregation in that this is organized and orderly. As in the tertiary structure, the quaternary structure usually takes on two forms, globular or rodlike. Similarly, the bonds stabilizing these structures are the same as those listed for the tertiary structure.

The structure of the protein, as well as the forces maintaining it, are not the sole determining factors of the native state of the protein. The role of the solvent must also be considered. The role of the solvent in maintaining the native structure of the protein is depicted schematically in Figure 7 with water as the solvent. Water attempts to maintain its own structured arrangement and therefore resists changes in the shape of the protein molecule. This forces the hydrophobic groups into the interior of the protein where they react with one another. Hence, the solvent can also affect the three-dimensional arrangement of the protein.

1.3.3 PROTEIN DENATURATION

In living organisms, proteins appear in their native states. After the processes of extraction, purification, and fractionation, a homoge-

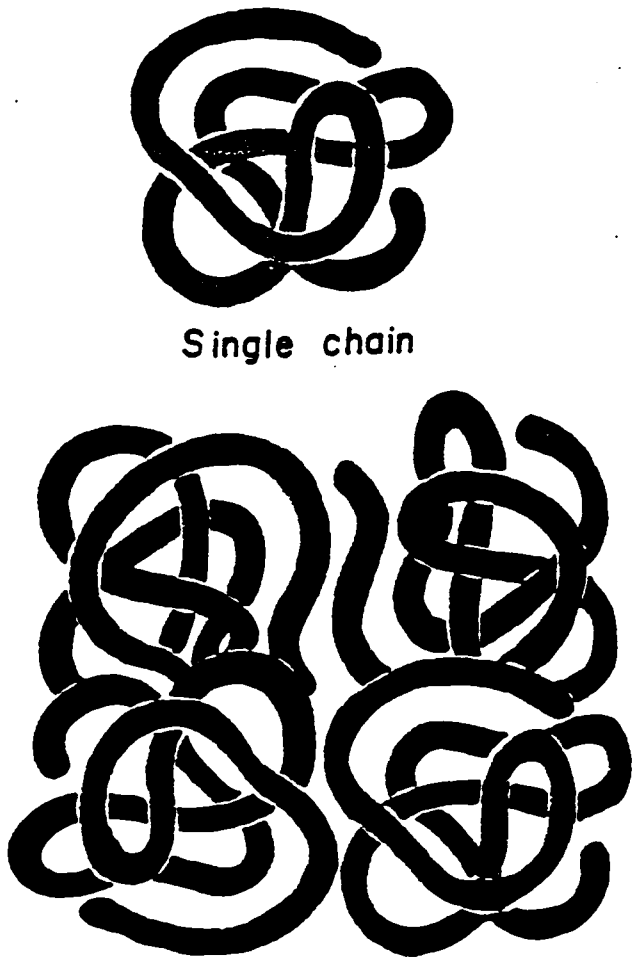

Figure 6. Globular structure of a protein [6].

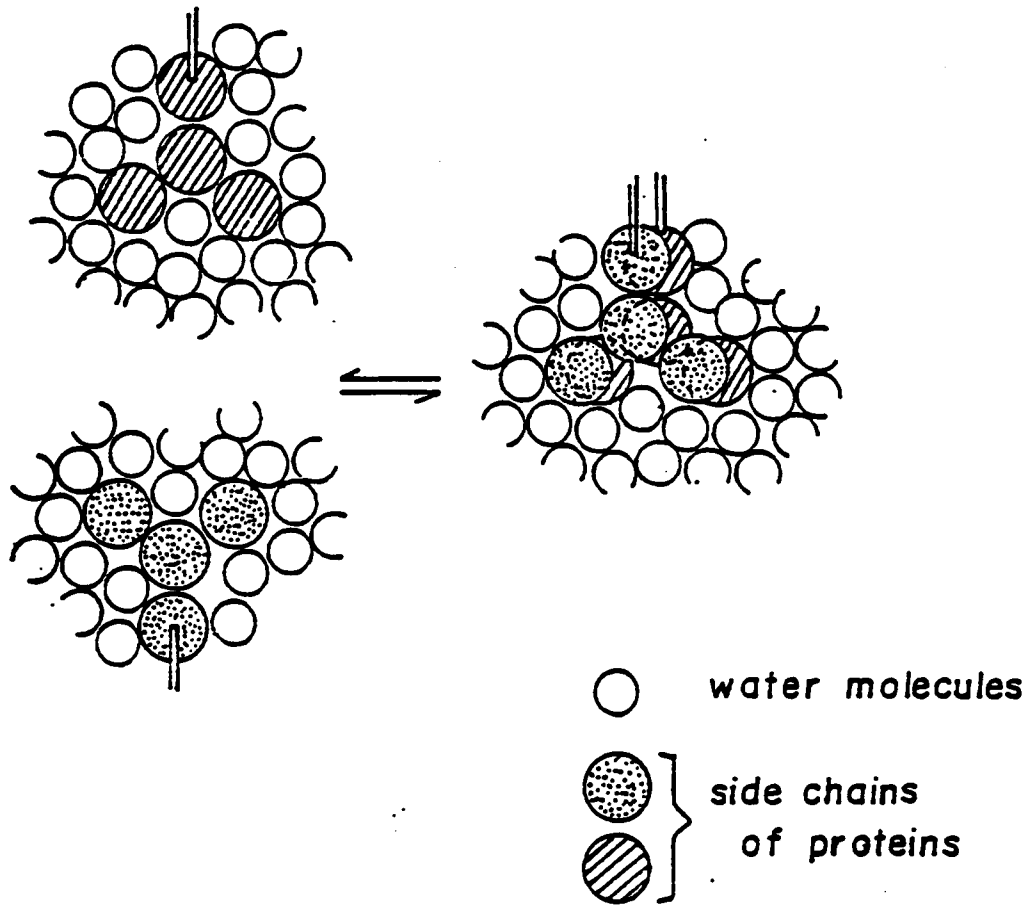

Figure 7. Role of water in maintaining structure [7].

neous product consisting of molecules in an identical state can in principle be obtained. Nevertheless, some question arises as to whether some irreversible changes have occurred during the preparation process of the product. Measurements during which proteins in solution are exposed to external disturbances may also cause some type of changes. In fact, structural changes may occur simply in the dissolution in water.

Denaturation is a process in which the native protein conformation undergoes a major change without rupture of the primary valence bonds, that is, without a change in primary structure. Another term, unfolding, is often used in place of denaturation, emphasizing the conformational aspects of the phenomenon. A schematic of the denaturation process is given in Figure 8. With respect to the overall structure of a native protein, the definition of denaturation implies changes in a single-chain protein of the secondary and tertiary structure. Denaturation can be a reversible process. Renaturation is the process of the protein converting back to a state with all the characteristics of its original native state. Once the critical temperature range for denaturation is reached, slightly increased severity of the conditions, such as a small increase in temperature, greatly increases the speed of denaturation. It is for this reason that proteins are considered extremely sensitive to denaturation in commercial processing procedures.

As previously stated, the solvent may play a role in determining the structure of the denatured protein. Changes in shape require a disruption of water structure with a required subsequent reorganization. When a protein has undergone a major unfolding, aggregation involving the hydrophobic regions of the molecule would be favored as the water reor-

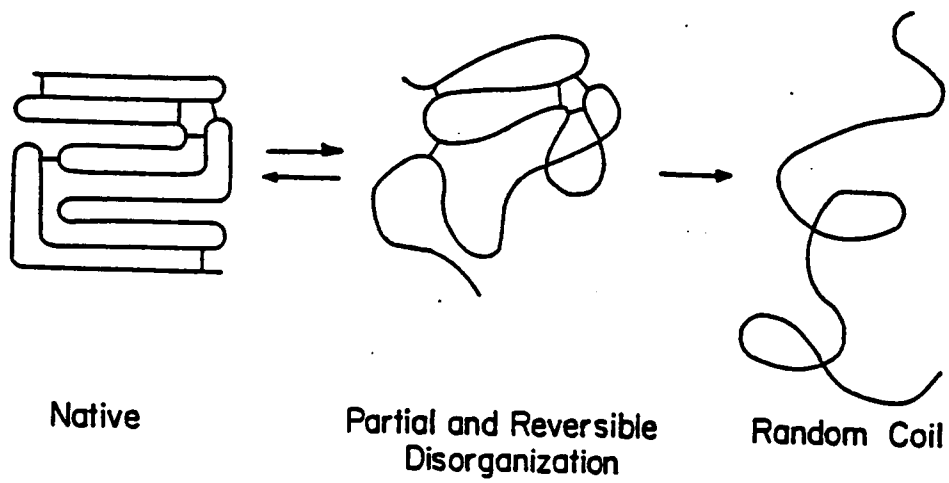

Figure 8. Schematic of the denaturation process [7].

ganizes to maintain its structure. As mentioned, upon denaturation, the protein may interact differently with the solvent. Lewin [10] has suggested several possible explanations for the increase in bound water which has been documented [11,12] upon denaturation of the protein. These are presented schematically in Figure 9. Collectively, these changes involve an increase in protein interfacial area, a decrease in protein-protein interactions, and an increase in protein-water interactions.

1.4 RESEARCH OBJECTIVES

Cooking extruders are becoming an essential processing step in a number of modern food processes. Their extensive capabilities to cook, minimize nutrient loss, form, mix, texturize, and shape food products under conditions of high production and low cost have been discussed.

To date, food extrusion has been developed through the art of trial and error. A review of polymer processing literature, however, reveals the great strides which have been made in this industry toward modeling extruder performance in the last years. The food industry has relied heavily on the theory of plastics extrusion for its development of food extruders. Hence, similar strides concerning the prediction of product qualities based on the governing extruder properties are desired for food extrusion despite the added complexities imposed because of the reactive nature of food ingredients and their natural variability.

Food systems are extremely complex due to their multicomponent nature and the interaction between many of the food constituents. To further complicate the picture, many food components such as starch and protein change their physical character through gelatinization or denaturation.

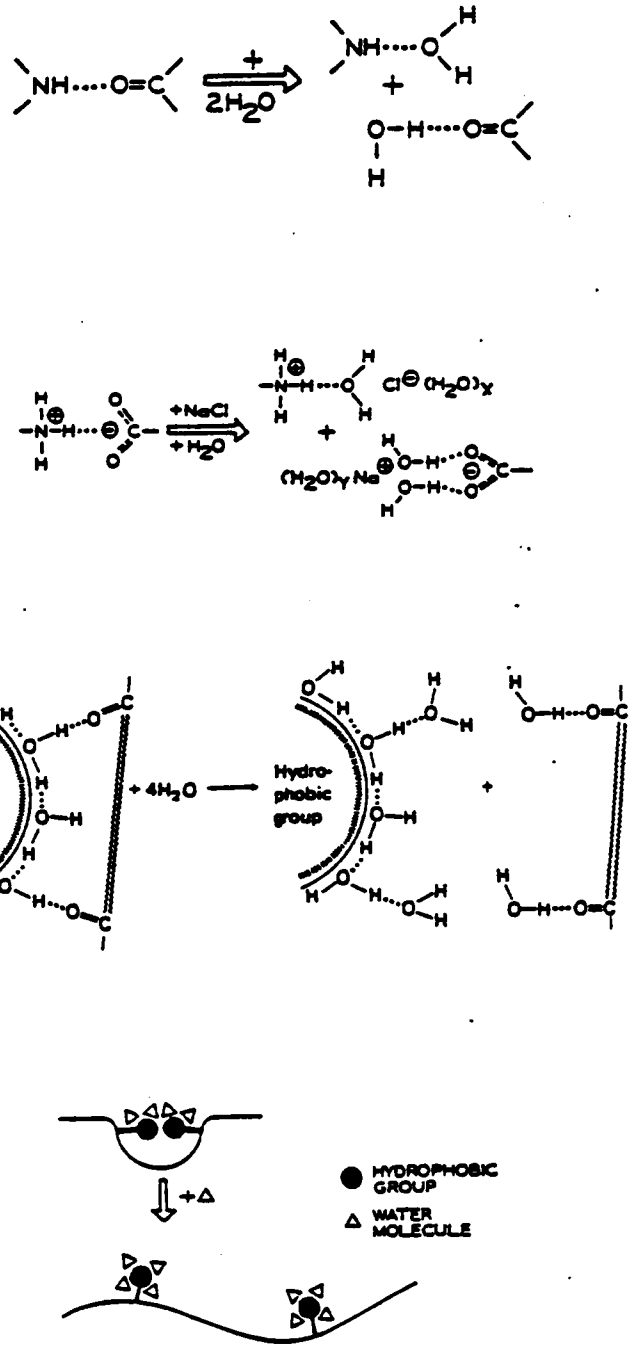

Figure 9. Explanations for increase in bound water upon denaturation [10].

Such complexity has made it difficult to quantitatively describe the changes of the food material occurring in the extruder in a manner which can be coupled with flow and energy inputs to the extruder. Consequently, mathematical models of the process are almost non-existent in food extrusion.

In this study an attempt will be made to numerically model the cooking extrusion process. Soy protein flour is chosen for the material of study because of its principal use in industrial processes. The development of a numerical model of the cooking extrusion process involves many facets of investigation. To begin, the material properties of the soy flour dough will be determined. Next, the nature of the cooking phenomenon which occurs during extrusion will be investigated. Presently, there exist many different theories as to the phenomenon associated with cooking. In one theory, cooking is described as a chemical reaction involving crosslinking of the protein molecules. Another theory postulates that cooking simply involves conformational changes, entanglements, and non-permanent interactions. The nature

of the cooking phenomenon in the soy dough system employed in this study must be determined. These findings will then be incorporated in a three dimensional finite element model of an extruder. Test cases for this model will be performed for varying flow rates and temperatures. Finally, the results of the model will be compared to actual laboratory experiments of an extruder under the test case conditions. From these comparisons, the ability of the numerical model to simulate actual conditions will be judged.

1.5 SUMMARY

In conclusion, this chapter has introduced the versatility of cooking extrusion. The advantages of this process were outlined as well as its developmental role in the food processing industry. A short description of the fundamental process was discussed for a better understanding of cooking extrusion. Also introduced in this chapter was soy protein flour, one of the major materials being explored for use in the food extrusion process. As stated, soy protein flour, in any of its various forms, can be made into a viable food product through food extrusion. Finally, a short discussion of the goals of this research was presented. Chapter Two will discuss the research in the fields of cooking phenomenon of soy protein and cooking extrusion of soy protein as they relate to this study. The information presented in this chapter should provide adequate background for an understanding of the research discussed in Chapter Two.

2.0 CHAPTER TWO: LITERATURE REVIEW

2.1 INTRODUCTION

In Chapter One, an introduction to cooking extrusion was presented. This chapter will discuss the research performed in connection with cooking extrusion. The major objective of this dissertation is to determine whether a three-dimensional finite element program can be used to numerically simulate the cooking extrusion process. In the development of this model, not only does a three dimensional finite element model of the extruder need to be used but also the material parameters of the soy flour dough must be determined. The material parameters include viscosity, thermal conductivity, heat capacity, and heat of reaction. In reference to the latter parameter, it must be determined if a reaction associated with the cooking extrusion process does exist, the nature of the cooking reaction taking place explained and the method developed to handle the enthalpy associated with the cooking process.

To date, very little has been reported on work directed toward this objective. Efforts toward obtaining information on certain parameters needed for modeling of food systems have been recorded in the literature. Some parameters, however, have not been documented as a topic of research for the material of study. Other parameters have been determined, but not under the conditions found in extrusion. Hence, no one has put all the necessary characteristics together to model the process. The purpose of this chapter is to present the work that has been performed, highlight

the important conclusions, and report the work that needs to be performed to complete the objective of this dissertation.

Included in this review will be a discussion of the research performed in all areas concerned with cooking extrusion. The first section of this review then will report the work done on the determination of the composition of soy protein. A knowledge of the composition of soy protein is essential for understanding the research connected with the cooking phenomenon. The next section will deal with the work performed in regard to the cooking phenomenon in soy flour systems. This section will present the methods used by researchers to determine the reactions occurring during cooking and the conclusions they reached from their results. Closely related are some of the studies of viscosity. In many cases viscosity was a means of examining the cooking phenomenon as the changes in the viscosity of the soy dough reflected the changes in microstructure. Therefore, the results of the studies of the viscosity are discussed in the following section. This section will include not only the qualitative studies as those mentioned in connection with the cooking phenomenon but also quantitative studies where models were fitted to viscosity or derived according to results. The work done in the area of thermal conductivity is described in Section 2.5. The experimental method and theory upon which the determination of thermal conductivity is based will be reviewed. The next section will describe differential scanning calorimetry as it is the means of determining both heat capacity and heat of reaction. Again, a description of experimental method and theory will be presented as well as the results of other researchers using this method of analysis on soy systems. Some of the models suggested for the cooking extrusion

of doughs are discussed in Section 2.7. In addition, the next section will describe some of the work performed in numerical modeling of extrusion. The final section addresses the research objectives of this dissertation.

2.2 COMPOSITION

As mentioned, it is necessary to know the composition of soy protein to interpret the research performed on soy protein preparations such as fractionate samples, isolates, and flours. The significance of the work, especially on fractionated soy protein samples, concerning the reactions involved in the cooking phenomenon cannot be understood without a basic understanding of the composition. Hence, this section will report the findings of the research into the composition of soy protein.

Soybean protein, which amounts to about 40% of the seed, consists of four main components. These are 2S, 7S, 11S, and 15S [32] as is shown in Table 4. The 7S and 11S fractions are the main storage proteins. Together they comprise approximately 70% of the total protein content. The 7S globulin has a molecular weight of approximately 200,000, and the 11S about 350,000 [40]. They are, however, composed of totally different components, and hence, are distinctly different in their functional properties. Complex quaternary structures and a high tendency to association-dissociation reactions are characteristic of both the 7S and 11S globulins. Both have a low content of α-helix and are primarily composed of antiparallel β-structure and disordered regions [50,51]. An in-depth description of the molecular make-up of the 7S and 11S globulins is found elsewhere [34].

TABLE 4

COMPONENTS IN THE ULTRACENTRIFUGE FRACTION OF WATER-EXTRACTABLE SOYBEAN PROTEINS SHOWING THEIR MOLECULAR WEIGHTS AND PERCENTAGES

Sedimentation Value	Percent of total	Known Components	Molecular Weights
2S	22	Trypsin inhibitors	8000-21,500
		cytochrome c	12,000
7S	37	Hemagglutinins	110,000
		lipoxygenases	102,000
		-amylases	61,700
		7S globulin	180,000-210,000
11S	31	11S globulin	350,000
15S	11	-----	600,000

Although it has been reported [30,31] that different soybean varieties contain different ratios of the major soy proteins, an analysis of the soy flour used in this study to determine the exact protein ratios is not performed. It is noted from this work that the soy protein is composed of different fractions, the presence of which may or may not affect the behavior of the soy flour. Hence, the soy protein composition is acknowledged as a possible factor contributing to the experimental response.

2.3 COOKING PHENOMENON

Cooking extrusion [86] is the process most often chosen to impart structural integrity and the first level of meatlike texture to soy meal, flour, or concentrate. Although it has been assumed that the structure of the soy extrudate is a result of alterations occurring in the protein fraction, the molecular changes that accompany the development of structure are poorly understood. These changes in the protein fraction are thought to be complex, involving alteration of both covalent and noncovalent interactions as well as possible conformational changes. Collectively it is these changes, resulting in structural and textural properties of the soy extrudate, which are referred to as the cooking phenomenon.

For higher moisture systems, the cooking phenomenon involves the formation of a gel. The definition of a gel has not yet been stated clearly. Many definitions have been proposed as the term encompasses a multitude of substances. In general, an essential characteristic of a gel is its solid-like behavior with a certain degree of elasticity [53].

The formation of a gel from globular proteins can be described as an intermediate state between a protein solution and a protein precipitate formed above a certain critical level of concentration with just the right balance of protein-protein and protein-solvent interactions [34]. This gel forming property is considered to be responsible for many functional properties including not only texture, or chewiness, but also for holding water and other components in a food system.

Few detailed studies exist which describe the cooking phenomenon which occurs during extrusion of soy dough. However, careful studies of the covalent bonding changes accompanying the formation of spun soy flour have been performed. Both Kelley and Pressey [72] and Chiang and Sternberg [54] have shown that spun soy fibers are held together by intermolecular disulfide bonds. Studies have also been performed on the unprocessed soy flour with regards to the bonds formed in the heat induced gels with varying conclusions.

From his work on these latter systems, Ferry [39] proposed gelation as a two-stage process; initial denaturation of the soy proteins into folded peptides, then gradual association to form the protein gel matrix. Hence, he concluded the protein gel is composed of three-dimensional networks in which water in entrapped. In some studies, attempts have been made to relate the textural properties to the gel microstructure. However, this relationship has not been investigated in depth though some studies have examined the effects of certain chemicals upon the textural properties. These experiments were performed to gain an understanding of the reactions related to the gelation phenomena. Much of the work performed in the attempt to establish the nature of the bonding is based

on the insolubilization of the cooked product. If the insoluble protein could be resolubilized by reagents whose modes of action were known it might then be possible to identify the forces producing this effect. Consequently, the microstructure of the gel could be determined.

To begin, the initial part of the section will discuss the results of work performed on the soy protein fractions. As mentioned in the section on composition of soy, there exists two major soy protein fractions, 7S and 11S. It is these two fractions upon which the research is concentrated. Further on in this discussion, the findings related to the unfractionated soy preparations will be reported. This includes studies of soy isolate, composed of the pure soy proteins, as well as other soy compositions such as soy milk and soybean meal.

Some researchers believe that because of the complexity of soybean proteins it is therefore difficult to interpret studies on the unfractionated protein mixture. Consequently, it is thought more meaningful conclusions should result from studies of purified components. While the soy protein products, such as flours and isolates, and their preparation were discussed in the introduction, the isolated soy protein fractions were not. Therefore, a flow diagram of a typical procedure for preparing the 7S and 11S fractions is shown in Figure 10. Their part in the overall composition of the soybean protein as well as their structure has already been discussed in the section on composition.

In order to establish the validity of studies using fractionated proteins, Kamata et al. [56] used fluorescence, ORD, and CD as structural probes. They reported that, under the conditions used in isolation of the 11S subunits, the peptides regain virtually all their native secondary

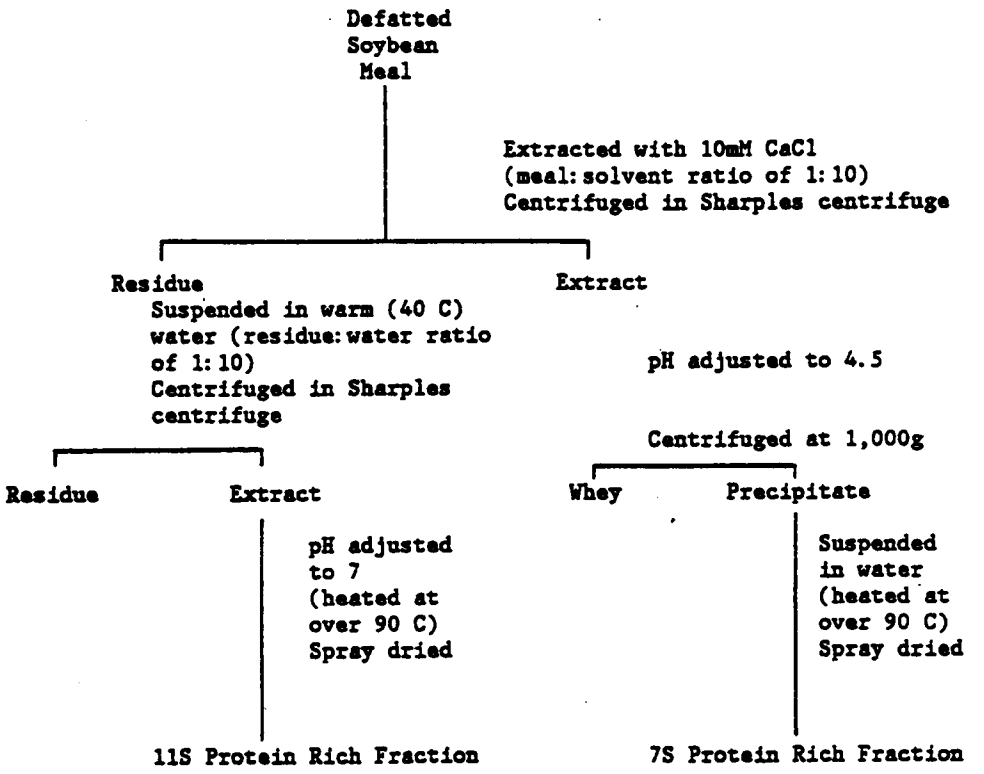

Figure 10. Procedure for preparing fractionated soy proteins [4].

structure. This suggests that while the subunits are dissociated, they are otherwise minimally altered. Hence, the reactions which occur during the cooking phenomenon should be the same. Similar studies, however, concerning the other protein fractions could not be found.

One of the most obvious changes resulting from heating soybean meal is insolubility of major proteins in aqueous solvents [41,42]. Changes in solubility of proteins are a measure of the extent of denaturation but give no information about the protein components involved or nature of the changes in proteins on a molecular level. As denaturation is involved in the gelation process, more information concerning insolubilization effects upon protein structure on the molecular level was sought.

Wolf [43] conducted preliminary studies on solutions of the crude 11S component. His results indicated that heating at 100°C caused two changes: about one half of the protein aggregated and precipitated while the remaining protein sedimented much more slowly than the 11S component. He also found in the presence of a reducing agent the precipitation action was accelerated but in the presence of N-ethylmaleimide, which blocks sulfhydryl groups, precipitation did not occur.

Wolf and Tamura [44] re-examined these preliminary investigations and studied them in more detail. Their results confirmed the previous information and extended the knowledge of the process; the overall conclusion being that heating disrupts the quaternary structure of the 11S protein and separates the subunits into two fractions. One fraction is considered to represent the 3-4S fraction formed on heating while the other is the portion of the 11S molecule which is converted into aggregates. This is shown schematically in Figure 11.

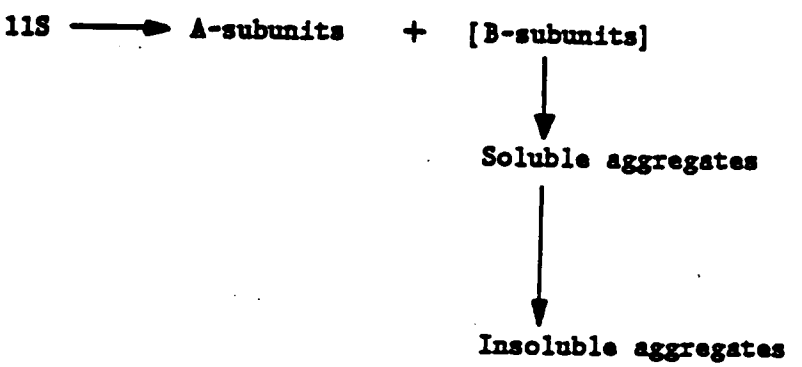

Figure 11. Aggregation of 11S protein [44]

Wolf and Tamura also employed N-ethylmaleimide, and mercaptoethanol, which is used to provide sulfhydryl groups to promote the sulfhydryl-disulfide interchange reaction of proteins [45], in their study of the reaction occurring during the insolubilization of the proteins. The results with the N-ethylmaleimide indicated that a well-developed intermediate in the aggregation process can be isolated. Hence, aggregation involves at least two reactions. The results with mercaptoethanol are not quite so conclusive. The mechanism for disulfide exchange predicts that the interchange to produce high molecular weight aggregates will not occur at high concentrations of sulfhydryl reagent. In their experiments, heating the 11S protein in 0.01M and 0.5M mercaptoethanol solutions gave almost the same amount of precipitate. However, the high concentration of sulfhydryl groups provided by the 0.5M mercaptoethanol solution along with the high temperature would be expected to result in a completely reduced protein rather than one crosslinked by intermolecular disulfide bonds. Hence, it was concluded that the ionic and hydrogen bonds are unlikely to be involved in the formation of the precipitated aggregate. They suggest that hydrophobic interactions may possibly be responsible for conversion of soluble aggregate to an insoluble state.

Hashizume et al. [61] conducted similar studies to that of Wolf and Tamura. They examined the ultracentrifugation patterns of the 7S globulin after heat treatment. Unlike the results of Wolf and Tamura concerning the 11S globulin, heating does not cause formation of stable dissociated products of the 7S globulin even at low ionic strength. Aggregation did occur on heating, however, and was enhanced by the presence of salt. No further investigation into the nature of aggregation was performed.

Based on the results of Wolf and Tamura [36] relating sulfhydryl groups to insolubility of soybean proteins, Saio and co-workers [46] investigated how the changes in the amount of sulfhydryl groups of soybean protein affected the textural properties of tofu. Tofu is a coagulated protein gel. The tofu used in this study was prepared from 7S and 11S protein solutions. The results of the effects upon textural properties are shown in Figure 12. Hardness, cohesiveness, and springiness increased rapidly in the 11S tofu as the amount of sulfhydryl groups increased. However, the 7S tofu showed little change in these three areas. Adhesiveness decreased in both the 11S and 7S tofu with increasing sulfhydryl groups. These results lead to the conclusion that changes in sulfhydryl groups have a significant effect upon the textural properties of 11S tofu but not so much on the 7S.

Saio and co-workers [46] also compared solubilization of the tofu in different concentrations of mercaptoethanol, urea, and sodium dodecylsulfate. In general, 7S tofu dissolved in more dilute mercaptoethanol solutions than did 11S tofu. They concluded that the tofu gel appears to be formed through the action of many forces including disulfide bonds and hydrophobic bonding with the contributions of these forces different in each gel. Disulfide bonds appear to be more dominant in 11S tofu. It was also observed that the 11S tofu had much bigger aggregates than 7S tofu. As the amount of sulfhydryl groups increased in the 11S solution, heat aggregation increased and resulted in larger size of protein aggregates.

In further experiments, measurements of the dependency of tensile properties in 7S, 11S, and isolate gels on the proportion of added water

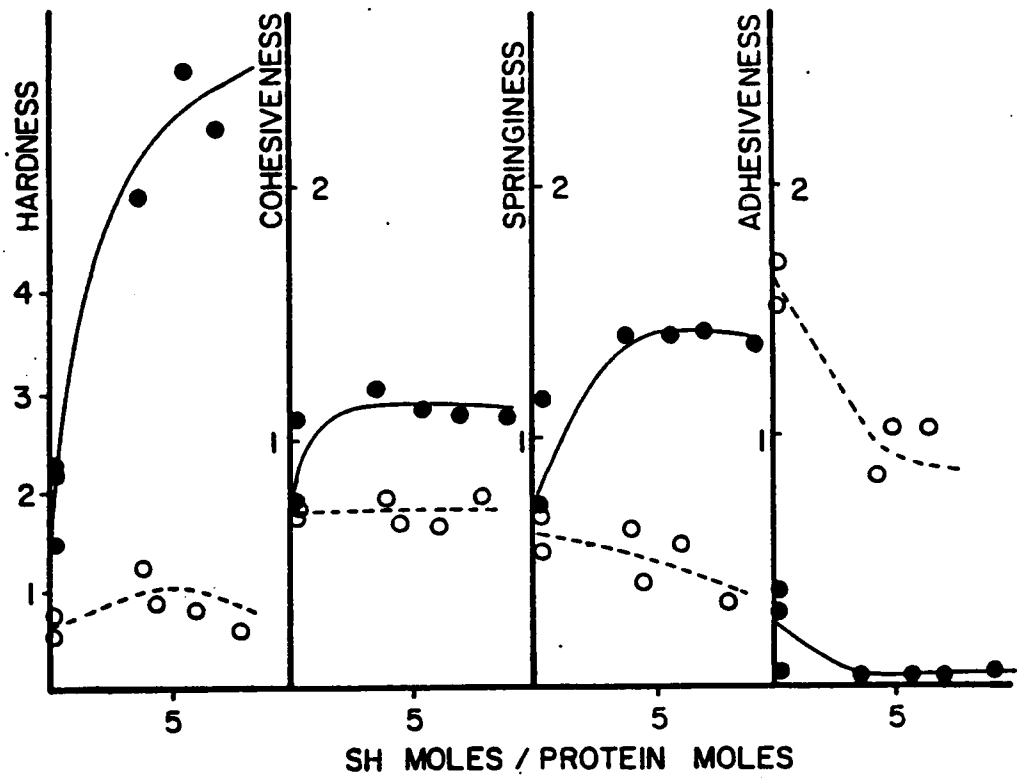

Figure 12. The effect of sulfhydryl content upon textural properties [46].

were also performed by Saio et al. [47]. At all levels of added water, 11S gels exhibited higher breaking stress and strain than 7S or protein isolate. This is attributed to the higher water holding capacity of the 11S gels [47]. In additional studies, Saio et al. [48] found that the 11S gels have a greater potential for expansion. The 11S gels were elastic and pliable while 7S gels were hard and fragile.

A short review of the work performed on the individual protein fractions has been presented. From this discussion it has been shown that the two major protein fractions, namely 7S and 11S, react differently upon subjection to various tests. It has been concluded that aggregation and gelation occur through the action of different forces for the two protein fractions. Hence, the reaction exhibited by one isolated protein fraction can not be generalized to apply to all fractions nor to the total system as the total system is a combination of all protein fractions. A conclusive statement as to the forces involved in the cooking reaction cannot be made as individual researchers suggest differing conclusions based on their results.

Some researchers believe that interactions occur between the soy protein fractions. Hence, the reactions cannot be fully explained simply by individual component reactions. Therefore, many researchers have performed experimental studies employing unfractionated soy samples. First, a study concerning the interaction of the two main fractions, 7S and 11S, will be discussed. Then, the studies involving unfractionated soy samples, in particular soy isolate, will be presented.

German et al. [13] conducted studies to investigate the physicochemical basis of the stabilization of soy 11S by 7S. Their research stemmed from

an interesting observation: one of the factors limiting the use of soy proteins as a highly functional food protein is their rather high stability to heat. This has generally been interpreted to be the result of disulfide bridging within the 11S globulin [55]. However, under conditions favoring thermal dissociation and aggregation of 11S, the thermal aggregation of the whole soy protein mixtures is observed to be minimal. This suggests that interactions between different globulins in whole soy proteins affect the net thermal properties imparting stability to the system.

Therefore, German et al. undertook the study of the solubility of the basic subunits to investigate the forces responsible for the association of proteins. They concluded from their results of the effect of reductant and low ionic strength upon thermal aggregation of 11S that the increased rate and extent of aggregation are because the reductant and low ionic strength facilitate thermal dissociation of the quaternary structure. They suggest that subsequent aggregation is spontaneous and is not a consequence of disulfide rearrangement or electrostatic attractions. This implies that hydrophobic forces may be involved in the aggregation of basic subunits at neutral pH.

To further investigate the role of hydrophobic forces, German and co-workers examined the effect of water structure upon the solubility of the subunits. They found a very strong correlation between solubility and the disruption of water structure. This indicates that hydrophobic forces strongly contribute to the association of basic subunits. Their results indicate that basic subunits tend to readily aggregate when released from their association with the acidic subunits in the oligomeric

11S. However, in the presence of the 7S fraction no precipitation occurs under the conditions employed. Two mechanisms are suggested to account for the 7S inhibiting aggregation. The 7S could interact directly with the 11S molecule or its constituent monomers could interact with the basic subunits once released, and by forming a complex, solubilize them.

German et al. also used differential scanning calorimetry (DSC) in their study of the associations of the 11S and 7S proteins. Thermograms of the isolated 11S subunits showed no endothermic transition below 100°C which indicates that transitions occuring below this temperature by the 11S must be due entirely to dissociation of quaternary structure. They also found that the transition temperatures of the 7S and 11S proteins are independent of the presence of the other. This supports the second mechanism postulated for the interaction of the 7S with the 11S. If the 7S interacted directly with the 11S, the transition temperatures of the two fractions would not be independent of the presence of the other. Reversible crosslinking experiments suggested that heating 11S in the presence of 7S results in complex formation between dissociated 7S subunits and 11S basic subunits.

Soy protein isolate is very similar to the fractions of soy protein just discussed. In fact, it is manufactured in a similar manner with the difference lying in the fact that the protein rich product is not separated into individually rich protein fractions, but instead is, in theory, composed of all fractions making up soy protein in the amounts present in the natural state. Although gelation studies on isolated soybean globulins are desirable from a theoretical viewpoint, the pure globulins are difficult to obtain in large quantities. Furthermore, such studies

may not be characteristic of the properties of the protein mixture which is commercially available for use in food applications. Therefore, research which has been performed with soy protein isolate as the material of study will be the next topic of discussion.

Hermansson [34] studied the denaturation and aggregation of soy protein isolate under various conditions. In this study, turbidity measurements were used to examine aggregation of a 0.5% soy protein dispersion in 0.2 NaCl as a function of temperature and pH. Aggregation was found to be suppressed at both high and low pH with no aggregation occurring in the range of 3.0<pH>11.0. This is explained as intermolecular repulsion forces occurring at high net charge. Hence, this suggests that protein-solvent interactions are favored rather than protein-protein interaction. He also found reversible aggregation to occur with cooling and reheating of solutions. Through experiments involving cryoprecipitation, the 11S fraction alone was found to be responsible for reversible aggregation in the intermediate pH range investigated. This result correlates with the work performed on the 11S fraction [43,44] discussed earlier in the section.

When the effect of salt concentration was investigated in this study, it was found that reversible aggregates formed in 0.1 NaCl, that thermal aggregation was maximal in 0.2M NaCl, and that aggregation was suppressed by increasing the salt concentration above 0.2M. Association and aggregation, thus, seem to be favored in 0.1-0.2M NaCl. At NaCl concentration lower that 0.1M, dissociation into subunits may occur, aggregation being suppressed due to the electric double layer and intramolecular repulsion in the absence of counter ions. It was also shown that salt stabilized

against denaturation as well as against aggregation. Hermansson concluded that although it is unlikely that protein-protein and protein-solvent interactions be favored by the same agent, this special behavior is due to the complex quaternary structure of the soy proteins.

The gelling of soy protein isolates under various conditions has been studied by Catsimpoolas and Meyer [93]. They performed their experiments on 8% dispersions of soy isolate in water with heating to 80°C. From their results, Catsimpoolas and Meyer were able to divide the gelling process into three steps. The first step was suggested to be an irreversible conversion of the sol into a progel caused by heat. The progel state was characterized by a significantly higher viscosity than the unheated material. The second step was concerned with the setting to a gel upon cooling which was considered reversible. This second step was compared with the formation of reversible aggregates. The third step was again irreversible where the progel turns into a metasol after chemical degradation caused by an excess of heat or chemical agents. This reaction sequence can be seen schematically in Figure 13.

The progel-gel transition was considered to be of a noncovalent nature because of its reversibility. The irreversibility of the sol-progel transition may be attributed to irreversible disruption of the quaternary structure and/or formation of covalent bonds in the progel state. However, the latter was determined incorrect as a 'set' gel could be liquefied by layering solid urea on the gel. Thus, if significant covalent bonding occurred in the progel state, it should have been maintained in the gel state and addition of urea should not have liquefied the gel.

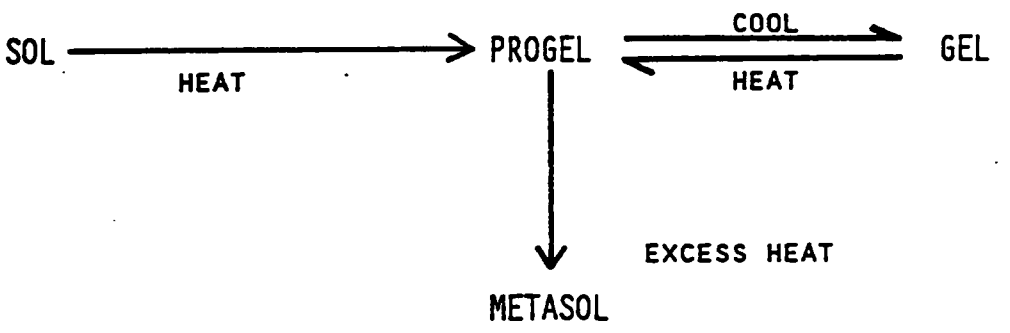

Figure 13. Gelation mechanism [93].

Hence, they suggested that heat causes dissociation into subunits and unfolding of the soybean protein molecules resulting in exposure of groups capable of hydrophobic bonding. They postulated that hydrophobic interactions of the nonpolar groups to form an associated network was involved in the formation of the progel state as this type of bonding is favored by a rise in temperature [68]. They further postulated that hydrogen bonds surrounded by water may be the main source of increased viscosity observed during the progel to gel transition. The thermal reversibility of this transition further supports the hypothesis of hydrogen bonding.

Circle et al. [67] also performed some experiments to determine the forces responsible for the gelation or cooking phenomenon of a commercial isolated soy proteinate preparation. They found the viscosity of both unheated and heated 10% dispersions significantly lowered and gelation prevented in experiments employing specific disulfide reducing agents. They interpreted the irreversibility of the soy proteinate heated gels to indicate that primary covalent bonds are involved in the network formation. They believed that the effect of the disulfide reducing agents points to the possibility of disulfide crosslinks involved in network formation. However, the ineffectiveness of a sulfur dioxide treatment at a 20% concentration leads to the conclusion that one or more other primary bonds may be involved in the crosslinking.

Whereas Catsimpoolas and Meyer and Circle et al. studied the gelation of soy protein isolate, Furukawa et al. [62] studied the textural properties of the gels produced. Specifically, they investigated the structural factors responsible for textural properties of heat induced soy protein gels using microscopic and mechanical testing techniques. The

gels were prepared by heating 20% soy protein isolate pastes at various temperatures. The gel structure was studied through its rheological properties, through solubility measurements, and through scanning electron microscopy (SEM).

In their studies, gels formed at temperatures ranging from 25°C to 130°C. They classified the resulting gels into three groups; soft gels which resulted from heating of pastes below 50°C, hard gels which were formed when pastes were heated from 60°C to 110°C, and fragile gels which resulted from heating at temperatures above 120°C. Gel hardness increased with heating temperature up to 80°C, but the gel was weakened by heating over 90°C, and especially over 120°C. The increasing hardness up to 80°C was postulated to be the increased hydrophobic interaction of nonpolar groups of the proteins to form an associated network. The drop in hardness was speculated as an indication of a partial collapse of the internal structure by excess heat. Upon cooling, the increased hardness was attributed to hydrogen bonds.

In the tensile stress relaxation experiments, Furukawa et al. determined the equilibrium modulus to be on the order of 10^4-10^5 dyne/cm^2 for the gels formed at all temperatures. A modulus of this magnitude suggested the presence of crosslinks in the gels. They concluded from these results that one of the factors responsible for textural properties may be the formation of crosslinks. Their results from solubility experiments with urea, mercaptoethanol, and various phosphate buffers indicated the existence of disulfide, hydrogen and hydrophobic bonds in the gels.

One additional study of interest is the work performed on soy milk by Fukushima [50]. Although soy milk is not the same as soy isolate, it is composed of all protein fractions. Fukushima investigated the plausibility of two possible mechanisms for the formation of the three dimensional structure formed upon cooking. He refers to this cooking phenomenon as a molecular polymerization of the protein with the first postulated mechanism to be polymerization by disulfide bonds and the second to be by hydrophobic interactions. A schematic of these two mechanisms can be seen in Figure 14. To test his theories he employed a solubility test using N-ethylmaleimide, the results of which are shown in Figure 15. His study involved comparing the amount of insolubilized protein in samples prepared with and without the addition of N-ethylmaleimide as a function of time of heating. By subtracting the amount of insolubilized protein in the sample with N-ethylmaleimide, which is indicative of the amount of protein insolubilized by mechanisms other than intermolecular disulfide bond formation, from the amount of insolubilized protein in the pure sample, he found that with increasing time at both temperatures of investigation (100° and 120°C) the amount of protein insolubilized by disulfide bond formation was very small. In fact, the 120°C samples approach a zero value for the amount insolubilized by disulfide bonds. From these results, he concludes that the insoluble protein is due mostly to hydrophobic bonding.

Unlike many of the researchers who studied the gelation effect of soy protein in an isolated environment, i.e., a soy dispersion subjected simply to heat, Cumming et al. [60] studied the effect of on the water soluble soybean. They analyzed both qualitatively and quantitatively the

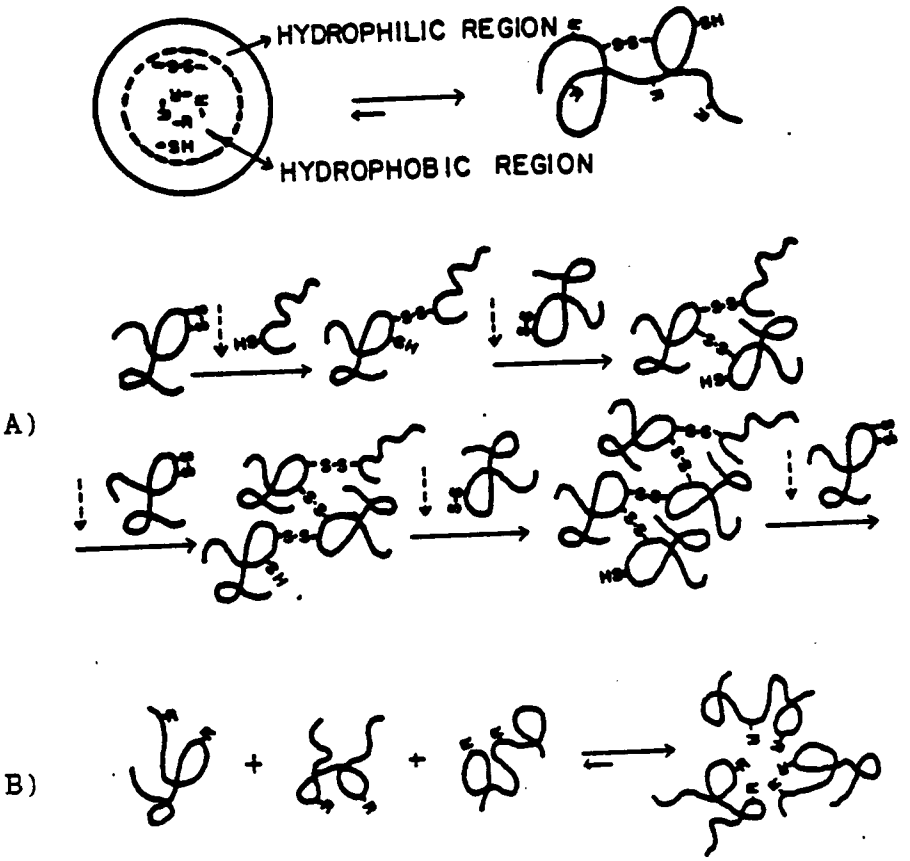

A)DISULFIDE BONDS B)HYDROPHOBIC INTERACTIONS

Figure 14. Intermolecular Polymerization Mechanisms [50].

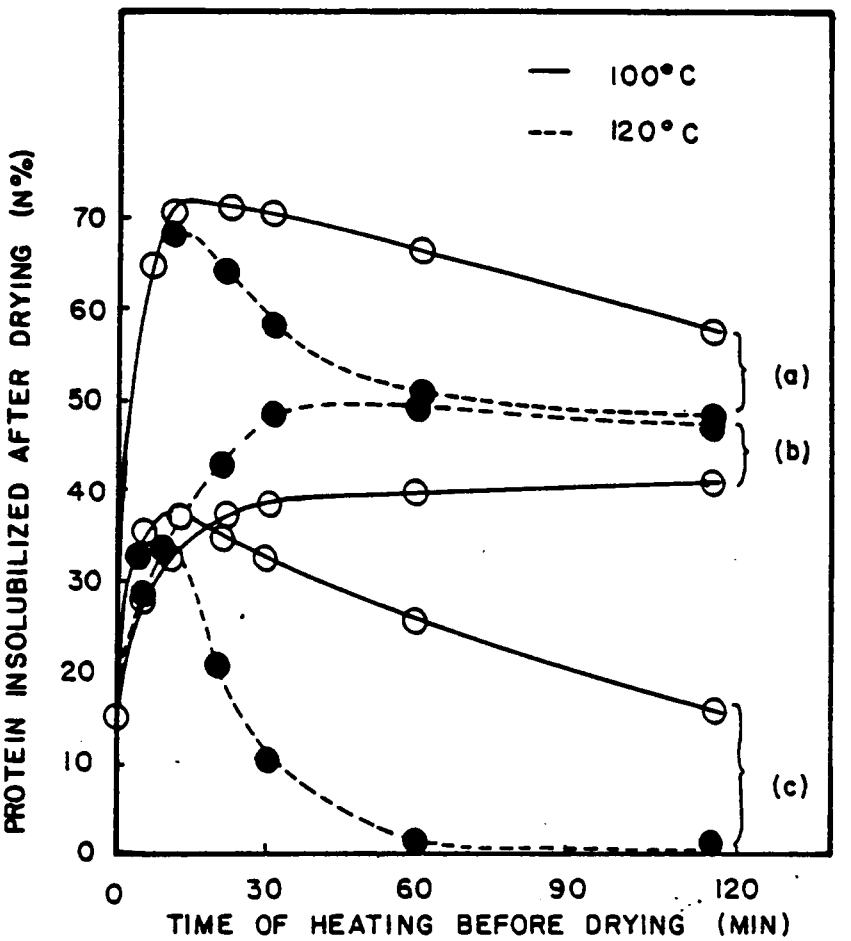

Figure 15. Solubilization tests studying the effect of heat on soy milk [50]

changes in soy protein from extrusion in an effort to correlate the theoretical findings for isolated proteins with the reactions occurring as a result of processing. They extruded a 30% added moisture soy flour and from the extrudate extracted the protein fractions. They also extracted protein fractions from the unprocessed flour for comparison.

From their studies, three major observations were made. It appeared that the unprocessed flour had large quantities of 11S and 15S while at higher extruder temperatures, there is a reduction of 15S, 11S, and to a lesser extent 7S protein. This is accompanied by a noticeable increase in the breakdown of products. Secondly, the more highly texturized the sample, the less soluble it becomes. In fact, the texturized material contained only 27% as much soluble protein as the unprocessed meal. The last observation of interest was that various proteins were affected unequally by processing, as evidenced by the various densitometer peak intensities changing at different rates during processing.

Burgess and Stanley [80] also studied the effects of extrusion upon soy. They suggest a different mechanism from any other previously postulated for the cooking phenomenon experienced during extrusion. Their work was performed on a 27% moisture soybean meal extruded at 178°C. Their conclusions were based on solubility studies using urea, 2-mercaptoethanol, and sodium dodecyl sulfate; these three reagents again chosen for the ability to disrupt disulfide bonds and hydrogen bonds and hydrophobic interactions. They found that none of the reagents were greatly effective in disrupting the bonding forces in the texturized soy product. Also, upon performing sulfhydryl and disulfide analyses, it was found that while extrusion produced an increase in moles of SH per mg

protein, a decrease occurred in level of SS. They remarked that it seems improbable that an increase in sulfhydryls or a decrease in disulfides would result due to extrusion if disulfide bonds are responsible for texturization. From this data they concluded that disulfide bonds do not play a significant role in the formation of the network structure. They instead proposed that the network is composed of intermolecular peptide bonds. This was investigated by adding a reagent to free amino and carboxyl groups and extruding the resulting material. The texture was tested for structure by means of a shear force test with the mean shear force of the reagent added product one fifth that of the pure soy extruded product. Hence they concluded that the mechanism for the formation of structure and texture in the extruded product involves intermolecular peptide bonds.

Melius [23] has reported that thermal polymerization by peptide bond formation requires a temperature of at least 180°. This finding substantiates the results and conclusion of the work of Burgess and Stanley but stipulates that a minimum temperature must be reached for this conclusion to be true.

Similar to Burgess and Stanley's work with high temperature extrusion, Hager [70] studied the effects of low temperature extrusion (<150°C) upon soy concentrate solubility. Measurements of the solubility of the original soy concentrate and of the extruded soy concentrate were performed to determine the forces which insolubilize the soy concentrate after extrusion. Urea was used to disrupt insolubilization due primarily to noncovalent forces, hydrogen bonding and hydrophobic interactions, and sodium bisulfite in combination with acrylonitrite was used to disrupt

insolubilization due to intermediate disulfide bridges. The major result of this work is that for the extrudate tested all but 3-4% of the protein can be solubilized by using urea and a disulfide cleaving agent. The data support the hypothesis that insolubilization and formation of structure caused by extrusion were strongly influenced by an increase in covalent bonded molecular aggregation due to intermolecular disulfide bridging. The absolute amount insolubilized by each type of bond was not determined. The fractions determined were obtained from indirect measurements and therefore were viewed as qualitative indicators of relative importance. Upon performing sulfhydryl and disulfide analyses, the level of SH increased while the SS content remained approximately the same (see Table 5). The findings of Burgess and Stanley are also included for comparison. Hager concluded that these differences reflect a difference in bonding mechanism between the high temperature extrusion of Burgess and Stanley (150-190°C) and their lower temperature extrusion (110-150°C).

From this discussion it can be seen that there are varied conclusions as to the mechanism for the cooking reaction. Cooking is viewed by some researchers to be similar to crosslinking primarily with the formations of disulfide bonds, though Burgess and Stanley propose peptide bonds as the crosslinks; while others viewed the bonds as less permanent.

Some interesting observations have been reported in the literature that may be the cause of the varying results of the studies performed. A point to note is that it has been reported by Saio et al. [30] and Wolf et al. [31] that different soybean varieties contain different ratios of 11S to 7S proteins. As it is seen that each fraction is distinctly different in its functional properties, it can be surmised that soy flour

TABLE 5

DISULFIDE AND SULHYDRYL CONCENTRATIONS IN NATIVE AND EXTRUDED SOY CONCENTRATE [70]

	native soy concentrate	extruded soy concentrate
Hager (140 C extrusion)		
(1) -S-S- content, mol/mg	22.7×10^{-6}	19.6×10^{-6}
(2) -SH- content, mol/mg	0.5×10^{-6}	4.1×10^{-6}
Burgess and Stanley (178 C extrusion)		
(1) -S-S- content, mol/mg	4.5×10^{-6}	0.9×10^{-6}
(2) -SH- content, mol/mg	3.3×10^{-6}	48.9×10^{-6}
Wolf and Cowan		
(1) -S-S- content, mol/mg	$\sim 20.0 \times 10^{-6}$	

products will differ in their functionality depending on the soybean variety used in its manufacture. As the studies on unfractionated soy preparations were not performed on the same soy from the same manufacturer from the same crop, the results can definitely be a function of the natural variability of the soybean. Also, Hermansson [34] performed calorimetric studies on commercially available isolates. He found that many of the commercial preparations showed no endothermic peaks on the DSC thermograms. Hence, these commercial preparations are completely denatured. As denaturation has been shown to play a significant role in the cooking process[34,41,42,44], the use of one of these commercial preparations which is denatured versus one which is not may produce different results in experimental studies. Another interesting observation by researchers is concerned with the dependence of the cooking reaction on the moisture content. Although most studies concentrated on the cooking phenomenon as a function of temperature, the moisture content was observed to be a factor. However, in most cases, it was simply reported that a minimum soy content was needed for the gelling of the dispersions with heat. As a number of the theories for cooking relate protein-solvent interaction as a force binding the network, the moisture content must be regarded as an important factor. A 10% dispersion of soy surely cannot possess the same protein-solvent interactions to the same degree as a 27% added moisture soy flour. This may in fact be an important observation in that different moisture content samples may not be compared as a different mechanism for cooking may be occurring depending on moisture content.

Now that the research involving the cooking reaction has been discussed, the effect of this reaction upon the rheological properties, namely the viscosity will be presented. In many cases the viscosity was viewed qualitatively in order to help determine the cooking reaction. However, other studies involved the modeling of the viscosity of soy flour preparations.

2.4 VISCOSITY

Viscosity is defined as the consistency of a fluid or, in other words, the resistance offered to a deformation such as that produced by shear stress. Viscosity can then be considered to be a momentum conductivity analogous to the heat transfer property of thermal conductivity. Of the material properties needed for modeling, viscosity has been investigated the most. In this section an overview of the investigation into the viscosity of soy materials will be presented. Also included will be the results of other rheological behavior which give insight into the behavior of soy products. The studies in this area range from qualitative reports on viscosity behavior as a function of external elements to development of models to describe the viscosity behavior of a specific system. This discussion will begin with some of the general observations and progress to include some of the postulated models for viscosity of soy systems.

Circle et al. [225] studied the viscosity of aqueous dispersions of a commercial isolated soy proteinate preparation. Experiments were performed on dispersions of the proteinate to concentrations of 14% in water. They found that in the absence of heat, the viscosity rises exponentially

with increased concentration. In concentrations above 7% by weight, heat causes thickening, and above 65°C, gelation. They found the rate of gelation and the firmness of the gel to be dependent upon temperature, time of heating, and protein concentration. For concentrations of 8-14% gels are formed within 10 to 30 minutes at 70° to 100°C but are disrupted if overheated at 125°C. Additional studies showed that at concentrations above 17%, the gels formed upon heating are firm and less susceptible to disruption by overheating.

Baird [65] has reported work on the effect of heat and shear on the rheological properties of soy; that is, not only viscosity but also storage, G', and loss, G", moduli. His studies included work on defatted soy dispersions and doughs of 30 to 60% flour by weight. In his studies of the effect of heat on the linear viscoelastic response of a 40% dispersion and a 50% dough, G' and η^*, the complex viscosity, for a 40% dispersion were seen to increase with temperature whereas the 50% dough exhibited the opposite behavior as shown in Figure 16. G' for both moisture contents was seen to depend on ω. The dependence of G' upon ω suggests that the results are due to the proteins being highly constrained but not permanently crosslinked. From these results he concluded that the increase in rheological properties which has been associated with protein gelation may be due to the expansion of globular protein by moisture. He explained this as the globular proteins expand, they overlap increasing molecular contacts which raises the rheological properties. The doughs have a high enough concentration of flour that the interactions are already present and increasing temperature only makes it more easily deformable. The effect of shear on the linear viscoelastic response of

these materials was negligible. Even high shear rates with strong entry flow effects produced no significant change in their rheological behavior. However, Baird then studied the combination of the two, heat and shear simultaneously, and concluded that shear may promote diffusion of the water into the protein during the cooking phenomenon, leaving them more swollen and increasing the degree of intermolecular interactions. Finally, in experiments monitoring G' as a functions of time, Baird found that although G' for the 50% dough was not a function of time, G' for the 40% dispersion increased significantly over a period of two to five minutes as can be seen in Figure 17, indicating a reaction kinetics.

Hermansson [66] not only studied the flow properties of dispersions of soy protein isolate as well as dispersions of other protein forms but also correlated his results with an empirical equation for viscosity. Experiments were performed on dispersions of 4-20% soy protein isolate. Flow properties were expressed by a power law equation with a yield stress as many of the protein dispersions had yield stress values. However, the Casson equation, which Hermansson stated is equally valid over a certain range, was used instead. Results showed an increasing deviation from Newtonian behavior with increasing concentration and at concentrations above 8% a yield value is apparent. The yield value was seen to increase greatly with protein concentration. Also, the consistency index was seen to increase with concentration but to a lesser extent than the yield value. Continuous shear curves showed that a dispersion of 12% soy isolate was thixotropic.

Hermansson also investigated the effect of processing by examining various commercially prepared soy isolates. He concluded that not only

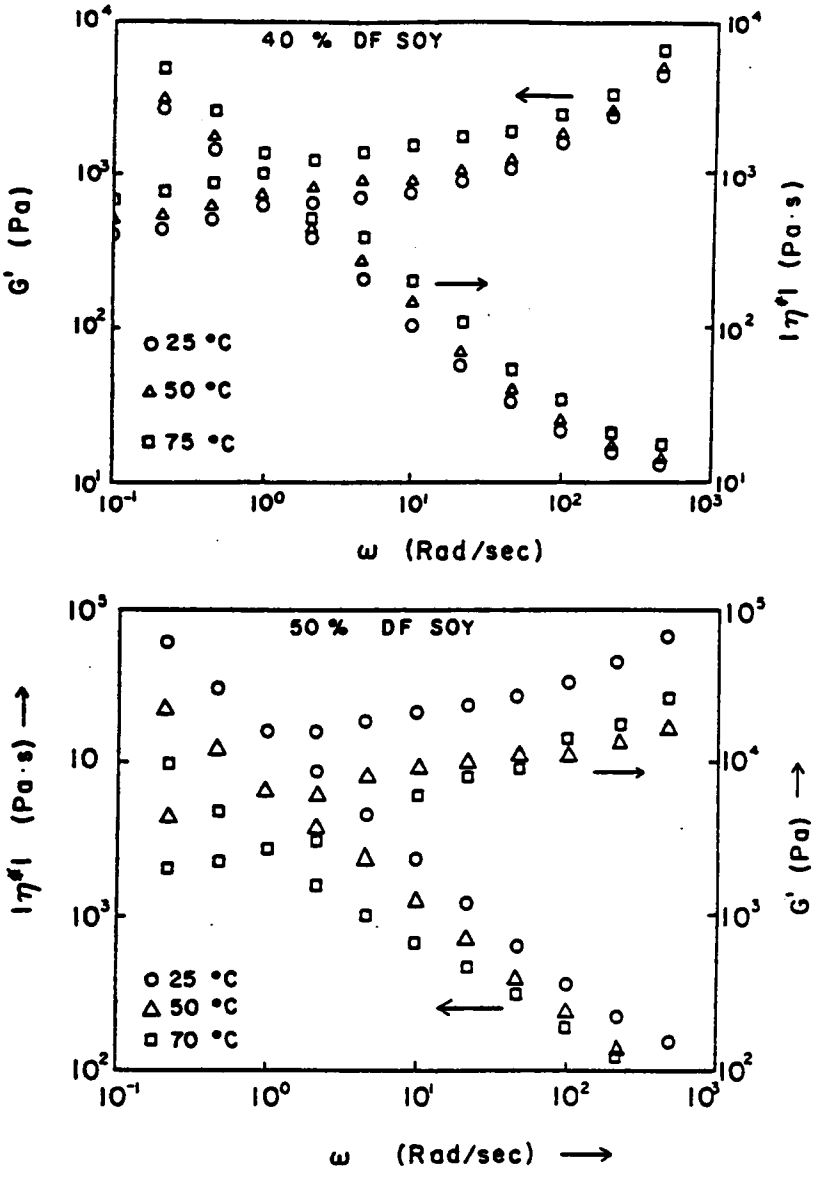

Figure 16. Temperature effects on 40% dispersion and 50% dough [65]

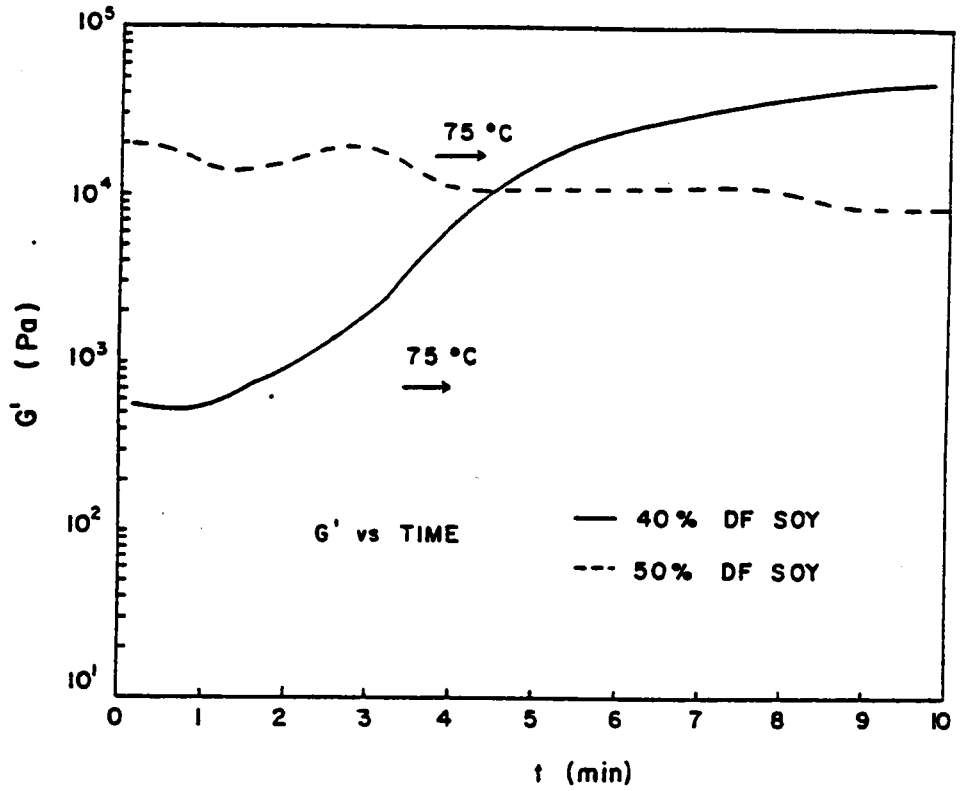

Figure 17. Kinetics associated with heating of soy doughs as shown by G' data[65]

is the consistency index affected but also that processing has caused the development of yield values. Addition of salt reduced viscosity as well as swelling and solubility. This effect of decreasing viscosity as less swelled, more rigid aggregates and less solvated protein molecules would be in the continuous phase. The same relations among flow properties, swelling, and solubility were obtained with increasing pH where the increase in net negative charge caused increased solubility and swelling as well as viscosity and yield values.

Jao et al. [40] studied the effects of moisture level, temperature, and shear rate on the viscosity of a defatted soy dough during extrusion. Process conditions involved in this study were temperature range from 100° to 160°C, added moisture content from 22% to 32% , and shear rate range from 50 to 10,500 s^{-1}. A Brabender laboratory extruder with four capillary dies was used. As they found that the pressure drop was undetectable when there was no die in the channel of the die head, the observed pressure value at the port 45 mm from the die face was considered to be the sum of the entrance and capillary pressure drops. Both the Bagley correction [38] on pressure drop and the Rabinowitsch correction [63] on shear rate were employed. This extrusion study revealed that entrance pressure loss is related to shear rate, temperature, and moisture. Entrance pressure loss increased with increasing shear rate but decreased with increasing temperature and moisture content. Viscosity curves of the 32% added moisture soy dough at 130°C were seen to be similar to that at 100°C. However, the effect of temperature on viscosity had a much more pronounced effect between 130°C and 160°C as can be seen in Figure 18. This behavior suggests that the material may

be of different structure above 130°C as compared to that below 130°C. The effect of temperature was also exhibited in the entrance pressure loss. Below 130°C, the entrance pressure contributed up to one quarter of the total pressure suggesting elasticity whereas above 130°C, the entrance pressure loss drops significantly, contributing less than 2% of the total pressure at 160°C. Viscosity data of the 25% added moisture dough exhibits a drastic drop with shear rate at 100°C crossing over that of 130° as can be seen in Figure 18. At 22% added moisture, the power law equation became inadequate to describe the flow characteristics at 100°C and 130°C as can be seen in Figure 18. An empirical fit of the viscosity data was developed with multiple regression analysis expressing the viscosity as a function of shear rate, temperature, and added moisture.

Chen et al.[220] took the work of Jao et al. [40] one step further. Based on established theories, they developed a viscosity model for defatted soy dough under various conditions of shear rate, temperature, and moisture level in an extrusion process. Their model combines the theories of power law, logarithmic mixing rule, and Eyring kinetic theory. The viscosity model obtained from applying the preceding concepts is shown in the following equation:

$$\mu = 93641\ \dot{\gamma}^{\,0.873}\ e^{3327/T}\ e^{\,0.0631H} \qquad 2.1$$

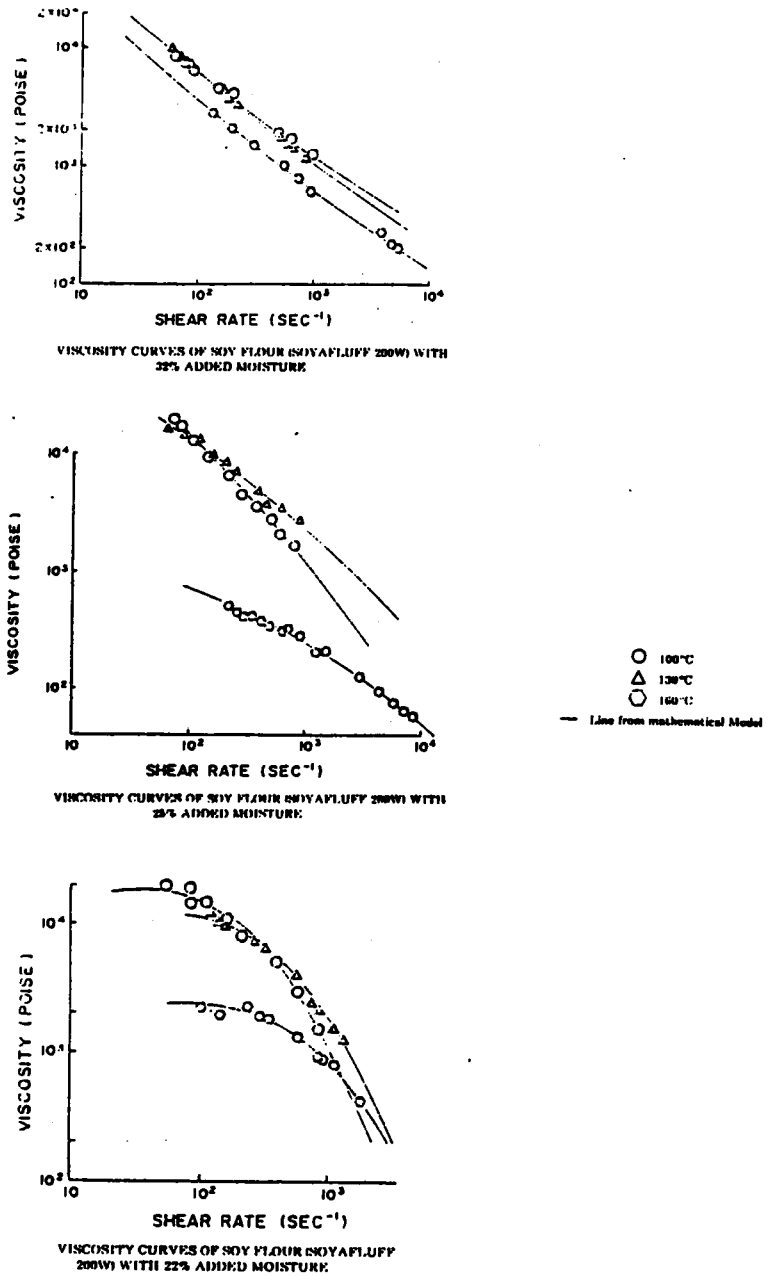

Figure 18. Effects of moisture level, temperature, and shear rate on viscosity [40].

This model represents data within the shear rate range of 50 to 100 s^{-1}, the temperature range of 100° to 160°C, and the added moisture range of 22% to 32%. This data was obtained by the same procedure as Jao et al. [40]. The flow index for this soy dough was determined to be 0.127. Examination of the viscosity model reveals that increases in the shear rate, temperature, and added moisture will cause a reduction in viscosity.

Remsen and Clark [71] recognized the presence of a kinetics in the cooking phenomenon as the network structure was formed. They developed a five parameter semi-empirical model to describe the apparent viscosity of a soy flour dough as a function of not only shear rate and temperature but also time-temperature history. Their model is based on the combination of the power law equation for shear rate dependence, an Arrhenius expression for temperature dependence, and an expression as shown in equation 2.2 developed by Roller [69] in his study of curing epoxy resins to describe the time-temperature dependence.

$$\ln\eta(T,\dot{\gamma},t) = \ln(\eta^*) + \Delta E_\eta/RT + (n-1)\ln\dot{\gamma} + \int_{t_0}^{t} k_\infty \exp(\Delta E_k/RT)\,dt \qquad 2.2$$

This latter expression accounts not only for the kinetics of the reaction but also includes a modification for non-isothermal reaction conditions. Upon first examination, their model appears to be quite in-depth and thorough. However, upon closer examination, many problems exist. First, their model is developed for a 32% moisture defatted soy dough. Hence,

moisture effects are neglected. The Instron capillary rheometer was used for experimental viscosity measurements. A value of 0.34 for the flow index was determined from the results of these experiments. This value was found to be essentially independent of temperature. However, the temperature span examined was narrow with no data reported for temperatures higher than 90°C. Finally, reaction effects were determined in Amylograph experiments. However, the Amylograph experiments were performed on a 25% dispersion of flour in water. As other investigators have shown that moisture percent has an effect upon the behavior of the soy dough, the reaction effects for the 25% dispersion could not realistically be applied to a 32% moisture soy dough. Therefore, their model not only was limited in its applicability but also was based on incorrect assumptions.

2.5 THERMAL CONDUCTIVITY

Thermal conductivity is the ability of a material to transmit heat when subjected to a change in thermal surroundings. As stated in Fourier's Law of heat conduction, the heat flux by conduction is proportional to the temperature gradient. The thermal conductivity of a material depends upon its porosity, structure, and chemical constituents. For food materials, the thermal conductivity depends primarily upon the content and properties of air, fat, and water. Since the thermal conductivity of fat is lower than water and air even lower, high levels of fat or entrapped air will decrease the thermal conductivity of a foodstuff. Also, the thermal conductivity of a liquid has been found to decrease with increasing concentration of solutes [81].

Thermal conductivity is a difficult material property to determine experimentally. The most accurate method currently employed in that of the guarded hot plate (ASTM Method C 177) [85]. Measurements of thermal conductivity by this method is time consuming and requires skilled operators. Other methods have been developed for measurement of the thermal conductivity insulating materials [100,101]; however, these methods are not functionally applicable to the consistency of most food materials.

Dickerson [102] developed an apparatus for the measurement of thermal diffusivity of foods. The thermal diffusivity of a material determines the rate of heat propagation through the material. It is related to thermal conductivity as well as density and specific heat. These properties are related by the equation:

$$\alpha = k / (\rho * Cp) \qquad 2.3$$

where: α - thermal diffusivity

k - thermal conductivity

ρ - density

Cp - specific heat

Hence, thermal conductivity of a material may be obtained from thermal diffusivity data if the density and heat capacity are known.

Dickerson's method determines the thermal diffusivity experimentally under transient heat transfer conditions. The apparatus shown in Figure 19 consists of a constant temperature water bath and a thermal diffusivity

tube that is filled with the food sample. Dickerson derived the following equation to compute thermal diffusivity from his experimental apparatus:

$$\alpha = [A * R^2] / [4 * (Tr - To)] \qquad 2.4$$

where: A - linear rate of heating

R - inside radius of tube

Tr - temperature at surface of cylinder

To - temperature at center of cylinder

The equation allows determination of thermal diffusivity if the constant temperature difference between the outside surface of the tube and the center of the tube (Tr - To) are known. The apparatus was designed to minimize experimental error. Although the mathematical derivation is for an infinite cylinder, its application to the designed diffusivity tube results in an error of less than 2%. The derivation assumes homogeniety of the food material measured. Dickerson reports an accuracy of 5% in his experimental results.

Dickerson also modified his apparatus to determine the thermal conductivity by the hot wire method described by Vos [99]. For these determinations, the end caps and thermocouple probe of Figure 20 were replaced by rubber stoppers with a heater wire placed at the axis of the tube and a thermocouple located on the midpoint of the axis of the tube.

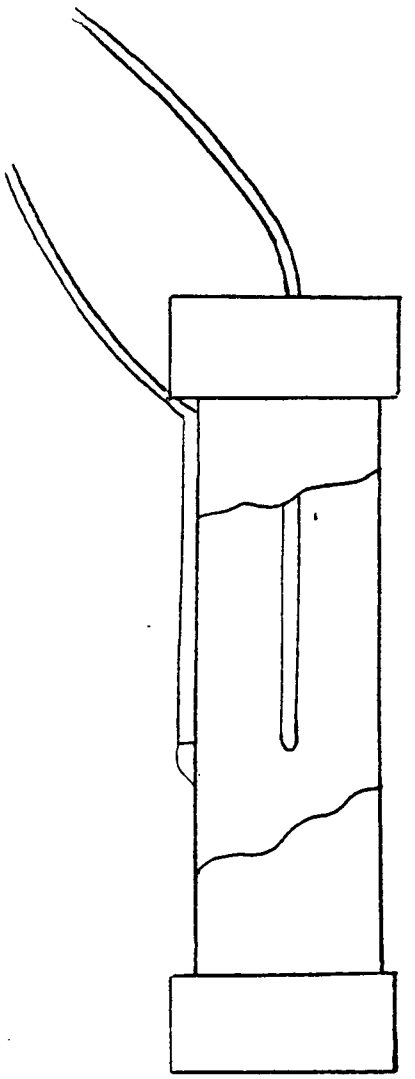

Figure 19. Schematic of the thermal diffusivity tube.

The hot wire method operates on the principle that as a constant rate of energy is supplied to the heater wire, the energy must be dissipated in the sample near the wire. The temperature of the sample near the wire will depend on how well the sample conducts heat away from the wire. Thermal conductivity, then, is determined from data obtained while heating the wire by the following equation:

$$k = \frac{[3.413 I^2 Z * \ln(\tau_1 / \tau_2)]}{[4\pi(T_1 - T_2)]} \qquad 2.5$$

where I - current
Z - resistance per unit length of heater wire
τ - time
T - temperature

where the subscripts 1 and 2 represent any two points on the curve after the initial transient response. Again, the apparatus dimensions were designed to minimize error.

Thermal diffusivity values for foods are in the range of 1-2 x 10^{-7} m^2/ s [82]. The values usually increase with increasing temperature. The only thermal property associated with soy reported in literature is the thermal conductivity for soybean oil meal reported to be 0.0692 (W / m *°K) [102].

2.6 DIFFERENTIAL SCANNING CALORIMETRY

Differential scanning calorimetry (DSC) is a particularly pertinent technique for studying the behavior of proteins in foods because of its

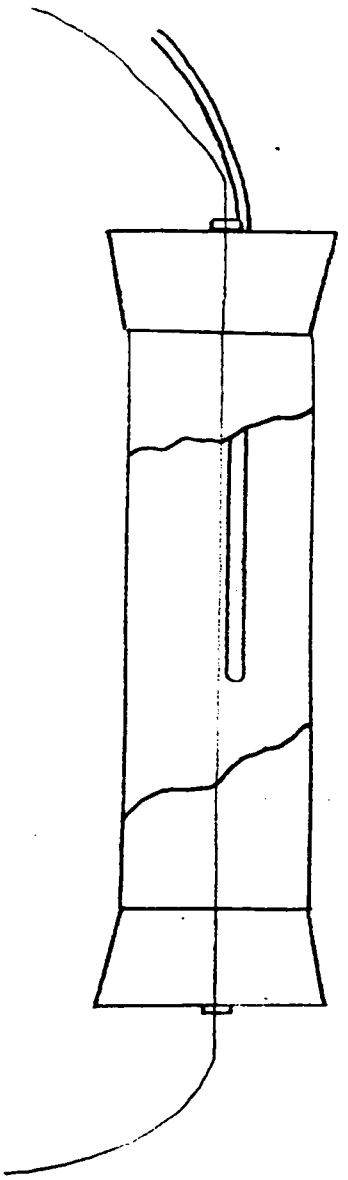

Figure 20. Schematic of the thermal conductivity tube.

inherent utilization of heat. Heating probably constitutes the most common form of processing treatment applied to food systems and is a definite component of cooking extrusion. Thus, basic information concerning the effect of temperature and rate of heating on denaturation undergone by the proteins during cooking can be obtained. Also, the determination of other reactions occurring in the system may be made and these in turn can be monitored. A discussion of the thermal scans found in literature which have been performed on soy protein is included in this section.

The thermally induced process exhibited by most proteins and detectable by DSC is the structural melting or unfolding of the molecule. This has been designated as denaturation, defined as the transformation from the native or ordered state to the denatured or disordered state. In order for the process of denaturation to be discerned by DSC, the rupture of the inter- and intra-molecular bonds must occur in a cooperative manner. The less cooperative a process, the broader the resulting transition and hence, the more difficult it is to detect by DSC. In fact, it has only been the recent advent of calorimeters with high sensitivity that analysis of the denaturation process has become possible as the enthalpies associated with denaturation are small, for the most part less than 5 cal/gram [98].

For the most part very little work has been performed on soy proteins using DSC to monitor the transitions which occur in the system upon application of heat. From studies of other protein systems [98,97] it has been found that the heating rate is an important factor when analyzing DSC data. Heating rate has been found to influence both apparent

denaturation temperature and enthalpy. The effect of temperature is explained in terms of denaturation kinetics. The result observed is one of increasing denaturation temperature with increasing rate of heating. Apparent enthalpy is seen to decrease as heating rate is reduced.

As mentioned, very little work has been performed using DSC on soy proteins. Hermansson [34] used DSC to investigate the denaturation and correlate the network formation of soy proteins. A dispersion of 10% soy protein isolate in distilled water was used in his study. A DSC thermogram of his results is seen in Figure 21. In his investigation, Hermansson looked at the denaturation of soy protein as a function of pH. As seen in the figure, only one peak was observed at low (2-3) and high (10) pH, while two peaks were observed in the middle (4-9) pH range. After complementary thermograms were performed on a fractionated 11S sample, he found that the 11S globulin is responsible for the second peak, and hence, the 7S globulin is responsible for the first peak. The enthalpy involved with these peaks was not determined in this study. No explanation of the effect of pH on denaturation was offered. A point to note was mentioned that the peaks were seen to be overlapping in many of the cases. Additional studies on commercially prepared isolates showed no endothermic peaks on DSC thermograms, which means that they are completely denatured. One isolate was found to be partially denatured exhibiting one broad peak encompassing both the 7S and 11S peaks. Hermansson concluded that the method of preparation is critical to the state of the proteins which may in turn be of consequence in the network forming process.

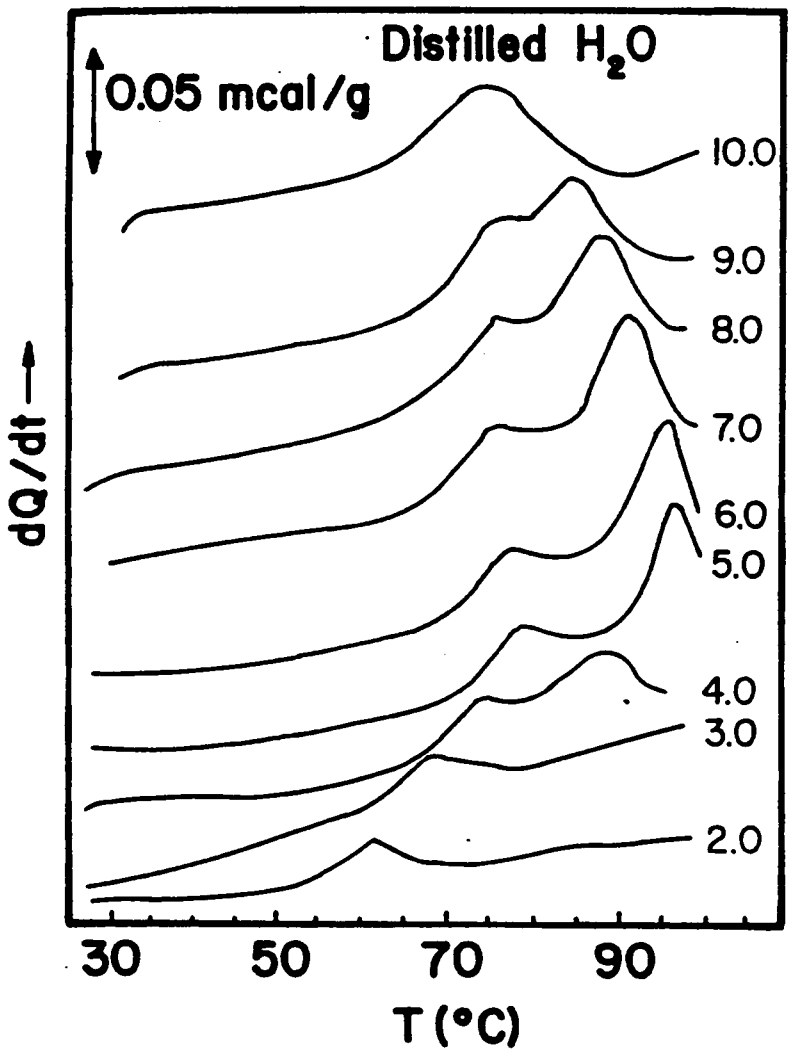

Figure 21. 10% soy dispersion thermograms [34]

Hermansson was able to correlate the temperature of denaturation of 7S globulin with the beginning of gel formation as seen in the work of Catsimpoolas and Meyer [93]. The temperature associated with denaturation of the 11S globulin is correlated with gel strength maximum also found in the work of Catsimpoolas and Meyer [93]. This, he concluded, implied that denaturation as well as the dissociation of protein structure is integral in the gelation process.

DSC has also been used to investigate protein-water interactions. The role of water is central in the denaturation of proteins since it is the balance between protein-protein and protein-solvent forces which largely determine the stability of the protein. In addition, the protein itself influences the structure and properties of the surrounding water. Muffett and Snyder [95] investigated the effect of water in a soya protein system. They found that the amount of non-freezable water which is determined by DSC increased with total water content of the system. This effect was most pronounced at concentration of 0.3g to 0.5g water per gram of protein. In this range, approximately 50% of the added water became 'bound'. In experiments on other protein systems [94,97] as water content increased, denaturation enthalpy increased while denaturation temperature decreased.

Although DSC is the preferred method for determination of heat of reaction and specific heat of a sample, some researchers have used other methods to gain values for these properties. Fong [104] determined the specific heat of 25, 28, and 33% moisture extracted soy flour dough. He performed an energy balance around the feeding and exiting ends of the extruder assuming adiabatic conditions. In his calculations, he based

the specific heat determination solely on the amount of water vaporized as measured by comparing the feed and product moisture contents. However, he did not take into account that the moisture flashes off outside of the extruder. Hence, the specific heat calculated reflected the vaporization of water outside the extruder and not the actual soy dough under processing conditions. Hence, his results are of no real value and could not be compared in anyway to those determined through DSC experimentation.

2.7 EXTRUSION

The material properties of food doughs needed to model the extrusion process have now been discussed. It is seen that, for the most part, the information regarding these parameters is scarce. That which does exist is conflicting and incomplete. In addition, the overall process of food extrusion is complex and inadequately understood. In the introduction, a basic description of the process is outlined. A summary of the different types of food extruders is given in an informative review by Harper [90].

The operation of the extruder in its various capacitites is governed by a number of factos. These factors include process parameters which include rotational speed of the screw, flow rate of feed material, and the temperature profile achieved by heating or cooling the barrel or screw. Design parameters include diameter and length of the barrel, channel depth profile of the screw, the width and pitch of the screw flights, and the clearance between the screw and barrel. The consequent power consumption, pressure rise through the extruder , and product tem-

perature are results of the combination of process and design parameters. It is the prediction of these results i.e., temperature, pressure, and power, from a knowledge of the process and design parameters that is desired for modeling of the extrusion process.

Rossen and Miller [27] looked at food extrusion on a generalized scale. They discussed the classification and applications of food extruders; a summary of which can be seen in Table 6. One can see from the table the extruder whose application is toward protein supplements is a single screw extruder exhibiting continuous high shear cooking. Also included in their review is a summary of typical operating data for five types of single screw extruders commonly used in the food industry. This is shown in Table 7. The values shown for a high-shear cooking extruder are representative of those used in the processing of soy protein. Rossen and Miller go on to report that the extruders used to process puffed cereals and snacks which require the high-temperature, short-time cooking generate heat rapidly in the product by operating at high speeds and usually run starved so that a low residence time is assured. They also discussed a variety of operating problems such as surging, die plugging, and product flow variations and methods of overcoming these problems.

On a more narrow scale, Smith [57] discussed process equipment, technology, and factors controlling production efficiency and product quality with regard to high temperature/short-time extrusion cooking. He suggested four major ways in which desired textural and functional characteristics of the extrusion cooked foods can be controlled. These were selection of ingredients and additives; control of pH in process materials; selection and arrangement of components of the extruder as-

TABLE 6

CLASSIFICATIONS AND APPLICATIONS OF FOOD EXTRUDERS

Types of extruders	General characteristics	APPLICATIONS						
		Snacks	Cereals	Pasta	Confec-tionery	Pet foods, animal food	Sausage products	Protein supplements, meat analogs
Direct (positive-displacement)								
Hydraulic or pneumatic ram	Very low shear, continous	X			X		X	
Intermeshing twin screw	Low shear, continuous				X			
Hybrid of direct and indirect								
Non-intermeshing twin screw	High shear, continuous				X			
Indirect (viscous-drag)								
Roller	Low shear, continuous	X	X		X		X	
Single Screw	High shear, continuous	X	X	X	X	X		X

TABLE 7

TYPICAL OPERATING DATA FOR VARIOUS FOOD EXTRUDERS

Measurement	Description	TYPICAL OPERATING DATA				
		Pasta extruder	High-pressure forming extruder	Low-shear cooking extruder	Collet extruder	High-shear cooking extruder
Feed moisture (%) Product moisture (%)	Illustrates product characteristics and moisture loss due to flashing	32.00 32.00	25.00 25.00	28.00 25.00	11.00 2.00	15.00 4.00
Product temperature (°F)	The temperature reached within the extruder; when flashing occurs, the temperature drops to the boiling point as the product flows through the die, with a corresponding loss of moisture	175.00	175.00	300.00	390.00	390.00
D/h	Represents the relative flight depths of the extruders	6.00	4.50	7-15	9.00	7.00
n	Number of parallel screw channels (leads)	1-2	1.00	1.00	2-4	1-3
N (rpm)	Screw speed	30.00	90.00	60.00	300.00	450.00
Applied shear rate (sec^{-1})	A function of D/h and N, used as a rough measure of the intensity of shear applied to the product; other factors such as pressure gradient and leakage flow, especially in a grooved barrel, strongly affect the actual shear rate	9.50	9.50	22-47	100.00	163.00
Z_{max}/Q $\left(\frac{hp}{lb/hr}\right)$	The total motor horsepower per unit flow rate required to operate the extruder	0.03	0.07	0.07	0.12	0.20
$Z_m \cdot Q$ $\left(\frac{hp}{lb/hr}\right)$	That portion of Z_{max}/Q which is distributed as heat to the food as it goes through the extruder	0.01	0.02	0.01	0.06	0.07
H_i (BTU/lb)	$Z_m \cdot Q$ expressed in thermal units	25.00	50.00	25.00	160.00	175.00
H_a (BTU/lb)	Heat added to (+) or removed from (-) the food by application of external heating or cooling	0.00	0.00	175.00	0.00	-60.00
H_{max} (BTU/lb)	The total energy received by the product ($H_{max} = H_i + H_a$); related to product temperature and moisture loss	25.00	50.00	100.00	160.00	115.00

sembly; and control of processing variables to produce desired functional or rheological properties. With regard to the processing of soy proteins, he proposed that the following steps need to be accomplished to produce a texturized product. The steps were as follows: moistening and heating of the protein flour, effective destruction of residual growth inhibitors, denaturation of protein, rupture of the cellulose sac which surrounds each protein body, the joining of these liberated protein bodies into rivulets of protein, which subsequently twisted together into protein strands, and the stretching and twisting of these protein strands with the uniform, systematic layering of these strands one over another to produce a structure quite similar to the structure of muscle tissue. All these steps can be accomplished in extrusion cooking. He also stated that the raw material must have a minimum of 50% protein, a maximum of 3% fiber, and an NSI, nitrogen solubility index, which is a measure of how much of the protein is undenatured, of 50 to 70 to produce a successful product.

Williams et al. [58] discussed the cooking conditions attainable in an extruder on proteinaceous materials. Many proteinaceous materials require cooking if they are to be used for food because they contain certain proteinaceous constituents which provide for poor taste, poor storage qualities, or poor digestibility. Enzymes present in the soy flour contribute to all three undesirable properties unless they are inactivated by the cooking process causing denaturation. Williams et al. [58] found that they could manipulate the moisture-temperature conditions required to denature proteins to serve specific requirements of the process. For

example, in a high moisture process one can denature protein at a lower temperature than would be required at a low moisture process.

With regard to soy flour protein meat analogs, Williams et. al. found that attention must be paid to two particular aspects of extruder operation. First, the process conditions must be correct to convert the protein into a condition where it can polymerize into the desired structure. They found an important process parameter is to start with a raw material that has the protein in a condition where it can undergo the reactions required. The protein in the raw feed material must be undenatured and capable of forming a gel. For making meat analogues, the NSI should be preferably around 90 and not less than 60. As the proteinaceous material passes through the extruder, it should first undergo a reaction where it forms a gelatinous mass by mixing and reacting with water and then remain in the extruder long enough for the protein molecules to begin to polymerize and form the chain interactions. While the material is polymerizing, the flow pattern should be such that it can form the desired structure, and then it should leave the extruder before the structure is destroyed. Apart from these process conditions, the extruder must be mechanically capable of providing an atmosphere where these reactions can occur.

As Smith stated, the composition of the starting material is one of the most important variables in food extrusion. Williams et al. [59] provides a good review of considerations in selection of a food extruder. They bring out the importance of moisture content not only to the type of cook desired which includes both temperature and time of exposure to elevated temperature but also to the extruder design. The moisture con-

tent of the material inside the extruder has an effect on capacity by controlling the frictional resistance of the material being conveyed through the extruder. Low moisture materials have high frictional resistance and draw high horsepower, whereas high moisture materials have less friction and less horsepower. Hence, food extruders are available at capacities of 20,000 pounds per hour depending on the food product being processed. Selection of the die may also control some important processing elements. These can include degree of orientation and expansion as well as controlling the pressure achieved in the extruder.

2.8 EXTRUSION MODELS

Very little modeling of food extruders has been done. A few models with varying constraints have been proposed. A short description of these models and their constraints and performance is now provided.

Levine [88] proposed a simplified model for food extrusion with extruder output and power consumption described by dimensionless groups. The conceptual model of the extruder is illustrated in Figure 22. This model was composed of three parts; an ideal screw which allows no backflow, a recycle pipe through which all backflow travels, and a valve which provides the flow resistance normally attributed to that of the die and breaker plate. He developed a mathematical approach for each section's flowrate. The ideal screw was approached as two plates moving relative to each other; the barrel being the moving top plate, and the screw being the stationary plate. The backflow is calculated using a cylindrical approximation to the helical flow path and the friction factor/Reynolds number correlation. Although he investigated the material properties of

the wheat dough he used in his studies and found the viscosity to be extremely temperature and moisture dependent the viscosity for a single moisture content dough at an average temperature was the sole viscosity value used in the calculations. Experimental results using a simple screw (non-varying thread depth) and isothermal conditions compared to theoretical prediction fairly well.

Levine acknowledged that this approach is too idealized for application to real extrusion processes. He suggested a method to approach the more complex extrusion process where processing conditions are not isothermal and the screw is not simple in design. For this situation, the screw is broken up into a 'chain' of short screws in series. The performance of the chain is then obtained by trial and error on section discharge pressure. This method however, is not only mathematically cumbersome, but also has problems with continuity across chain segments. Also, the case tested was for only one material, an uncooked wheat flour dough. A model for its viscosity was developed, but it was over a narrow moisture and temperature range. In addition, as stated, the dough did not get cooked in the extrusion process. In addition, although a viscosity model dependent upon temperature, shear rate, and moisture content was developed, the average temperature and moisture constants were used to simplify calculations.

Jasberg et al. [84] observed that during the extrusion of soy flakes the back pressure from the die had little influence on the volumetric flowrate. Hence, they believed that the soy flakes were conveyed as a powder and therefore plug flow would describe the process rather than viscous drag flow. Although they admitted that the normal operating

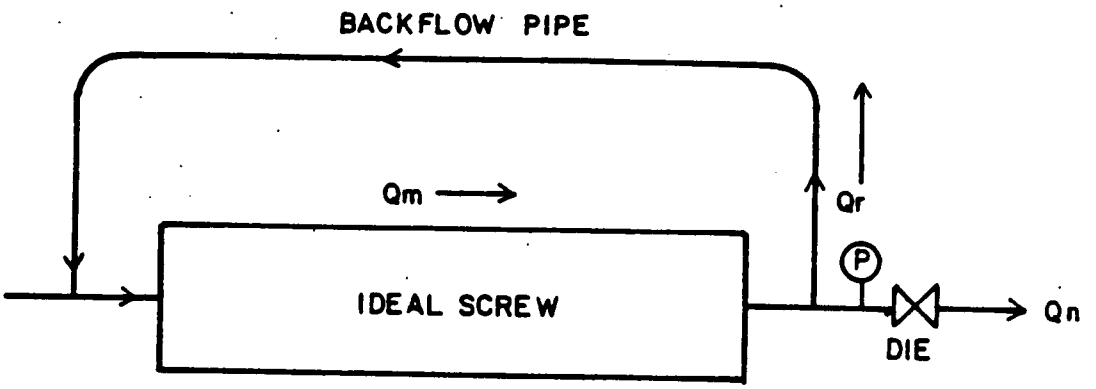

Figure 22. Conceptual model simulating food extrusion [88].

temperature in the compression and metering zones would be much higher (150°C) and the dough would behave as a pseudoplastic fluid as shown by Chung [79] and Jao [78], because of the low operating temperatures the extruder was analyzed using a plug flow model for the entire screw length. Therefore, Jasberg et al. used the Darnel and Mol model of plug flow based on solids conveying to predict the extrusion of defatted soy flakes at low temperature (30-50°C).

Darnell and Mol [77] analyzed the plug flow of solids in the feed section of a plastics extruder. According to their theory the volumetric flowrate of a single screw extruder can be predicted from the geometry and speed of the screw, and the coefficients of friction between the solid plug and extruder surfaces. By performing a force balance on the plug traveling in the screw channel as shown in Figure 23, the conveying angle of the plug is determined. The conveying angle is then used to solve for volumetric output per revolution.

Jasberg et al. examined moisture levels for the dough ranging from 25 to 35 % water. Coefficients of friction were determined experimentally using a method similar to ASTM Method D1894-63 where a sled covered with the material is pulled across a plate. The coefficients of friction were seen to increase with moisture content, a value of 0.2 was found at 8% moisture content increasing to 0.7 at 36% mositure content. Screw speed and die length were other variables investigated in the experiments.

The theoretical predictions for volumetric flow rate were in good agreement with experimental results. The theoretical curve describing volumetric flow rate as a function of moisture appears to be slightly lower than experimental values at lower moistures and slightly higher at

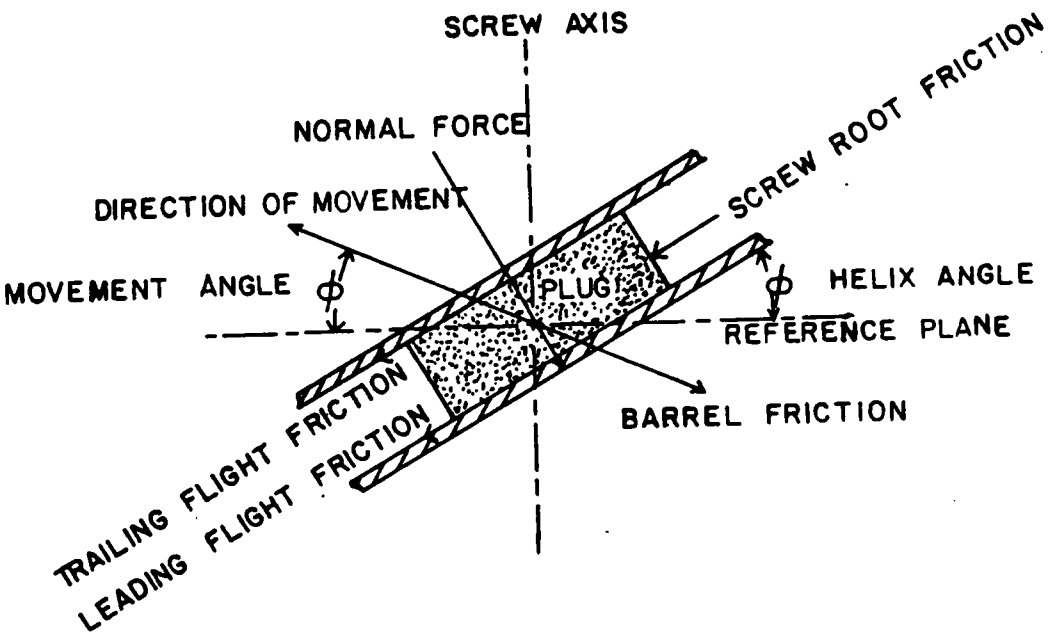

Figure 23. Forces on the plug traveling in the screw channel [77].

higher moistures. This phenomenon was not explained, but the average error was only 5%. Moisture content was found to be the most significant factor involved of the variables examined. Output versus pressure drop curves showed an unusual slope in some cases unlike that seen in the flow of polymer melts. Jasberg et al. attributed this phenomenon to plug flow occuring in the die rather than viscous drag flow.

Harper [87] discussed a common model used in food extrusion. This model borrows heavily from that developed in the plastics industry. In this model a set of assumptions is made to solve the basic flow equations. The assumptions are that flow is fully developed, steady-state and laminar, the fluid is incompressible, gravity and inertial forces are negligible, the barrel is rotating and the screw is stationary and slip does not occur at the walls. In this model, the channel is 'peeled' off the screw and laid flat. A schematic of this method of approach is seen in Figure 24. Basically, these assumptions are valid for food extrusion though some are of question. Only if the channel of the screw is shallow may it be unwound from the screw with little distortion. Also, assuming no slip conditions is not always true of all food systems but as incorporating slip into the model is difficult it is not included. The initial model he discusses is for a Newtonian fluid under isothermal conditions. For these conditions, mathematical expression for volumetric output and pressure drop across a die have been derived. This model is very useful in understanding how the primary geometry and operating characteristics affect the output.

Harmann and Harper [86] performed a study with this model using pregelatinized corn flour hydrated to 32% and isothermally extruded at

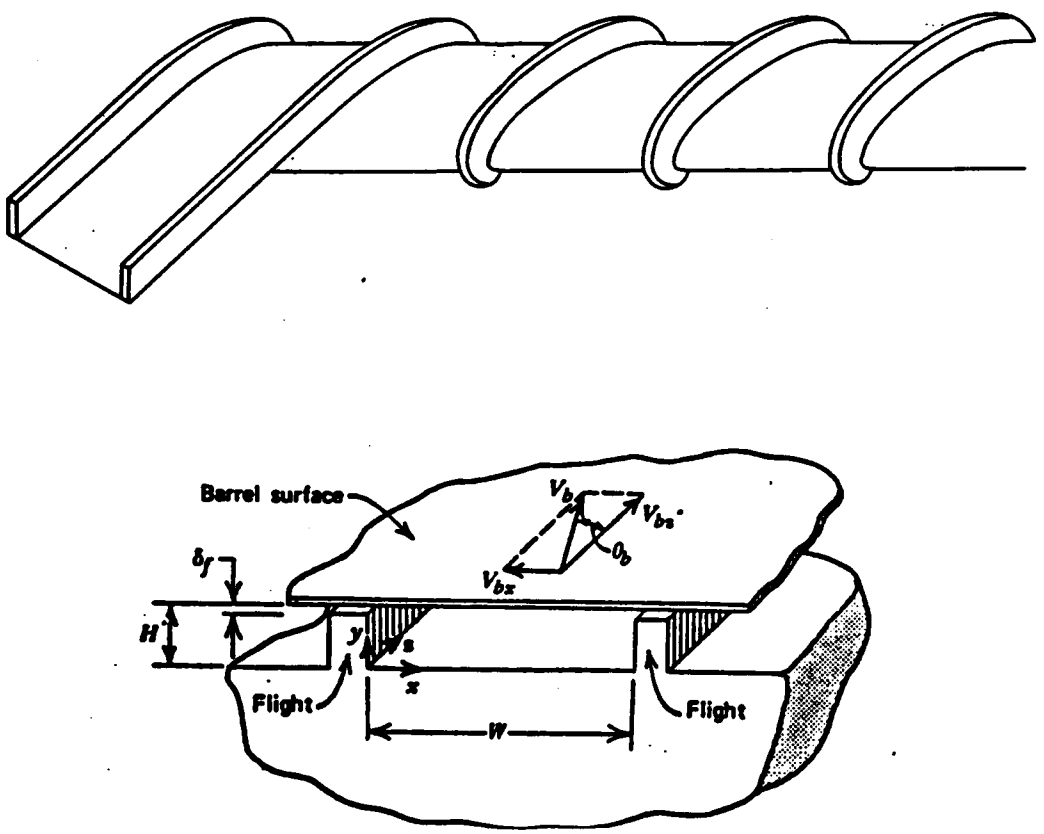

Figure 24. Schematic demonstrating the extruder channel peeled off of the screw.

88°C. Flow rate and temperature were reported as a function of screw speed, compression ratio, and moisture content. These values were compared to the predictions of the model based on the Newtonian analysis of a metering section of the screw. Flow rate increased linearly with screw speed which indicated that drag flow was dominant. In addition, flow rate increased with channel depth which was what the model predicted if drag flow dominated. Their results showed that theory underpredicted volumetric flow by 9 to 13% for shallow screws whereas for deep flighted screws theory overpredicted flow by up to 21%. These deviations from theory are attributed to the non-Newtonian behavior of the doughs altering the velocity profile in the screw. However, torque measurements disagreed totally with model predictions, decreasing with increasing channel depth. They attribute this phenomenon to the non-Newtonian behavior of the fluid. In addition, some other questionnable results were found in their study. Flow rate as a function of screw speed should alter with changing die geometry as the die geometry controls the contribution of the pressure flow term. However, flow rate was found to be directly proportional to screw speed even when the die geometry was changed.

Mustakas et al. [19] studied the preparation of full-fat soy flour from soybean by an extrusion method. Their objective was to develop a system for cooking the soybeans to achieve a full-fat soybean flour with high nutritional value, sufficient palatability, high storage stability and inactivated growth inhibitors. They performed a series of twenty four extrusion cooking experiments under various combinations of time, temperature, and moisture content to determine optimum cooking conditions in the preparation of a high-quality soy flour. Through their studies,

they found that they could produce a full fat soybean flour of good flavor, nutritive value, and oxidative stability through an extrusion cooking process. Retention time, temperature, and moisture all proved to be important factors correlating to the quality of the product produced. The range of operating conditions which satisfy all requirements was found to be small.

The studies of Mustakas et al. were restricted purely to the equipment at hand with no suggestions as to the influence of parameters other than moisture, time, and temperature could play in the process. No extrusion model was developed by Mustakas et al. based on their work.

However, Fricke et al. [22] decided to employ the findings of Mustakas et al. and determine if such an extrusion system could be modeled. Fricke et al. studied the extrusion of soy flour and attempted to model this operation using a theoretical treatment derived for plasticating extruders. They used a simplistic model of treating the flour as a Newtonian fluid and neglecting any transitions which take place during extrusion. This treatment allowed the food extruder to be treated as the melt conveying zone of a plasticating extruder. Using Tadmor and Klein's [29] development for shallow prismatic channels operating at steady state with fully developed laminar flow of an incompressible Newtonian fluid, they developed relationships for volumetric flowrate, overall change in temperature due to both viscous dissipation and transferred heat, and mechanical energy required by the extruder. Simultaneous solution of these three relationships given certain extruder and material properties resulted in pressure and temperature profiles along the extruder as well as power requirements. They accomplished the solution by a program which

integrated the equations in increments along the length of the screw. They compared their results with the experimental work of Mustakas et al. [19]. The correlation was only fair at best with some large discrepancies. They purported that these differences arise either because of inaccuracies in estimating viscosities and densities or because of surging in some of the extrusion tests. They specifically point out the problem of using a simple viscosity model for the soy which is most likely going through at least one phase change which would drastically affect viscosity and density parameters.

Tsao et al. [24] also looked at Tadmor and Klein's [29] model of the metering section in comparison with actual results of a food extrusion process. They focused on the effects of screw geometry on extruder operational characteristics rather than feed parameters. They conducted a series of studies on fourteen specially designed extruder screws with varying flight depths, pitches, compression ratios, and lengths of metering section by using a single screw extruder with a high moisture feed product. The extruder was operated with varying screw rotation speeds and barrel temperatures. The deviations in their results from the theoretical predictions were thought to be due to the non-Newtonian character of the food product and possible slippage occurring at the extruder barrel and screw surfaces. They concluded that food extrusion was significantly affected by extruder screw geometry and operating conditions. Although the experimental results did not correlate well with the theoretical predictions, they proposed that Tadmor and Klein's model does describe the relationship between important geometrical and processing variables

with the differences in results lying in the non-Newtonian behavior of the food material and the slippage at the walls of the extruder.

Harmann and Harper [15] also tested equations derived for the metering zone of a plastics extruder [29]. They examined the flowrate and torque equations for their applicability to the metering zone of a foods extruder. The theoretical predictions were compared to the actual experimental results from two extruders of different diameter, each having a series of screws of different geometries. They found that for screws with a taper, the equations underpredicted the actual flowrate but for straight screws, the equations overpredicted the flowrate. These deviations were attributed to non-Newtonian effects. Their results agree with the predictions of non-Newtonian flow in single scre extrusion of Tadmor and Klein [29]. Tadmor and Klein stated that underprediction would occur with a negative pressure gradient and overprediction would occur with a positive pressure gradient. Harmann and Harper found that the tapered screws exhibited a negative pressure gradient and the straight screws exhibited a positive gradient. Other possible error was introduced in the geometrical constants which were measured from the screws, in some cases averaged, and used in the equations. Harmann and Harper found that the torque equations best modeled the straight screws with torque estimations using screws with an overall taper having the worst correlations to experimental results. Again they suggested that error was due to the non-Newtonian behavior of the fluid. They concluded however that their results support the validity of using a power law model, for cereal dough viscosity. They also concluded that the equations were sufficiently accurate for engineering design. This conclusion is of question due to the

large deviations in the predictions from their experimental results. Although non-Newtonian fluid behavior may be one of the explanations for the deviations, using it as the sole explanation of the deviations does not justify the validity of the model.

Thompson and Rosenau [37] took a different approach to the modeling of the food extrusion process. They instrumented a laboratory scale extruder to aid in the development and verification of extrusion models. Pressure and temperature transducers were installed at -45° and $+45^{\circ}$ from the vertical of six sections of the barrel. Additional temperature transducers were located near the inlet of the die and in a seventh barrel section. Screw speed and torque were also monitored. Thompson and Rosenau discussed in great detail the justification for their design of instrumentation and the accuracy they could obtain. Data collection and analysis was also discussed in detail. However, no actual data collected from this equipment was reported nor any correlation between theoretical predictions and their results was made. In addition, their experiments simply monitored the processing conditions. No model which in any way could predict cooking extrusion was offered. Hence, the system was basically an in-depth data collection system and the use of the term model of the extrusion process is false.

The research presented so far has either been concerned with a model of the extrusion process, in many cases examining specific contributory factors to the overall performance, or a detailed data collection system. Ideally, a combination of the two would provide the best information. However, the texturization of the final product is the goal of the food extrusion process. Hence the parameters controlling texturization are

instrumental for the modeling of a system to predict a satisfactory food product. A cooking extrusion model cannot simply predict temperature, pressure, and power to be adequate. The model must also include the conditions for texturization. A few studies have been performed which describe how the texture of extruded soy protein can be manipulated by control of process conditions and feed material composition. Thus it should be feasible to produce extruded materials with specific textural characteristics by regulating appropriate processing and compositional variables.

Aguilera et al. [28] studied the extrusion of soybean grits in an interesting way. They monitored the changes occurring in the ultrastructure of soybean grits during extrusion using scanning electron microscopy. The extruder product was obtained using a Wenger X-5 laboratory extruder under one set of conditions consisting of 25% moisture content, 800 rpm and 145°C barrel temperature. When steady state was reached, the extruder barrel was disassembled and samples taken from preselected areas along the length of the screw. Mixing predominates first until cooking temperatures were reached in the last turns of the screw. In this zone, they observed that the cells were completely disrupted and were rearranged into strands that orient into thin fibrils at the die. They suggest that the pressure release at the exit causes radial flow in the extrudate forming new, more extended surfaces. Hence, they concluded only the combined effects of shear, heat, and pressure release was shown to be responsible for texturization.

Cumming et al. [75] employed the extrusion process to a 30% added moisture defatted soybean meal to produce an experimentally texturized

soybean protein product. Extent of texturization and other physical properties such as density and water regain were examined in relation to process temperature. They found that product density decreased with increasing processing temperature. Although density changed quite markedly over the range of temperature used, product diameter remained constant. Cumming et al. stated that this phenomenon suggests that all physical changes occurred prior to final extrusion. Product rehydration showed the opposite trend with regards to process temperature. They purported the increase in water uptake with increasing temperature is largely a result of changes in density. Finally, microscopic examination of the product demonstrate major structural change. At 123°C they found the product to be cellular in appearance with some general indication of orientation whereas at 148°C, a highly oriented fiber system had developed. As temperature increased, orientation and degree of fiber formation increased. Cumming et al. described fiber formation phenomenon as the protein bodies during processing were reformed into continuous fiber-like structures. Many fissures and holes were observed and were explained as possibly the abrupt release of pressure which occurs during and just prior to extrusion.

Maurice et al. [74] performed similar studies on a 24% moisture soybean meal. Mechanical and sensory panel testing as well as SEM analysis were used to evaluate product texture as a function of temperature. Their findings corresponded to those of Cumming et al. [75]. At the lowest temperature, 130°C, the sample was dense and compacted in nature and the amorphous character of the soy was in evidence. At 165°C some partial alignment was observed and a few fibers were seen. However, the

density of the material was still quite high. By 180°C definite fibration and orientation of these fibers was attained. It is the oriented fiber structure thought to be responsible for texture. The oriented fiber structure was less dense giving rise to a spongy texture.

Maurice et al. [73] in further studies looked at the effect of not only temperature but also composition and screw speed upon texturization. They found that protein level was the factor most responsible for texturization with temperature being the next most important factor. Temperature becomes more critical with shorter residence times. They attribute this depence upon residence time to more efficient heat transfer to the material through better mixing. Feed moisture at a constant protein level was found to have very little influence. Hence, from these studies it is seen that protein level and process temperature are the most important parameters to control for the production of a texturized product.

So far, the extrusion models used in food processing have been the only ones discussed. Many models of the extrusion process used in other industries have been proposed. For a more complete discussion of extrusion models, one is referred to a review by Fenner [105] or to Tadmor and Klein [29] which in addition to melt flow in extruders, also covers the analysis of solids conveying and melting zones. Although these models have been developed for the single screw extrusion process for polymers, they are used for the basis of many other models developed including those used in the food industry. Hence, their development is of interest in all fields. In his review, detailed consideration is given to the many published theoretical models of the various zones. The development of these

models is traced in terms of the gradual relaxation of simplifying assumptions to provide methods of analysis which give realistic predictions of machine performance. He also compares the results of some of the analyses to observed machine behavior.

Some of the extrusion models postulated for food extrusion have now been presented. Included were models derived from the equations of mass, motion, and energy to those which simply described the dependence of extrudate properties upon extrusion conditions. The next section of the literature review will deal with the numerical modeling of extrusion.

2.9 NUMERICAL MODELING

To date, no attempt has been recorded to numerically model a food extrusion process. Some simplified calculations employing a computer to solve the equations

have been documented; however, these were not true numerical models of the system. A discussion of the finite element method, the numerical technique used in this dissertation, will be presented in Chapter Four. Now, however, a short discussion of the numerical work performed on extruders used in the polymer industry will be presented. In most cases, some if not all of the models developed can apply with some modification to food extrusion.

In an early work, Griffith [106] looked at the fully developed compressible fluid in a metering screw. The differential equations for the thermally and hydrodynamically fully developed flow for a power law fluid were presented in dimensionless form. By specifying the helix angle, the power law exponent, heat generation parameter, and the pressure gra-

dient in the downstream direction, and estimating cross channel pressure gradient and temperature, approximate velocities were obtained by Runge-Kutta integrations of the momentum equations. Approximate temperatures were then obtained by Runge-Kutta integrations of the energy equation using the derived velocities. The new approximation to temperature was then used in the momentum equation to obtain a second approximation and so on. Depending on the accuracy of the initial guesses, Griffith stated calculation required three trials taking about 2 to 3 hours on a Burroughs 205 computer. Good agreement was found between the numerical and experimental results in most cases. However, not only were the numerical calculations lengthy and entailed but these calculations were made with many simplifying assumptions which were not all applicable. For example, Griffith assumed that the flow was so rapid that temperature was essentially constant on a streamline. Since the screw and barrel surfaces constitute sections of a single streamline, Griffith supposed that jacketing one or both walls would produce the same results. However, the different results achieved experimentally without core cooling indicated the theory to be defective.

Agur and Vlachopoulas [107] developed one of the few fully predictive steady-state computer models for a single screw plasticating extruder. Their model combined variations of established models for the different regions or zones of flow. These included a model for solids flow in the feed hopper, a variation of the Darnell and Mol model [77] for the solids conveying zone, and a variation of Tadmor's [29] melting model for the melting zone. An implicit finite difference solution of the mass, momentum, and energy conservation equtions for the melt conveying zone of the

extruder and die was used along with a predictive correlation for extrudate swell. A temperature and shear rate dependent viscosity equation, obtained by linear regression analysis applied to Instron capillary data, was used to describe the melt-flow behavior in the model. Basically, specification of the material and rheological properties of the polymer, the screw geometry and dimension, and the extruder operating conditions yielded prediction of flow rate of the polymer, pressure and temperature profiles along the extruder screw channel and in the die, and extrudate swell at the die exit. To solve the model, a pressure was calculated at the base of the feed hopper. Then, a mass flow rate was assumed for the solids conveying zone and maintained through the length of the extruder. If computed exit pressure was greater than zero, a new mass flow rate was assumed and calculation repeated. Their predicted results agreed well with experimentally measured values. However, many simplifying assumptions were made in the various models employed. Also, no mention was made as to how the various models were connected. Some of the models are for fully developed flow and do not take into account any entry flow. Their handling of the transition from section to section needs to be clarified to determine the true applicability of the model.

Zavadsky and Karnis [108] also developed a fully predictive mathematical model for a plasticating extruder. Similar to Agur and Vlachopoulas [107], the formulation of the mathematical model subdivided the extruder into zones such that each zone contained a characteristic physical process. Zavadsky and Karnis' mathematical model consisted of five zones; the zone under the hopper, the solids conveying zone, modeled by a variation of Tadmor and Broyer's theory [109], the delay zone, mod-

eled by the theory of Kaeir and Tadmor [110], the melting zone, employing the model given by Tadmor et. al. [111], and the melt conveying zone, modeled by a combination of models [112, 113, 114]. They neglected the breaker plate and die assembly and the extrudate swell zones included in Agur and Vlachopoulas' model. Although the two predictive models are alike in their approach, they differ in the handling of the calculations for each zone. Specifically, they differ in the adopted models used for each zone and hence, the simplifying assumptions for each case. For example, Agur and Vlachopoulas used a one-dimensional isothermal, isotropic model for their simulation of the solids conveying zone whereas Zavadsky and Karnis used a two-dimensional, non-isothermal, non-isotropic plug flow model.

A fortran computer program was constructed from Zavadsky and Karnis' mathematical model. This program enabled many different computation to be carried out. For example, it computed the design of an extruder for a given output with particular melt parameters at the outlet; the design of a new screw for an existing extruder to maximize output at given conditions; the output for given processing condition and extruder; and the axial pressure and temperature profiles, average residence time, and power consumption for given output, extruder, and processing conditions. The performance of the computer program had some problems. The temperature profile was not smooth in transition from zone to zone. This was attributed to the isothermal assumptions used in the zone under the hopper and the melting zone. Also, although a power law viscosity model was used, the power law parameters were constants which caused significant error in the axial pressure profile. Even with these problems, the authors re-

ported only 5% error in temperature and mass and 30% error in pressure when compared to polypropylene experiments.

To date, Viriyayuthakorn and Kassahun [121] have been the only ones to report a three dimensional finite element model for plasticating screw design. Their model included not only the melt conveying zone but also the phase change. The phase change was accounted for in the functional dependence of the specific heat capacity on temperature, thereby eliminating the need for any restrictive melt mechanism. A temperature dependent Newtonian viscosity was used in the calculations. The idealized geometry of the screw channel unwound from the screw such that the screw was kept stationary while the barrel surface was rotated was employed. Although they discussed the melting mechanism with the solid pelletized plastic moving slowly down the channel, melting and forming the pool of melt, no mention of the model for the solids conveying was made. They reported that predictions of the model for the phase change zone and the sectional temperature distributions, as well as temperature in the down channel and cross channel, agreed with the cooling experiments reported in literature. However, at no point do they report any values of the variables, boundary conditions, or computer methodology used in their calculations.

2.10 RESEARCH OBJECTIVES

A detailed discussion of all aspects pertaining to the modeling of a food extrusion process has now been presented. One can see that there are many facets and difficulties in modeling a food extruder. The goal of the dissertation is to determine if a three dimensional finite element method

can be used to numerically simulate cooking extrusion. This numerical simulation will consider the non— Newtonian, non-isothermal, reactive conditions found in a food extruder.

However, as there is very little information regarding any of the food systems used in extrusion from which the necessary material parameters may be obtained, a material of study must first be chosen. This is, in essence, the starting point of the research. A 50% added moisture defatted soy flour dough is chosen for the material of study. The material properties needed for the model are determined for this material. Although this narrows the scope of the research as the results are for one particular material, the methods used in determining the material properties will be of sufficient generality so as to be applied to other materials.

The material parameters of interest in modeling the extrusion process are viscosity, thermal conductivity, heat capacity, and heat of reaction. A section discussing each of these parameters has been included in the literature review.

To begin, the viscosity of the 50% moisture soy dough is found over a large range of shear rates similar to those experienced in the extruder. The viscosity is determined not only as a function of shear rate, but also as a function of temperature and thermal and shear history. In addition, the effect of moisture content is examined. A viscosity model which fits the data is then found. One can see that this procedure has been performed for other food materials. However, most of the studies have not been as extensive or have had some downfall. In some cases, the range of experimental conditions were very narrow, or one range of conditions was extrapolated to apply over the range found in the extruder. In other

studies, models which were found to fit the data were in fact simply a regression fit to the data with no theoretical background.

The next material parameter needed is the thermal conductivity. One can see from the literature that this parameter, in effect, has not been studied for the food preparations used in extrusion. The method developed by Dickerson[102] is employed for the determination of thermal diffusivity and thermal conductivity as a function of temperature. Again, in addition, the effect of moisture content upon these properties is investigated.

Heat capacity is the third material parameter mentioned that is needed for the modeling of the extrusion process. Again, one sees that information concerning the heat capacity of food materials is severly lacking. However, in this case there are developed techniques, specifically differential scanning calorimetry, which allows an accurate determination of this parameter. Hence, the determination of the 50% soy dough heat capacity is perforemd using DSC with certain modifications which will be discussed in the experimental section. The heat capacity is determined as a function of temperature and thermal and shear history. In addition, the effect of moisture content is found.

The final material parameter needed for modeling of the extrusion process is the heat of reaction. Heat of reaction is also determined using differential scanning calorimetry. Although many researchers have postulated the occurrence of a reaction in the formation of the textured structure for soy flour doughs, no detailed mechanism has been has been offered. The most specific mechanism postulated is the formation of disulfide bonds but no mention of the extent of the formation of these

bonds is made. In addition, most work has been performed on isolated proteins in very dilute solutions and are not representative of the true system. On the other hand, there are those researchers that believe that there is no true covalent bonding reaction occurring during texturization. Hence, not only is the heat of reaction required, but the presence, nature, and conditions under which a reaction may occur must be known.

Once the material parameters are found, they must then be incorporated into the finite element model of the extruder and die assembly. One has seen from the review of the literature that initial attempts at modeling a food extruder have met with only limited success. In nearly all cases the lack of agreement was attributed to non-Newtonian behavior of the food doughs. The three dimensional finite element model employed corrects for this shortcoming in the other models. Certain simplifying assumptions are still used for the model. The finite element method is used in modeling for its versatility and ease of handling the complexities associated with the extrusion process. A description of this method is presented in a later chapter.

Finally, extruder runs recording flow rate and pressure profiles data are made on a laboratory scale extruder. The data from these runs are compared to the results of the numerical model to determine the validity of the model.

The purpose of this chapter has been to introduce and review the research concerning cooking extrusion and soy flour dough, the material used in this dissertation, and to outline the basic research objectives of this work. In the following chapter, a detailed outline of the experimental

procedures which will be used in fulfilling the proposed objectives will be presented. Chapter Four will discuss the finite element method used in the numerical modeling of the extrusion process.

3.0 CHAPTER THREE: EXPERIMENTAL APPARATUS AND PROCEDURE

In the previous chapter the literature was reviewed and the research objectives associated with the modeling of food extrusion were proposed. In this chapter a detailed outline of the experimental methods used to fulfill those objectives is given. A description of the materials, apparatus, and range of investigation is included.

3.1 MATERIALS

A defatted soy flour, Soyafluff 200W (Central Soya, Fort Wayne, Indiana) was used. As discussed in the research objectives, a 50% added moisture soy dough was chosen as the major soy dough composition of study. In addition, studies were performed on samples from 0% added moisture soy flour to 70% added moisture soy dispersions in order to determine the effect of moisture on the material properties. However, the defatted soy flour from the distributor has an inherent moisture content of 5 to 8 % based on samples dried in a vacuum oven. Hence, the true moisture of a 50% added moisture sample is approximately 53%. All moisture content is reported based on added moisture on a weight basis. In all cases deionized distilled water was used in the preparation of the sample.

The preparation of the soy flour dough was complicated by two phenomenon inherent to the flour. Soy doughs are a natural food system lacking the preservatives necessary to prevent the growth of mold. Although the functional length of time for a sample can be extended as is described in the section on preparation of samples, there is a definite limit to its usability. Additionally soy flour aggregates upon exposure

to water. Hence, a careful method of preparation must be employed to obtain a homogenous sample.

3.1.1 SAMPLE PREPARATION

Samples were prepared using a KitchenAid mixer (model K5SS) with the dough hook attachment. The defatted soy flour and the deionized distilled water were weighed into separate containers. Batches of approximately 400 to 600 grams of each material were used to make a sample of total weight of 800 to 1200 grams. These size batches of sample were determined to provide the optimum mixing for the mixer assembly used. Sample batches of smaller size did not adequately contact the mixer hook and sample batches of larger size did not provide enough room for movement of the sample for mixing to occur. The soy flour was placed in the mixing bowl and a well formed in the center. The water was then poured into the well and the mixer started on its lowest speed. The sample was allowed to mix for 5 minutes. This amount of time permitted adequate mixing with minimum working of the dough as determined by observation. If the sample was not allowed to mix for sufficient time, the dough was not uniform in texture or appearance. If mixing occurred at higher speeds or for longer lengths of time, the sample temperature rose. The batch of dough was then sealed in plastic and refrigerated overnight to establish equilibrium moisture dispersion. The samples were used within the next 36 hours. Any portion of the sample batch not used in experimentation was kept refrigerated until use or until the time limit for use had expired.

3.2 APPARATUS

Four major apparatus were used in experimentation. These were a Rheometrics Mechanical Spectrometer (RMS), an Instron Capillary Rheometer (ICR), a Perkin-Elmer DSC-2 differential scanning calorimeter, and a Killion laboratory scale extruder. In addition, a thermal conductivity/diffusivity device was constructed. A brief description of each apparatus, pertinent operating information, and range of experimental analysis are included in this section.

3.2.1 RHEOLOGICAL MEASUREMENTS

The rheological properties of the soy samples were measured using a Rheometrics Mechanical Spectrometer (model RMS 605). The top plate of the rheometer was connected to a motor which rotated the plate in either a clockwise or counterwise direction which enabled the study of the steady shear viscosity. The motor was also used to oscillate the top plate at varying frequencies to generate the dynamic property data for the sample. The bottom plate was connected to a series of transducers which measure torque and normal forces. With a sample in the gap, rotation caused a torque to be transmitted through the fluid to the bottom plate. Knowledge of the experimental parameters of rotational speed of the top plate, the plate diameter, and the gap between the two plates allowed calculation of the apparent shear rate. The shear rate in combination with the recorded torque measurement gave the viscosity of the sample.

In these experiments two stainless steel plates of 2.5 cm diameter were used. A baffel attachment was fitted around the lower plate. The

gap, the distance between the plates, was set at 2.0 mm for all measurements. The shear rate range of investigation was between .01 and 1.0 s^{-1}. Above this shear rate the sample would become discontinuous and in some instances, come out of the gap.

3.2.1.1 SAMPLE LOADING

For these experiments, only moisture content doughs of 50% or greater could be handled. The solids content of doughs less than 50% was too high to flow in this geometry. Samples under 50% moisture simply cracked. Even the 50% moisture dough presented difficulties. To load a 50% moisture dough sample, it was first pressed into a disc slightly thicker than the gap width designated for the plate/plate geometry. The disc of sample was then placed in the gap and the top plate lowered until the gap was set correctly. The disc of sample could not be much greater than the gap of the plates or lowering the top plate to set the gap would impose large residual normal force. This normal force did not relax nor show any indication of relaxing in the hour which it was monitored. The 60% moisture dough, which in actuality was more the consistency of a paste, was much easier to load. No preshaping was necessary and a normal loading procedure was followed.

3.2.1.2 MODIFICATIONS

As mentioned, a baffel was used around the botton plate during the experiments performed. Normally, a baffel is used to allow flooding of the sample during measurement. However, in these experiments, the baffel served a different purpose. A swatch of fabric was saturated with

deionized distilled water and placed in the baffel around the sample. This procedure was performed to minimize the drying of the free edge of the sample during testing at elevated temperatures. Prior to the actual experiment, tests were run to determine the amount of time it took to dry the fabric at the experimental temperature. Then, during the actual experiment, the oven was opened and the fabric rewetted before the calculated time of drying. This operation continued until the end of the experiments. This operation must be done very quickly before a large temperature drop occurred.

3.2.1.3 CALCULATIONS

The torque and normal forces measured by the transducers attached to the bottom plate were fed to a central processing unit designated the CPU. First, the analog signals were filtered to eliminate any errors which might enter into the calculations due to noise. The analog signals were then converted into digital signals which the computer in the CPU used to calculate the viscosity in the steady shear expeiments. In the dynamic experiments, the same torque and normal force signals were used to calculate the dynamic mechanical properties. The major equations used by the CPU in calculation of these properties are described in detail elsewhere[119,120].

3.2.2 CAPILLARY RHEOMETRY

Although viscosity results were obtained by means of the Rheometrics Mechanical Spectrometer, the viscosity values were obtained at low shear rates only. Experiments were performed on an Instron capillary rheometer

(model 3211) in order to obtain high shear rate viscosity data. Experimental results gave viscosity values for the shear rate range of 1 to 1000 s^{-1}.

The capillary rheometer works on the principle of forcing a known quantity of fluid through a capillary of known geometry. The sample was placed in the reservoir and brought to operating temperature. A stainless steel plunger was used to drive the sample down the reservoir and subsequently through the capillary. The plunger was driven by a constant speed drive system, the speeds of which were controlled through the use of a set of drive gears. The plunger moving down the reservoir at constant speed resulted in a constant flowrate. The average velocity of the sample depended upon the capillary diameter and drive speed. Two sets of capillaries were used in the measurements: one set with 0.1" diameter and the other with 0.052" diameter. The length to diameter (L/D) ratios for the 0.1" diameter set were 15, 20, and 30, whereas the L/D ratios for the 0.052" diameter set were 31.35, 46.41, and 58.38. The resisting force on the plunger was measured by a load cell which is capable of measuring forces up to 2000 kg. A minimum of five separate experiments were performed to accurately determine the response of the material. New samples of the same batch of dough were loaded and tested as well as samples from different dough batches.

3.2.2.1 SAMPLE LOADING

A special method of loading the sample into the reservoir was devised due to the sample's doughy consistency. A cylinder was constructed with a plunger at the top and a hole the size of the opening of the reservoir

in the base. The sample was loaded into the cylinder, the hole in the base aligned with the entrance to the reservoir, and the plunger assembly attached to the drive system in the same manner as the plunger fitting the reservoir. The sample was then pushed through the hole into the reservoir using the slowest speed of the 1:1 gear ratio, 0.06 cm/min. Employing this method for sample loading ensured a sample free from entrapped air pockets.

3.2.2.2 MODIFICATIONS

In order to measure viscosity at temperatures above 100°C without vaporization of water, the capillary rheometer was pressurized above the vapor pressure of water at elevated temperature. As the highest temperature investigated was 150°C, the applied pressure was set at 80 psi, a little over the pressure of saturated water at that temperature. A vessel to fit around the capillary and receive extrudate which could be pressurized was manufactured. A schematic of the pressurized system is shown in Figure 25. Nitrogen was used to pressurize the system. Care was taken to make sure the plunger was sufficiently in the reservoir to form a seal so that the whole system was sealed before pressure was applied. An applied pressure of 80 psi was used for all measurements, even those below 100°C for consistency. In support of this procedure, experiments at temperatures below 100°C were also performed without an applied pressure and found to agree with those under pressure.

The addition of the applied pressure changed the force needed to extrude the sample through the capillary. This change in force was measured by pressurizing the sytem in the middle of the experimental run.

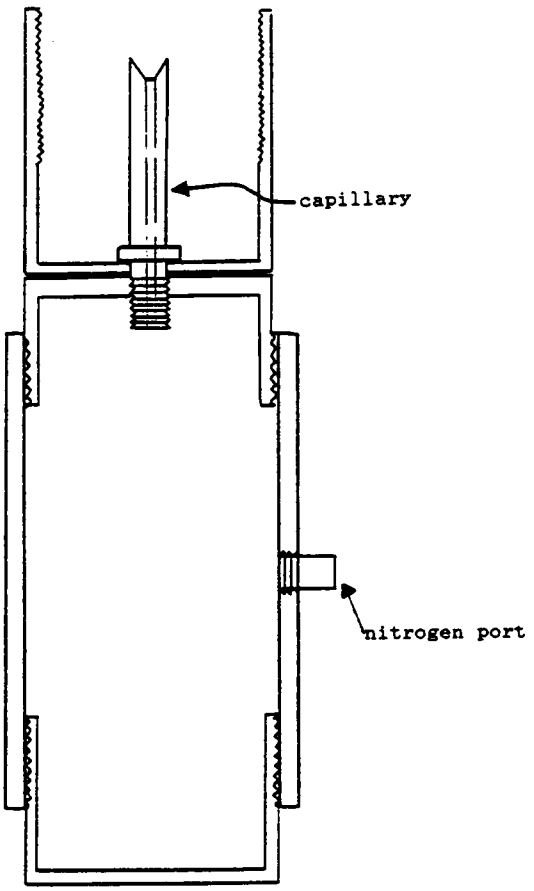

Figure 25. Pressure capsule modification for the Instron Capillary Rheometer.

While a steady state force was being recorded, the system was suddenly pressurized. An additional force reading of 3.84 kg was recorded. This same additional force reading was measured at a variety of temperature and speed combinations. Hence this additional force was subtracted from all recorded values of force before viscosity calculations were made.

During the capillary rheometry experiments, the extrudate is collected in the pressure capsule. For the experiments which employ the extrudate of the capillary rheometer as the test sample, the following procedure is used. At the conclusion of the capillary rheometer experiment, the pressure capsule was dismantled from the capillary rheometer. The capsule was then opened and sufficient sample for the subsequent test to be performed was collected and stored in a sealed container under refrigeration until needed.

During the capillary rheometry experiments, the extrudate is collected in the pressure capsule. For the experiments which employ the extrudate of the capillary rheometer as the test sample, the following procedure is used. At the conclusion of the capillary rheometer experiment, the pressure capsule was dismantled from the capillary rheometer. The capsule was then opened and sufficient sample for the subsequent test to be performed was collected and stored in a sealed container under refrigeration until needed.

3.2.2.3 CALCULATIONS

For a given die geometry, two parameters were recorded; the speed of the plunger and the steady state force. For the most part, the recorded force produced a smooth reading. In those cases where irregularities

occurred, an average force reading was used. These measurements were used to evaluate the shear stress at the wall. The relationship used was:

$$\tau w = \Delta P/(4 * (L/D)) \qquad 3.1$$

where: ΔP - pressure drop across capillary
D - capillary diameter
L - capillary length

The pressure drop was calculated by:

$$\Delta P = F / Ap \qquad 3.2$$

where: F - force measured by load cell
Ap - cross sectional area of the reservoir

The pressure drop evaluated from the force measured by the transducer must be corrected for the entrance pressure losses. The correction for the entrance pressure loss was calculated using the well known Bagley plot [38]. In essence, the plot presents pressure as a function of L/D at constant shear rate. Extrapolation to a zero L/D yielded the pressure loss in the entrance region. Hence the true shear stress was given by:

$$\tau w = (\Delta P - \Delta Pent) / (4 * (L/D)) \qquad 3.3$$

The apparent shear rate which the shear rate for a Newtonian fluid , was defined as:

$$\Gamma = (4 * Q) / (\pi * R^3) \qquad 3.4$$

where: R - capillary radius
Q - flowrate = speed of plunger * Ap

Again a correction was employed to account for the non-Newtonian behavior of the sample. The Rabinowitsch correction [122] for shear rate was applied in the following manner:

$$\gamma w = \frac{4\,Q}{\pi\,R^3}\left(\frac{3n + 1}{4n}\right) \qquad 3.5$$

where: $n = \delta \ln \tau w / \delta \ln \Gamma$

The viscosity was determined by the ratio of the wall shear stress to the corrected wall shear rate:

$$\eta = \tau w \; / \; \dot{\gamma} w \qquad 3.6$$

3.2.3 THERMAL CONDUCTIVITY/DIFFUSIVITY

The apparatus as described by Dickerson [83] was built as close to his description for the determination of the thermal conductivity and thermal diffusivity. The general apparatus is shown in Figure 26. It consisted of a brass cylinder immersed in a four gallon oil bath. The oil was heated by a coiled wire supplied with a voltage controlled by a Variac votage regulator. The oil bath was mixed by a Lightnin stirrer in order to ensure a consistent temperature throughout the bath.

The conductivity tube constructed was a nine inch long, 2.125 inch ID brass tube, sealed at the ends by Teflon caps. In the center of the top end cap a hole was made and fitted with a pressure seal. A shielded type J thermocouple was placed through the seal, measuring the temperature along the axis of the tube. A second shielded type T thermocouple was welded to the outer wall of the tube in such a way the its tip was at the same height of the inner thermocouple. A resistance wire was passed down parallel and as close to the axis of the cylinder. A current provided by a Tyco Pro electrical racing system transformer was passed through the wire. Assuming all energy produced by the wire was absorbed by the surrounding sample, the temperature increase measured by the thermocouple inside the tube was used to calculate the thermal conductivity. The thermocouple on the outside was used to monitor the temperature at which

the measurement was taken. Conductivity was measured at ambient temperature for 0, 25, and 50 % moisture samples.

The modifications for the thermal diffusivity measurements were slight. The resistance wire was removed. The Teflon caps of diffusivity 0.0625 cm^2/min, which approximate that of the dough studied, maintained the assumption of the infinite cylinder approach of negligible temperature gradient in the axial direction. The temperatures measured at both the inside and outside thermocouples were monitored. Finally, unlike the conductivity measurements which were made at constant temperature, the oil bath was heated at a constant rate to satisfy the transient relationship upon which the calculations were based. Thermal diffusivity was measured over the range of 25 to 150°C.

3.2.3.1 SAMPLE LOADING

Three moisture content samples were used in experimentation: 0, 25, and 50% moisture. The 0% moisture sample gave no problem in filling the conductivity tube. However, the 25 and 50% moisture samples did have difficulties. The 25% moisture samples was crumbly in consistency, hence although it would pour into the tube, much entrapped air was present without compaction. The 50% moisture sample was a dough which had to be packed into the tube. Air pockets were also a problem as good compaction could not always be achieved. Density measurements were taken for each experiment to ensure consistent packing of the samples.

3.2.3.2 CALCULATIONS

As stated, the thermal conductivity was calculated by monitoring the

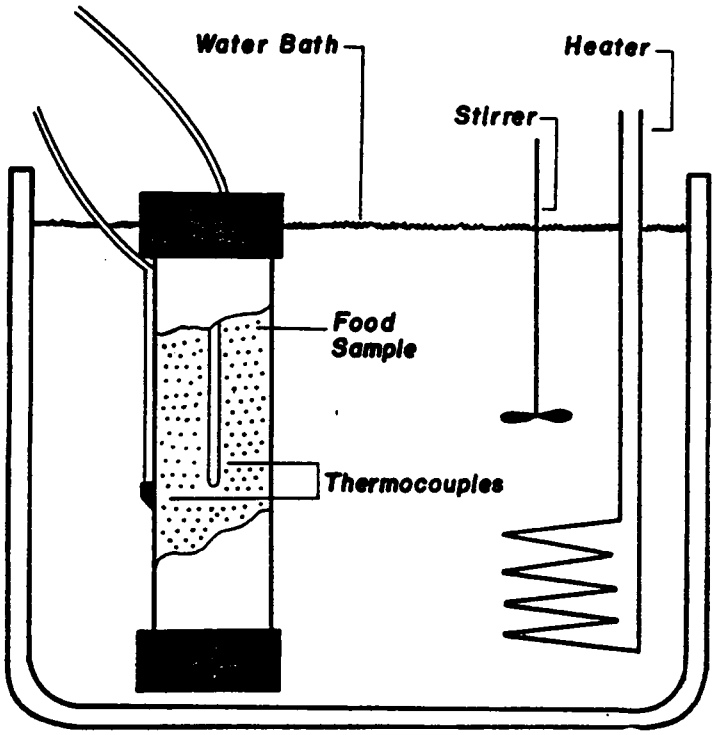

Figure 26. Thermal diffusivity/conductivity apparatus.

temperature increase in the sample as current was passed through the resistance wire. Thermal conducitivity, k, was determined from the following relationship:

$$k = \frac{3.413\ I^2\ Z\ \ln(\tau 2\ /\tau 1)}{4\ \pi\ (T2 - T1)} \qquad 3.7$$

where: I - current
Z - resistance
τ - time
T - temperature

The thermal diffusivity was determined by monitoring the temperature difference as recorded by the thermocouples positioned at the wall and center of the sample. Using these measurements, the thermal diffusivity, α, was calculated by the following equation:

$$\alpha = A * R^2 / (\ 4* (Tr - To)) \qquad 3.8$$

where: A - heating rate
R - cylinder radius
Tr - wall temperature
To - axial temperature

Then, from the calculated thermal diffusivity, the thermal conductivity was determined by the following relationship:

$$K = \alpha * \rho * Cp \qquad 3.9$$

where: ρ - density
Cp - specific heat

In determining both thermal conductivity and thermal diffusivity an initial transient period in the measurements was recorded. Dickerson [83] gave relationships to calculate the length of time of this transient period. His procedure was followed to calculate the transient period for each experimental measurement.

3.2.4 DIFFERENTIAL SCANNING CALORIMETRY

The operating principle of DSC is based on two fundamental facts. First, when a system or material undergoes a change of state, there is an adsorption or liberation of heat. Second, this change can often be initiated by the application of heat itself. An example of this type of change of state would be a melting process where raising the temperature induces melting. In this technique, a sample and an inert reference material are maintained at the same temperature while the temperature of both is gradually raised. In most cases, the experiment is performed using a programmed linear rate of rise in temperature. Any thermally induced changes occurring in the sample are then recorded as a differential heat flow. These are normally displayed as a peak on a thermogram. An example thermogram can be seen in Figure 27 demonstrating these transitions. Integration of this heat flow with respect to temperature or time yields a value for the enthalpy change associated with the process. This technique also affords a means of measuring heat capacity, reaction kinetics, and transition temperature for a given material.

Experiments were performed to determine both the heat capcity and the heat of reaction for the soy samples. The heat capacity was determined over the range of temperature for 20° C to 170° C which encompasses the range of processing temperatures. The heat of reaction was also determined over this temperature range. Additional experiments were performed which looked at the behavior of the soy samples at a constant temperature, or isotherm, as a function of time.

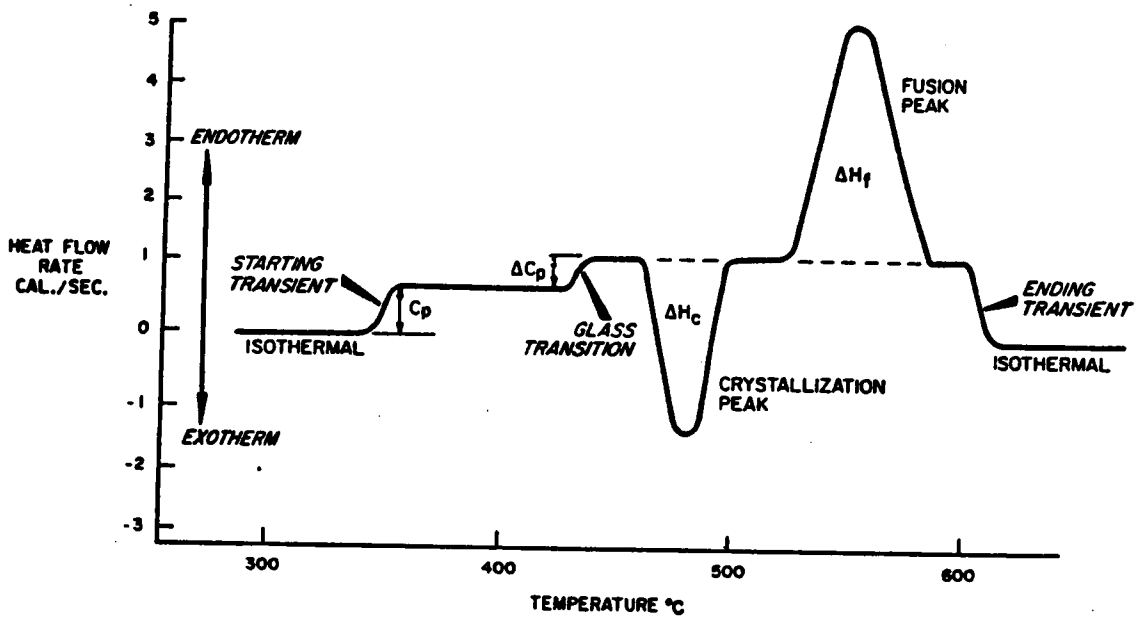

Figure 27. Example thermogram exhibiting possible transitions detected by a DSC scan.

3.2.4.1 SAMPLE LOADING/MODIFICATIONS

Normally the sample is loaded into an aluminum pan with a cover which is crimped shut. Crimping the sample pan shut does not form a seal, it simply encloses the sample. However, as the samples consisted of some percentage of water and it was necessary to measure the heat capacity and the heat of reaction at temperatures above that of the vaporization of water, some modification to the normal sample container was needed to prevent moisture from flashing off at elevated temperatures. Hence, special pressure cells were used to contain the sample. These were stainless steel capsules constructed of two separate pieces which screwed together forming a seal. An aluminum sample pan was filled with the dough sample and placed inside one side of the pressure capsule. The other side of the capsule was positioned over the sample and screwed down tightly. If a seal was not formed, a sharp peak occurred at ~100°C corresponding to the vaporization of water in the sample. If this peak was observed, the experimental run was discarded. Measurement of the total weight of the sample before and after an experimental run verified that no moisture was lost during the experiment.

3.2.4.2 CALCULATIONS

The Perkin-Elmer DSC-2 is equipped with a computer to receive, process, and record the output from the differential scanning calorimeter. Different software was used depending on which information, heat capacity or heat of reaction, was desired. In either case, an initial run, called the baseline, was performed over the temperature range under investi-

gation using the two empty sample pans. This established the inherent difference in the heat capacity of the two sample pans. The sample was then loaded into one sample pan and the experiment performed. The computer continuously recorded the differential heat flow required to keep the sample and empty sample pan at the same temperature. If heat capacity of the sample was desired, the difference between the experimental scan and the baseline at a discrete temperature was calculated and divided by the weight of the sample. A continuous graph could then be generated and plotted or a table of heat capacities at discrete temperature intervals could be printed out.

If a reaction occurred in the sample, a peak would be displayed in the data. The area under the peak represented the heat associated with the reaction. The direction of the peak, negative or positive deviation from the baseline heat, indicated endothermic or exothermic. The operator designated the initial and final temperatures of the reaction and the computer extrapolated the baseline heat of the sample over the range of temperature of the reaction. The area under the curve was then calculated and divided by the weight of the sample to give the heat of reaction.

3.2.5 EXTRUSION

Extrusion experiments were performed using a Killion (KL Series) one-inch laboratory scale single screw extruder. An explanation of the operation of a single screw extruder has been outlined previously. The extruder was equipped with three controllable temperature zones on the barrel and a fourth on the die. Two pressure transducers were mounted along the barrel. The screw characteristics are listed in Table 8. Ex-

TABLE 8

EXTRUDER SCREW CHARACTERISTICS

Description	Dimension
number of parallel screw flights	1.00
helix angle at flight tip	17.66 deg
helix angle at screw root	23.20 deg
mean root diamter of screw	1.914 cm
barrel inside diameter	2.54 cm
channel depth at entrance	1.14 cm
channel depth at exit	0.32 cm
flight thickness	0.409 cm
channel width at barrel surface	2.08 cm
channel width at screw root	1.88 cm
length of screw channel	146.2 cm

periments were performed at barrel temperatures ranging from 25° to 140° C. Constant temperature profiles, barrel and die assembly, were employed. Extrusion rates of 4 to 40 rpm were used.

3.2.5.1 SAMPLE LOADING/MODIFICATIONS

The normal method for feeding material is a gravity feed chamber. However, the material of study, 50% moisture soy dough, is not of the consistency that can be gravity fed. Hence, a special pressure feed system was designed and constructed to overcome this difficulty. A schematic of the pressure feed system is shown in Figure 28. As the hydraulic jack was pumped, the plunger descended pushing the dough down the feed cylinder into the opening of the extruder feed port. A constant pressure of 15 psig, monitored by the pressure transducer at the base of the feed cylinder, was maintained throughout the experiments. The applied pressure required was determined by two criteria. The first was to apply a particular pressure, stop the extruder, and pull the screw to see if it was flooded. The second was to monitor the flow for consistency. A pressure of 15 psig was the minimum pressure needed to maintain a constant ouput and provide a flooded screw.

3.2.5.2 CALCULATIONS

As mentioned, two pressure transducers were mounted along the length of the barrel. These pressures were monitored and recorded during the course of all experiments. In addition, mass flowrate was determined for each experiment. Ten samples were collected and weighted for each exper-

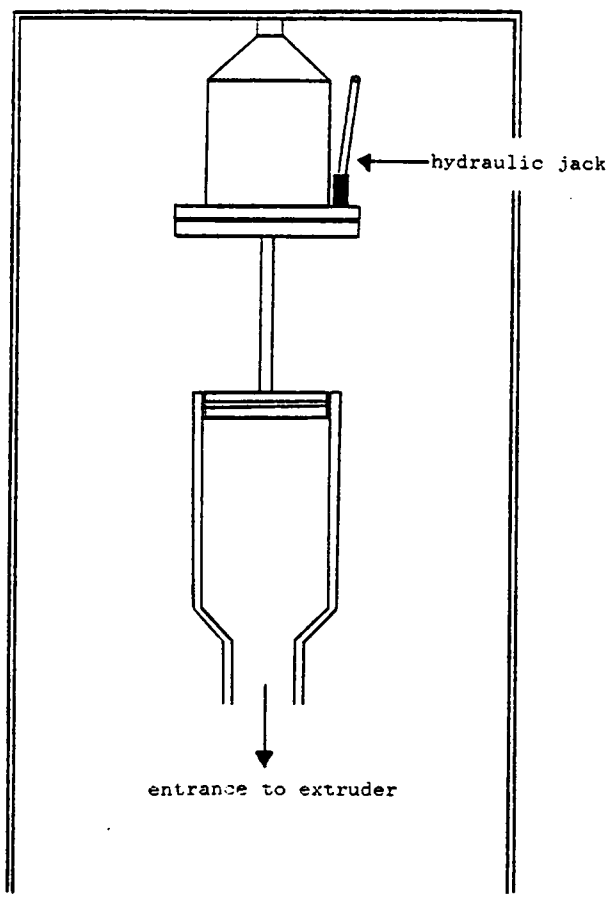

Figure 28. Schematic of Pressure Feed System

imental run. To calculate mass flowrate, the following relation was employed:

$$M = \pi r^2 \, wl \, / \, t \qquad 3.10$$

where r - radius of the die
l - sample length
w - sample weight
t - time of sample collection

It was assumed that the diameter of the extrudate remained as that of the die used. Any puffing of the extrudate was neglected.

4.0 CHAPTER FOUR: FINITE ELEMENT METHOD

4.1 INTRODUCTION

The finite element method is a general technique for constructing approximate solutions to boundary value problems. The method involves division of a given irregularly shaped domain into an assembly of geometrically simple subdomains called elements. These elements are interconnected at specific spatial coordinates or nodes. An approximation of the solution over the collection of elements is then constructed using variational concepts. The field variables are approximated as a linear combination by simple functions, usually polynomials. Then, the field equations are rewritten for each element using the interpolating functions. At this point, the equations over all the elements are assembled using the principle of continuity of the primary variables. Once the proper boundary conditions are imposed, the assembled system of equations can be solved. A continuous global solution at any point in the domain is found by using the approximation polynomials.

Because of the generality and richness of the ideas underlying the method, it has been used with remarkable success in solving a wide range of problems in virtually all areas of engineering. The finite element methodology lends itself readily to the development of general purpose programs; it allows for easy handling of complex geometries and simple implementation of a variety of boundary conditions. One such computer code employing the finite element method is called FIDAP. FIDAP is de-

signed for analysis of viscous, incompressible fluid flows including the effects of heat transfer.

As stated, FIDAP is a general purpose computer program which can simulate many classes of incompressible fluid flow. Two dimensional, axi-symmetric, and three dimensional steady state or transient simulations in complex geometries are possible. For a complete list of the capabilities and options available in FIDAP, one is referred to the FIDAP manual. The limits of the analysis are solely practical considerations of computer time and ultimate capacity of secondary storage devices when required for problems that cannot be solved in core.

In this chapter, a discussion of the theory of the methods employed in the FIDAP finite element code is presented in general form. In particular, only those methods used in the solution of the problem of study, i.e., the modeling of a foods extruder in three dimensions, will be detailed. For information regarding the other methods and options available in the FIDAP program, one is referred to the FIDAP theoretical manual. For an in-depth, overall discussion of all methods involved in the finite element method, one is directed to a number of publications regarding this topic [117,118,119].

As mentioned, the finite element method involves division of the domain into an assembly of elements. Hence,the next section in this chapter discusses the discretization of the domain. Next, the formulation of the continuum problem is reviewed in abbreviated form. The following section then presents the formulation of the discrete problem. Section 4.5 discusses the computational details of the individual element formulation. The next section presents the method for evaluation of the various coef-

ficient matrices. Then the imposition of the boundary conditions is detailed. Finally, the last section discusses the solution procedure used.

4.2 DISCRETIZATION OF THE DOMAIN

In the finite element method, the domain of the problem is divided into a number of geometrically simple elements. The discretization process involves the choice of the shape, size, and number of elements to represent the domain. The number and size of the elements in the mesh influences the accuracy and convergence of the solution. There can exist an error associated with the discretization of the domain. This is usually found for curved boundaries. The discretization error is defined as the region in a domain not included in the area mapped by the collection of elements. The discretization error may be reduced by increasing the number of elements along the boundary, thereby approximating the boundary closer. Increasing the number of elements should, in most cases, increase the accuracy of any problem, but at the expense of increased computational time. Above a certain number of elements, however, increasing accuracy is insignificant. In discretizing the domain, the physical aspects of the problem should be considered in order to optimize the numerical procedure. In areas of high gradients, the use of more elements may improve the solution. Indeed, the use of fine meshes in areas of high gradients and course meshes in areas of low gradients will improve solution accuracy without excessive computation and storage requirements.

In discretizing the domain of the food extruder, a mesh generator called GEN2D was used for the two dimensional discretization and a mesh generator called GEN3D was used for the three dimensional discretization.

These mesh generators are capable of generating 3 noded triangles and 4, 8, and 9 noded isoparametric quadrilaterals in two dimensions and 8, 20, and 27 noded isoparametric bricks in three dimensions. The programs do have the limitation that different element types may not be combined in a given mesh. The details of the mesh generation procedure employed by these programs can be found in their respective manuals [115, 116]. With proper massage of the data as to format position, the output file from these mesh generators is complete for that required for input to the FIDAP code.

4.3 FORMULATION OF THE CONTINUUM PROBLEM

To begin, the equations used to describe fluid flow are derived from the basic physical principles of conservation of mass, momentum, and energy. In FIDAP, an Eulerian formulation of these equations is employed. The equations presented here are expressed in Cartesian tensor notation with summation over repeated indices implied. The list of variables and symbols associated with the following formulation is given in Appendix A. In order to handle these equations in a numerical simulation, certain simplifying assumptions have been incorporated in the FIDAP formulation. These are as follows:

1. The Boussinesq approximation is assumed. In essence, this approximation assumes density variations are negligible for all terms except in the body force term, ρf_i, where temperature induced variations give rise to a body force, ρg_i, which contributes to the fluid motion. This approximation in temperature independent flows is simply that of incompressibility.

2. The density, ρ, in the ρg term, satisfies an equation of state if the form $\rho = \rho_0[1 - B(T - T_\beta)]$ where ρ_0 is at a reference state.

3. The enthalpy is a function of temperature only with $dh = Cp\ dT$.

4. The fluid motion is laminar.

With these assumptions and defining the strain rate or deformation tensor, $\varepsilon_{ij} = \frac{1}{2}(u_{i,j} + u_{j,i})$ the final set of equations which represent the class of fluid flows which can be simulated using the FIDAP program is now presented.

Equations of continuity, motion with a constitutive equation, and energy:

$$u_{i,i} = 0 \qquad 4.1$$

$$\rho\left(\frac{\partial u_i}{\partial t} + u_j u_{i,j}\right) = -p_{,i} + \rho f_i + \rho g_i[1 - \beta(T - T_\beta)] + [\mu(u_{i,j} + u_{j,i})]_{,j} \qquad 4.2$$

$$\rho c_p\left(\frac{\partial T}{\partial t} + u_j T_{,j}\right) = (kT_{,j})_{,j} + \mu\Phi + q_s \qquad 4.3$$

where: $\Phi = 2\varepsilon_{i,\delta}\ \varepsilon_{i,\delta}$

with boundary conditions:

$$\begin{aligned} u_i &= \bar{u}_i(s,t) && \text{on } \Gamma_u \\ t_i &= \sigma_{ij} n_j(s) = \bar{t}_i(s,t) && \text{on } \Gamma_t \\ T &= \bar{T}(s,t) && \text{on } \Gamma_T \\ q &= (kT_{,j})n_j(s) = q_a(s,t) + q_c(s) + q_r(s) && \text{on } \Gamma_q \end{aligned} \qquad 4.4$$

and initial conditions:

$$u_i(x,0) = u_i^0(x)$$

$$T(x,0) = T^0(x) \qquad 4.5$$

In these equations, the fluid properties Cp, μ, B, h, k, may be constant or temperature dependent. In the case of non-Newtonian flow, μ may be a function of $\dot{\varepsilon}_{ij}$. In particular, viscosity empiricisms, Bingham fluid and power-law fluid, are presently incorporated as options in the FIDAP program.

4.3.1 PENALTY FUNCTION APPROXIMATION

Many times the finite element method is not applied directly to the system of equation just presented. Instead, rather than including the pressure as an additional unknown in the formulation, as in the velocity-pressure formulation, the penalty function method is employed. The penalty function method also provides a means of including the mass continuity constraint , but in an approximate way. Now the finite element method is applied to a perturbed system of equations in which the continuity requirement is weakened and replaced by:

$$u_{i,i} = -\varepsilon P \qquad 4.6$$

where ε, the penalty parameter, is small; on the order of 10^{-9} In a physical sense, this could be equated to simulating the flow of a very slightly compressible fluid. The method is, by definition, an approximate one and yields the true solution only in the limit as the penalty parameter approaches zero. The pressure is recovered by a post-processing step from the velocity field by:

$$P = \frac{1}{\varepsilon} u_{i,i} \qquad 4.7$$

Most important, the penalty method offers the significant advantage of not requiring the inclusion of pressure as an extra unknown. In many instances, this property leads to finite element formulations which have significantly fewer unknowns then those obtained through the velocity-pressure formulation. In large meshes, especially those in three dimensions, this saves considerable computational time by reducing the size of the matrix problem. Hence, for this reason the penalty method was employed in these calculations. In the remainder of the description of the finite element method, only the penalty method formulation will be discussed.

A short description of the fluid flow problem which can be handled in the FIDAP program has now been presented. The problem has been presented in a continuous formulation. The next step in the finite element method is the formulation of the discrete problem. This formulation will be addressed in the next section.

4.4 FORMULATION OF THE DISCRETE PROBLEM

As mentioned, the basic objective of the finite element method is to reduce the continuous problem represented by equations 4.1-4.3 which consists of an infinite number of degrees of freedom to a discrete problem described by a system of algebraic equations consisting of a finite number of degrees of freedom.

The formulation of the discrete problem begins with the discretization of the domain. As discussed, this entails division of the continuum region

into a number of simply shaped regions called elements. As an Eulerian approach was used in development of the continuum problem, the elements are assumed to be fixed in space. Within each element, the dependent variables u and T (P would be included in a velocity-pressure method formulation) are interpolated by functions of compatible order in terms of values to be determined by a set of nodal points. In order to develop the equations for the nodal point unknowns, an individual element is separated from the system.

Integral to the formulation and solution of the discrete problem is the type of element used. Although there are many element types available in the FIDAP program for both two and three dimensional problems, the 8 noded brick used in three dimensional simulations is the one employed in this problem. In this element, velocity and temperature are the primary degrees of freedom at each node. The velocity components and temperature are approximated using trilinear interpolation functions, the details of which are outlined in the FIDAP manual. The same order of interpolation for the velocity and temperature is used for cost effectiveness reasons.

As stated, the velocity and temperature fields are approximated over each element. This is given by:

$$u(x,t) = \psi^{T} U(t) \qquad 4.8$$

$$T(x,t) = \nu^{T} T(t)$$

where U and T are column vectors of element nodal point unknowns and ψ and ν are column vectors of the interpolating functions. These approximations are substituted into the field equations and boundary conditions to yield the following set of equations:

$$f_i(\rho, \vartheta, U_i, T) = R_i \qquad \text{Momentum}$$

$$f_2(\varphi, \vartheta, U, T) = R_2 \qquad \text{Energy} \qquad 4.9$$

where R_1 and R_2 are the residuals or errors resulting from the use of the approximations.

In FIDAP, the Galerkin form of the Method of Weighted Residuals is used. This method seeks to reduce the residual errors to zero by making the residuals orthogonal to the interpolation functions of each element. The manipulations involved in this procedure are presented in the following section. The results of those computations can be expressed by the following matrix equations:

$$MU + A(U)U + K(U,T)U + \varepsilon C M_\rho^{-1} C^T U + B(T)T = F(T) \quad \text{Momentum}$$

$$NT + D(U)T + L(T)T = G(U,T) \qquad \text{Energy} \qquad 4.10$$

For simplicity, these may be combined into the single matrix equation:

$$\begin{bmatrix} M & 0 \\ 0 & N \end{bmatrix} \begin{bmatrix} \dot{U} \\ \dot{T} \end{bmatrix} + \begin{bmatrix} A(U) + K(U,T) + \varepsilon C M_\rho^{-1} C^T & B(T) \\ 0 & D(U) + L(T) \end{bmatrix} \begin{bmatrix} U \\ T \end{bmatrix} = \begin{bmatrix} F(T) \\ G(U,T) \end{bmatrix} \qquad 4.11$$

In this equation, the A and D matrices represent the convection of momentum and energy, respectively and the K and L matrices represent the diffusion of momentum and energy, respectively. The M and N matrices represent the mass and capacitance terms in the field equations. The B is related to the buoyancy term discussed in the density equation of state. The F and G vectors represent the forces on the system, both volumetric and surface forces, as well as viscous dissipation.

This summary has focused on a single element of the discretized system. To obtain the discrete representation of the entire continuum region, the elements are assembled such that interelement continuity of velocity and temperature is met. This continuity requirement is enforced through the direct stiffness approach. In essence, the direct stiffness

approach is the the summation of equations for nodes common to adjacent elements. The result of such a assembly process is a system of matrix equations of the form 4.11.

This completes the overall formulation of the discrete problem. In the next section, the details of the derivation of the matrix coefficient matrices will be given.

4.5 DERIVATION OF MATRIX COEFFICIENTS

As stated, the construction of the matrix coefficient matrices will be discussed in this section. An outline of the manipulations required to transform the field equations into the discrete form is now presented. To begin, one is referred to the equations 4.2, 4.3, and 4.6 which are the continuum equations to be discretized in the penalty method formulation. By using the finite element approximations to the velocity, temperature, and pressure and the definition of the Galerkin method requiring orthogonality of the residuals to the interpolating functions, the following equations can be written. The Green-Gauss theorem is used in the derivation to reduce the second-order terms in the momentum and energy equations and the penalty pressure term to first-order terms plus a surface integral.

(Momentum)

$$\left(\int_V \rho\varphi\varphi^T dV\right)\frac{dU_i}{dt} + \left(\int_V \rho\varphi u_j \frac{\partial\varphi^T}{\partial x_j} dV\right)U_i - \left(\int_V \frac{\partial\varphi}{\partial x_i}\psi^T dV\right)P + \left(\int_V \rho\beta g_i \varphi\vartheta^T dV\right)T$$
$$+ \left(\int_V \mu \frac{\partial\varphi}{\partial x_j}\frac{\partial\varphi^T}{\partial x_j} dV\right)U_i + \left(\int_V \mu \frac{\partial\varphi}{\partial x_j}\frac{\partial\varphi^T}{\partial x_i} dV\right)U_j$$
$$= \int_S \bar{t}_i \varphi dS + \int_V \rho f_i \varphi dV + \int_V \rho g_i (1 + \beta T_\beta)\varphi dV.$$

(Compressibility)

$$\left(\int_V \psi \frac{\partial \varphi^T}{\partial x_i} dV\right) U_i = 0 \quad \left[\text{ or } \quad \left(\int_V \psi \frac{\partial \varphi^T}{\partial x_i} dV\right) U_i = -\varepsilon \left(\int_V \psi \psi^T dV\right) P \right]$$

(Energy)

$$\left(\int_V \rho c_p \vartheta \vartheta^T dV\right) \frac{dT}{dt} + \left(\int_V \rho c_p \vartheta u_j \frac{\partial \vartheta^T}{\partial x_j} dV\right) T + \left(\int_V k \frac{\partial \vartheta}{\partial x_j} \frac{\partial \vartheta^T}{\partial x_j} dV\right) T$$

$$= -\int_S (q_a + q_c + q_r) \vartheta dS + \int_V q_s \vartheta dV + \int_V \mu \Phi \vartheta dV$$

The various coefficient matrices are taken from these equations and defined by:

$$M = \int_V \rho \varphi \varphi^T dV$$

$$M_p = \int_V \psi \psi^T dV$$

$$N = \int_V \rho c_p \vartheta \vartheta^T dV$$

$$K_{ij} = \int_V \mu \frac{\partial \varphi}{\partial x_j} \frac{\partial \varphi^T}{\partial x_i} dV$$

$$C_i = \int_V \frac{\partial \varphi}{\partial x_i} \psi^T dV$$

$$L_{ij} = \int_V k \frac{\partial \vartheta}{\partial x_i} \frac{\partial \vartheta^T}{\partial x_j} dV$$

$$A_i(U_j) = \int_V \rho \varphi u_j \frac{\partial \varphi^T}{\partial x_i} dV$$

$$D_i(U_j) = \int_V \rho \vartheta u_j \frac{\partial \vartheta^T}{\partial x_i} dV$$

$$B_i = \int_V \rho g_i \beta \varphi \vartheta^T dV$$

$$F_i = \int_S \bar{t}_i \varphi dS + \int_V \rho f_i \varphi dV + \int_V \rho g_i (1 + \beta T_\beta) \varphi dV$$

$$G = -\int_S (q_a + q_c + q_r) \vartheta dS + \int_V q_s \vartheta dV + \int_V \mu \Phi \vartheta dV$$

4.6 EVALUATION OF THE MATRIX COEFFICIENTS

The various element matrices have just been defined. They are, in effect, spatial intergrals of the various interpolation functions and their derivatives. The form of the integrand is such that classical or exact integration methods are difficult or impossible to employ. Hence, numerical integration, or quadrature, techniques are used. This section will describe the method employed in evaluation of these matrices.

In the FIDAP program, a numerical quadrature procedure is used in evaluation of the matrix coefficients. In particular, the method of Gaussian quadrature is employed. For a detailed description of this method one is referred elsewhere [120]. The FIDAP program allows the user a certain degree of freedom of choice of the integration order for the different matrices. However, certain rules apply and are outlined in the FIDAP manual as to the specification of the order for the different matrices. For example, the use of fourth order Gaussian integration is required for the coefficient matrices representing the diffusion of momentum and energy in a non-Newtonian fluid problem. Also, depending on the pressure formulation, consistent or reduced penalty formulation and the type of element employed, the order of the matrices involved with pressure is determined.

4.7 BOUNDARY CONDITION EVALUATION

The previous two sections have discussed the construction and evaluation of the various coefficient matrices. However, the specification of

the boundary conditions was not included. Therefore, this section will address the various boundary conditions.

4.7.1 CONSTRAINED VELOCITIES AND TEMPERATURES

The constrained velocities and/or temperatures are the essential boundary conditions of the problem. The specification of particular constant values for the velocity components or temperature at boundary nodes results in the field equation for that particular degree of freedom being deleted. The specified value is them imposed for the degree of freedom in the other equations.

4.7.2 APPLIED SURFACE FORCES AND FLUXES

The boundary conditions in this section are often referred to as the natural boundary conditions because of the natural way they arise in the integral equations. Two types of surface force or fluxes are possible; applied heat flux or applied traction forces. The heat flux is of the form:

$$G = \int_S \phi q_a \, dS$$

and the applied stress boundary condition is of the form:

$$F_i = \int_S \phi \xi_i \, dS = \int_S \phi \sigma_{ij} n_j \, dS$$

By expressing the surface of the element parametrically, the details of of which are outlined in the FIDAP manual, the boundary conditions can be expressed in an integral form similar to the coefficient matrices. From there, they can be directly evaluated.

A point to note is that the applied stress boundary condition is in terms of the total normal stress or traction which is different from the

pressure. However, in many cases, the viscous part of the stress is negligible and the normal stress is essentially the pressure. Whichever the case, negligible viscous term or not, the application of the stress boundary condition does not distinguish between contribution from the pressure and viscous parts but simply reflects their net effect.

4.8 SOLUTION PROCEDURE

As stated, the system of equations can be written in the form:

$$[K(U)]U = F$$

This system of equations is solved by a combination of methods; these are successive substitution and quasi-Newton. In the method of successive substitution the nonlinear terms are evaluated with values of U from the previous iteration. This scheme has a fairly large radius of convergence but for many problems, especially non-Newtonian flows, the convergence rate can be very slow. The Newton-Raphson method has a rate of convergence superior to that of the successive substitution method. Its convergence rate is quadratic as long as the initial solution vector is within the radius of convergence. However, this radius of convergence is smaller than that of successive substitution. For both methods, the Gaussian LU factorization of the matrix must be performed at each iteration. In the quasi-Newton procedure, however, the LU decomposition is updated in a simpler manner at each iteration. In addition, the quasi-Newton method has superlinear convergence with its rate of convergence approaching that of Newton-Raphson while the cost of one quasi-Newton iteration is typically 10 to 20% of the cost of a Newton-Raphson iteration.

Hence, with this knowledge of the methods available, the following iteration strategy was employed. First, one iteration of successive substitution was performed to obtain a guess within the radius of convergence of the quasi-Newton method. Subsequent iterations were performed until convergence using the quasi-Newton method.

5.0 CHAPTER FIVE: RESULTS AND DISCUSSION

5.1 INTRODUCTION

The goals of this dissertation were outlined in Chapter Two. In this chapter, the experimental work employed to obtain these goals is discussed. The first section presents the work performed to study the rheological behavior of the soy dough. The next section examines the thermal behavior of the system as determined through differential scanning calorimetry. This includes determination of the cooking reaction and the heat capacity of the soy dough. Closely related to these thermal properties are the thermal conductivity and diffusivity of the material. The determination of these two properties will be addressed in the following section. The experimental extruder runs are the topic of section 5.5. Finally, combining the results from these previous sections, the last section of this chapter is concerned with the three dimensional finite element model of the extruder and compares the predictions to the flowrate and pressure data obtained from the extruder experiments.

5.2 RHEOLOGICAL MEASUREMENTS

The experiments used to determine the rheological behavior of the soy dough are discussed in this first section. Of most importance is the determination of the viscosity of the 50% added moisture soy dough. This is determined as a function of shear rate and temperature. In addition, the effect of moisture content on the viscosity is explored. Although the

majority of the work is centered on the viscosity of the soy dough, some additional rheological measurements examine storage and loss moduli as a function of temperature and time. The results of these experiments are discussed at the end of this section.

To begin, capillary rheometry experiments used to determine the viscosity of the 50% added moisture soy dough are discussed. These experiments follow the procedure outlined in Chapter Three. As mentioned in the experimental chapter, a special sample preparation procedure was developed. The results from experiments prior to the adoption of the sample preparation procedure as well as those following the adoption of the procedure are shown in Figure 29. These results demonstrate the necessity of a consistent sample preparation technique. The reproducibility of the data for the samples with a controlled preparation is much better than that of the samples with a random preparation. There are many factors which could contribute to the scatter associated with the random preparation. These include non-uniform dispersion of moisture, inconsistent mixing, varying storage time, and improper storage. Hence, a controlled sample preparation as outlined in the experimental chapter is employed for all experimental samples.

As mentioned in the experimental chapter, calculation of the entrance pressure loss must be performed before calculation of the viscosity. The Bagley plot technique is used for calculation of this quantity. In Figure 30 are presented the results of these calculations displaying entrance pressure loss as a function of temperature at different shear rates. The different symbols represent different shear rates. At any one temperature, the symbol corresponding to the lowest entrance pressure cor-

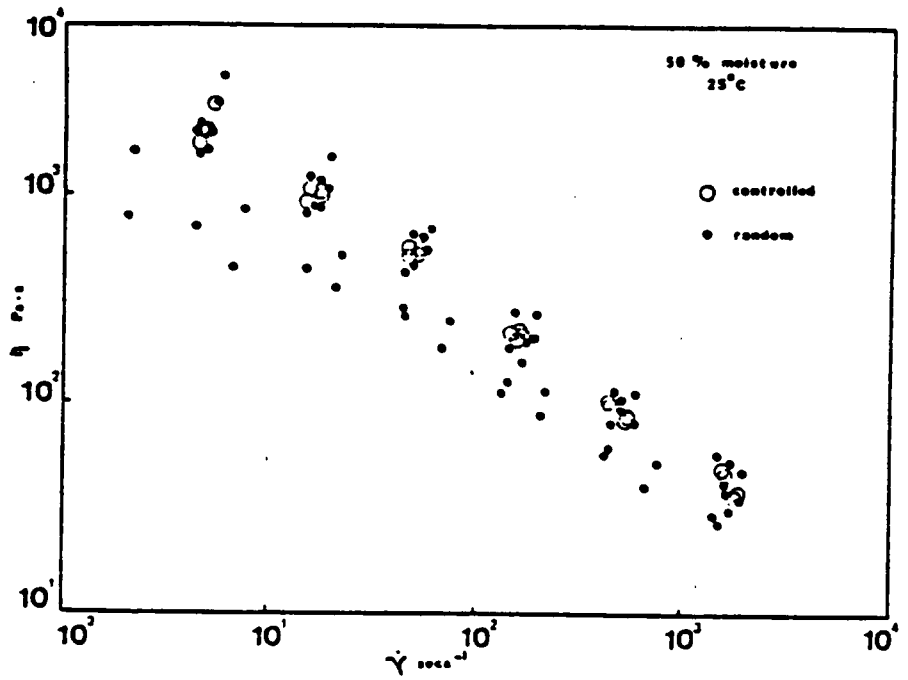

Figure 29. Viscosity curves for random vs. controlled samples

rection factor coincides with the lowest shear rate and the symbol corresponding to the highest entrance pressure correction factor coincides with the highest shear rate with the other symbols' positions agreeing accordingly to shear rate. Hence, at a constant temperature, increasing shear rate increases the entrance pressure for the 50% added moisture soy dough. However, this is not the case at all temperatures. At the lower temperatures increasing the shear rate did not always increase the entrance pressure loss. For example, at 25°C the entrance pressure loss is zero for the first four shear rates and not until a shear rate in the range of 450 s^{-1} is employed is an increase in entrance pressure loss obtained. It is significant to note that this is true only at the lower temperatures. At the higher temperatures the entrance pressure loss increased with increasing shear rate.

This dependence of entrance pressure loss on shear rate was expected. It is the dependence of entrance pressure on temperature which is of greater interest. At a constant shear rate, an increase in entrance pressure loss is observed with increasing temperature. Of special note is the large increase in entrance pressure loss which occurs between 75 and 85°C for all shear rates examined. Similarly, a large increase is seen for the entrance pressure loss between the 85 and 100°C values for most of the shear rates examined. However, at the two highest shear rates, a decrease rather than an increase in entrance pressure loss is observed. As entrance pressure loss is related to the primary normal stress difference which in turn is related to the elasticity of the material, the increase in entrance pressure loss at the higher temperatures can be attributed to an increase in elasticity [40]. The exact reason for the in-

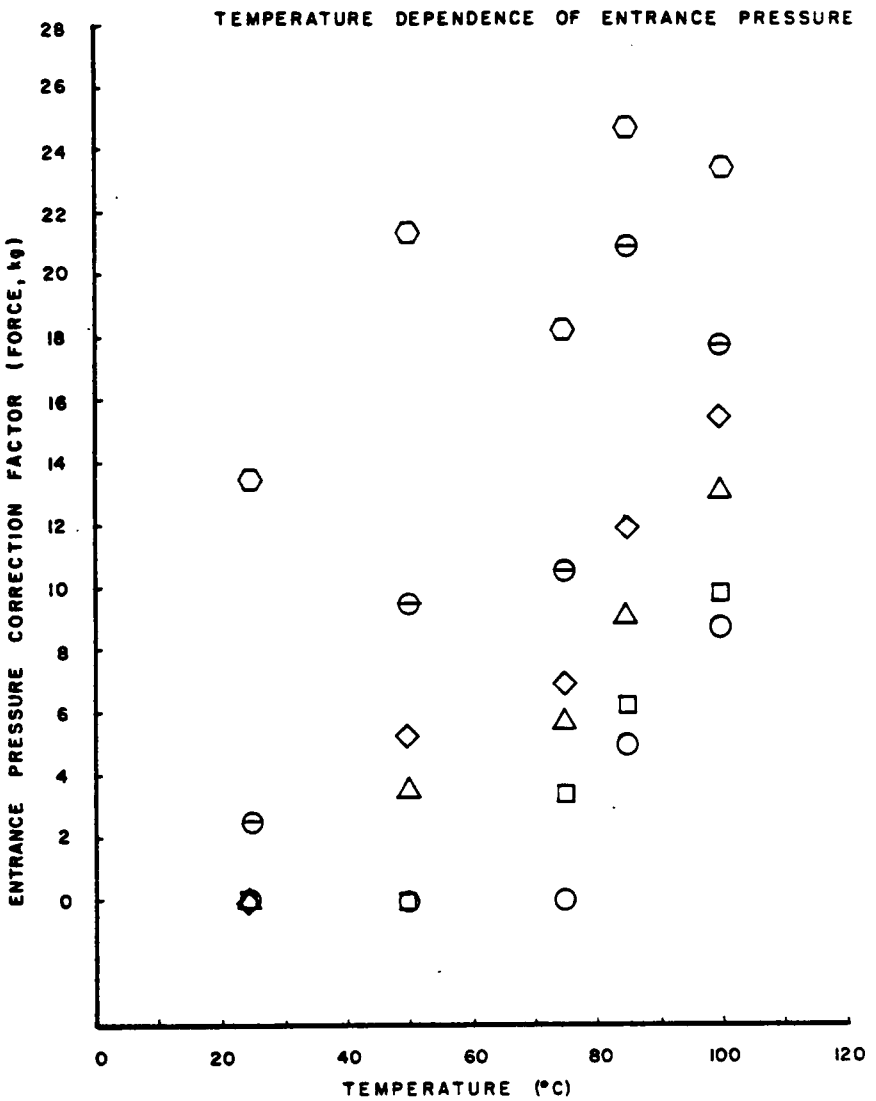

Figure 30. Temperature dependence of entrance pressure for 50% moisture dough

crease in elasticity is not known at this point. From the knowledge of protein chemistry, it is possible to suggest that denaturation of the proteins may have occurred at the higher temperatures, 85 and 100°C specifically. The random coil conformation of the denatured proteins is likely to form a more elastic sample as there is no rigidity to the molecules as there is in the structured state of the molecules before denaturation.

The results for the entrance pressure loss data were not consistent for all samples measured. In a few experiments, the extrapolations to zero length on the Bagley plots, and hence, entrance pressure values, gave values for entrance pressure loss which were larger than the pressure drops observed. This behavior was not observed at any one particular temperature or shear rate condition. However, it was more likely to be observed at the lower temperatures and shear rates. Two possible explanations for this erratic behavior are offered. The first involves the possibility of a yield stress in the soy dough. It has been previously suggested in the literature that the soy doughs exhibit a yield stress [40]. It is possible that the presence of the yield stress complicates the entrance pressure measurement, or that for the lower shear rates, the yield stress is higher than the stress experienced in the sample. The yield stress would most likely be greater at the low temperatures and would have more of an effect at the lower shear rates. Hence, the inconsistencies would be more prevalent at these conditions.

The other explanation is the possibility of the partial clogging or blocking of the capillary from soy particles cooked on to the walls. If a particle or particles of dough were to adhere to the wall of the

capillary, the diameter would be decreased and increased pressure would be required for flow to occur. Although this would be a constant increase in pressure over all shear rates if the particle were not tightly adhered, it is possible that the higher shear rates could clear the capillary by forcing the blockage to flow out. Hence, this type of experimental error could cause two behaviors: either a consistent increase in pressure over the whole range of flows or simply an increase in pressure at the lower shear rates. Both of these behaviors were observed. Whatever causes an abnormal pressure reading for an experimental sample, inclusion of those points in the Bagley plots would create an inaccurate extrapolation. Consequently, the entrance pressure loss would be incorrect and inaccurate viscosity results would be obtained.

In addition to the Bagley plots that were used to obtain the entrance pressure loss correction, the Rabinowitsch correction was also applied to the capillary rheometer data. Once these correction factors were obtained, the viscosity of the soy dough was calculated. For these viscosity calculations the dough was considered incompressible. Viscosity was assumed to be independent of pressure. This assumption was tested with the aid of the pressure capsule on the capillary rheometer. The system was pressurized to different pressure levels and viscosity measured. The viscosities calculated from the experimental results at the different pressures were all within experimental error of one another. Hence, the viscosity was assumed independent of pressure. The results are shown in Figure 31 with viscosity displayed as a function of shear rate and temperature. In addition, the viscosity values calculated without the entrance pressure loss correction are shown. In this figure,

viscosity is reported as a function of temperature only up to temperatures of 100°C. Additional experiments were performed to obtain the viscosity at elevated temperatures but will be discussed later.

The most noticeable aspect of Figure 31 is the sharp slope of the viscosity data. The slopes of the various viscosity curves range from -0.6 to -0.8 depending on temperature. Furthermore, the viscosity curves do not shown any indication of leveling off at the lower shear rates. This suggests the presence of a yield stress. The leveling off of the viscosity curve would be indicative of the plateau associated with the zero shear rate viscosity observed in most polymeric materials. However, if a yield stress is present in a material, the viscosity of the material continually increases with decreasing shear rate, theoretically approaching infinity. To better determine the presence of a yield stress, viscosity measurements at lower shear rates must be made.

As mentioned, the results of viscosity calculations before the inclusion of the entrance pressure loss are included in Figure 31. The behavior of the uncorrected data will be addressed first. The viscosity curves dependence upon temperature is seen to be unique. For most polymeric systems, viscosity decreases with increasing temperature. The viscosity data for the soy dough follows this trend of decreasing with increasing temperature but only up to 75°C. At 85°C, a rise in viscosity is seen as compared to the viscosity measured at 75°C. After 85°C, the viscosity continues to decrease with increasing temperature. Hence, the anomalous behavior occurs around the 85° experimental temperature.

Recalling the large increase in entrance pressure loss at this temperature, it is possible that the inclusion of the entrance pressure loss

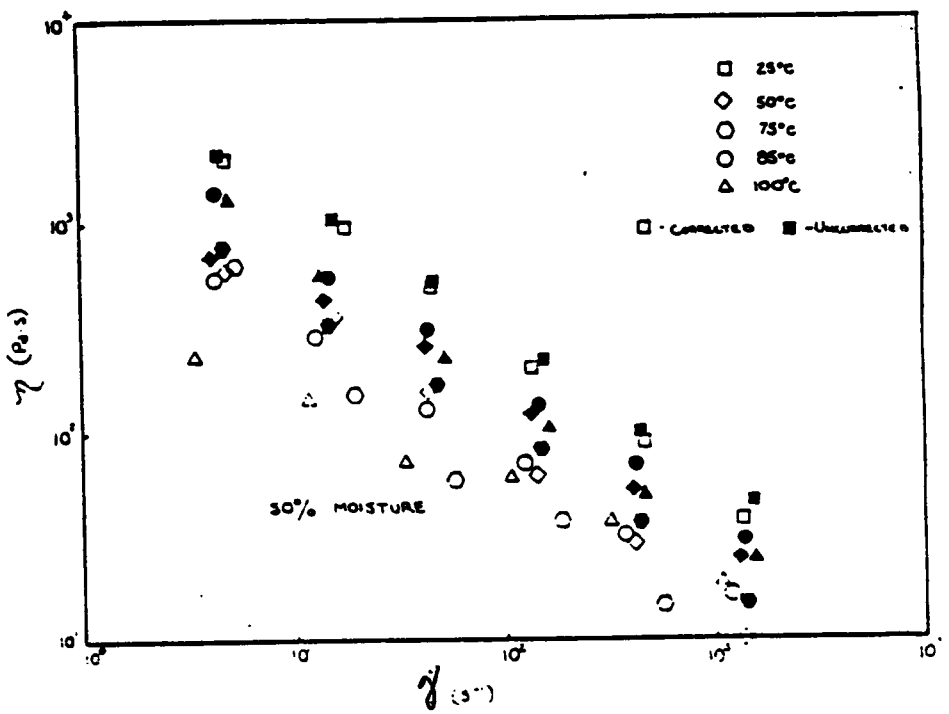

Figure 31. Viscosity curves of 50% moisture dough

factor corrects the inconsistency of the data's dependence upon temperature. However, this is not the case. The same temperature dependence is found for the viscosity after correcting for the entrance pressure loss. The dependence of the viscosity on temperature can be seen more clearly in Figure 32. Here, the viscosity is presented as a function of temperature at a constant shear rate; data are presented for both a low and high shear rate. The same trend is observed regardless of the shear rate employed. Viscosity is seen to decrease with increasing temperature up to 75°C. At the next experimental temperature, 85°C, the viscosity data is seen to be significantly greater than that measured at 75°C. In fact, it is even greater than the viscosity data found at 50°C. After 85°, the viscosity is again observed to decrease with increasing temperature. The error bars associated with the measurement of the data, the details of which are presented in Appendix B, are included in Figure 32. As the error bars associated with the 75 and 85°C viscosity data do not even overlap, the viscosity behavior as a function of temperature is concluded to be a true phenomenon.

The appearance of the extrudate was monitored throughout the experiments. A change in the appearance was noticed at 85°C. For experimental temperatures up to and including 75°C, the extrudate had basically the same appearance as the as-mixed sample. The extrudate was yellow-gold in color, tacky to the touch, and broke when bent, not exhibiting any elasticity. However, the extrudate of the 85 and 100°C experiments were still a yellow-gold color but now were smooth and non-tacky to the touch, and had a rubbery behavior. When they were bent, they did not break but would give and stretch, and when pressure was relieved they would spring

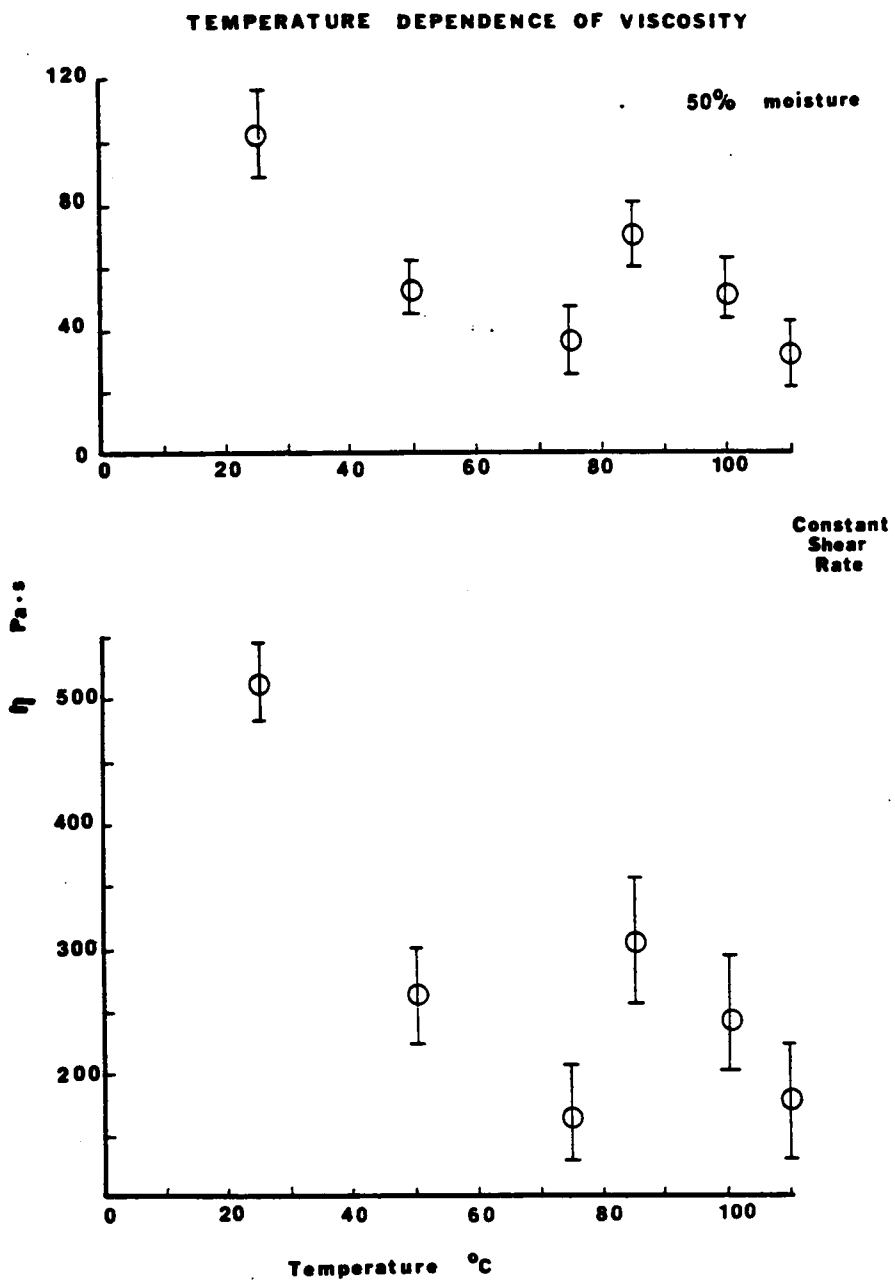

Figure 32. Temperature dependence of viscosity for 50% moisture dough

back. Hence, not only do the viscosity measurements exhibit a change in the material at 85°C but also the appearance of the extrudate.

Additional experiments were performed using the capillary rheometer with a larger diameter capillary. By employing a larger diameter capillary, the shear rates obtained during experimentation are lower for the same instrument speeds. The results from these experiments are presented in Figure 33. The results from the measurements made with the original capillary are included in this figure for comparison. Essentially good agreement is obtained as the differences are within the error bounds calculated earlier. If the viscosities calculated by the two different capillaries did not agree, it is possible that an instability in the experiment may exist. In particular, the question of slippage occurring in the capillary arises for this experiment. However, if slippage of the sample were occurring in the capillary, the results from capillaries of two different diameters, and therefore, different contact area, would not coincide. Hence, it can be concluded that the experiments reflect a true viscosity for the material.

As discussed, the shear rates experienced in the larger diameter capillary are lower than those of the smaller diameter capillary. The viscosity at these lower shear rates still indicate the presence of a yield stress. No leveling off of the data is yet exhibited.

As mentioned earlier, additional experiments using the capillary rheometer to determine viscosity were performed at elevated temperatures. Values of viscosity were desired for temperatures up to and including those normally experienced in the cooking extrusion process, on the order of 150°C. The results from these experiments are shown in Figure 34. The

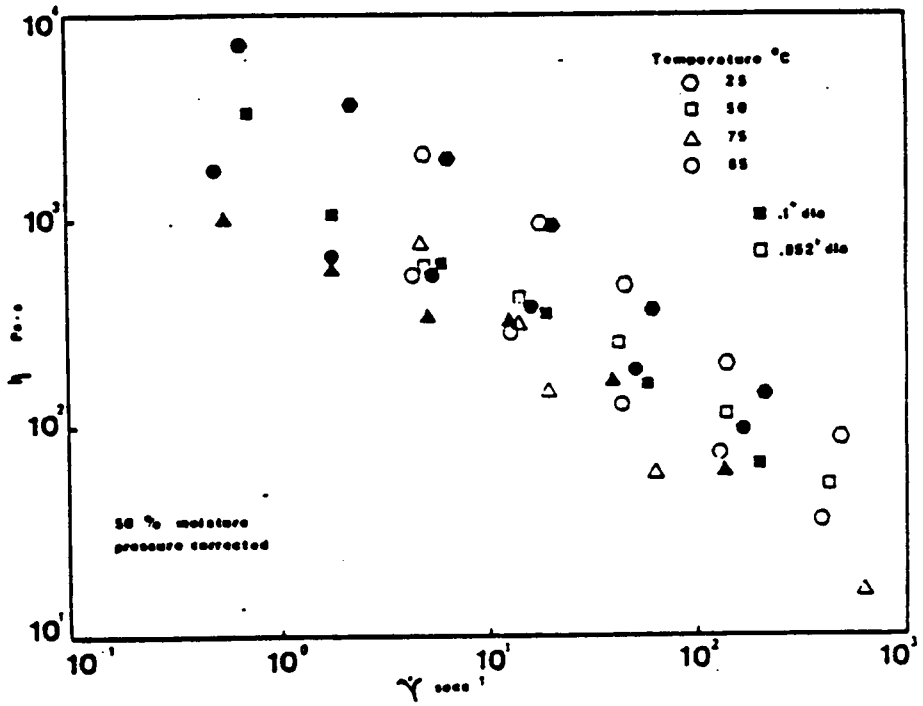

Figure 33. Viscosity curves comparing data from two capillary diameters

viscosity results at 110°C appear to agree with the trend of the previous data. The viscosity is slightly lower than that at 100°C as was expected, and the slope of the curve is approximately the same as that of the other lower temperature data.

The viscosity results for 130 and 140°C, however, are of question. The first difference observed, before the viscosity was even calculated from the capillary rheometer data, was the appearance of the extrudate. For temperatures up to and including 110°C, the extrudate was a light golden color and pliable. However, at 130 and 140°C, the extrudate appeared brown and burned. It was no longer as pliable and had a hard crust. At that point the results were suspect. Once viscosity was calculated for these temperatures and compared to the viscosity at other temperatures, additional differences were observed. First, the viscosity at 130 and 140°C was much lower than the values at 100 and 110°C. It was expected that the results for these higher temperatures would decrease in proportion to the decrease shown between 85 and 110°C. In addition, the slope of the two curves differ from the range of slopes encountered for the lower temperature measurements. The slopes now are on the order of -1.0 which is indicative of plug flow. In essence, the material is no longer flowing but simply moving as a solid plug through the capillary. The appearance of the crust on the extrudate supports this idea.

While extrusion cooking typically occurs at 130°C or higher; the extrudate from the extrusion cooking process does not appear burned. However, it appears that for some reason, possibly the long exposure time to the elevated temperature, the sample is burning in the capillary rheometer. Consequently, another procedure for measuring the viscosity

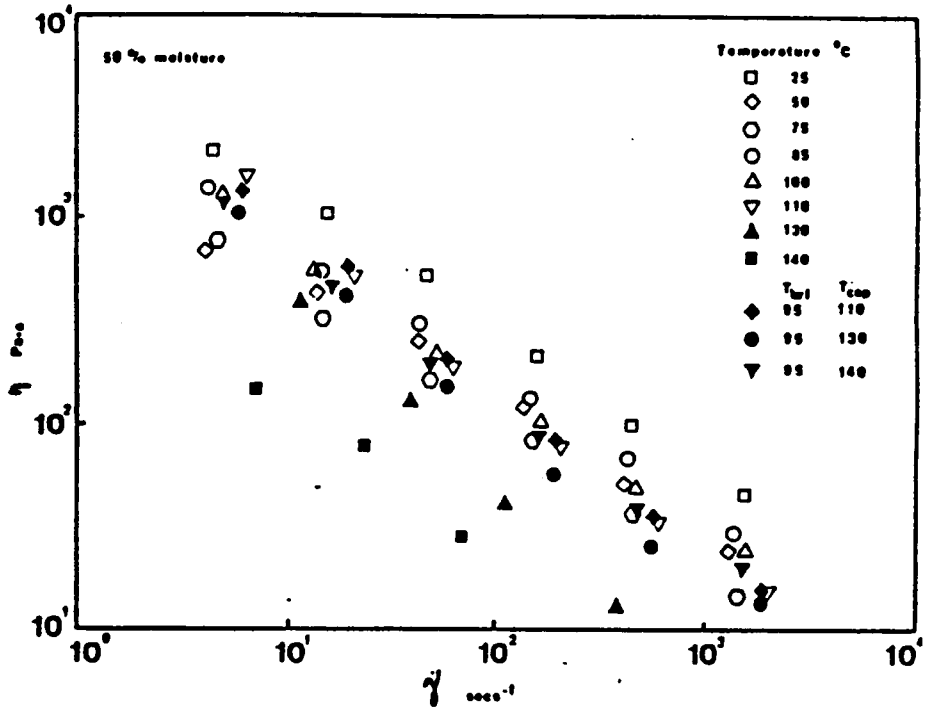

Figure 34. Viscosity curves for 50% moisture dough for full temperature range

at the elevated temperatures was developed. Assuming it was the extended exposure to the elevated temperature which created the inconsistencies, the normal capillary rheometer procedure was modified. Instead of setting the capillary reservoir and the capillary to the experimental temperature, only the capillary was set to the experimental temperature. The capillary reservoir was set to 95°C. This is below the temperatures where inconsistencies started to be seen but high enough that heating of the sample to experimental temperature would occur quickly. The results from these experiments are also presented in Figure 34. The viscosity curves for all three capillary temperatures are essentially the same. In addition, the results do not agree with the results from the experiments where both the capillary and the reservoir were at the experimental temperature. This can be seen better in Figure 35 where the isolated results of the experiments at elevated temperatures are presented. The results from the experiments with both capillary and reservoir at 110°C and those with reservoir at 95°C and capillary at 110°C agree completely. This is expected as the temperature difference is not large and it was seen that the viscosity curves for 100 and 110°C are very close. However, it was also observed that the experiment with the reservoir at 95°C and the capillary at 140°C gave the same results as the 110°C experiments. These results are in contrast to the results of the experiment with both capillary and reservoir at 140°C. The validity of the results of either method of determining the high temperature viscosity are doubtful. Hence, only the results for measurements of viscosity up to 110°C are considered reliable.

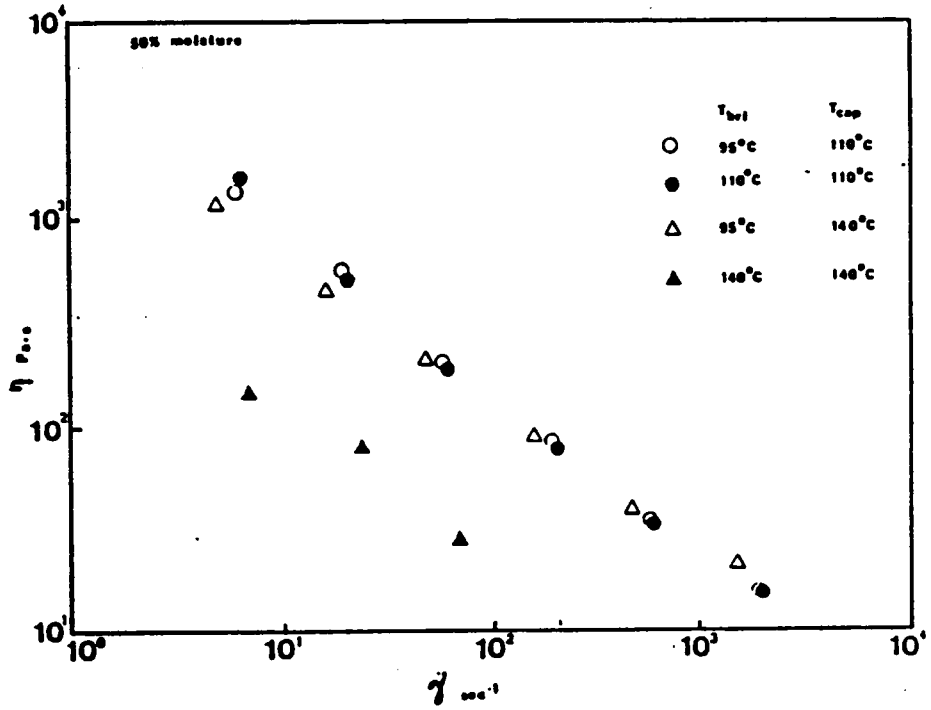

Figure 35. Viscosity curves for elevated temperatures

The viscosity of 40 and 60% added moisture soy doughs was also determined using the capillary rheometer as a function of shear rate and temperature. The results of these studies are seen in Figures 36 and 37. The viscosity curves for the 40% added moisture soy dough, shown in Figure 36, do not exhibit the same behavior as the viscosity curves for the 50% moisture soy dough. The slopes of the curves are consistently nearer to -0.6 to -0.5 range. This is surprising as the higher solids content sample would be expected to approach plug flow rather than exhibit a higher flow index than the lower solids content dough. The temperature dependence of the viscosity is also different than that of the 50% moisture dough. Similar to the 50% moisture dough, the viscosity measured at ambient temperature is noticeably higher than the viscosity at elevated temperatures. However, unlike the 50% moisture dough, the viscosity curves for the 40% moisture dough show no distinguishable dependence upon temperature at raised temperatures. Some dependence on temperature is seen at the lowest shear rates with viscosity decreasing with increasing temperature up to 75°C then increasing at both 85 and 100°C. This behavior could partly be influenced by the presence of a yield stress in the material as has been discussed earlier. For the most part, however, the values determined for viscosity at the various temperatures are within the error range of the other viscosity measurements.

The viscosity results of the 60% added moisture soy dough are different again from either of the 40 or 50% moisture soy dough results. The slopes of the viscosity curves for the 60% moisture dough are between -0.85 and -0.7. This slope is approaching that of plug flow. This is in contrast to the expected results. With increased moisture it is expected

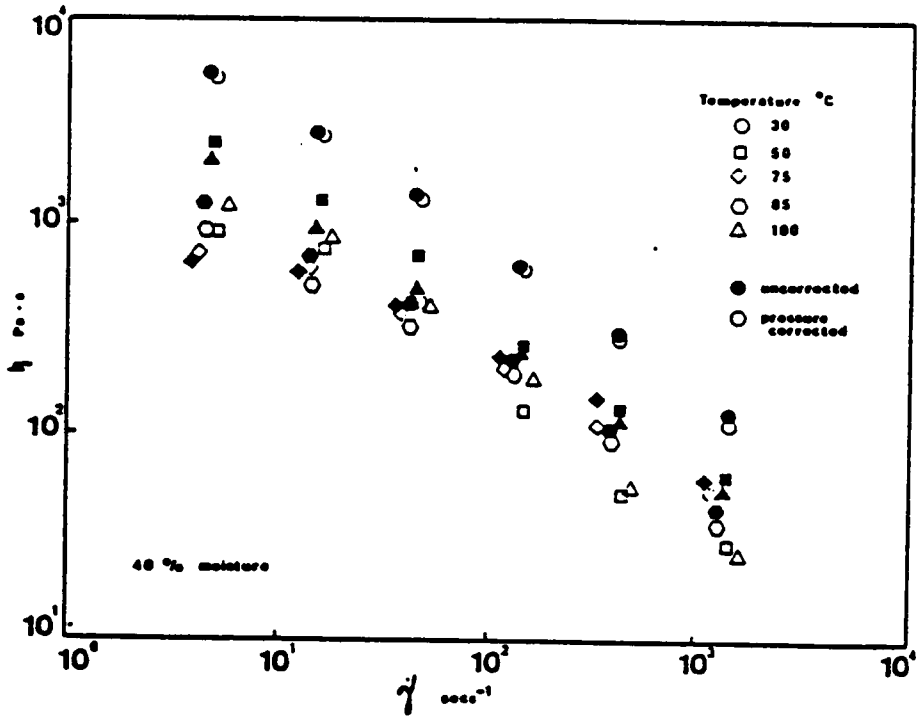

Figure 36. Viscosity curves for 40% moisture dough

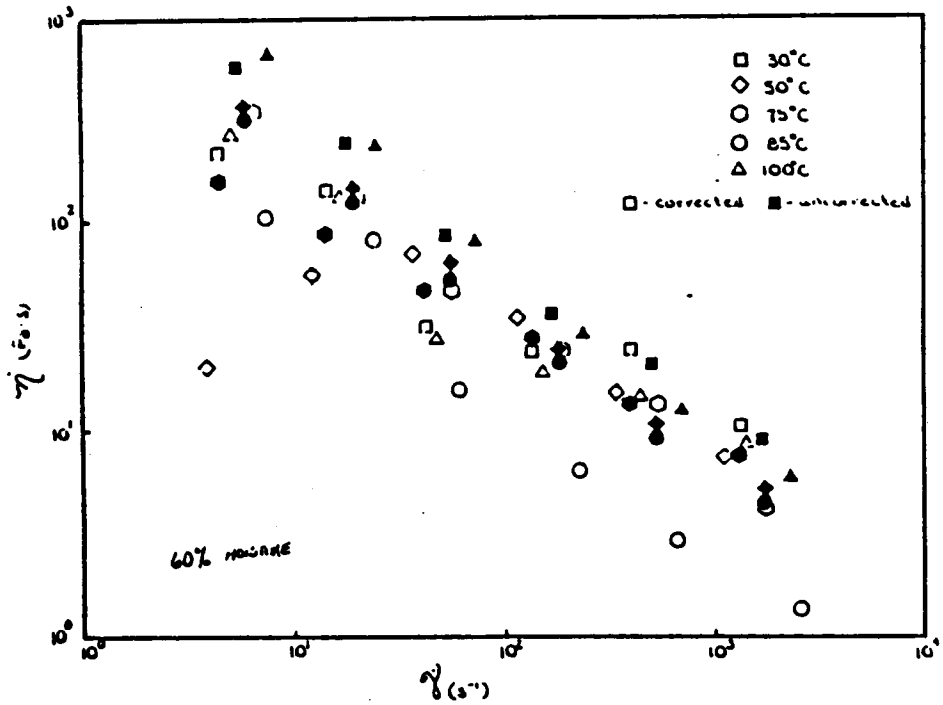

Figure 37. Viscosity curves for 60% moisture dough

that the material would flow better but instead the additional moisture seems to make the flow behavior approach that of plug flow. The temperature dependence of the viscosity curves are also different than either of the previously noted temperature dependencies for the 40 and 50% moisture samples. For the 60% moisture dough, viscosity is seen to decrease slightly with increasing temperature up to and including 85°C and increase at 100°C. This is similar to the behavior of the 50% moisture dough except the increase in viscosity occurs at a slightly higher temperature, 100°C instead of 85°C previously seen. It is possible that the same mechanism is responsible for the increase in viscosity in the 60% moisture dough as in the 50% moisture dough. The slightly higher temperature of 100°C as opposed to 85°C may be due to the dilution of the system. For the same reasoning, the absence of this behavior in the 40% moisture dough may be the lack of enough water present in the system for the increase in viscosity to occur. Hence, it is concluded that the moisture content may be responsible for the temperature dependence observed.

Although the behavior of the different moisture soy doughs has been discussed, the actual effect of moisture has not clearly been stated. In all cases, the viscosity values for the 60% added moisture soy dough were lower than those for the 50% added moisture soy dough which in turn were lower than the 40% added moisture soy dough. The magnitude of the difference, however, depended on the temperature at which the viscosity was measured. At ambient temperature, the effect of the additional moisture of the 60% moisture dough was much greater than the effect of the reduced moisture of the 40% moisture dough as compared to the 50% moisture dough.

The values for the viscosity for the 60% moisture dough were approximately an order of magnitude less than the 50% moisture dough viscosity values whereas the 40% moisture dough viscosity values were only one half a magnitude higher. Once heat is applied, however, the difference in the viscosity values as a function of moisture decrease. At 50°C, the difference between the 40 and 50% moisture dough viscosity values was on the order of one half magnitude difference. The viscosity values for the 50 and 60 moisture samples also differ by the one half order of magnitude. At 75°C, the 60% moisture dough viscosity values are only slightly lower than those of the 50% moisture dough while the 40% moisture dough viscosity values were still one half a magnitude higher than those of the 50% moisture dough. At 85°C, where the 50% moisture dough behavior rose suddenly with temperature, the 40% moisture dough viscosity values are not only approximately one third a magnitude higher than the 50% moisture dough values but the 60% moisture dough viscosity values are one whole order of magnitude less. At 100°C, it was seen that the 60% moisture dough viscosity displayed a discontinuity similar to that observed in the 50% moisture dough at 85°C. It is no surprise then that at 100°C the difference between the 50 and 60% moisture doughs has decreased. In fact, the difference in viscosity values for these two moisture content doughs is now only on the order of one quarter of a magnitude. The difference between the 40 and 50% moisture doughs is approximately one half magnitude. Hence, the difference between viscosity values for the 40 and 50% mositure doughs is relatively constant while the difference between viscosity values for 50 and 60% moisture doughs is very temperature dependent. It can be concluded then that any experimental error which would include a

reduced moisture content would have a consistent error whereas an increase in moisture would cause different percent error in the results as a function of temperature.

To expand the knowledge of viscosity as a function of shear rate and temperature, experiments were performed using the Rheometrics Mechanical Spectrometer (RMS). The results of these experiments are presented in Figure 38. Although modifications were made to the instrument as described in the experimental chapter to minimize the loss of moisture from the sample, the highest temperature at which the viscosity was determined was 85°C. At 100°C, moisture flashed off from the sample resulting in inaccurate viscosity measurements. In the figure, the viscosity results display a sharp slope as a function of shear rate which is similar to that seen in the capillary rheometer data. However, the viscosity curves do not exhibit as strong a temperature dependence as seen in the capillary rheometer results. While the viscosity curve for the ambient temperature, 30°C, is higher than the viscosity curves at higher temperatures, it is not significantly higher as it was at the higher shear rates. The viscosity curves for the elevated temperatures are all very close in value. The data for these curves are all within the error limits of each other. Hence, no true temperature dependence is found.

Similar to the capillary rheometry experiments, once shear rate and temperature dependence were determined for the soy dough, the effect of moisture content was explored. The 40% added moisture soy dough is too viscous for the RMS. Hence, only the 60% added moisture dough was examined. The results of these experiments are presented in Figure 39. The behavior of the viscosity curves for the 60% moisture dough is similar

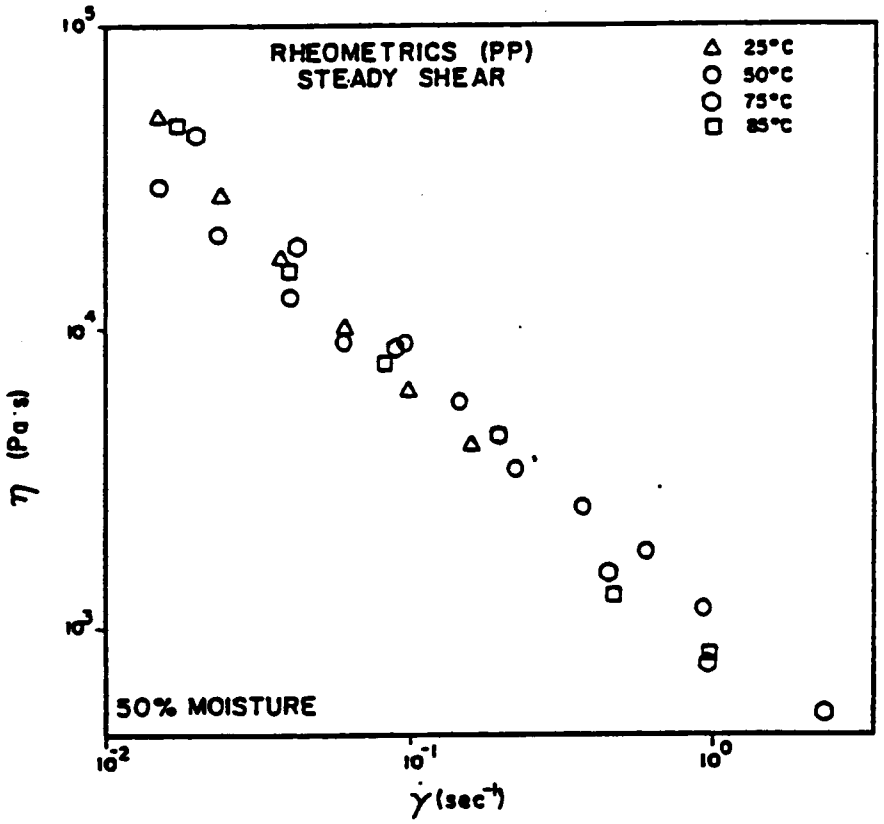

Figure 38. Rheometrics steady shear vicosity curves for 50% moisture dough

to that of the 50% moisture soy dough. The viscosity curves as a function of shear rate exhibit a sharp slope. The viscosity curve for the ambient temperature, experiment is slightly higher than the viscosity curves at elevated temperatures. Again, the viscosity curves at the higher temperatures are all approximately the same with all values falling within the margin of error. Once more, no true temperature dependence of the viscosity can be observed.

As mentioned, the slopes of the viscosity curves for both the 50 and 60% moisture doughs were still very sharp, approximately -0.7 slope, even over the low range of shear rates investigated. Hence, a yield stress is present in the soy dough. The convergence of the viscosity curves to the same value at the elevated temperatures may be due to the presence of the yield stress. If the yield stress for the material is not very temperature dependent, the curves would converge at lower shear rates. The divergence of the viscosity curves as a function of temperature which occurs at the higher shear rates occurs because of the temperature dependence of the slope.

Finally, the viscosity calculated from the RMS data was compared to that obtained from the capillary rheometer data. The results for one temperature, 50°C, are shown in Figure 40. Good agreement is found between the data. This is true for the data at all experimental temperatures. As the data were obtained by means of two different apparatus employing two different techniques of measurement, the agreement between data substantiates the viscosity results.

As mentioned, the viscosity results have indicated the presence of a yield stress in the material. Hence, the data were replotted in a form

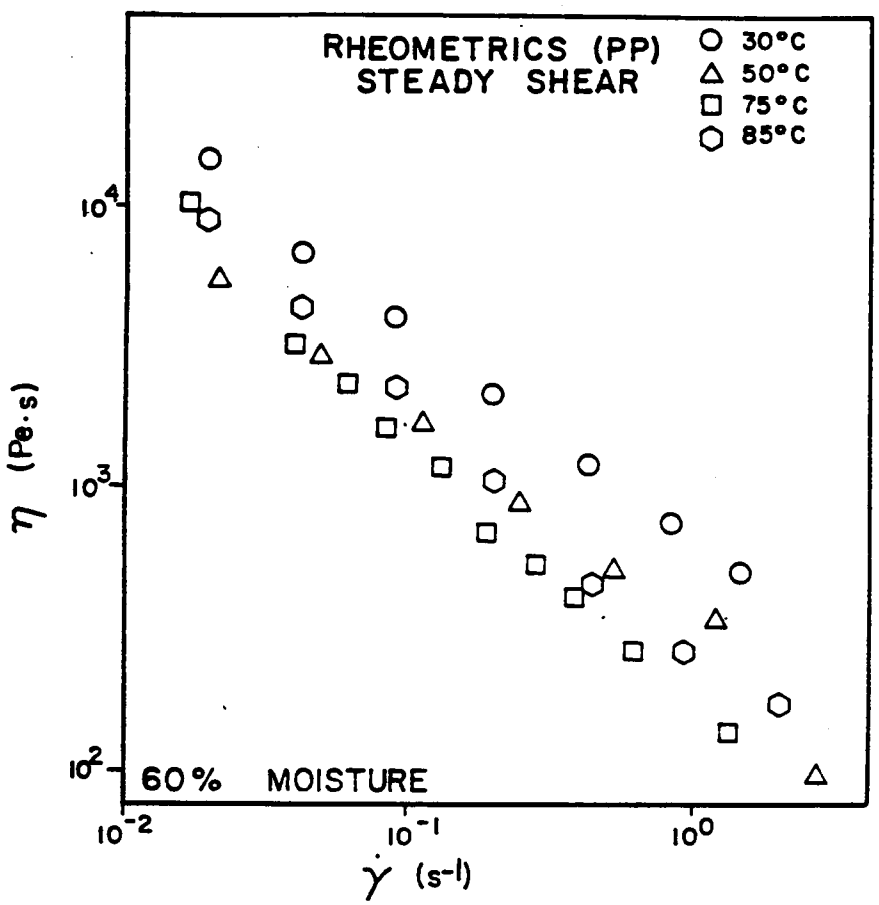

Figure 39. Rheometrics steady shear viscosity curves for 60% moisture dough

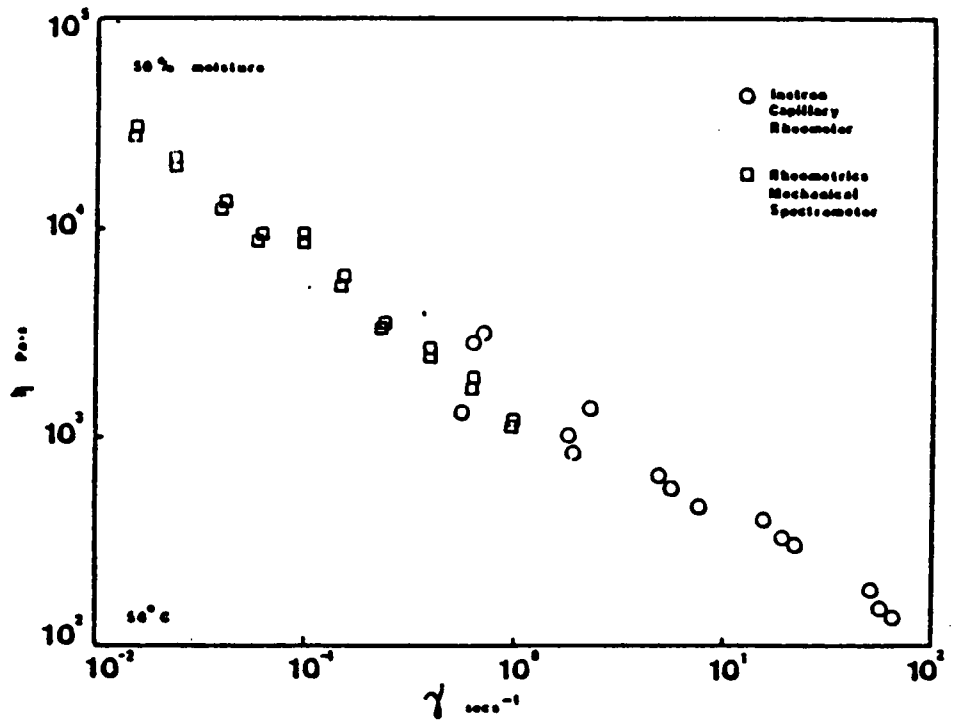

Figure 40. Capillary rheometer data compared to plate/plate steady shear data

from which the yield stress could be determined. In Figure 41 is displayed the replotted data. The shear stress value at which the slope of the viscosity versus shear stress curve becomes infinite indicates multiple values of viscosity for a constant shear stress. This shear stress value is the yield stress for the material.

The yield stress is seen to be a function of temperature. As the temperature increases, the yield stress decreases. The relationship between yield stress and temperature is displayed in Figure 42. The yield stress values are seen to be relatively small. In comparison to the results of the capillary rheometry experiments, the yield stress represents approximately 10% of the shear stress or less at the shear rates experienced in the capillary rheometer. The dependence of the yield stress on temperature is also seen to be relatively small.

Viscosity for the 50% added moisture soy dough has now been determined as a function of shear rate, temperature, and moisture content. The dependence on shear rate and temperature is used in determining the model to represent the viscosity. The dependence of viscosity on moisture content was found solely to determine if variations in moisture content could greatly affect viscosity measurements. It is not a goal of this research to model the the viscosity as a function of moisture content. The 50% added moisture soy dough is the sole material of interest. Also, the presence of a yield stress in the soy dough was determined as well as its dependence on temperature. All that remains is to determine the best viscosity model to use. This requires finding a model which accounts for the flow geometry, fits the data, and is sufficiently simple to use in the numerical model.

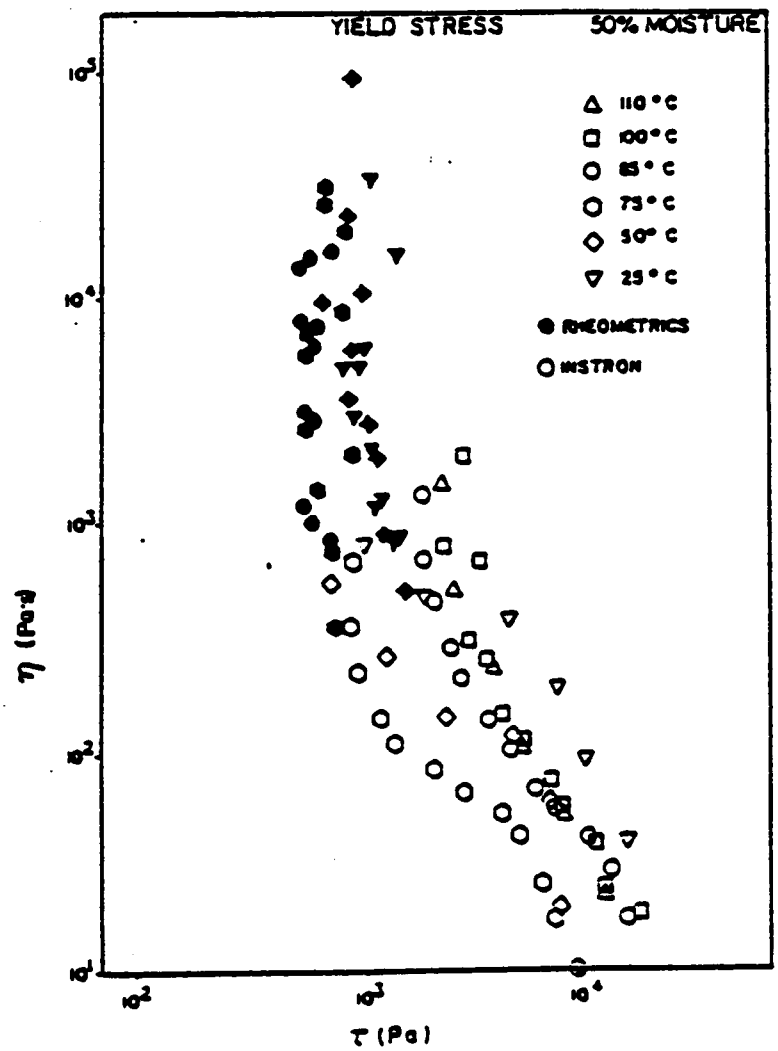

Figure 41. Determination of yield stress for 50% moisture dough

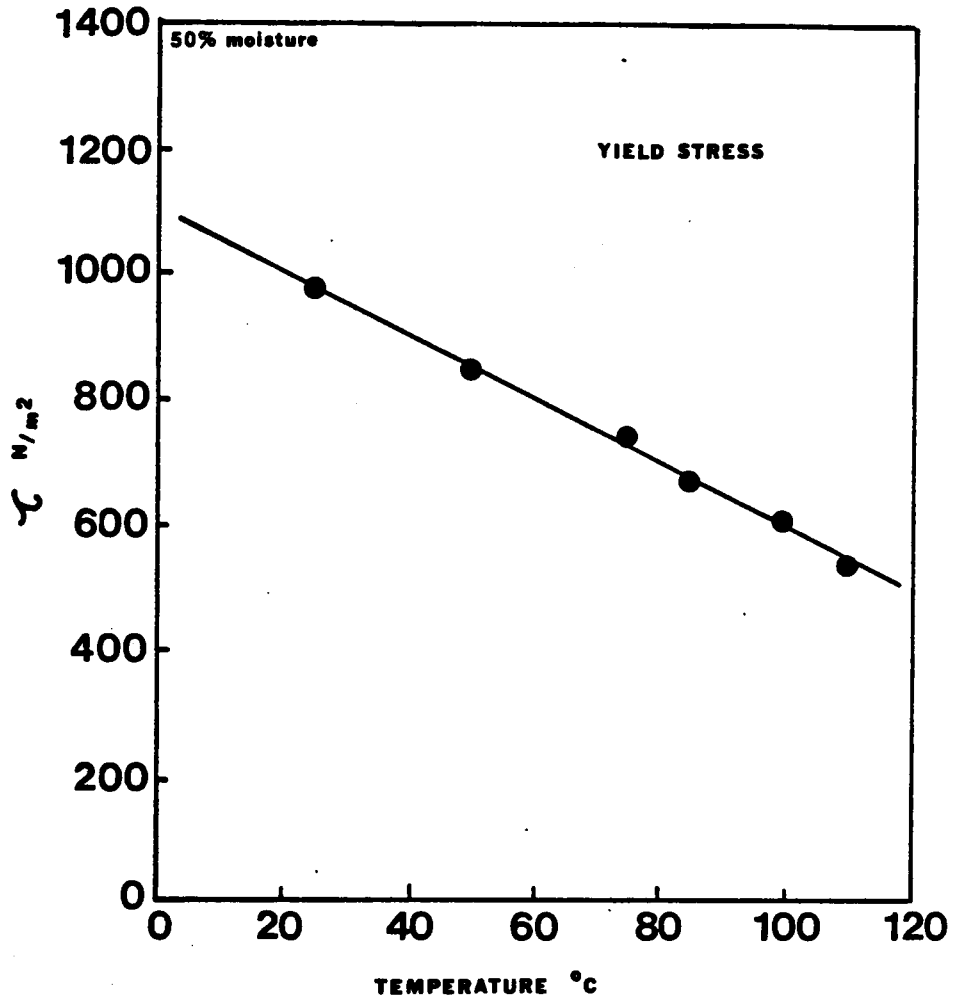

Figure 42. Yield stress as a function of temperature

The last requirement is, in some respects, the most restricting. Problems have arisen in two-dimensional modelling of fluids with viscosities possessing elastic components, specifically instabilities and high Weissenberg numbers. Hence, to avoid these problems which would only be worse in three dimensional modelling, only models which address the viscous effects will be examined. Next, in examination of the flow field it is not known which stresses are important. It is assumed, however, after examination of the velocity components present in the extruder and die that the stresses which predominate are shear stresses. Therefore, with this assumption, an adequate model simply needs to predict shear flow well. Finally, having identified two of the model requirements, the model fit to the data is examined next.

To keep to simple models which predict shear flow well the Generalized Newtonian Fluid (GNF) is examined. The GNF encompasses a family of viscosity empiricisms of which four are considered. They are as follows:

Bingham Fluid

Power Law Fluid of Ostwald de Waele

Casson Fluid

Herschel-Bulkley Fluid

One of the most common GNF empiricisms, the Power Law fluid of Ostwald de Waele is a two parameter model which predicts viscosity as a function of shear rate in a limited range of shear rates under the assumption that a plot of viscosity versus shear rate is linear on a log-log plot. The Bingham fluid exmpiricism is a two parameter model commonly used to model pastes and slurries. A material which follows this model remains rigid when the shear stress is of smaller magnitude than

the yield stress but flows somewhat like a Newtonian fluid when the shear stress exceeds the yield stress [123]. Similarly, the Casson equation, used frequently to model biological fluids includes a yield stress but predicts near Newtonian flow when shear stress is above the yield stress. Finally, the Hershel-Bulkley empiricism is a three parameter model which combines the behavior of the Bingham fluid and Power Law models. Hence, it includes the yield stress with shear rate dependent viscosisty function.

Having examined the viscosity models for a preliminary agreement with the viscosity behavior exhibited by the soy dough, the next step was to evaluate the fit of the viscosity data to the various models. The Casson, power law, and Herschel-Bulkley fluid models were tested for agreement. The Bingham fluid model was neglected because of the low values of yield stresses and high dependence on shear rate of the viscosity curves. Although the Casson equation is thought to have the same detriments as the Bingham fluid model, it is included because of its application in other biological fluids and for a comparison of a model which includes yield stresses to the other models which do not. The results of the fit of these models to the data are shown in Table 9. The details of these calculations are shown in Appendix C.

The results are not conclusive as to one model being better than the others in modeling the viscosity data results. The correlation coefficients for the various models change with temperature. This results in different models displaying the best fit at the different experimental temperatures. For example, based on the correlation coefficients, at 25°C the power law and Herschel-Bulkley models fit the data better than the

TABLE 9

COMPARISON OF VISCOSITY MODEL FIT TO DATA

TEMPERATURE °C	CORRELATION COEFFICIENT		
	CASSON	POWER LAW	HERSHEL-BULKLEY
30	0.93	0.98	0.98
50	0.84	0.93	0.92
75	0.85	0.88	0.90
85	0.96	0.97	0.96
100	0.96	0.92	0.94

Casson equation. In contrast, at 85°C, the Casson equation models the data better than the other two models investigated according to comparison of the correlation coefficients. However, the yield stress in the Casson model, due to the method of evaluation of the fit of the equation, was calculated from the shear stress versus shear rate data. Although the correlation coefficient for the model suggests that the Casson equation is the best fit, comparison of the predicted yield stress, 3109 Pa, to that calculated from the data, 668 Pa, shows a large discrepancy. Hence, the Casson equation is not the best fit to the data regardless of what the correlation coefficient results imply.

Therefore, the power law and the Herschel-Bulkley equations are concluded to be the better models for the data. From comparisons of the correlation coefficients of the two models at the various temperatures, the power law equation appears to be the better of the two models for viscosity over the whole temperature range. Except for the data at 100°C, the correlation coefficient for the power law model was the same or better than that for the Herschel-Bulkley model. This is contrary to what is expected as the power law equation neglects the yield stress present in the system. For the most part, however, the values of the correlation coefficients are close for the two models. Therefore, the power law equation can not be concluded to be conclusively the best model especially as the yield stress, however small, is not included in the model. Consequently, the Herschel-Bulkley model is concluded to be the best model for the data as the model includes the yield stress as well as the shear dependence of the viscosity.

Although the Herschel-Bulkley equation has been concluded to be the best model for the 50% moisture soy dough viscosity, the power law equation is chosen for use in the numerical model. The following are the Power Law viscosity constants as determined at the different experimental temperatures:

TEMPERATURE	n	m
25	0.29	71152.8
50	0.28	23922.7
75	0.21	21006.5
85	0.40	13261.0

The power law equation has been shown to adequately model the viscosity data as indicated by the correlation coefficients. In addition, the power law equation is simpler to employ as a yield stress is not included in the model. Hence, conditional shear rates above and below which the deformable solid versus fluid flow models apply, do not have to be programmed into the model. Finally, the finite element program already has the ability to handle a power law constitutive equation.

Now that the model for the viscosity of the 50% added moisture soy dough has been decided, the major objective of the rheological experiments has been achieved. However, some additional rheological experiments were performed in an effort to gain some insight into the behavior of the soy dough, in particular its behavior as a function of temperature. The experiments and their results are now presented.

To begin, dynamic mechanical experiments were performed on both the 50 and 60% added moisture soy doughs. Strains of 1, 10, and 99% were used

in testing. A strain within the linear region of strain, in theory, should give information as to the presence of a structure in the material. The small oscillation at the 1% strain is more of a vibration which reflects the material structure without breaking it up. In contrast, a strain of 99% approaches the results for the steady shear experiments, essentially breaking up any structure in the material just as in the steady shear experiment. An intermediate strain was included for comparison.

The results of these experiments for the 50% moisture dough are shown in Figure 43. Data for a strain of 99% are not included as the sample became discontinuous and came out of the gap. The dynamic viscosity results for both strains, 1 and 10%, are greater than the steady state viscosity measured and reported previously. This behavior is indicative of a structure in the material. This structure is partially broken up with increasing strain to 10% as indicated by the slightly lower values for viscosity. For the 1% strain experiments, the results reflect the same temperature dependence as the RMS steady shear experiment. However, the 10% strain experiments exhibit the same temperature dependence as the capillary rheometer results where the viscosity decrease with temperature up to 75°C but increases at 85°C. No explanation is offered for this behavior as the only change experienced by the sample is increased strain. As the steady shear viscosity results which in essence, represents the results of a sample experiencing greater strain do not exhibit the behavior of the 10% strain data, the change in behavior cannot be assumed to be caused by the increased strain. Therefore no explanation can be postulated.

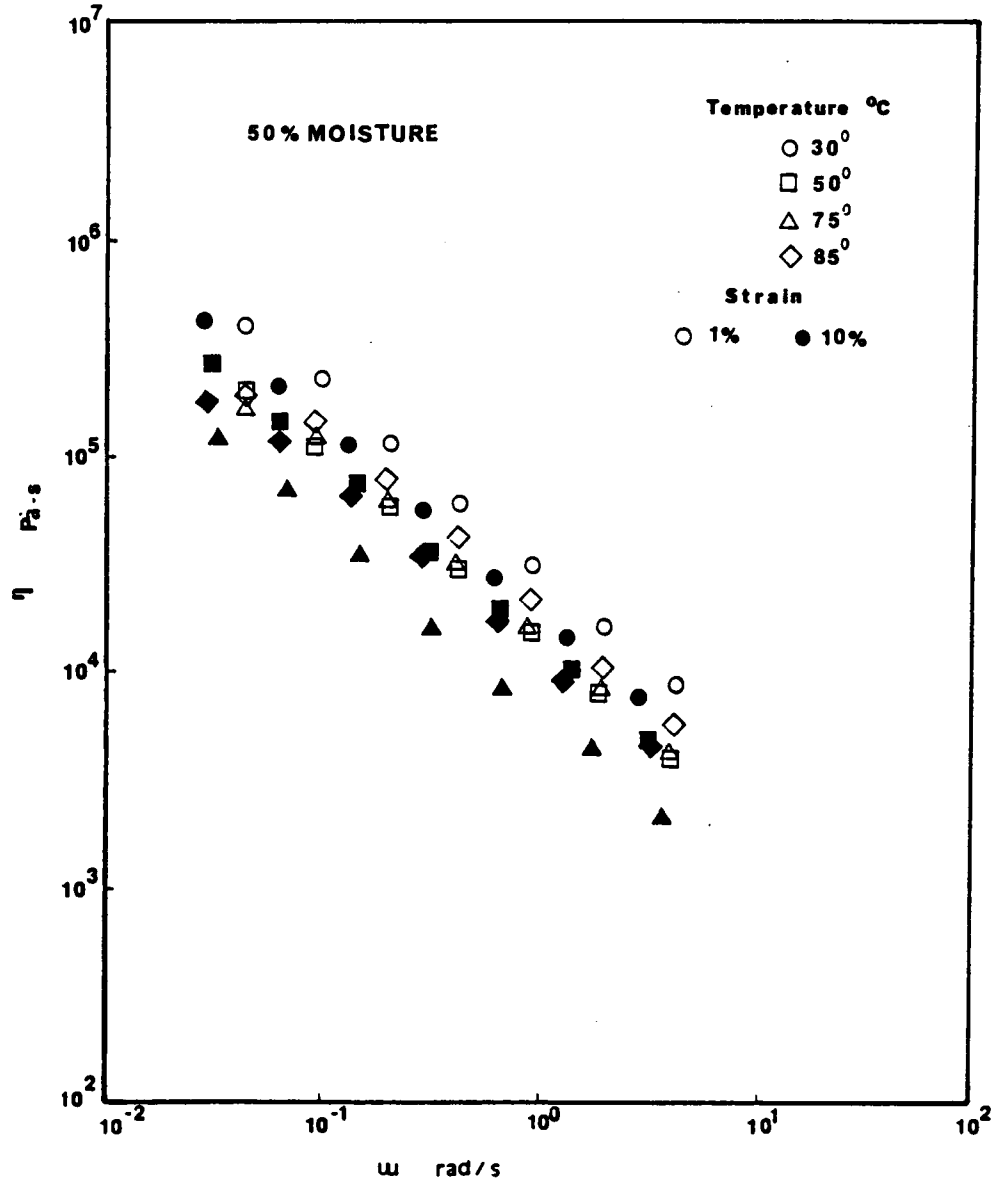

Figure 43. Dynamic viscosity curves for 50% moisture dough

The results of the dynamic mechanical experiments for the 60% added moisture dough are shown in Figure 44. These results are similar to those of the 50% moisture dough. The dynamic viscosity results for both the 1 and 10% strain experiments are higher than the steady shear viscosity determined previously. As stated, this indicates a structure in the material. The 99% strain data reflects the results of the steady shear experiments with the dynamic viscosity values falling within the error limits of the steady shear viscosity. The fact that the 10% strain data is lower than the 1% strain data but higher than the 99% strain data demonstrates that the increase in strain to 10% partially breaks up the structure while the increase in strain to 99% breaks up the structure to the same point as the steady shear experiments. No abnormal temperature depedence is observed. For the most part the values are within the error limits of the other temperature values similar to the behavior of the steady shear results. From the results of these experiments, then, it can be concluded that there is an inherent structure to the soy dough which can be disrupted by shear.

Another set of dynamic mechanical experiments examined the irreversibility of the soy dough. It was seen in the capillary rheometry experiments that whatever structure was created in the soy dough upon heating remained in the dough. Dynamic viscosity experiments were carried out under the following temperature conditions. The first experiment was at 30°C, the second at 85°C, the third heated to 85°C and cooled to 30°C, and the fourth heated to 85°C, held 5 minutes and cooled to 30°C. The results of these experiments are shown in Figure 45. The viscosity curve for the experiment carried out at 30°C is higher than the viscosity curve

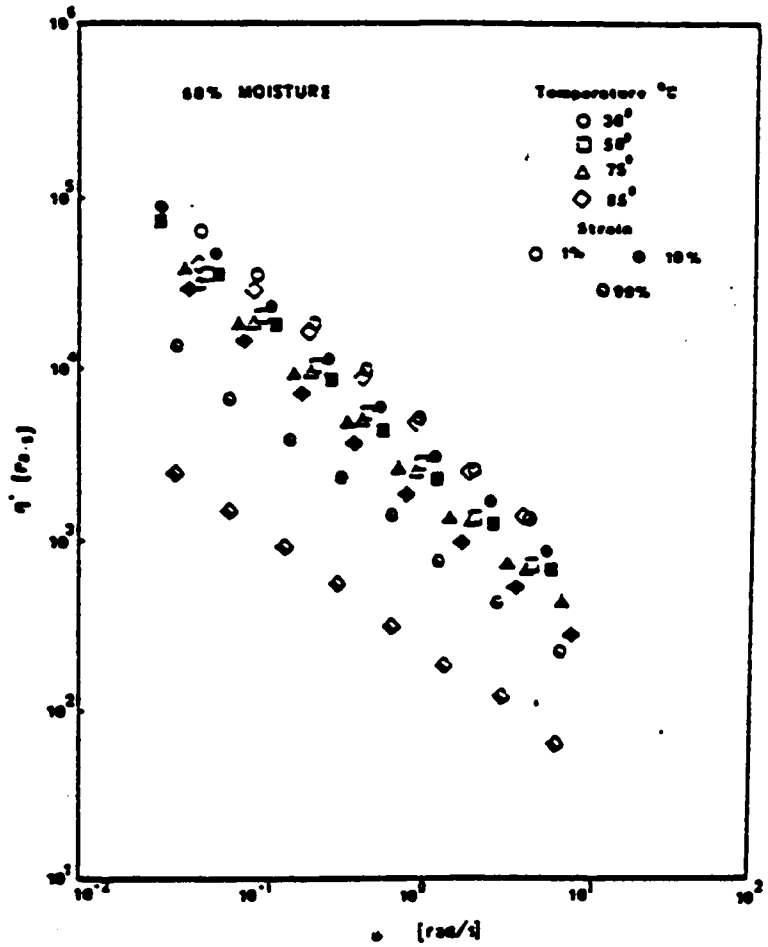

Figure 44. Dynamic viscosity curves of 60% moisture dough

for the experiment carried out at 85°C as expected. However, the other two experiments yield viscosity curves comparable to 85°C results even though the actual viscosity measurement occurred at 30°C. Hence, from a different set of experiments it is again concluded that the structure formed at elevated temperature, specifically 85°C, is irreversible.

A discrepancy is found in these results, however. This set of experiments was performed on a 60% moisture dough. In the capillary rheometer experiments the rise in viscosity, linked to the formation of a structure in the dough, occurs at 100°C for the 60% moisture dough. This discrepancy can be explained in terms of the conditions of the experiments. The viscosity found by capillary rheometry is determined at higher shear rates whereas the dynamic viscosity is investigated at low strain. Hence, it is possible that the development of structure would be observed at a lower temperature at the lower strain. Since there is additional moisture in the 60% moisture dough, the high shear rates of the capillary rheometer could be disrupting the structure at 85°C. The higher moisture content of the dough might require a higher temperature to firmly establish the structure so that it is not disrupted in shear.

In the final set of experiments, the development of structure in the 50 and 60% moisture soy dough is examined as a function of time. The storage modulus, G', was monitored as a function of time at various temperature conditions. The results for the 50% moisture dough are shown in Figure 46. The storage modulus is seen to be essentially constant over the 28 minute experimental time range for the 30°C experimental temperature. For the 85° experimental temperature, the storage modulus is seen to increase over time, eventually reaching the value exhibited by the 30°C

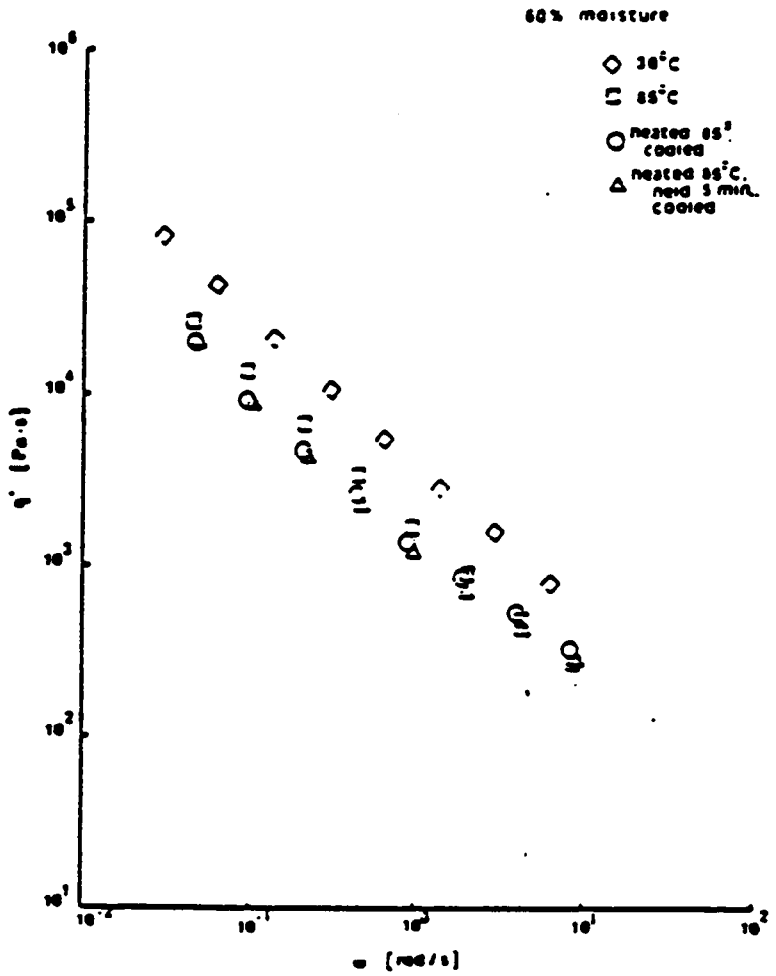

Figure 45. Irreversibility of heat treated soy dough

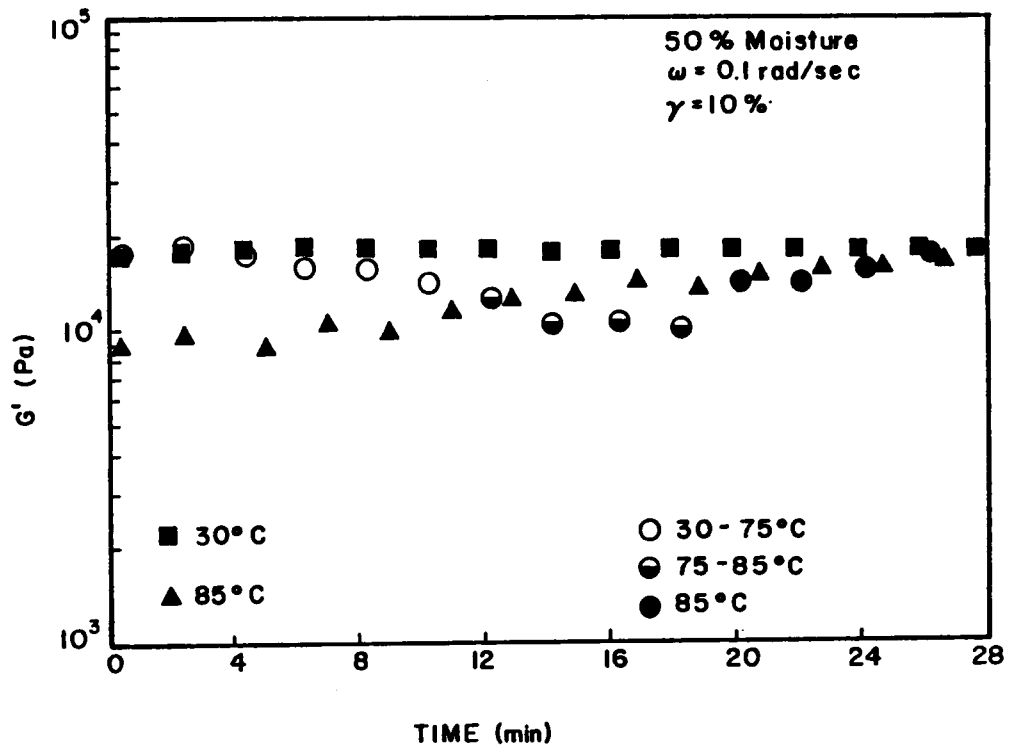

Figure 46. Storage modulus vs. time for 50% moisture dough

sample. Even though the graph displays data only up to 28 minutes, the experiment was continued past the 28 minutes and the 85°C results were seen to level off at the same value as the 30°C results. Finally, the storage modulus was monitored as the sample was heated from 30°C to 85°C. From 30 to 75°C, the modulus is essentially constant reflecting the same value as the constant 30°C experiment. Over the 75 to 85°C temperature range the modulus decreases in value to the value initially displayed by the constant 85°C experiment. Once the sample reaches 85°C, the modulus increases once more to the value exhibited at 30°C and remains constant for the remaining experimental time interval.

Similar results are exhibited by the 60% moisture dough as shown in Figure 47. The change in modulus as a function of time and temperature is much more dramatic than for the 50% moisture dough results. For the constant 85°C temperature experiment, the modulus constantly increases over a 12 minute time period, then levels off for the remainder of the experiment. The other data shows the results for the sample as it is heated. For the 40 to 75°c temperature range, the modulus decreases with temperature. The 75 to 85°C temperature range data gives a constant modulus. Finally, once the temperature reaches 85°C, the modulus increases with time to the same value achieved by the constant 85°C experiment. From these experiments then it can be concluded that the structure which develops in the soy dough at 85°C is a function of time.

5.3 DIFFERENTIAL SCANNING CALORIMETRY

Differential scanning calorimetry (DSC) is used to determine the presence and nature of a reaction occurring in the soy dough during

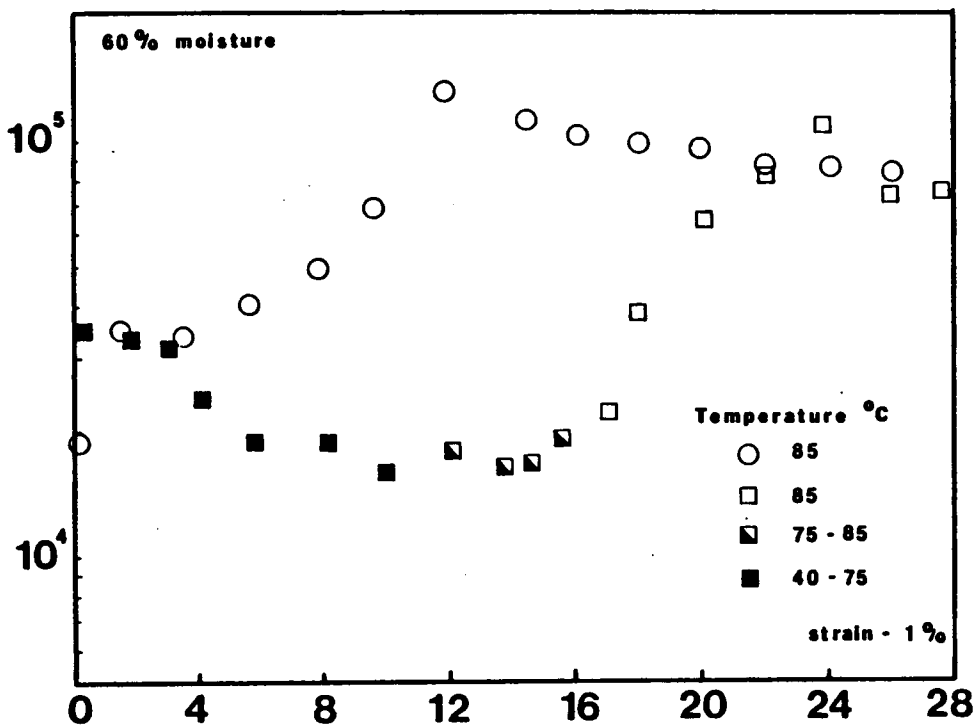

Figure 47. Storage modulus vs. time for 60% moisture dough

cooking. Also, the heat capacity as a function of temperature is measured using this experimental technique. To begin, this section discusses the results involved in the determination of the cooking reaction. In order to understand these results in light of the literature, samples having moisture contents ranging from 0% added moisture up to 70% added moisture are employed in experimentation. However, experiments concentrate on the material of study, the 50% added moisture soy dough. Various experiments involving heat and shear treatment are performed to determine the nature of the reaction. These experiments and others, as well as their results, are discussed. The second part of this section discusses the heat capacity of varying moisture content soy doughs with regard to temperature and shear dependence.

5.3.1 HEAT OF REACTION

In this section a description of the various experiments performed in the determination of the cooking reaction of soy dough is presented. The results of these experiments are then discussed as they relate to the cooking reaction. The experiments are outlined in a logical progression presenting the results from which the conclusion concerning the inclusion of the heat of reaction in the modeling process can be drawn. The details of each experiment are explained and the significance of the results are presented. All experiments followed the experimental procedure outlined in Chapter Three. The DSC scans presented in the figures are representative of the repetitive experimental runs. In all cases, as mentioned in Chapter Three, a minimum of five experiments were performed under the same conditions to establish repeatability of the results. Small vari-

ations in peak area are observed but are expected due to the natural variations of the soy system as well as small variations in the moisture content of the sample incurred in sample preparation or due to relative humidity.

In the first experiment performed, the effect of added moisture upon the soy dough was examined. Experiments were performed on samples ranging from 0% added moisture to 70% added moisture. This wide range of added moisture samples encompassed most forms of the soy flour moistures; from dry flour to dough consistency to dispersion in water. The results from these experiments are presented in Figures 48 and 49. In Figure 48 is displayed the results for 0% to 20% added moisture samples whereas in Figure 49 is displayed that of 30% to 70% added moisture. The characteristic scan of the two figures is seen to be very different. In Figure 48, one large peak is exhibited by all samples. The energy associated with the endothermic reaction represented by this peak is approximately 25 cal/gram. No particular trend was noticed in terms of the energy associated with the endothermic reaction as a function of moisture content in this range of moisture. In the second figure, Figure 49, the scans now exhibit, for the most part, two very small peaks. The energy associated with these endothermic reactions is on the order of one cal/gram or less. Again, no correlation of the energy associated with the endothermic reaction to the moisture contents was found. Additional experiments were performed with samples having moisture contents between the 20 and 30% range. Up to 24%, the results mirrored those of the lower moisture samples. Between 24 and 28%, varying results were obtained. Some samples exhibited the one larger peak, and others, at the same moisture content,

exhibited the two small peaks. From 28 to 30% moisture content, two small peaks were consistently observed. For the range of 24 to 28% moisture content, the inconsistent results were attributed to variations in the dispersion of the water throughout the sample. Hence, the division between the two types of behavior is concluded to be between 24 and 28% added moisture.

The two different behaviors of the soy mixtures depending upon moisture content can be attributed to two different types of interaction occurring in the system. The behavior exhibited in the higher moisture soy doughs and dispersions has been previously documented by Hermansson [80]. The small endothermic peaks are representative of the denaturation of the protein fractions. The energy associated with these peaks is of the correct order of magnitude and the temperature range agrees with that previously published as the range of denaturation. Also, as mentioned in the literature review, soy consists of four major protein fractions, two of those fractions present in much larger amounts than the others. Hence, the two small peaks could represent the denaturation of those two protein fractions. The other fractions are either too small to be noticed or are incorporated in the two peaks exhibited, i.e., their denaturation temperature is the same as one of the other fractions.

The behavior of the lower moisture soy systems is not as easily explained. As stated in the literature review, the energy associated with denaturation is on the order of 1 cal/g. Hence, the energy associated with the endothermic peak is too large to represent solely denaturation of proteins. Hence, some other type of interaction must be associated with the endothermic reaction. Denaturation of the protein molecule may still

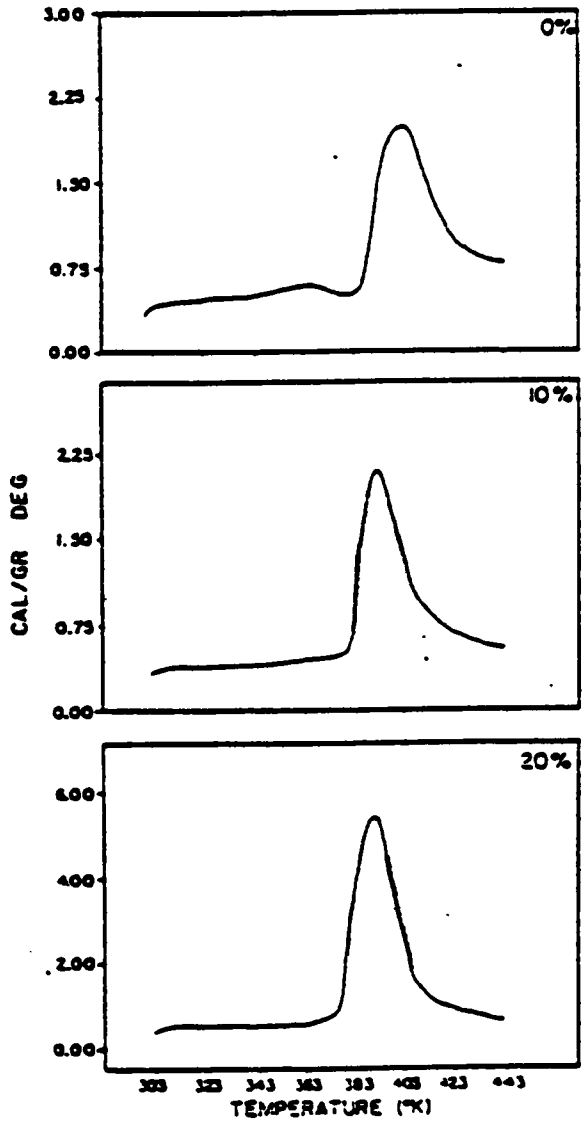

Figure 48. DSC thermograms for 0 to 20% added moisture soy doughs.

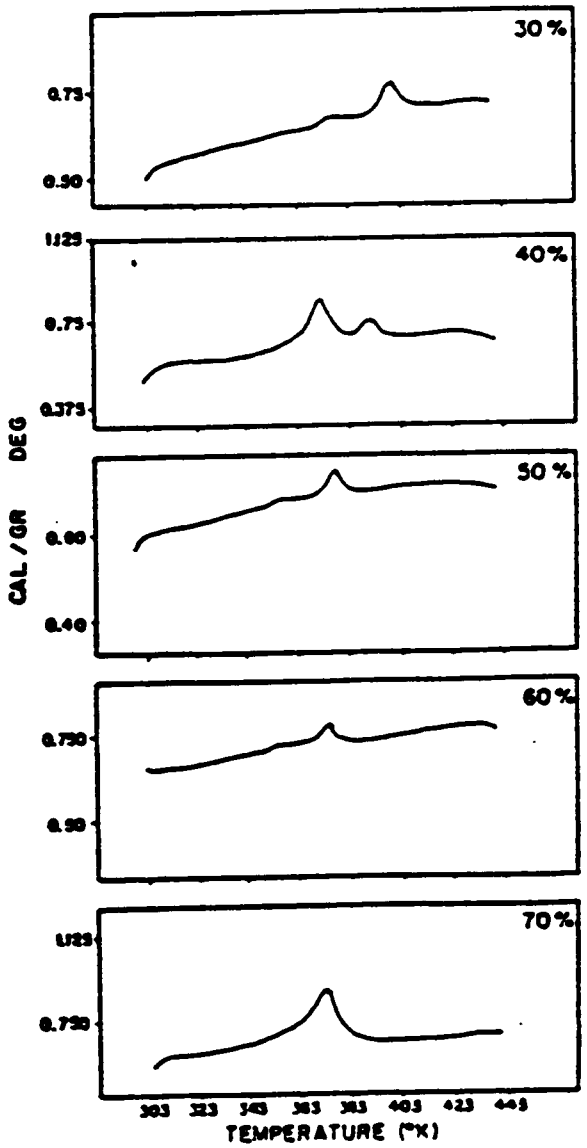

Figure 49. DSC thermograms for 30 to 70% added moisture soy doughs.

occur in the lower moisture system but the endothermic peak associated with this conformational change is masked by the additional endothermic reaction occurring in the system. With the knowledge of protein systems and their interaction with water as presented in the introduction, it is possible to explain the two different behavioral phenomenon. At the higher moisture concentration, i.e., above 28% moisture content, the water forms a continuous phase around the soy protein molecules. Therefore, the molecules are essentially isolated or are in small clusters surrounded by water molecules. In addition, the hydrophobic side chains are turned into the interior of the molecule forming a hydrophobic region isolated from the water, making the molecule more compact. For either reason, few if any inter-molecular interactions between side chains can occur. However, in the lower moisture soy systems, inter-molecular interactions between the side chains of the protein molecule can occur. Hence, upon addition of heat, as undergone in the DSC experiments, the interactions are broken up and displayed as the endothermic peak. Later, this behavior will discussed more in view of other experiments.

In addition to the differing mechanisms, the results of these experiments demonstrate another phenomenon dependent upon the moisture content. Taking the two reaction behaviors separately, upon addition of water the maximum peak temperature of the reaction decreases as water content increases. This behavior holds with that known of the addition of diluents to a system. This behavior, however, is not consistent over the whole range of added moisture but only over the 0 to 24% added moisture range, and then again over the 28 to 70% added moisture range. As the reactions

are different it could not be expected that the maximum peak temperatures could be compared.

One more interesting point to notice is the temperature at which the first peak appears in the 50% soy dough. The first peak occurs approximately at 85°C, the same temperature at which the rise in viscosity was observed as discussed previously. Hence, the rise in viscosity can possibly be linked to the denaturation of proteins in the system. The change in conformation associated with denaturation could cause the increase in viscosity as the result of additional entanglements and interactions arising due to the random coil state of the molecule.

The next experiment performed examined the reversibility of the reaction indicated by the endothermic peak. For all samples, the following procedure was followed. An initial DSC scan was performed on a sample. The sample was then quenched to 25°C and re-scanned, again recording the results. The results for the two characteristic responses are shown in Figures 50 and 51. Figure 50 is characteristic of the samples exhibiting the lower moisture reaction and Figure 51 is characteristic of the samples exhibiting the higher moisture reaction. These experimental results demonstrate that for either reaction mechanism, the change which is involved with the endothermic reaction is irreversible, at least for the length of time studied. The length of time between repetition of the experimental run was approximately 30 minutes from the beginning of the quench to the start of the re-scan. As some reversal processes can be extremely slow in occurring, an additional experiment was performed where the sample after being quenched, was left in the pressure capsule and refrigerated overnight. It was then re-scanned approximately 24 hours after being

quenched. Again, regardless of the sample moisture and hence, the reaction mechanism, the re-scan was completely featureless demonstrating the irreversibility of the reaction. With regards to the higher moisture reaction mechanism surmised simply to be denaturation of the proteins in the system, this behavior agrees with that found for most proteins. Although some proteins have been found to renature; for the most part, denaturation is an irreversible process. Therefore, if the reaction behavior of the lower moisture system is attributed to inter-molecular interactions involved with the conformation of the proteins before denaturation, then this reaction mechanism would also be irreversible.

Throughout the extent of this investigation, the reversibility of all reaction exhibited was tested. In all cases, the re-scan of the sample proved void of any peaks indicating a reaction and therefore reversibility. Hence, although the reactions observed may be different depending on moisture content, as shown so far, or temperature and shear treatment, as will be discussed; they all are irreversible in nature.

So far, simply the as-mixed samples have been investigated. The next step is to explore the response of heat and shear treated samples as the soy dough experiences both heat and shear during cooking extrusion. Samples of the extrudate from viscosity measurements on 50% soy doughs using the capillary rheometer were collected. The DSC scans of these samples are presented in Figure 52. An as-mixed sample is included for comparison. The sample, from which viscosity at room temperature was determined using capillary rheometry and hence simply experienced a shear environment, exhibited the same results as the as-mixed sample. Therefore, the scan labelled as-mixed is, in fact, characteristic of both the as-mixed and

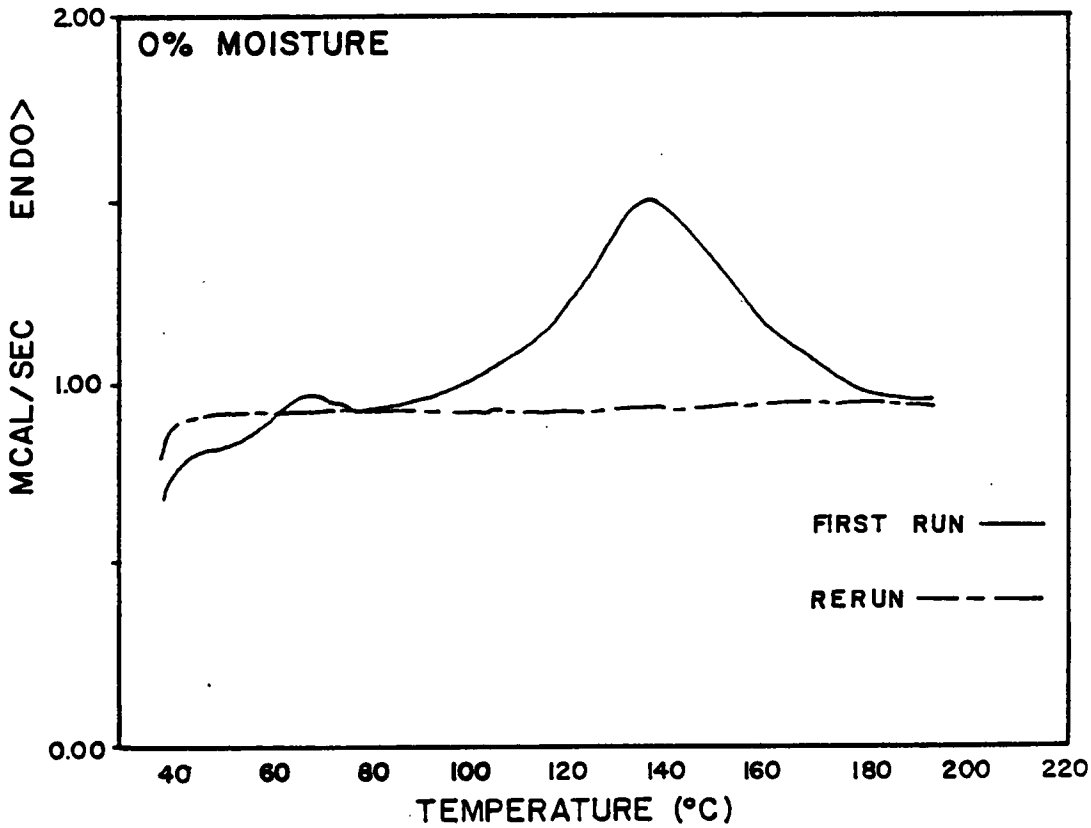

Figure 50. Comparison of initial and rerun thermograms of lower moisture soy dough.

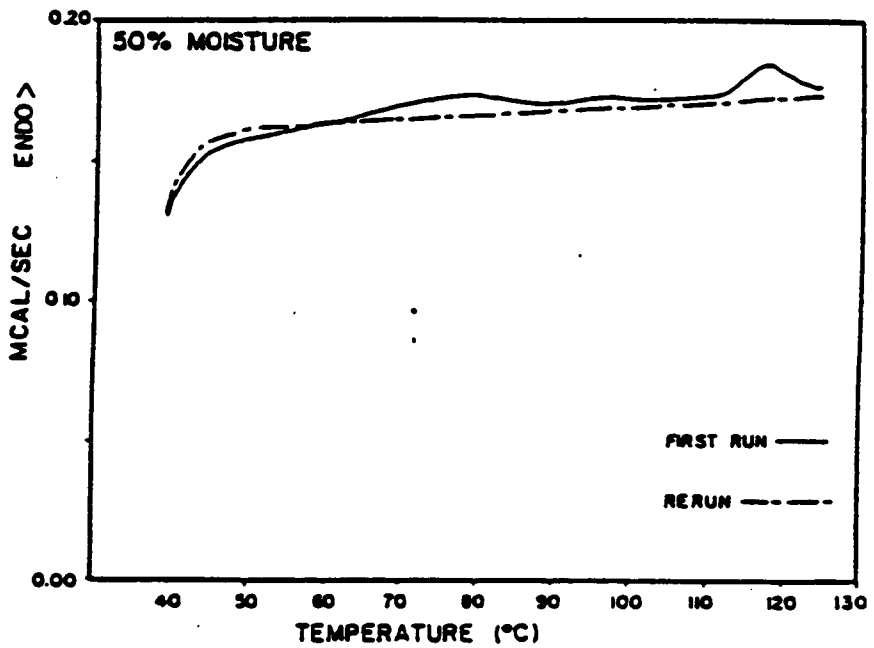

Figure 51. Comparison of initial and rerun thermograms of higher moisture soy dough.

the room temperature extrudate. This implies that at least for the range of shear rates experienced in the capillary rheometer shear does not affect the response of the soy dough. In addition, the same results as the as-mixed sample are exhibited by the samples heated to 50 and 75°C. Therefore, not only does shear experienced by the dough in the capillary rheometer not have any effect on the reaction mechanism, but also temperatures up to 75°C. A slight increase in the maximum peak temperatures can be observed. This behavior, however, can be attributed to a slight drying of the sample due to exposure to the higher temperature and subsequently the collection procedure.

However, the sample which experienced the 85°C experimental temperature exhibited a very different behavior displaying a large endothermic peak representing approximately 125 cal/g of energy. The first small peak no longer is present. The second peak is no longer present in the same form as in the previous scans. If the reaction corresponding to the second small peak was still present, it would be masked by the larger peak shown in the scan. The larger peak encompasses the temperature range of the second samll peak and hence, the energy associated with the small peak would simply be incorporated in the energy associated with the larger peak.

Perhaps, however, this large endothermic peak is in actuality the same reaction represented by the second small peak. It is possible that the reaction mechanism is not denaturation as first postulated but some mechanism that could be enhanced due to the conditions experienced in the capillary rheometer at 85°C. The onset of the reaction occurs at approximately the same temperature; hence this too is a possible explanation.

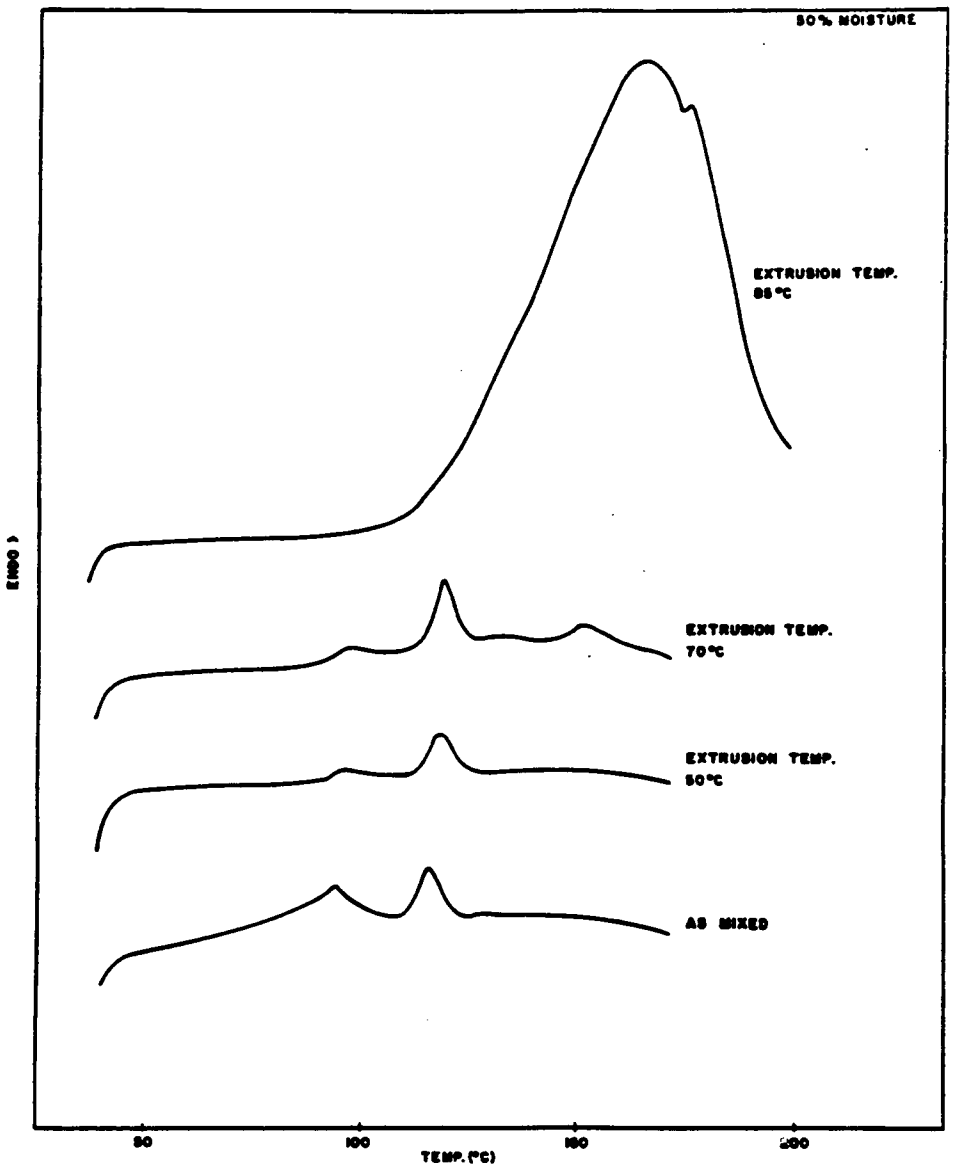

Figure 52. DSC thermograms of extrudate samples from the capillary rheometer.

It is significant to note that the key temperature associated with the large endothermic reaction was 85°C, the temperature at which the first small peak of the as-mixed sample occurred. This first small peak is no longer present in the 85°C sample scan. Therefore, it can be concluded that the denaturation of the protein fraction associated with this peak occurred during the capillary rheometry experiments. Hence, it can be postulated that the denaturation of this protein fraction may in some way be responsible for the large endothermic reaction. In addition, as mentioned earlier in connection with the increase in viscosity at 85°, it is seen that the proteins are in fact denatured at the 85°C experimental temperature. The increase in viscosity may then be linked to the denaturation of the proteins.

Another interesting observation is gained through this experiment. As stated, the samples used in this series of experiments were collected from capillary rheometry measurements. They were sealed in plastic and refrigerated overnight with the DSC experiments being performed the following day. Whatever is occurring in the soy dough when it experiences the 85°C temperature that generates the endothermic reaction observed is irreversible. Again, this statement is limited to the time frame of investigation. Therefore, not only is the endothermic reaction irreversible as proven by the re-scan of the sample, but also the generation of the interactions responsible for the endothermic reaction displayed by the 85°C sample.

The results pertaining to the 85°C sample are of question. If the sole reason for the generation of the large endothermic peak in the sample is the exposure to an 85°C environment and consequently the denaturation

of the proteins, then why is a large peak not found on the DSC trace. The sample experiences 85°C and denaturation of the proteins occurs during any DSC experiment performed so far. Hence, something else besides the 85°C environment must contribute to the generation of the endothermic reaction. In an examination of the processing of the two samples, it is seen that there are two major differences. The first is the fact that the sample from the capillary rheometer is not only heated to 85°C but also sheared at that temperature. The second is the heating conditions to which the samples are exposed are different. The former explanation does not seem particularly plausible as the shearing had no effect on any of the other samples at the lower temperatures. It is still regarded as a possible explanation but for this time is ignored and the latter explanation is more thoroughly investigated.

First, the two heating conditions will be discussed. In the DSC experiment, the sample undergoes continuous heating at a rate of 10°C/min. The sample is not only heated to 85°C but continues to heat at the constant rate up to 160°C. In contrast, the sample from the capillary rheometer is heated up to 85°C with an unknown heating rate and then is kept at 85°C throughout the experiment. A capillary rheometer experiment takes approximately 25 minutes to perform. Hence, the sample from the capillary rheometer experiences the 85° environment for much longer amounts of time. To test out this theory as to the length of time the sample undergoes the 85°C environment, an experiment was performed where the sample was allowed to soak (incubate) at 85°C in the barrel of the capillary rheometer before the viscosity was measured. The viscosity of this sample was found to be the same as the samples measured without any

soak time at 85°C. However, a much larger endothermic reaction is now exhibited when the sample is run on the DSC as shown in Figure 53. The original 85°C sample scan is included for comparison. The reaction is seen to begin at approximately the same temperature although the shape of the peak is different than that of the original 85°C sample. The energy associated with this reaction is almost twice as large, now approximately 225 cal/g. Therefore, it can be concluded that the length of dwell time at 85°C controls the energy associated with the endothermic reaction.

The role of shear in the generation of the large endothermic peak has still not been reconciled. Although it was found that the length of time that a sample was held at 85°C influenced the reaction, shear was still a component of the experiment. Therefore, experiments devoid of shear which employed different dwell times at 85°C were performed. The experiments were performed using the DSC. The samples were placed in the sample capsules and to begin, the DSC was operated in the isothermal mode. This involved raising the sample quickly to the set temperature of 85° and allowing it to soak at that temperature for varying amounts of time. The sample was then quenched to 25°C and the normal DSC experiment performed. The results from two different sample soak times are shown in Figure 54. The DSC results of the sample with soak time of five minutes exhibit one small peak. This peak corresponds to the second peak of the as-mixed sample. The absence of the first peak indicates that the denaturation of the proteins associated with that peak has occurred during the 85°C soak period. These results were expected for this soak time. The DSC results of the sample experiencing a soak time of 35 minutes are also presented in Figure 54. These results are not the expected ones. From the results

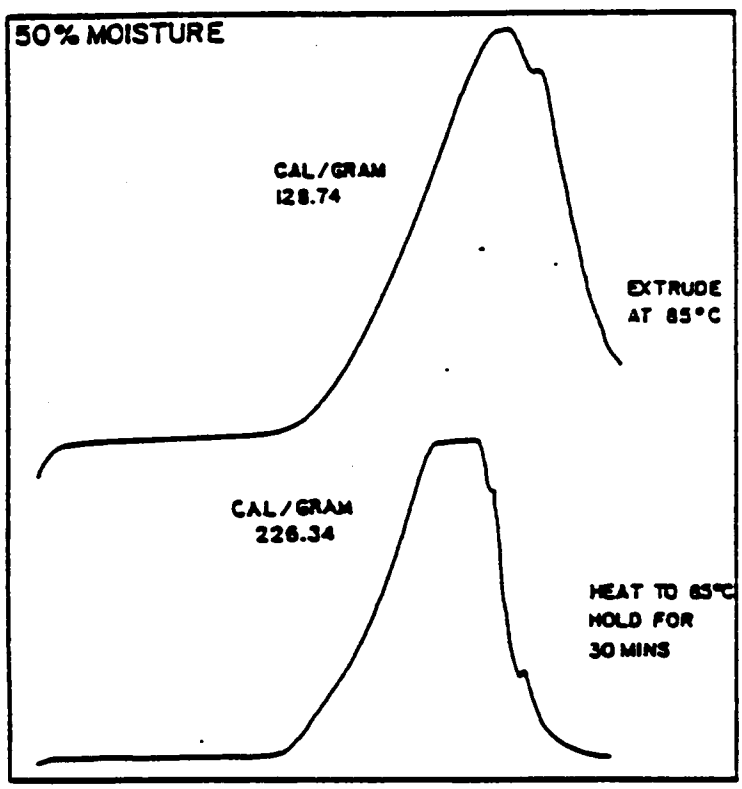

Figure 53. Comparison of DSC thermograms of samples experiencing 0 and 30 minute soak times at 85°C in the capillary rheometer.

of the experiments involving the capillary rheometer samples, it was concluded that holding the sample for 30 minutes at 85°C was one of the controlling factors in the generation of the large endothermic peak. However, exposure of the sample to 85°C for a length of time longer than that needed to generate the peak in the capillary rheometer did not generate any large peak. In fact, the energy associated with the one peak exhibited in the scan of the sample held at 85°C for 35 minutes in the DSC is less than 1 cal/g. Essentially, the results from this experiment are the same as those for a soak time of only five minutes. Therefore, although the denaturation of the proteins associated with the first small peak occurred nothing occurred in the sample to generate the large endothermic peak as seen in the 85°C sample from the capillary rheometer.

Hence, the possibility of shear also contributing to the generation of the large peak is probable. Only one other condition is different between the two experiments. In the capillary rheometer, the sample is heated in the bulk whereas in the DSC samples were very small, approximately 20 mg in weight. It is possible that the samples were too small or an inadequate sampling was taken to create the interaction necessary for the endothermic reaction to happen.

As shear is the parameter of question in generation of the large endothermic peak, more controlled experiments were developed to create and monitor sheared samples. A Rheometrics Mechanical Spectrometer (RMS) was used in this set of experiments. The response of samples exposed to shear at 85°C as well as the other temperatures previously investigated was tested. Basically, each experiment conducted at a specific temperature consisted of two parts. In the first part, the response of a sample

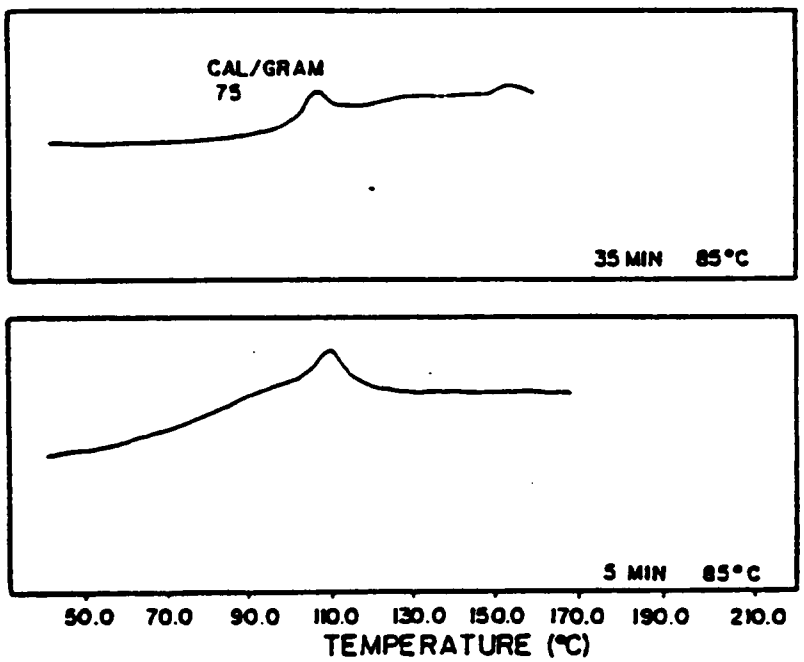

Figure 54. Comparison of DSC thermograms of samples experiencing 5 and 35 minute soak times at 85°C in the DSC.

simply heated in the RMS was examined. In the second part, the response of a sample experiencing both heat and shear in the same instrument was investigated. A comparison of the results for the two samples may determine the direct contribution of shear as both samples experienced heating under the same conditions.

The first experiment tested the response of a sample exposed to shear but not heat. The results are shown in Figure 55. Once more, two small peaks are exhibited in the DSC scans of the soy sample. From these results it is seen that shearing has no effect upon the room temperature sample. Only one small difference is exhibited. The maximum peak temperature is shifted to a lower temperature. This may be explained with regards to the possible loss of moisture due to the handling of the samples under shear conditions or simply the natural variation in the soy dough. Figure 56 presents the results of samples heated to 50°C. Here again two small peaks are observed. However, shearing begins to exhibit some effect as the energy associated with the second peak in the heated and sheared sample is five times as great as that of the sample simply heated. However, the energy is still on the order of 1 cal/g and definitely not reflective of the energy associated with the large endothermic peak seen previously. The difference may possibly lie within the natural variations of soy dough. Finally, the experiment was performed with samples heated to 85°C. The results of this experiment are shown in Figure 57. These results demonstrate a definite dependence of the generation of the endothermic peak upon shearing. The energy associated with the peak displayed by the heated and sheared sample is much larger than the energy associated with the sample that was simply heated. However, it is still

not of the magnitude of that generated in the capillary rheometer. This discrepancy is justified by two possible explanations. One, the shear experienced by the samples in the capillary rheometry experiments is much greater than that experienced by the samples in this experiment. Two, the samples were held at 85°C for a longer amount of time in the capillary rheometer than in these experiments. The capillary rheometer was pressurized as discussed in the experimental chapter to prevent loss of moisture. Hence, the sample could be left for extended lengths of time without moisture loss. Although precautions were taken to minimize moisture loss in the mechanical spectrometer, moisture is continuously lost through the drying edge of the sample and consequently the experimental time is kept to a minimum. As it was shown that the magnitude of the peak energy increased with soak time, the latter explanation is the more likely one. Based on this explanation, the difference between the sheared and non-sheared sample peak energy may not be as great as the results indicate. Although care was taken to duplicate experimental conditions as closely as possible, the sheared samples did experience a slightly longer time, on the order of one minute, at the elevated temperature. It is questionnable, however, if the minute could make such a great difference.

Up to this point, 50% soy dough has been investigated in its as-mixed state and under varying degress of heat and/or shear. In addition, the response of the soy dough system as a function of moisture was explored. It was found that two basic responses exist as a function of moisture: one broad endothermic peak for the lower moistures and two small endothermic peaks at the higher moistures. Although the combination of

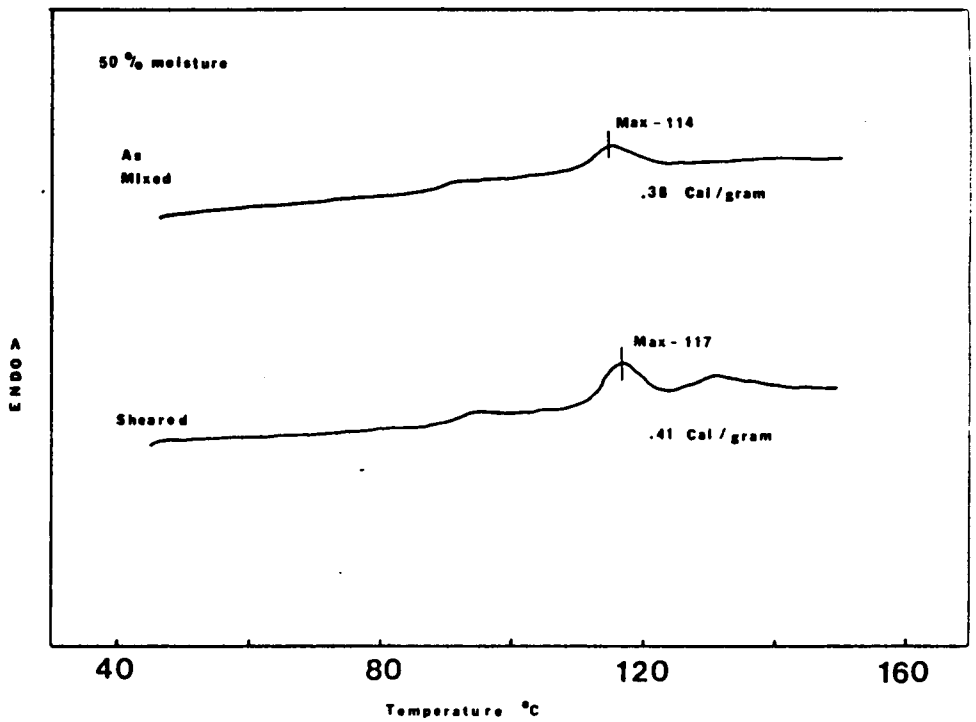

Figure 55. Comparison of DSC thermograms of samples which have and have not experienced shear in the RMS at room temperature.

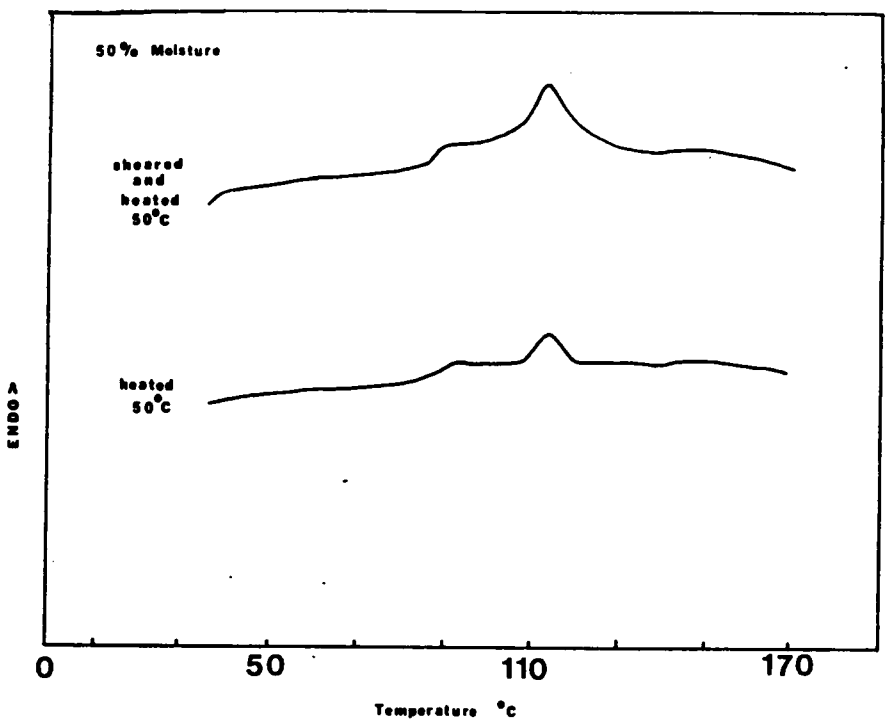

Figure 56. Comparison of DSC thermograms of samples which have and have not experienced shear in the RMS at 50°C.

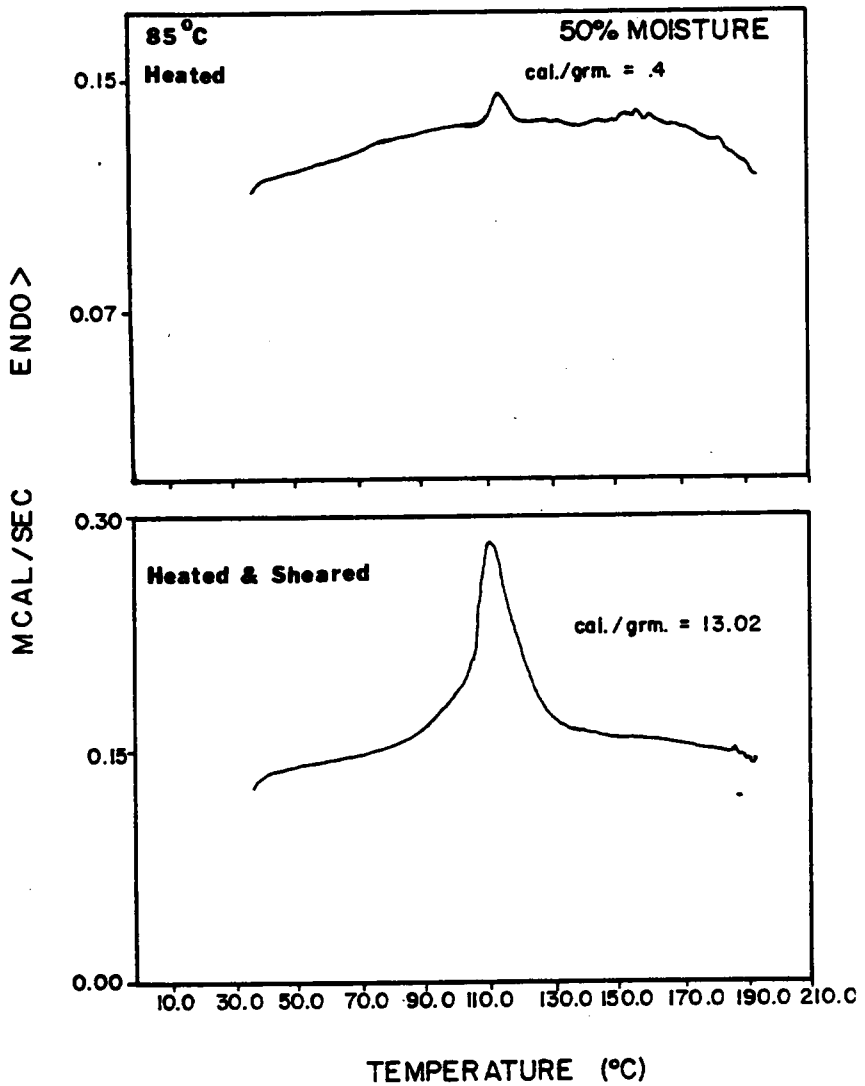

Figure 57. Comparison of DSC thermograms of samples which have and have not experienced shear in the RMS at 85°C.

heat and shear has been investigated, the flow geometry of those experiments was not comparable to that of the extruder. In addition, some questionable results as to the factors responsible for the generation of the large endothermic peak were obtained. It is of particular importance to determine the existence and extent of the endothermic reaction which would occur during the cooking extrusion process. If a large endothermic reaction were to occur in the process, it would have to be accounted for in the numerical model of cooking extrusion. Therefore, to obtain a true account of what would occur in the extruder, experiments involving extruder samples were performed.

To diverge from the material of study for a moment, the results for a 25% added moisture soy mixture extruded at two temperatures, 60 and 99°C, are presented in Figure 58. These samples are taken from the extrudate of an experimental run performed on the laboratory scale extruder. For the sample extruded at 60°C, one large endothermic peak is observed. The energy corresponding to this reaction is approximately 100 cal/g. This is much larger than the 25 cal/g peak exhibited by the as-mixed sample. Hence, it is concluded that the action of extrusion creates interactions which exhibit an endothermic reaction upon heating. The sample extruded at 99°C does not exhibit a large endothermic peak. In fact, only a small endothermic peak representing an energy of approximately one cal/g is seen. This peak does not correspond to any seen previously. It does not correspond to the peak exhibited by the as-mixed samples as the 25% moisture as-mixed sample exhibited one broad endothermic peak. This broad endothermic peak is representative of a much larger energy and hence, most probably a different reaction. Nor could

it be correlated to the small peaks seen in the higher moisture samples as the temperature at which the onset of the peak occurs is much higher than that of the other peaks. One explanation is that with the exposure to 99°C, the majority of the large endothermic reaction exhibited in the scan of the sample extruded at 60°C occurs. The small peak seen then is actually just the remainder of the reaction that did not occur in the extruder. This is not a particularly plausible explanation as the onset of the reaction that occurred in the sample extruded at 60°C occurred at temperatures above 100°C. The sample extruded at 99°C never experienced these higher temperatures required by the endothermic reaction seen in the scan of the 60°C extruded sample. Unless the reaction had a kinetics which allowed it to occur because of the extended amount of time at 99°C experienced in the extruder, the two reaction mechanisms are different.

The results of the DSC scans of the extruded samples were obtained previously to all other experimental DSC work presented here. In essence, it was these results that were the catalyst of the investigation into the endothermic reaction associated with cooking extrusion. Up until now, all the literature discussed a cooking reaction and possible mechanisms associated with the reaction. As seen in the literature review, one of the most prevalent theories of the cooking reaction is the formation of disulfide bonds in the manner of a crosslinking reaction. It this were the case, a DSC scan of the sample would show a broad exothermic peak of large energy and not an endothermic peak. In fact, none of the theories presented in the literature would produce an endothermic reaction. Hence, the results which have been presented are of great interest. As the 25% moisture soy dough is not the material of study, further investigation

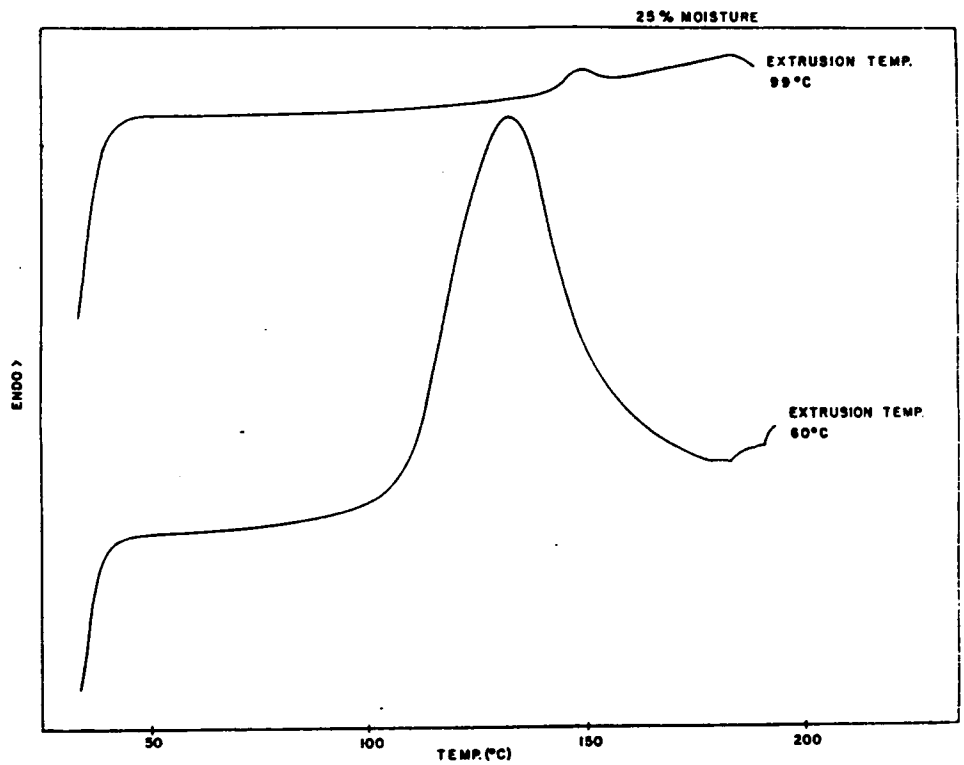

Figure 58. DSC thermograms of two 25% moisture soy dough samples extruded at 60 and 99°C.

is not warranted at this time. However, the results from the DSC work performed on the two extruded samples definitely indicated that extruder samples need be taken and examined for the presence of a reaction. Samples of the extrudate of experimental extruder runs were collected for testing in the DSC. Experimental conditions included temperatures ranging from 25 to 85°C, and varying extrusion rates ranging from 4 to 40 rpm. The results for samples extruded at 25, 50, and 75°C exhibited two small endothermic peaks. These results were consistent throughout the range of extrusion rates. No significant difference between the as-mixed and these extruded samples was observed. The results for the 25, 50, and 75°C extruded samples were expected as the results from all previous experiments also demonstrated no deviation from the as-mixed sample behavior as a results of exposure to shear or heat up to 75°C.

The results of most interest were those of the sample extruded at 85°C as this is the temperature where large endothermic reactions could be generated under certain experimental conditions. As the factors controlling the generation of the endothermic reaction have not been defined, there were no expected results of this experiment. However, experimental parameters were varied regardless of the actual parameter values which are to be incorporated in the model to see the conditions under which the endothermic reaction might be generated. The major parameter varied was the extrusion rate. Other parameters were die assembly and feed pressure; both of which contribute to the pressure profile experienced by the sample. The basic reason for varying the extrusion rate in the experiments is that the extrusion rate controls the two factors which have been seen to generate the endothermic reaction; soak time and shear. In the

extruder, unfortunately, these parameters cannot be separated during operation. If a slower extrusion rate is used, a longer residence time occurs. Hence, the soy dough experiences a longer soak time at temperature at the cost of experiencing low shear rates. If high high shear rate is the controlling factor of the reaction generation, high extrusion rates would produce high shear rates. This, however, shortens the residence time and the sample experiences a shorter soak time at temperature. The only way to produce a longer soak time at higher shear rates would be to change the extruder dimensions.

The results of the 85°C extruded sample exhibited one small endothermic peak similar to the results of the sample heated to 85° in the DSC. The first peak no longer was evident and the second peak represented an energy of approximately one cal/g. No large endothermic peak was exhibited regardless of the extrusion rate.

Actually, testing the extrudate in the DSC only demonstrates the reaction that would occur in the sample and not those that did occur. Hence, it is not a true diagnosis of the reaction occurring in the system. Based on the other experimental results which display only small endothermic peaks, it could be assumed that no reaction occurs in the system over the temperature range investigated. However, to be thorough in investigating the possibility of a reaction occurring during the extrusion process, the following experiment was performed. The extruder was operated at 85°C at various extrusion speeds. For each speed, the extruder was stopped and the screw was pulled, taking samples every five turns along the screw. These samples were then tested using the DSC. The reasoning behind this experiment is that if a reaction were to occur in the extruder, the DSC

results would register a peak in one sample and not in the next sample taken further along the screw. The results of this experiment are shown in Figure 59. The results were the same regardless of the extrusion rate. No matter what position along the screw, the results for the sample were the same as the those from other sample positions. This proves that no reaction is occurring during the cooking extrusion process through the temperature range investigated.

One point of contention in the results of this experiment is the lack of two small peaks present in the DSC scans for the samples taken closest to the feed port. As the soy dough is entering the extruder at room temperature and has to be heated to experimental temperature in the extruder, the first samples taken might not be up to the 85°C temperature. Previous results have shown that the first peak exists up to 85°C. Hence, the soy dough must heat quickly to the 85°C experimental temperature and actually be up to temperature before the fifth turn of the screw.

As discussed, the results of the extrusion experiments have indicated that for extruder operation conditions, no heat of reaction term need be incorporated into the numerical model of the process. However, one additional experiment was performed out of interest to see if the large endothermic peak could be generated in the extruder. So far, the only sample which exhibited this reaction has been that collected from the capillary rheometer with an experimental temperature of 85°C. As the extruded samples experienced shear, the other major parameter in generation of the endothermic reaction was the additional soak time of the capillary rheometer. Therefore, the following experimental procedure was performed. The extruder was stopped in the middle of an experiemntal run

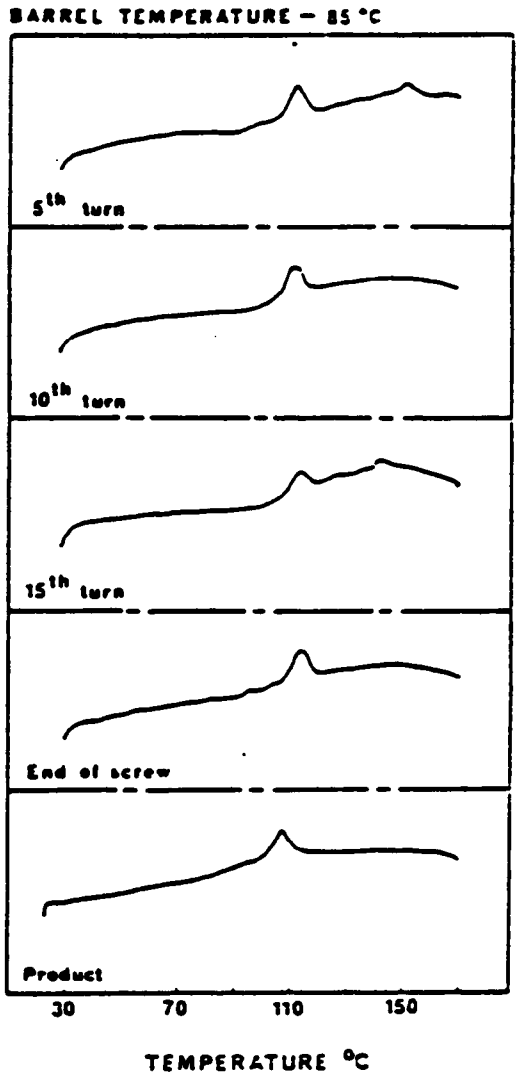

Figure 59. DSC thermograms of 50% moisture soy dough samples collected along the length of the extruder.

but the temperature was held at the experimental conditions. Temperatures ranging from 25 to 85°C were investigated. This sample was allowed to sit in the extruder for 30 minutes at which point the extruder was started again and the extrudate collected. The extrudate was then tested in the DSC. Two of the more informative sample results at extrusion temperatures of 80 and 85°C are presented in Figure 60. For temperatures up to 80°C, the scan presented for the 80°C samples is representative of all samples. Once more two small endothermic peaks are observed. However, the 85°C sample exhibited a large endothermic peak with energy corresponding to 140 cal/g. This energy is on the same order of magnitude as the energy associated with the endothermic reaction of the 85°C samples from the capillary rheometer. The shape of the peak differs from that of the capillary rheometer but the onset temperature is approximately the same. These results show that the endothermic peak can be generated under conditions other than those of the capillary rheometer.

Finally, an argument has been presented to counteract the conclusion that a reaction does not occur during the cooking extrusion process. Although this does not directly involve the experimental conditions found in this dissertation due to the limitation of temperature caused by the moisture content of the soy dough, it will be addressed. Industrial processing of soy normally is in the range of 130 to 160°C. It is argued that the direct exposure to the high temperature is responsible for the cooking reaction. Although this is in opposition to the results which indicate a soak time at a key temperature, an experiment was performed to simulate this condition. Once again the DSC was operated in isothermal mode where the sample was immediately brought up to set temperature and

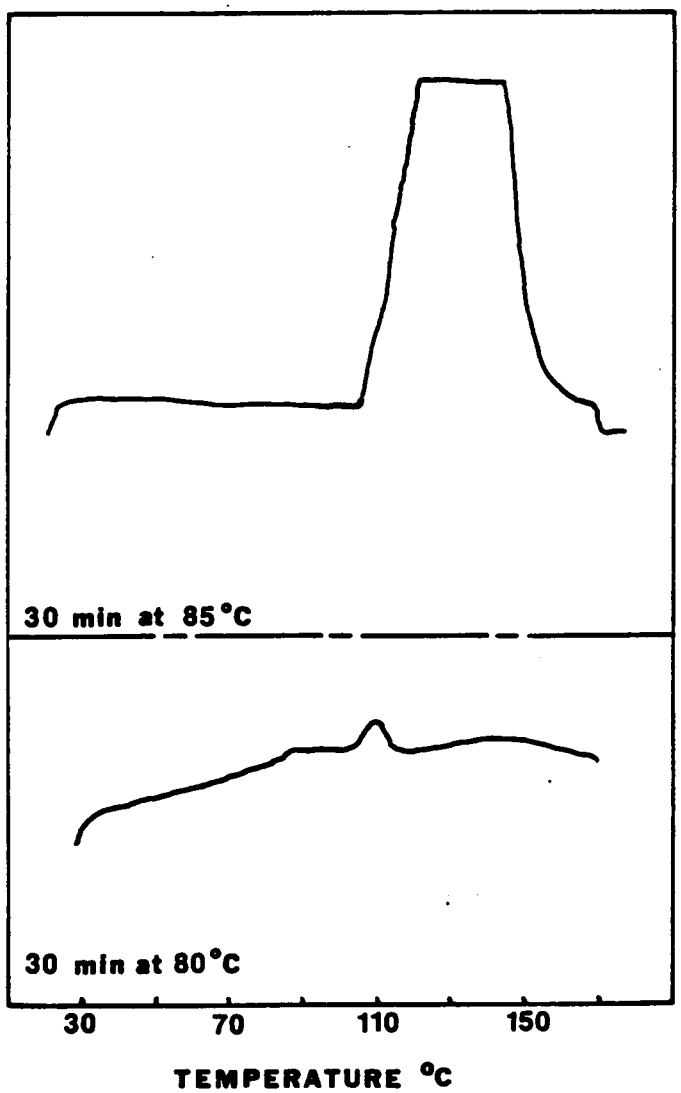

Figure 60. Comparison of DSC thermograms of samples extruded at 80 and 85°C.

scanned as a function of time. Even though residence time in the extruder is low, the sample is exposed to the high temperature for an extended length of time just to be sure that the reaction is not present. The results of these experiments are presented in Figure 61. The scans are seen to be completely featureless. From the previous experiments it is known that at least for the heating rate used in the DSC experiments, only two small endothermic peaks occur during the heating from 25 to 160°C. Once at the elevated temperature, no reactions occur no matter how long it is exposed to that temperature.

In conclusion, the most important finding of the experiments designed to determine the cooking reaction of the 50% added moisture soy dough was that for the temperatures under consideration only one small endothermic reaction would occur during the extrusion process. In addition, that reaction, which has been associated with the denaturation of proteins, would only occur at experimental temperatures of 85°C. Below this temperature, the DSC results are the same for all samples, and hence, no reaction would occur in the soy dough during heating or shearing. Therefore, no term representing the heat of reaction need be incorporated in the numerical model to be developed. Although the one endothermic reaction associated with denaturation would occur at 85°C, the energy associated with the reaction is negligible and therefore will not be considered.

There were many other findings associated with these experiments which are not of direct use in satisfying the goals of this dissertation but are of definite interest. A short summary is now presented.

To begin, it was seen that different reactions occurred in the soy mixtures depending on the moisture content. Two small endothermic peaks

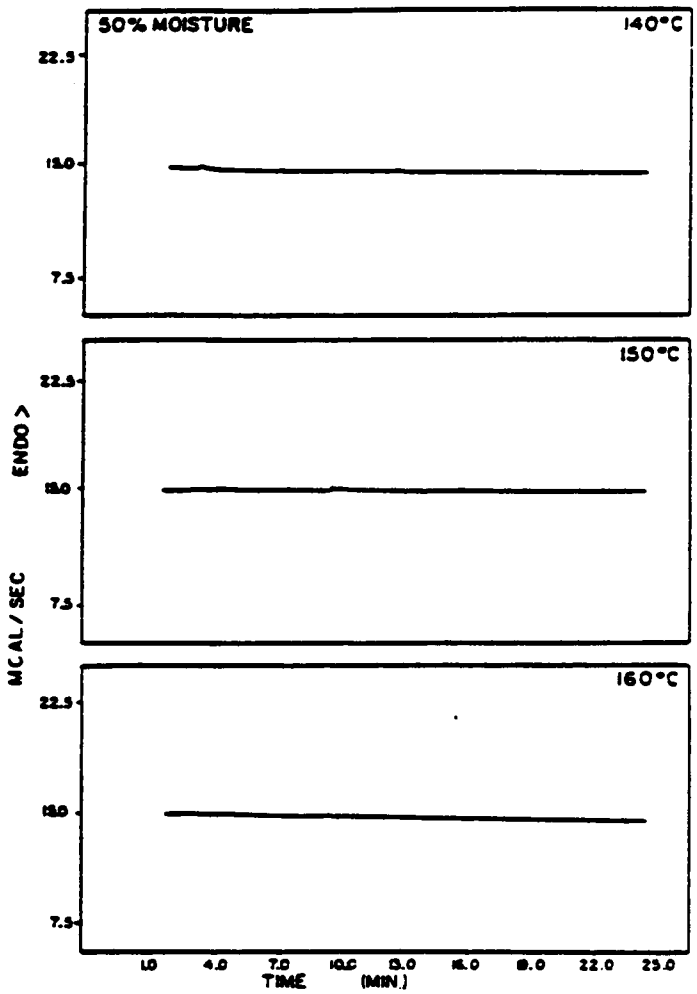

Figure 61. Isotherms at 140, 150, and 160°C of 50% moisture soy dough.

of approximately one cal/gram were observed for the higher moisture systems consisting of 28 to 70% added moisture, and one larger endothermic peak of approximately 25 cal/gram was observed for the lower moisture systems consisting of 0 to 24% added moisture. The transition from one reaction mechanism to the other occurred in the moisture range of 24 to 28% added moisture. From the results of that experiment alone, it can be concluded that the response of soy mixtures are a function of water content and generalizations should not be made between various moisture content soy mixtures.

Next it was seen that the temperature of the first peak observed in the 50% added moisture soy dough coincided with the temperature at which an increase in viscosity was observed. As this first peak is attributed to the denaturation of the proteins, the increase in viscosity could then be attributed to the entanglements and interactions which could occur because of the new conformation of the proteins following denaturation.

Third, a large endothermic reaction could be generated under certain experimental conditions. From the results of the experiments used to explore the factors contributing to the generation of the reaction, it was concluded that soak time at 85°C was definitely one of the factors. Shear was another factor which possible contributed to the generation of the reaction. A definite correlation was never drawn conclusively. The conditions surrounding the heating, bulk sample as experienced in the extruder and capillary rheometer versus small isolated sample as experienced by the small sample used in DSC experiments were also postulated to affect the reaction.

Finally, all reactions which occurred in the soy samples were irreversible for the period of study. This irreversibility applied doubly to the generated endothermic reaction. Not only was the endothermic reaction irreversible but also the interactions which were formed due to the soak time and other factors in the experiment.

If, for example, a reaction were found to occur in the system over the processing temperature range, the energy associated with that reaction would have to be included in the model. The incorporation of this energy into the model would be handled in the manner displayed in Figure 62. The reaction itself is represented by the apparent heat capacity whereas the true heat capacity is termed the sensible heat capacity. Knowing that the reaction energy is the integral of the apparent heat capacity over the temperature range, and the thermal energy absorbed by the soy dough is the integral of the sensible heat capacity over the total temperature range, the total thermal behavior of the system can be represented by the combination of the two heat capacities. In other words, for the numerical model, the heat of reaction would be incorporated into the heat capacity term. This is the method Virayauthakorn et. al. employed in their three dimensional model for extrusion of polymers. The energy associated with the melting of the polymer was included in the heat capacity term.

5.3.2 HEAT CAPACITY

Since the heat capacity of the 50% moisture soy dough is needed for the numerical model, it also was determined from the results of the DSC experiments. In addition, the heat capacity for soy mixtures ranging from

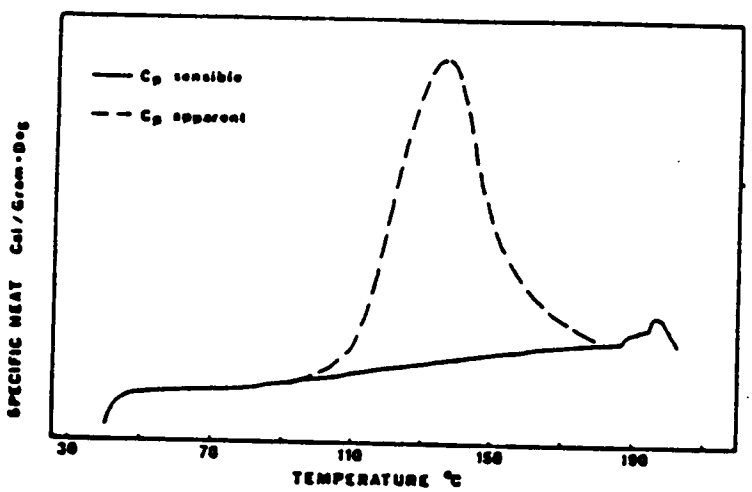

$$C_p = C_{p_{sens}} + C_{p_{app}} \qquad \Delta H = \int C_{p_{app}}\, dT$$

Figure 62. Schematic of sensible versus apparent heat capacity.

0 to 70% added moisture was found in order to ascertain the effect of moisture content. In this section, the various experiments performed in the determination of the heat capacity and the results from these experiments are presented. The method used in the heat capacity determination was described in Chapter Three.

As discussed in the experimental section, the Perkin-Elmer DSC-2 system has the ability with the aid of a special software package to calculate the heat capacity for any sample as a function of temperature. The heat capacity results can then be displayed in either graphic or tabular form. The results for a 50% added moisture soy dough are presented in both manners in Figure 63 and Table 10. In Figure 63, the heat capacity is shown as a continuous function of temperature. The dependence of heat capacity upon temperature is slight as indicated by the slope of the curve. The small endothermic peaks, which were discussed in the previous section concerning the reactions present in the system, are evident in these results. Hence, the DSC calculation of heat capacity is of the combined sense discussed in the previous section. Both the sensible and apparent heat capacity are combined into an overall heat capacity function. If simply the sensible heat capacity is desired, the sample would have to be run and then rerun on the DSC. The first time would allow the reactions to occur so that the rerun would be indicative only of the sensible heat capacity. This procedure has two limitations. First the reaction must be irreversible for the method to work. Second, the occurrence of the reaction must in no way alter the heat capacity of the sample. The former of these limitations has been proven for this system while the latter will be discussed later. In Table 10, the values are

printed for the heat capacity at a 5^0 temperature interval. However, the temperature interval is user specified and may be set to any convenient number.

The next three figures present the results of the heat capacity as a function of moisture content. In Figure 64, the average heat capacity over the temperature range of 25 to 170°C is presented as a function of moisture. Three categories of data are displayed: data representative of the low moisture samples exhibiting the larger enodothermic peak, data representative of the high moisture samples exhibiting the two smaller peaks, and data representative of the reruns of all moisture content samples. As discussed above, the heat capacity determined by the DSC is a comprehensive heat capacity combining both the sensible and apparent heat capacity of the material. Those samples with a lower moisture content exhibited a large average heat capacity compared to those with the higher moisture content due to the energy assocated with the endothermic peak. As discussed, a method for determining the sensible heat capacity only would be to rerun the sample. The reruns of the samples with the lower moisture content exhibit a much lower average heat capacity, now, as the energy of the endothermic reaction is no longer averaged in. The reruns of the higher moisture samples, however, do not exhibit much, if any, change in the average heat capacity as the energy associated with the small peaks is relatively insignificant. A least squares fit of the higher moisture data is shown by the dashed line. It is seen, however, that neither the results of the first run nor of the rerun of the lower moisture samples fall anywhere near the extrapolation of the higher moisture correlation.

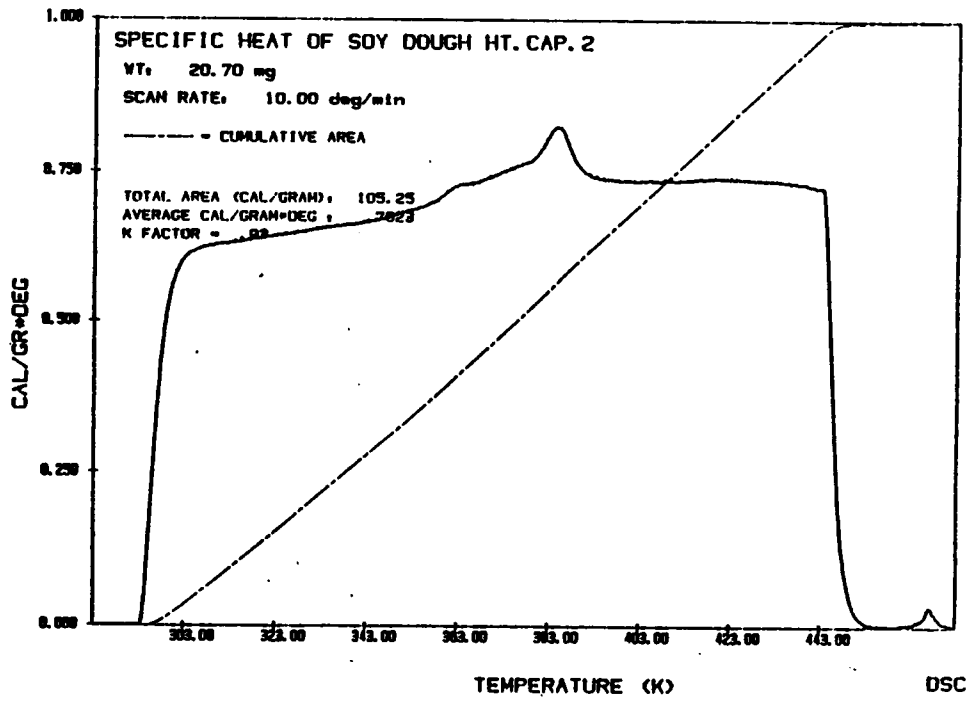

Figure 63. Heat capacity as a function of temperature for a 50% moisture soy dough.

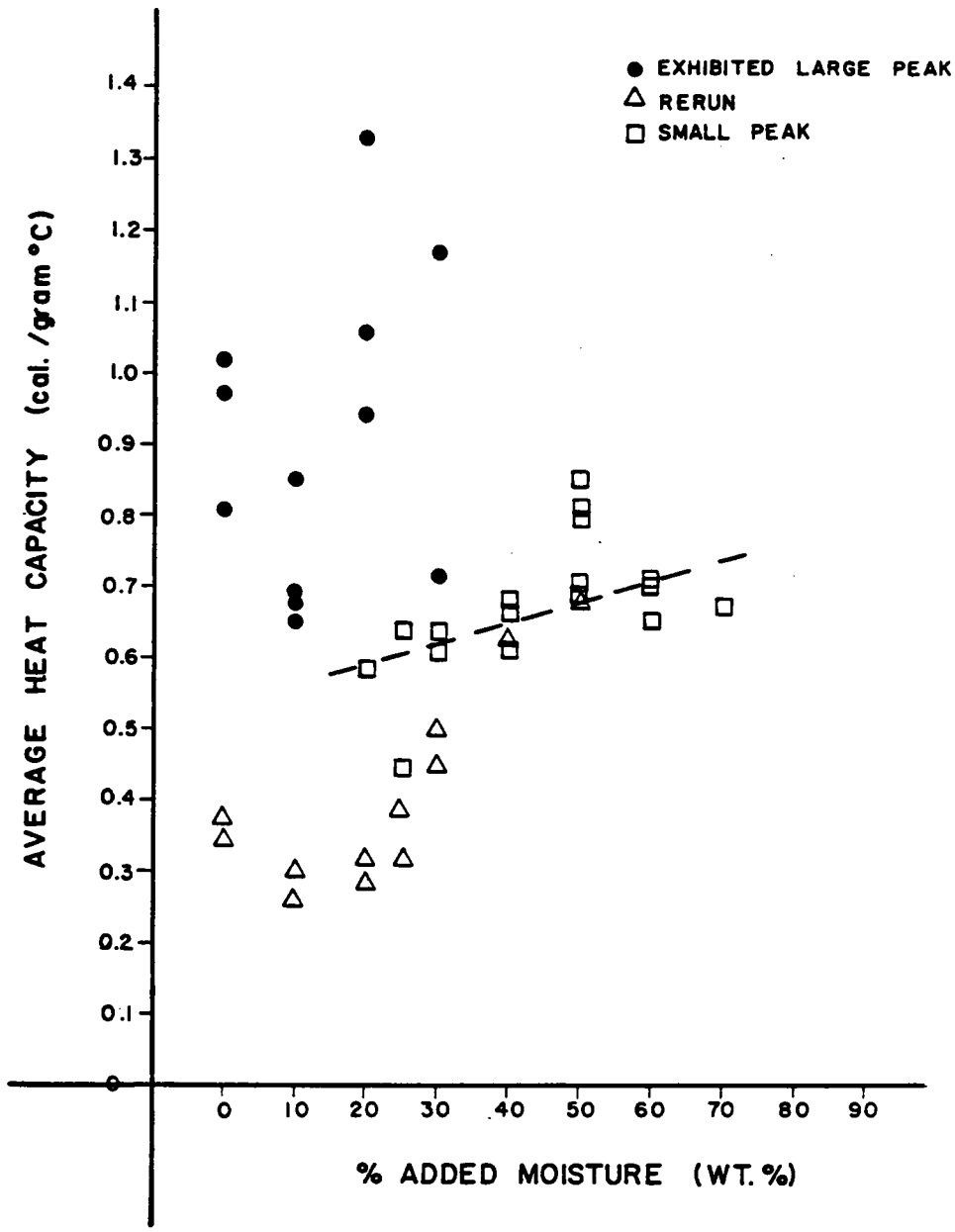

Figure 64. Average heat capacity as a function of moisture.

TABLE 1C

SPECIFIC HEAT OF 50% ADDED MOISTURE SOY DOUGH

TEMP. <K>	CAL/GRAM*DEG	TEMP. <K>	CAL/GRAM*DEG
303	.6089	383	.8183
308	.6267	388	.7682
313	.6321	393	.7413
318	.6361	398	.7348
323	.6442	403	.7356
328	.6491	408	.7364
333	.6577	413	.7375
338	.6623	418	.7402
343	.6658	423	.7383
348	.6763	428	.7372
353	.6879	433	.7329
358	.7024	438	.7299
363	.7297		
368	.7369		
373	.7531		
378	.7677		

Previously, limitations were presented in the method of using the rerun of a sample to determine its sensible heat capacity. As the irreversibility limitation was already determined and satisfied, the other limitation pertaining to the occurrence of the reaction changing the heat capacity of the material is now explored. The initial and rerun results for heat capacity at 30°C for samples ranging in added moisture from 0 to 70% are presented in Figure 65. A large difference is seen between the heat capacity at 30°C for the initial and rerun experiments of the lower moisture samples. This is not the case with the higher moisture samples where the heat capacity at 30°C for the initial and rerun experiments are almost identical. Therefore, the occurrence of the reactions associated with the two small endothermic peaks are concluded not to have any effect on the system as to change the heat capacity. In contrast, the occurrence of the reaction in the lower moisture mixtures does have an effect on the system which changes the heat capacity of the material.

Finally, the heat capacity at 30° for all the samples tested and their reruns are displayed in Figure 66. From these results, it is seen that a continuous dependence of the heat capacity on temperature can be obtained over the entire moisture range investigated. This is contrary to the results of the average heat capacity which only could be empirically fit as a function of temperature over the higher moisture content range. However, the results demonstrated by the heat capacity at 30°C data explains this behavior. It was previously stated that the average heat capacity data would not agree over the entire moisture range for the inital run because of the inclusion of the energy associated with the reaction of the lower moisture soy mixtures. In addition it was stated that the

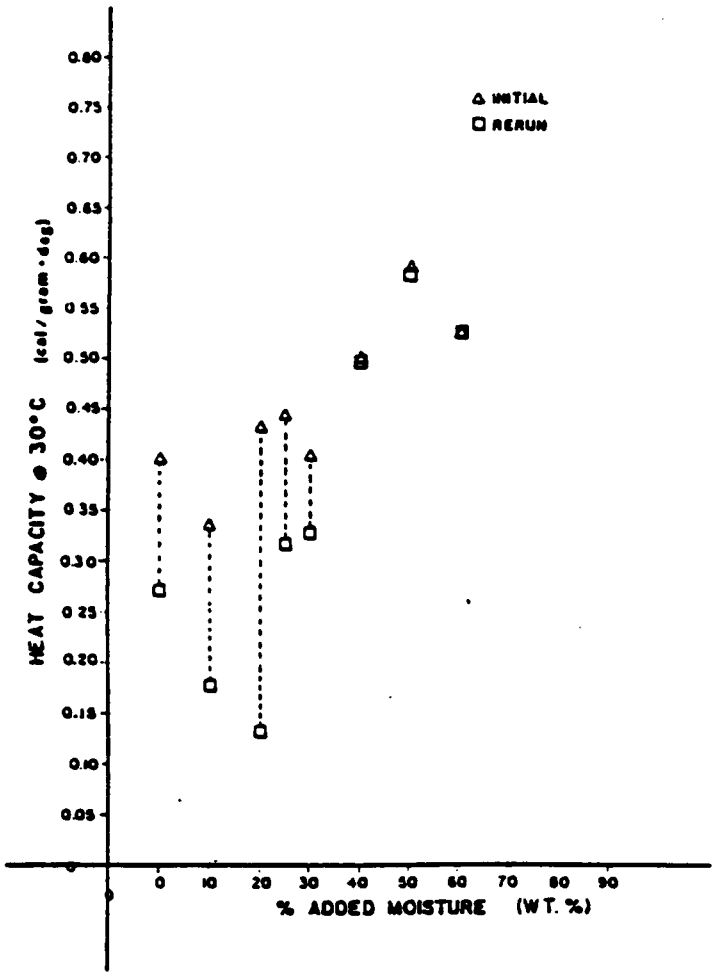

Figure 65. Heat capacity at 30°C as a function of moisture.

rerun data would only be valid if the reaction did not change the heat capacity of the system. However, from the heat capacity measurements at 30°C it was discovered that the reaction did in fact change the heat capacity of the soy sample. Hence, it could not be expected that the average heat capacity of the rerun sample would coincide with systems in which the reaction did not occur.

One additional point to notice is the actual dependence of the system upon moisture content. Although the heat capacity does increase with the addition of water, which is expected as the heat capacity of the water is greater than that of the soy flour, the least squares fit of the data does not extrapolate to 1.0 cal/gram °C at 100% water. It is possible that the interactions between the soy and the water molecules affect the heat capacity and therefore would not extrapolate to the true value for the pure material. Remember that even the 0% added moisture sample does have some inherent moisture.

In conclusion, the heat capacity experiments revealed some interesting results. Most important, the heat capacity of the 50% added moisture soy dough was determined. It was found to have a slight dependence upon temperature. Second, the heat capacity calculations were found to reflect the overall heat capacity of the system, i.e., the heat of reaction or apparent heat capacity was included in the reported values. Third, it was found that the reactions associated with the higher moisture systems did not affect the heat capacity, however, the reaction associated with the lower moisture system did affect the heat capacity, lowering the heat capacity of the material over the remperature range up to the onset temperature of the reaction and possibly more. Finally, an empirical fit to

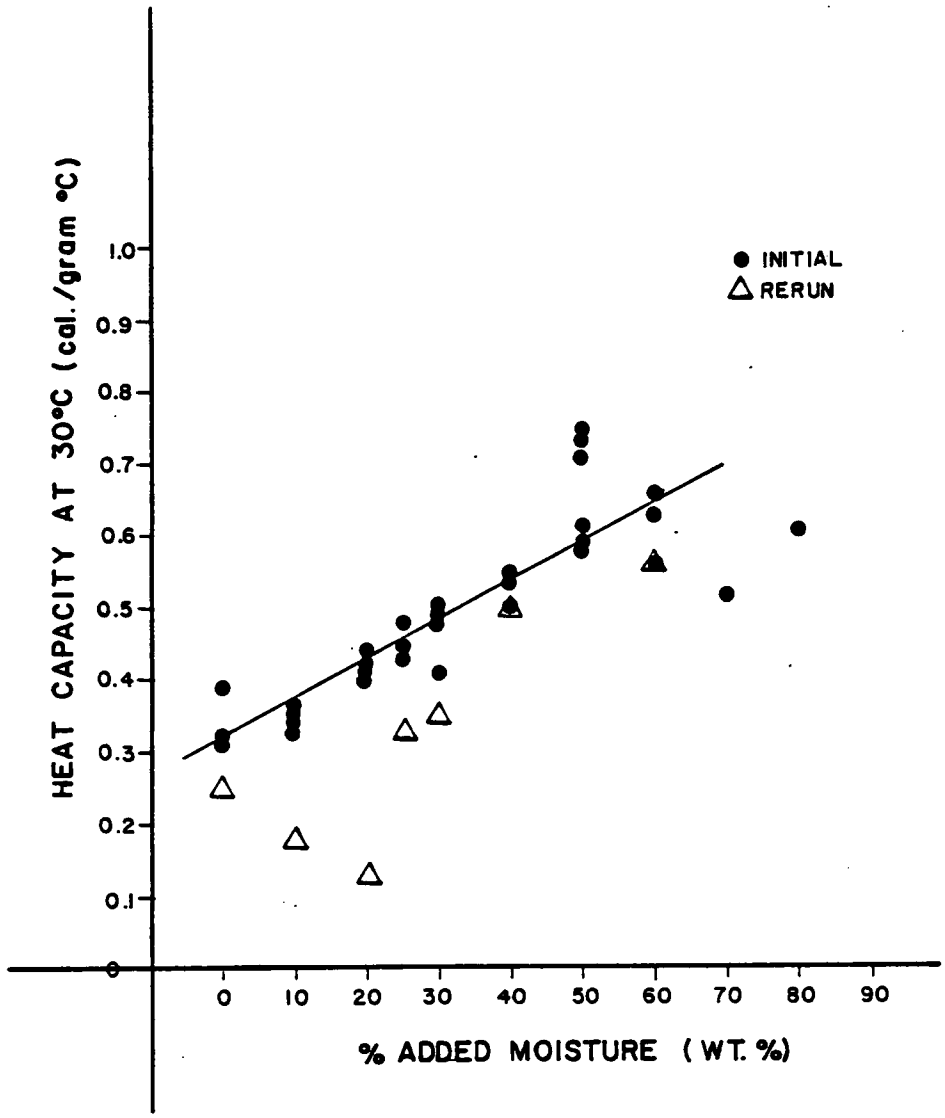

Figure 66. Heat capacity at 30°C as a function of moisture.

the data was determined to correlate heat capacity at temperatures lower than the lower moisture reaction onset temperature to moisture content over the 0 to 70% added moisture range.

5.4 THERMAL CONDUCTIVITY AND THERMAL DIFFUSIVITY

Along with the thermal properties of heat capacity and heat of reaction which were just discussed, the thermal conductivity of the 50% moisture soy dough is also needed for the numerical model. No instrument is commercially available to measure the thermal conductivity of food materials. Hence, a method had to be developed and apparatus built to determine the thermal conductivity of the soy dough.

Two methods for determining the thermal conductivity were employed. To begin, the thermal conductivity was measured directly by the hot wire method described by Vos [99] and outlined in the experimental chapter. With a few changes, the apparatus was modified to measure the thermal diffusivity which in turn can be related to the thermal conductivity through a simple relationship. This method was described by Dickerson [83] and outlined in the experimental chapter. The results of the direct measurement method for determining thermal conductivity are discussed first. The results of the method which determined thermal diffusivity from which the thermal conductivity was calculated are presented second. Finally, a comparison of the results from the two methods is made.

The thermal conductivity of 0,25,and 50% added moisture soy dough was determined directly at ambient temperature by the hot wire method. As discussed in the experimental chapter, the method consists of a current being passed through a resistance wire which lies along the axis of a

cylindrically shaped sample. Assuming all the energy produced by the wire is absorbed by the surrounding sample, the thermal conductivity can then be determined by the temperature increase measured close to the wire as a function of time. The details of this calculation are given in the experimental chapter and a sample calculation is exhibited in Appendix D. A typical graph of the data obtained from a thermal conductivity experiment is shown in Figure 67. The solid line passing through the data for a particular trial run is a least squares fit of the data. Two temperatures and their corresponding times are taken from the least squares fit of the data and the conductivity calculated.

The calculated thermal conductivity values for the 0, 25, and 50% moisture doughs are given in Table 11. The density for the individual trial runs is included as an indication of the consistency of packing. However, as the method involves the detection of the energy given off by the wire by a thermocouple placed very close to the wire, the overall density is not a good indication of the packing. The most important area to concentrate on packing is that surrounding the thermocouple and wire. A small air space calculated in the overall density would have a small effect of the calculated thermal conductivity but if it was positioned between the wire and the thermocouple it would have a significant effect on the calculated thermal conductivity. Hence, the overall density could be exactly the same for multiple runs, but give different thermal conductivities due to air space positioning.

For this reason, no true correlation can be made between the density and the thermal conductivity calculated for a trial run. There is a very distinct dependence of thermal conductivity on moisture content. On com-

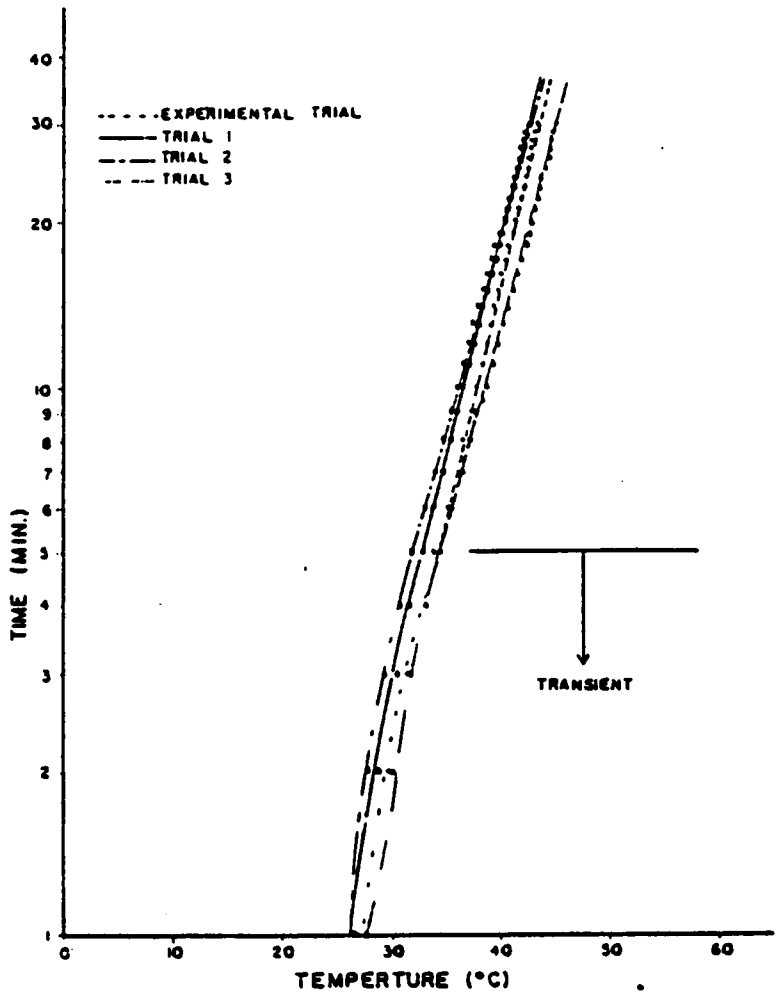

Figure 67. Thermal conductivity experimental data

TABLE 11

THERMAL CONDUCTIVITY OF DIFFERENT MOISTURE SOY DOUGHS

Soy Dough Moisture %	Conductivity ($kg*m/s^3*^oK$)	Density (kg/m^3)
0	0.0542	676.00
25	0.1061	732.00
50	0.2105	1,030.00

paring the average thermal conductivities, the thermal conductivity for the 50% moisture dough is approximately double that of the 25% moisture dough which is in turn twice that of the 0% moisture dough.

Next the thermal diffusivity is found by the transient method described in the experimental chapter. The thermal diffusivity of 0, 25, and 50~% moisture doughs was determined. Figures 68, 69, and 70 show the temperature versus time data collected from an experimental run for each moisture content. From these figures it is seen that the experimental temperature range was 30 to 150°C for the 0 and 25% moisture samples but only 30 to 110°C for the 50% moisture dough. During the experimental runs of the 0 and 25% moisture samples, vapor loss from the diffusivity tube was observed beginning at a temperature of 110°C and lasting through the end of the run. For the 50% moisture dough, vapor loss was first observed around 105°C. However, because of the large moisture content of the dough, the amount of vapor released was greater than what could escape around the top of the diffusivity tube and the top exploded off at 110°C. Due to the vapor loss, the data obtained at temperature above 110°C is questionable as the composition of the material is changing. This should not have a large effect on the 0% added moisture dough as the inherent moisture is low but it could seriously affect the validity of the 25% moisture dough results. As mentioned, no data above 110°C could be collected for the 50% moisture dough so the effects of moisture loss for this material can not be examined.

The shapes of the temperature versus time data for the three moisture soy samples are of interest. If a material possesses a constant diffusivity with temperature, the two curves will be parallel after the

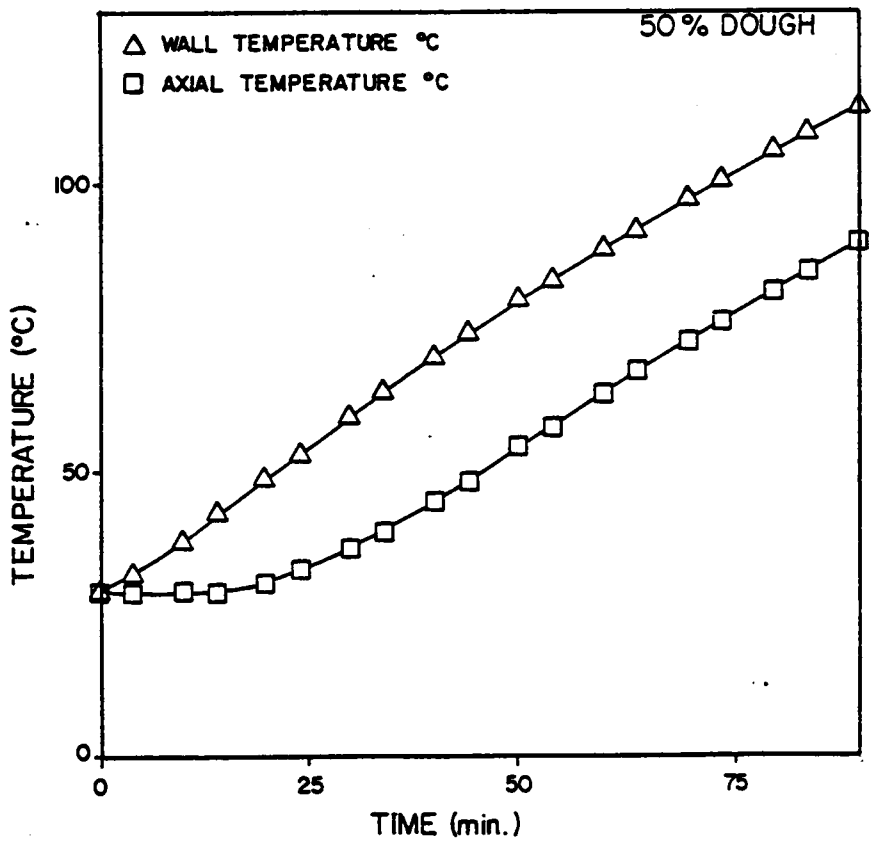

Figure 68. Thermal diffusivity experimental data for 50% moisture dough

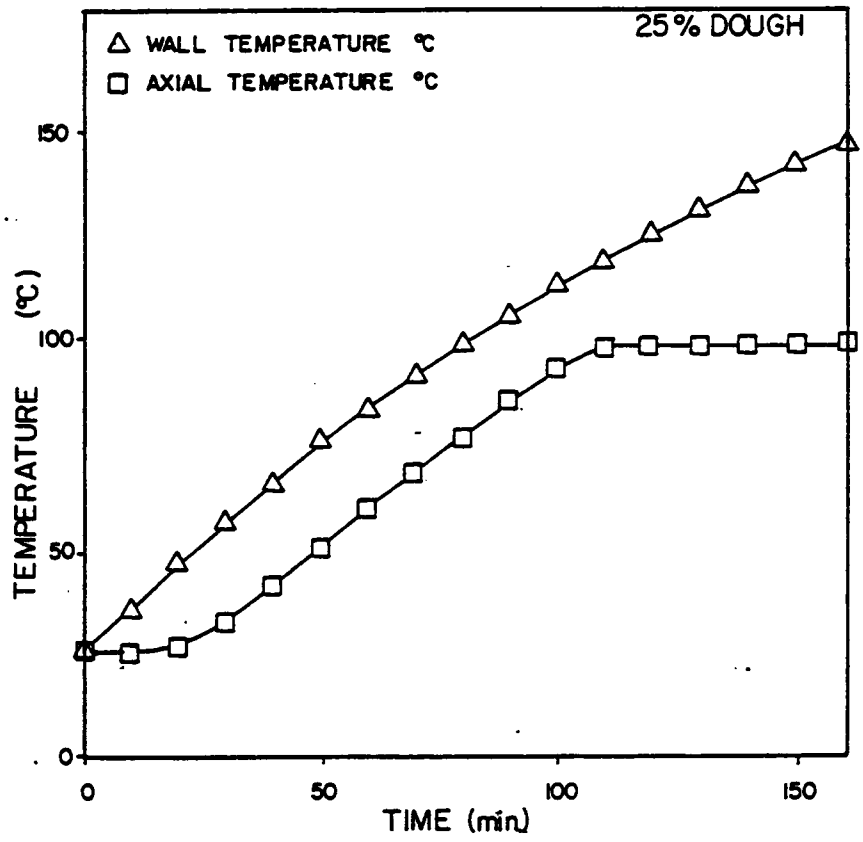

Figure 69. Thermal diffusivity experimental data for 25% moisture dough

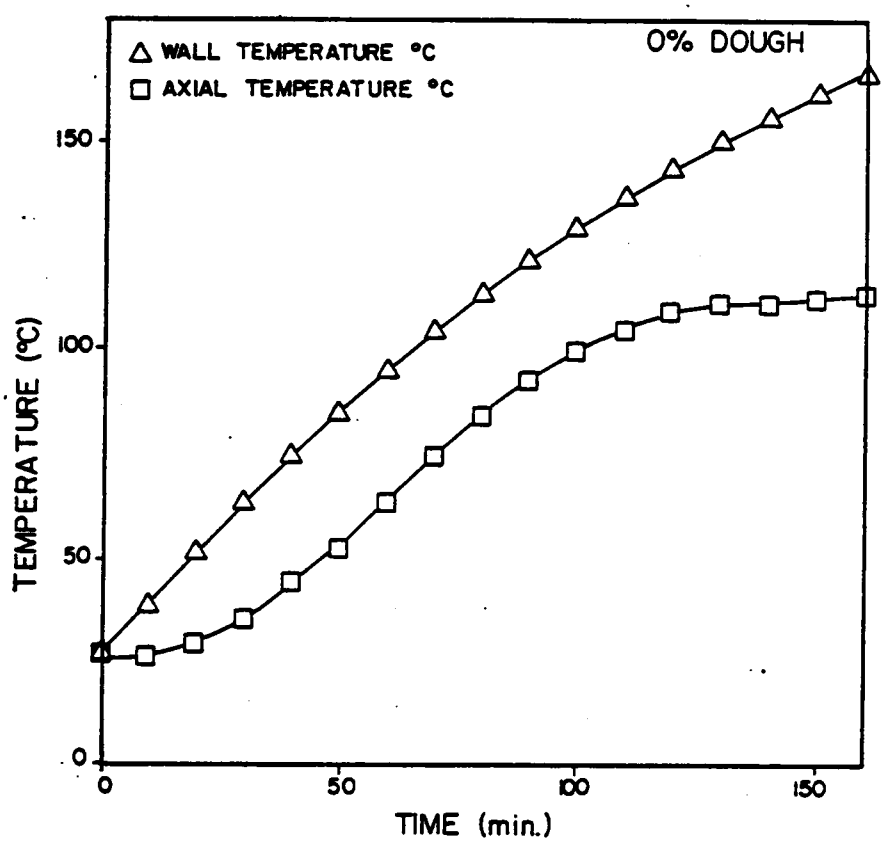

Figure 70. Thermal diffusivity experimental data for 0% moisture dough

initial transient period. This is the behavior of the 50% moisture dough shown in Figure 68. The two temperature curves are approximately parallel after the transient period indicating a constant thermal diffusivity for that temperature range. This, however, is not the behavior of the 0 and 25% moisture soy samples. The temperature curves presented in both Figure 69 and 70 are not parallel over the temperature range of investigation. For both materials, the axial temperature curve displays an isotherm at a temperature of approximately 100°C even though the wall temperature continues to increase to 150°C. Up to that temperature, the behavior of the two temperature curves is indicative of a constant thermal diffusivity. As the 50% moisture dough data could only be recorded up to 110°C it is impossible to tell if it would display the isotherm.

Two possible explanations for the occurrence of the isotherm exist. The isotherm is due to an endothermic reaction occurring within the system. Hence, rather than causing an increase in sample temperature, the energy supplied to the sample by the constant heating of the bath is absorbed in the reaction. The obvious explanation of the endothermic reaction would be the vaporization of the water in the system. Although the endotherm occurs slightly below an axial temperature of 100°C, the wall temperature is over 100°C and the sample between the wall and the center of the tube would definitely have reached vaporization temperature. The length of time of the isotherm should be indicative of the extent or length of the reaction. It would be expected then that the isotherm would occur for a much shorter length of time for the 0% moisture sample than the 25% moisture sample as there is significantly less moisture in the sample. This is not the case; both isotherms last until the end of the

experimental run. It is possible that the length of the isotherm might differ if the length of the experimental run was extended. It is questioned, however, if all the energy absorbed as indicated by the isotherm is necessary to vaporize the small moisture content of the 0% added moisture sample.

Therefore, it is possible that another endothermic reaction may be responsible for the isotherm, or perhaps a combination of the two. It was seen in the previous section on the differential scanning calorimetry work that an endothermic reaction occurred in 0 and 25% moisture soy samples. In addition, the onset of this reaction did in fact occur at approximately the same temperature as the isotherm. Consequently, this reaction could also play a part in the observed isotherm. Water vapor was definitely observed being released during these experiments, hence, if the endothermic reaction documented by the DSC work is involved with the isotherm, it must be a combination of the two reactions which generate the isotherm.

For whatever explanation of the isotherm, the reaction in the system causes a question to arise as to the validity of the thermal diffusivity calculation in that temperature range. Therefore, the calculation of the thermal diffusivity values is concentrated over the temperature range beginning approximately at 60°C which disregards the transient region at the lower temperatures to 110°C which is before the onset of the isotherm. One problem arises in the caluclation of the thermal diffusivities. The experimental runs did not comply completely to the theoretical model. In each trial, the heating rate was not constant but decreased by 50% over the two hour period. The non-linearity of the heating rate meant that the

diffusivity had to be calculated for each different heating rate. Temperatur measurements were obtained at two minute intervals. As the heating rate was not constant, the diffusivities were calculated every two minutes with an average heating rate for the interval. The heating rate was found to vary less than 5% over the time interval therefore introducing minimal error.

The results of these calculations are shown in Figures 71, 72, and 73. The thermal diffusivities were calculated over the full temperature range. In the 0 and 25% moisture sample graphs, two regions are seen; a constant thermal diffusivity for the lower temperatures and a decreasing thermal diffusivity over the temperature range where the isotherm was observed. The 50% moisture sample simply exhibits an essentially constant diffusivity. Average thermal diffusivity values were calculated over the 70 to 105°C temperature range and are given in Table 12. Unlike the thermal conductivity values, although the thermal diffusivity values are moisture dependent, the dependence is not seen to be great.

Finally, as discussed previously, the thermal diffusivity values were determined only to calculate the thermal conductivity values. The thermal conductivity was determined by the following equation:

$$k = \alpha * \rho * Cp$$

The heat capacity used in these calculations was an average value over the 70 to 105°C temperature as determined from the DSC experiments. The calculated thermal conductivity values are shown in Table 13. As the heat capacity and thermal diffusivity values were constant over the large temperature range, it was assumed that these values could be compared to

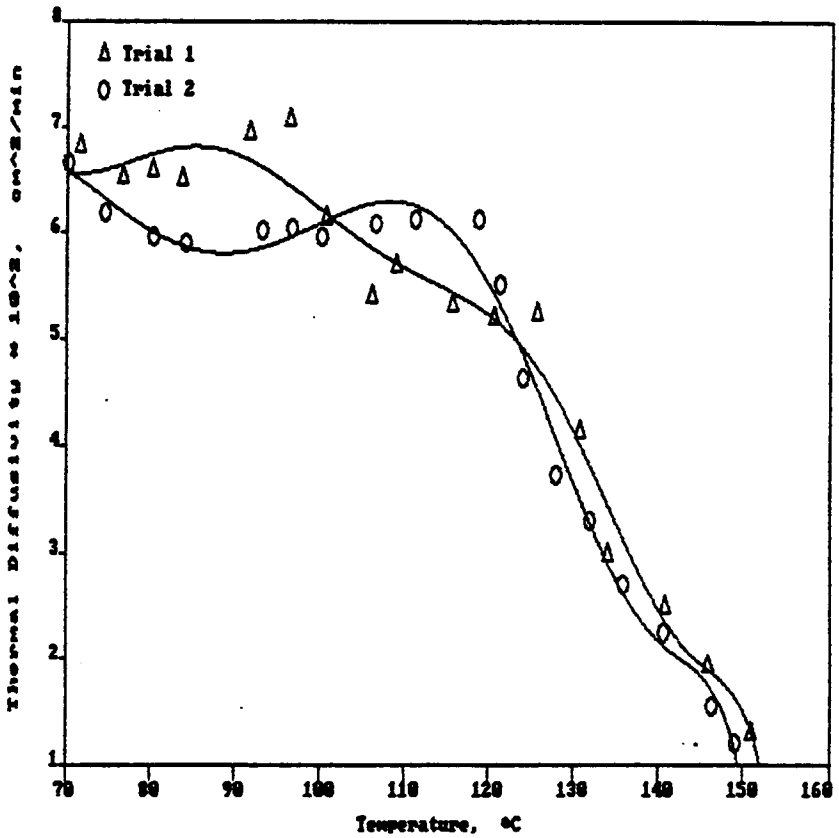

Figure 71. Thermal diffusivity vs. temperature for 0% moisture dough

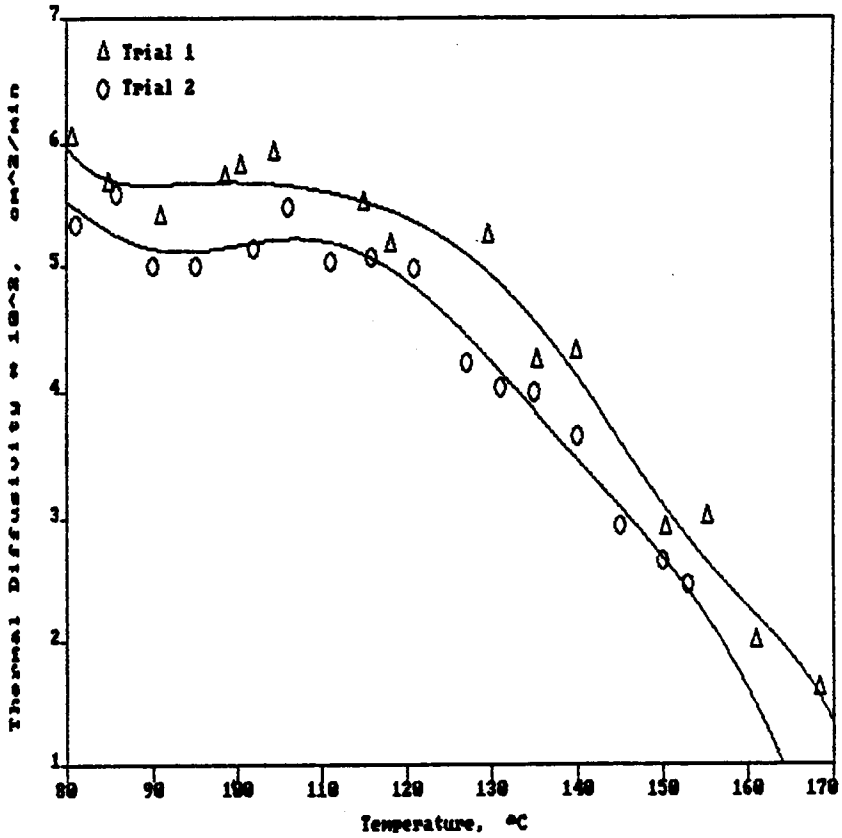

Figure 72. Thermal diffusivity vs. temperature for 25% moisture dough

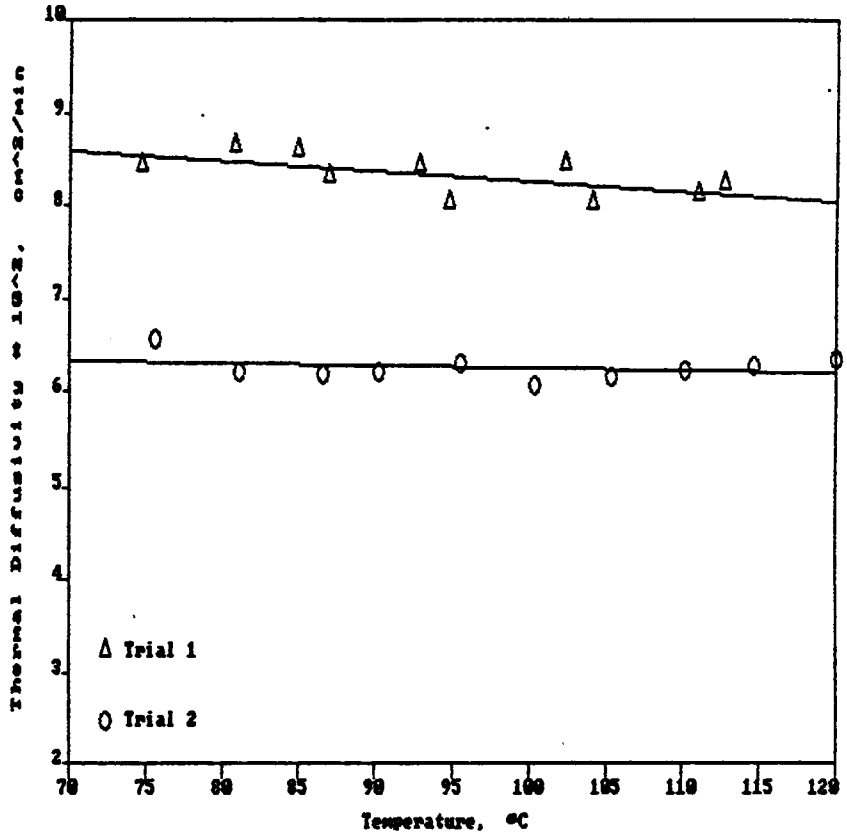

Figure 73. Thermal diffusivity vs. temperature for 50% moisture dough

TABLE 12

THERMAL DIFFUSIVITY OF DIFFERENT MOISTURE SOY DOUGH

Soy Dough Moisture %	Diffusivity (m^2/sec) * 10^{-8}
0	8.89
25	10.37
50	12.43

those measured at ambient temperature. Upon comparison, it is seen that the values calculated from the thermal diffusivity measurements are than those measured directly. Two explanations exist. One explanation lies in the possible error mentioned in connection with the packing of the conductivity tube during measurement. As moisture content increased, the difficulty level in uniformly packing the sample increased. Likewise, notice as the moisture content increases, the differences in the two conductivity values increases. The other is that on comparison of the methods associated with the measurement of the diffusivity versus conductivity one is inherently better because of the measurement technique producing more reliable results.

5.5 EXTRUSION

Once the material parameters of the 50% soy dough needed for the numerical model were determined, extrusion experiments were performed. Pressure at two points along the extruder and flowrate were monitored as a function of temperature and rpm. This information will later be used in comparison with the calculated numerical results for the same conditions to determine the validity of the numerical model. The details as well as the results of these experiments are presented in this section.

The initial plan of investigation for these extrusion experiments of the 50% added moisture soy dough included experimental temperatures up to and including 150°C which incorporates the temperature range usually experienced in the industrial extrusion process. However, after some initial investigatory experiments, it was found that the plan of investigation would have to be modified. For temperatures up to 50°C no prob-

TABLE 13

CALCULATED VERSUS EXPERIMENTAL CONDUCTIVITY VALUES

% ADDED MOISTURE SOY DOUGH	CONDUCTIVITY experimental ($kg*m/s^3*^\circ K$)	CONDUCTIVITY calculated ($kg*m/s^3 * K$)
0	0.0542	0.0792
25	0.1061	0.1410
50	0.2105	0.3400

lems were encountered for any extrusion rate. At 75 and 85°C, while inconsistencies in the flow were encountered at low rpm, a constant uniform flow could be obtained at higher rpm. Since the inconsistencies in flow were eliminated by increasing rpm, it was surmised that these inconsistencies were due to the prolonged exposure to the elevated temperature. As the industrial extrusion process normally operates at higher rpm, this procedure was thought to be acceptable. At temperatures of 100°C and higher inconsistencies in the pressure readings as well as the flow occurred at all extrusion rates. The flow inconsistencies included discontinuous extrudate, spattering, shooting of the extrudate to distances of five feet and more, vaporization of water, and a scaly, twisted appearance to the small segments of the extrudate which were collected. At temperatures above 120°C, no flow occurred. To determine what was happening in the extruder to retard flow, the extruder was stopped and the screw pulled. The soy dough in the flights of the screw appeared burnt, dried out, and somewhat shrunken. From this information, it was concluded that due to the very high temperature, the water in the dough was vaporizing and the sample was contracting slightly. Hence, contact was minimal between the soy dough and the barrel. With no friction, there was no force to move the dough and consequently no flow occurred.

These experiments were performed with a constant temperature profile over the length of the extruder and the die. As the flow inconsistencies which occurred at 75 and 85°C could be eliminated with increased rpm, or conversely, with decreased residence time which in effect lowers the time the dough is exposed to the temperature, modification of the temperature profile for the temperatures above 100°C was made. Three separate zones

for temperature control plus the die assembly control were used to manipulate the temperature profile. A number of temperature profiles were tested to see if a continuous flow at temperatures above 100°C could be obtained. The most extreme variation on the temperature profile occurred when the first extruder zone was set at 50°C, the second extruder zone at 85°C, the third extruder zone at 120°C, and the die assembly at ambient temperature. Even with this severe temperature gradient resulting in a short exposure time at the elevated temperature, no uniform continuous flow was achieved regardless of the extrusion rate employed. Therefore, from these experiments it was decided that the highest temperature at which the experiments could be performed with reliable results is 85°C.

Having determined the operable temperature range for the extruder, extruder experiments under the following conditions were performed and monitored. Extrusion rates of 4, 12, 20 and 40 rpm were used. Constant temperature profiles at ambient, 50, 75, and 85°C were employed. Temperature gradients in the extruder over the ambient to 85°C temperature range were tested. However, no large effect on flowrate or pressure was observed. The flowrate and pressure for the temperature gradient experiments were found to be similar to those of the highest temperature reached. Therefore only constant temperature profiles were used in experimentation.

As mentioned, the flowrate and pressure was monitored in the extrusion experiments. The results of the experiments are presented in Figures 74, 75, and 76. Figure 74 displays the volumetric flowrate as a function of rpm for the various experimental temperatures. As mentioned in the literature review, it is postulated that drag flow predominates in food

extrusion. Therefore, it is expected that increasing the rpm would correspondingly increase the flowrate. This is exactly what is observed. Tripling the rpm from 4 to 12 rpm approximately tripled the volumetric flowrate from 0.069 to 0.233 cm /s. The calculation of volumetric flowrate assumed no die swell, i.e., the diameter of the extrudate was the same as the die diameter. Special care in collecting the extrudate had to be taken as the extrudate would stretch with its own weight if it was left to hang. Therefore, the extrudate was collected on a flat sheet as it was extruded to eliminate any extension of the extrudate. The average length of ten collected samples was used in the calculation. However, some stretch may occur and introduce some error into the flowrate values. Therefore, the mass flowrate from these extrusion experiments was also monitored. Even if the extrudate stretches upon collection, the mass would stay constant. The average mass of ten collected samples is used in the calculation. The results of these measurements are shown in Figure 75. Again, on examining the data if the extrusion rate is tripled from 4 to 12 rpm, the mass flowrate is approximately tripled, 0.084 to 0.267 gram/s. These results are a more exact correspondence than the volumetric flowrate. Tripling the extrusion rate yielded a 3.1 factor increase in mass flowrate whereas it yielded a 3.4 factor increase in volumetric flowrate. Error associated with the rpm setting would enter into both measurements equally, hence, the volumetric flowrate over estimates the true flowrate probably due to the stretching of the sample upon collection. Therefore, it is concluded that the mass flowrate was a better measurement of the flowrate.

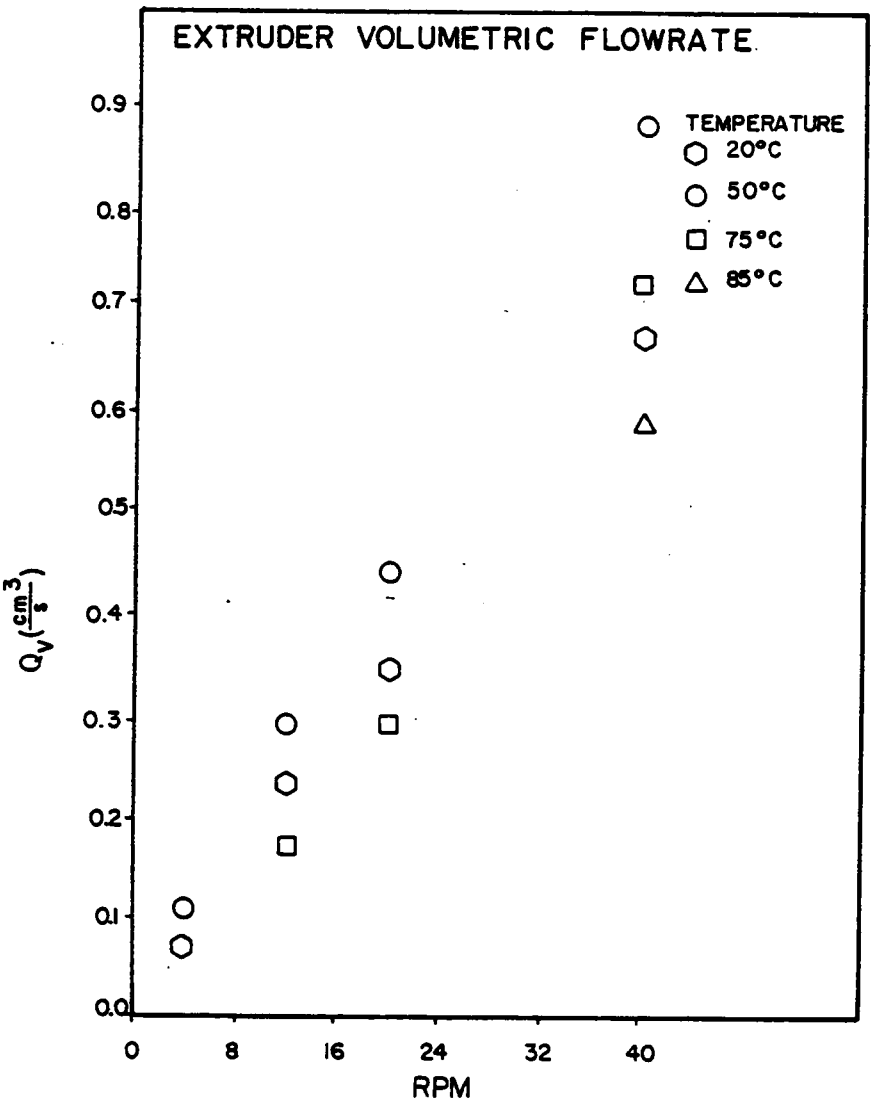

Figure 74. Extruder volumetric flowrate as a function of temperature and rpm.

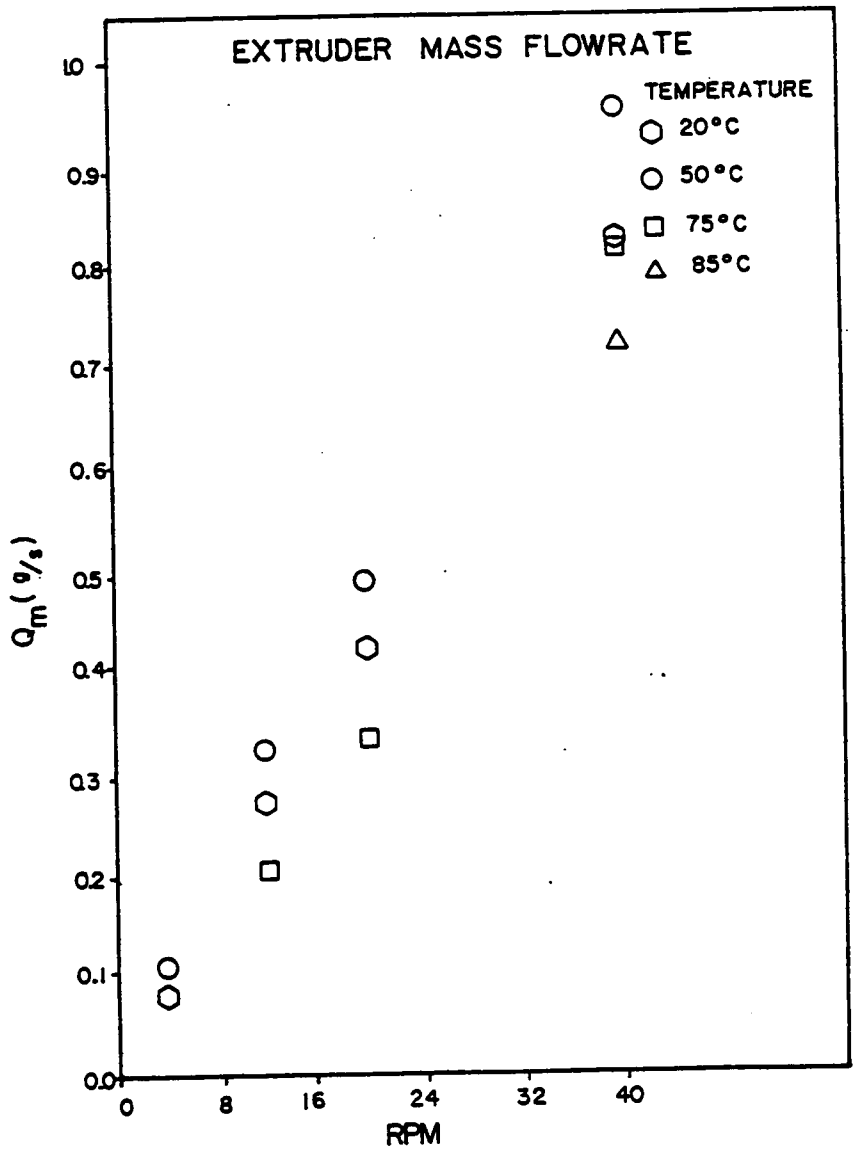

Figure 75. Extruder mass flowrate as a function of temperature and rpm.

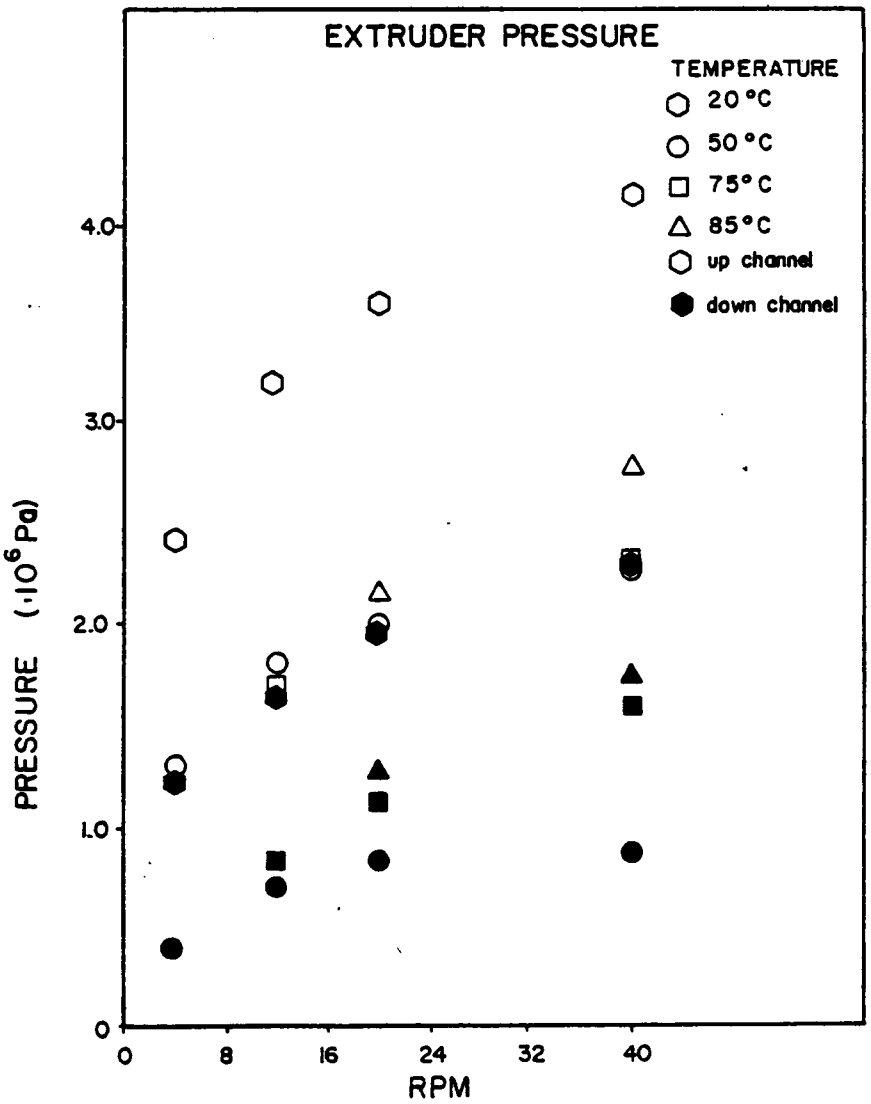

Figure 76. Extruder pressure profiles as a function of temperature and rpm.

Finally, in Figure 76 is displayed the pressure data collected during the experiments. Two pressure transducers were mounted on the extruder, one approximately half the distance down the length of the extruder axis designated the up-channel pressure, and one at the extruder exit designated the down-channel pressure. The most noticeable aspect of the data shown in Figure 76 is the fact that the up-channel pressure is greater than the down-channel pressure for all extrusion rates and temperatures. This is not the normal operative conditions for an extruder. Pressure normally builds for the length of the extruder reaching its highest value at the exit to the die. This abnormal pressure profile is most likely due to the feed system designed to feed the 50% moisture soy dough.

First some basic facts known about the extrusion process. The pressure build-up in the extruder is directly proportional to the flooded length of the screw. In most operations, the feed is gravity fed into the extruder. The feed particles drop into the deep flights of the feed section of the extruder screw. It is not until the compression section that the material is compacted and a flooded screw is achieved. However, due to the feed assembly manufactured to feed the 50% moisture dough, the entire length of the screw is flooded for these experiments, even the deep channels of the feed section of the screw. As the material moves down the tapered screw, the pressure builds as normally occurs in an extruder. A point is reached however, where the velocity of the material exceeds the rpm of the screw because of the taper of the screw. In other words, more material needs to be transported along the screw than drag flow mechanism provides. Hence, pressure then aides in the flow. This realizes a pressure maximum at the point where drag flow becomes insufficient. Before this

point pressure builds and after this point pressure decreases. For this reason, the down-channel pressure is lower than the up-channel pressure.

The curvature of the pressure curves as a function of rpm results because of the non-Newtonian nature of the 50% moisture dough. The most severe curve occurs at 50°C while the other temperatures exhibit approximately the same shape. No explanation is offered as there is no great difference in the viscosity of the 50°C from the of the other temperatures.

Finally, the temperature dependence of the pressure curves reflects the results found earlier. The most viscous material was seen to be the soy dough at 20°C, or ambient temperature. The pressure related to the ambient temperature extrusion experiment is much greater than the pressures associated with any of the other experiments. The pressure results of the heated extrusion experiments were all very close for the lower extrusion rates. The viscosity curves of the 50% moisture dough for the elevated temperatures were also very close. In effect, the temperature dependence of the pressure curves reflect the temperature dependence of the viscosity.

5.6 NUMERICAL EXPERIMENTATION

5.6.1 INTRODUCTION

In this section is discussed the aspects involved with the three dimensional finite element model of the extrusion of a 50% moisture soy dough. To begin, the conditions of the numerical model are presented. The conditions include the discretization of the domain, boundary conditions, and material parameters. Next, the limitation due to the FIDAP

program are outlined. The errors introduced into the formulation of the numerical model are then discussed. Finally, the results of the numerical model are presented and compared to experimental extrusion results.

5.6.2 CONDITIONS

The various conditions employed in the numerical model are now presented. Included in this discussion is the discretization of the domain, the boundary conditions employed, and the material parameters chosen for use in the model as discussed in the previous sections. First, the method of determining the discretization to be used in the finite element mesh is presented.

As discussed in the chapter on numerical methods, the accuracy of the numerical solution depends on the fineness of the mesh. However, too fine a mesh may give inaccuracies in the solution as well as long computing times which translate into large costs. Therefore, a mesh which is fine enough to give an accurate solution but coarse enough to minimize computational costs had to be found. As three dimensional runs in themselves require much greater amounts of computer time due to the additional unknowns and increase in number of nodes because of the third dimension, the determination of an appropriate mesh for the problem was performed in two dimension. By using the downchannel cross-section of the three dimensional problem, it was assumed that an adequate mesh could be found. Five meshes of different fineness were tested. The velocity and pressure results of the five meshes were compared at different points to determine the consistency of the results from mesh to mesh. If the results of a coarser mesh are within 2% of the finer mesh, the coarser mesh was con-

sidered to be sufficient to adequately model the process. This method was used to determine the best mesh of the five tested to be used in the three dimensional model. For the three dimensional model, the third dimension was added to the two dimensional mesh determined by the method just discussed in proportion to the dimensions of the elements used in the height of the channel in the two dimensional mesh. The aspect ratio of elements is an important factor in finite element calculations. An accepted rule is to keep the aspect ratio under ten for each element. However, due to the overall dimensions of the extruder channel and die, the length of the screw channel being over 100 times the height or width of the channel, this rule was broken in the construction of the meshes tested. It is known that a circulatory flow occurs in an extruder and hence, enough elements must be included in the cross-channel section of the extruder mesh to approximate this flow. Also, the areas nearest to the moving barrel wall will have a large shear gradient which would be difficult to handle unless the elements are sufficiently small. However, it was assumed that flow in the down channel direction would not change greatly in the middle length of the extruder but only at the entrance and exit sections and in the die. Therefore, the aspect ratio was not kept below ten for the down channel direction. When the third dimension, or cross-channel dimension, though was added to the two dimensional mesh, the aspect ratio for the elements in terms of height versus width was kept below ten for all meshes tested.

The next step was to determine the boundary conditions to use in the model. These consist of velocity, pressure, and temperature boundary conditions. The following section describes the boundary condition as

shwon in Figure 77. The notation employed specifies the y-direction being across the channel, the z-direction being the height of the channel, and the x-direction being along the downchannel direction along the screw and die. At the inlet to the extruder, if a pressure boundary condition is specified, it is specified in the stress vector. If the viscous terms are assumed to be negligible, then the applied stresses simply reduce to a pressure boundary condition. Hence by specifying the pressure in the appropriate direction it is equivalent to specifying applied stress. This pressure is atmospheric pressure plus the additional pressure applied due to the feed system. This pressure amounts to approximately 15 psi over atmospheric. The pressure acts normal to the inlet face, hence it is applied in the x-direction. As a pressure is specified, the velocity in the x-direction must be left as an unknown so as not to over specify the node conditions. If a velocity entrance boundary condition is employed the velocity in the x-direction is specified at the nodes on the entry face and no pressure is specified. The velocities in the z- and y-directions are specified to be zero at the inlet. If non-isothermal conditions are analyzed, the inlet temperature is specified at ambient, 25°C.

At the top of the channel, or the barrel face, the x- and y-velocities are specified as the components of the extruder velocity as calculated from the experimental rpm. The pressure is an unknown. Heat in the experiments was applied through band heaters around the barrel. Therefore, for the non-isothermal case, the temperature is specified according to the set temperature used during the experimental investigation.

At the screw surface or bottom of the channel, and the two walls of the channel all velocities are set to zero in accordance with the no slip conditions and the pressure is an unknown. In the laboratory extruder, there is no means of heating the screw. Hence, for the non-isothermal case, a zero heat flux is specified which in essence sets the wall temperature at the temperature of the material.

At the intersection of the extruder channel and die assembly, there is a wall which occurs in the geometric approximation to the extruder channel and die assembly. This is due to the extruder channel whose height is much smaller than the opening to the die assembly. At these points, the velocities are specified as zero, the pressure as an unknown, and the temperature at the experimental temperature which is the temperature the barrel was set at in the experiment.

At the walls of the die assembly, again the velocities are specified as zero, the pressure as an unknown, and the temperature as the temperature of investigation to match experimental temperature setting. Finally, at the outlet face of the die assembly, the pressure is set to atmospheric pressure. This again acts normal to the face of the die assembly outlet and therefore, the x-direction velocity must be an unknown. The z- and y- velocities are specified as zero with a zero heat flux condition across the face for the non-isothermal case.

Lastly, the material parameters to be used in the numerical model are outlined. The viscosity function used was a power law model with specified n and m values. For non-isothermal problems, the heat capacity and thermal conductivity employed were constants as it was found that for the tem-

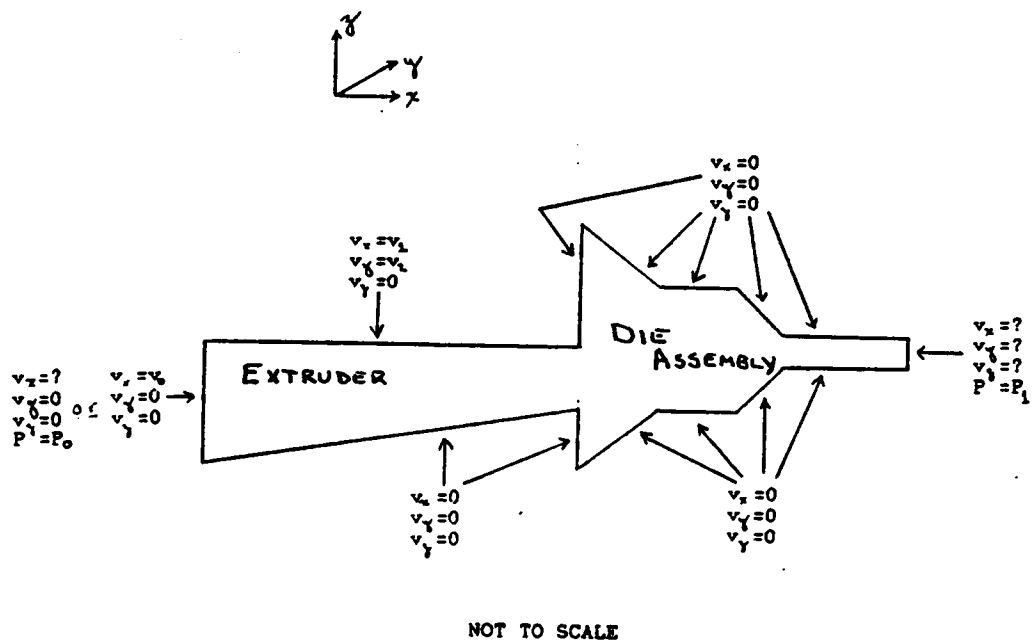

Figure 77. Boundary conditions for the numerical simulation.

perature range of investigation the values for both heat capacity and thermal conductivity were essentially constant.

5.6.3 LIMITATIONS

As mentioned in the numerical methods chapter, a commercially available finite element code, FIDAP, was used to perform the numerical model of the extrusion process. FIDAP, although being one of the few three-dimensional finite element programs available, and possibly the only developed to handle fluid flow at this time, possesses certain limitations due to the generality needed in a commercial code. These limitations will vary from problem to problem. One major limitation is encountered during the modeling of the extrusion of 50% moisture soy dough. It was found that the viscosity could be modeled by the power law equation. It was also found that the viscosity was temperature dependent. However, FIDAP has the ability to handle power law or temperature dependent viscosity, but not a temperature dependent power law model. As a result of this limitation, only the power law relationship at the experimental temperature for the viscosity was employed. In essence, then, this simplification neglected the entry flow in the extruder where the material was heating to the experimental temperature.

Whether this was a serious simplification had to be explored. Two things were explored in an effort to determine the importance of the temperature dependence of the viscosity upon the numerical results. First, the distance down the extruder required to heat the material to experimental temperature was calculated. Second, the velocity profiles for the different viscosity relationships were examined. With regards

to the former, the extruder was modeled in three dimensions without the die assembly to determine the distance down the extruder required to heat the material to experimental temperature. The extruder alone was modeled for these investigations for two reasons, it was assumed that the material reached experimental temperature in the extruder and modeling only the extruder saved calculation time which in turn saved computational costs. The results of these numerical experiments show that the material is heated to the experimental temperature within the first quarter of the extruder length as can be seen in Figure 78. In addition, 70% of the material reaches 50°C within the first eigth of the extruder length.

With regards to the latter investigation into the effect of the temperature dependence of the viscosity relationships upon the velocity profiles, the initial experiments were again performed in only the extruder section. The velocity profile results were compared to determine how different the velocity profiles were as a results of the different viscosity relationships. A comparison of the velocity profiles resulting from the 25 and 85°C viscosity relationships is shown in Figure 79. Two things are noticed in this figure. First, the differences between the two velocity profiles are insignificant over the length of the extruder. In fact, the largest difference is found to be only 12% between the two profiles. Second, in the beginning of the extruder the velocity of the material at 25°C is predicted to be slightly greater than the material at 85°C. However, by the end of the extruder this condition has changed and now the velocity of the 85°C material is slightly greater than that of the 25°C material. In addition, the shape of the velocity profile changes as the fluid progresses along the length of the extruder. This

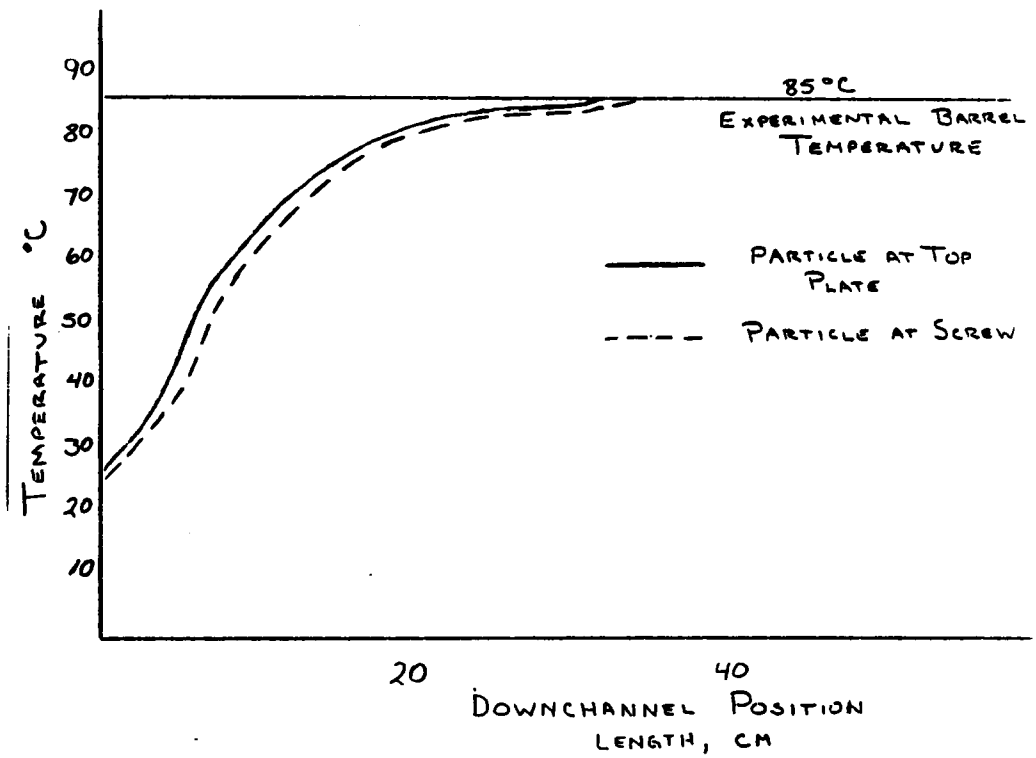

Figure 78. Temperature profile as a Function of Position in the Extruder

phenomenon is explained through the observations seen in the extrusion experiments. It was found that at some point in the extruder the pressure profile reached a maximum at which point the flow in the extruder went from drag flow with a negative pressure flow contribution to drag flow plus a positive pressure flow. It is expected that the material with the higher power law index would respond more to pressure flow than a material with a lower power law index. Hence, as the soy dough at 25°C has a lower power law index than that at 85°C the velocity profile at the beginning of the extruder exhibits less of a change due to the negative pressure flow. Likewise, at the end of the extruder, once the flow becomes pressure driven as well as drag flow, the material with the higher power law index would have the greater forward velocity as it is more responsive to the pressure force.

One factor which actually benefits from the inability to model a temperature dependent power law viscosity is the computational time. As the thermal conductivity and heat capacity are taken as constants and the viscosity cannot be temperature dependent and obey a power law relationship simultaneously, the analysis can be performed as if it were under isothermal conditions. This means that the temperature unknown as well as the whole energy equation are eliminated from the problem considerably reducing computational time.

In summary, justification of the use of isothermal conditions in all subsequent numerical simulations has been presented. First, it was shown that only the very initial section in the extruder is affected as the material rises quickly to the barrel temperature. Second, even with the different viscosity parameter constants, the velocity profiles do not

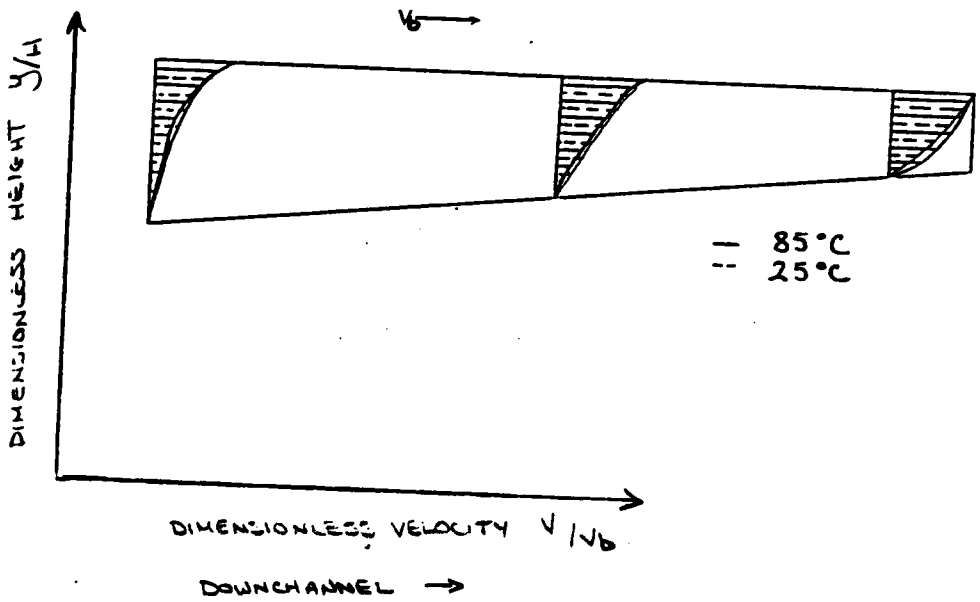

Figure 79. Comparison of the Velocity Profiles for Soy Dough at 25 and 85°C

differ greatly. Finally, the savings in computational time cannot be ignored.

Another limitation is that the computer program assumes that the channel is completely filled with material. Even with the pressure feed system it is not guaranteed that the channel is completely filled over the total length. This condition in reality may not occur until further along the screw where the channel is smaller and the dough would then be packed. As pressure build-up in the extruder is directly proportional to filled channel length, this assumption as to the length of filled channel could introduce error into the calculation.

5.6.4 ERRORS

Before the actual modeling even takes place, certain factors in the simulation are known to be sources of error. These factors exist for many different reasons. For instance, the first source of error is the simplification of the viscosity equation due to the limitation of the FIDAP code to handle temperature dependent power-law viscosity relationships. The next source of error is due to the discretization of the domain. Finally, another source of error is the geometric approximation to the extruder and die assembly. These sources of error are now discussed in more detail.

It was discussed in the section on limitations that temperature dependent power law viscosity function could not be used in conjunction with the FIDAP code. Hence, neglecting the temperature dependence of the viscosity is assumed to introduce error into the calculations. Two points were investigated toward determining the significance of the temperature

dependence: the processing length before experimental temperature was reached and the differences in the velocity profiles caused by the temperature dependence of the viscosity. Although it was shown that the temperature dependence effects were relatively small, some error will be introduced into the calculations due to the simplifying assumption of using the experimental temperature viscosity as the viscosity function for the whole processing operation. Both the calculated pressure and velocity profiles will be altered as a result of the viscosity simplification.

As mentioned in the chapter describing numerical methods, another error that arises in the use of the finite element method is the error due to the discretization of the domain. This occurs when the domain cannot be approximated exactly by the simple geometric shapes used in the mesh, in this case the three dimensional bricks. The extruder channel was approximated exactly as its shape is a parallelpiped due to the assumption of unwinding the channel from the screw and using parallel plate flow to describe the flow geometry. However, the die assembly is cylindrical and cannot be approximated exactly by bricks. Therefore, there is an error introduced into the solution due to the approximation of the circular cross-sectional area of the die assembly by quadrilaterals. The circular cross-section is approximated by six quadrilaterals as shown in Figure 80. The cross-sectional area is reduced by 8.7% by the approximation. Hence, one result of the approximation would be to increase the velocity through the die. Also, the pressure profile of the extruder should be somewhat higher due to the greater constriction of the die approximation geometry.

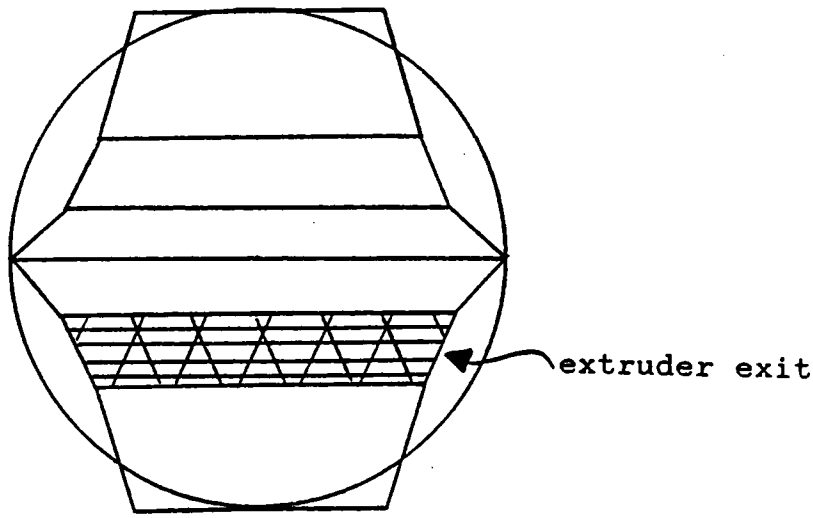

Figure 80. Cross-section of the die with finite element approximation

Finally, another source of error in the numerical model is the geometric approximation of the extruder and die assembly. Whereas the error associated with discretization is due to the geometric approximation of the finite element mesh to the domain, the error of interest now is due to the approximation of the domain to the actual physical system. Of greatest concern is the meeting of the extruder exit with the entrance to the die assembly. There is an error associated with the aproximation of the extruder in unwrapping of the channel but this has been investigated many times over in the literature [123] and will not be discussed here. It is simply mentioned as another source of geometric error.

Two specific errors are associated with the geometric approximation of the exit of the extruder into the entrance of the die. The first error is caused by the shape of the extruder exit and the second is caused by the positioning of the extruder exit with respect to the entrance to the die assembly. An error is introduced with the geometric approximation of a squared-off channel at the extruder exit. In reality, at the tip of the screw, the end of the extruder channel is actually on the diagonal rather than squared-off. This geometric approximation of a squared-off channel at the exit of the extruder then changes the flow pattern from the extruder into the die assembly. The second error is introduced with the positioning of the extruder exit at the entry of the die assembly. During extrusion, the screw is rotating and hence, the opening of the extruder channel into the die assembly would be rotating also. Instead, with the approximation of the unwrapped channel with top plate moving diagonally across it, the exit of the extruder is fixed rather than moving in the opening of the die assembly. In addition, an arbitrary stationary

position had to be specified as no one position in the entrance to the die assembly could be assumed to be better than another. The combination of the arbitrary positioning of the non-rotating extruder exit most probably changes the flow into the die influencing the flow throughout the die. Hence, the geometric approximations mentioned here most probably affect the flow out of the extruder and through the die introducing possibly significant error into the calculation.

5.6.5 NUMERICAL MODEL RESULTS

Several simplified problems were tested for solution by FIDAP in order to determine if the program could handle fluid flow in general and specifically handle the viscosity parameters adequately. All problems which were run initially had analytical solutions to which the experimental results could be compared. These numerical simulations included tube flow and parallel plate flow in two dimensions. The viscosity parameters used in these simulations consisted of first trial with a newtonian viscosity equal to the consistency coefficient, m, of the dough at 25°C after which selected power law viscosity parameters found at the different extruder experimental temperatures were employed. The different numerical simulations were performed with both pressure and velocity boundary conditions where applicable.

As mentioned, various fluid flow problems with analytical solutions were examined using FIDAP to determine the efficiency of the program in modeling the flow. First, tube flow using a newtonian viscosity was examined with pressure boundary conditions at the inlet and outlet. The numerical solution was found to match exactly the analytical solution.

Next, tube flow with the power law parameters for the soy dough at 25 and 85°C was examined with pressure boundary conditions at inlet and outlet. Again, good agreement was found between the numerical simulation and analytical solution with less than 2% variation in velocities found. Next parallel plate flow was examined employing both drag flow and a combination of drag flow and pressure backflow. For the drag flow case, the pressure at the entrance was specified to be the same as the pressure at the exit. Only the moving top plate causes flow in the fluid. As pure drag flow is simply related to the velocity of the top plate the calculated velocity profile is the same regardless of the viscosity function employed. For both newtonian and non-newtonian cases excellent agreement was found with less than 2% deviation from the analytical solution as can be seen in a typical solution plotted in Figure 81. For the drag flow with pressure backflow, the boundary conditions were set similar to that experienced in the extruder with the outlet pressure being higher than the inlet pressure. This causes backflow in the extruder and hence, the velocity profile is a combination of the positive drag flow and the negative pressure flow. Both newtonian and power-law viscosity relationships were used in conjunction with these boundary conditions. As can be seen in Figure 82, the numerical solution for the newtonian viscosity displayed excellent correspondence to the analytical solution. Again, less than 2% deviation in calculated versus analytical result was found. Once the power-law viscosity parameters were employed the agreement between numerical simulation and analytical solution was not found to be quite as good as can be seen in Figure 83. The general shape of the velocity profile is predicted correctly. However,, in the region where the

pressure backflow predominates the calculated velocities are greater than the analytical values. This is the first indication that the power law index may cause difficulties in solution of the numerical model. Other power law viscosity parameters corresponding to the soy dough at other experimental temperatures were also tried with this problem of parallel plate flow with pressure and drag flow. Figure 83 is characteristic of these solutions with the general shape of the velocity profile calculated correctly but the calcualted velocities in the lower part of the channel where pressure backflow occurs to be slightly greater than those predicted.

The next set of computer runs looked at the two dimension model for the extruder and die geometry of the system. No analytical solution for this problem exists. However, the shapes of the velocity profiles in the various sections of the extruder and die can be examined as well as the magnitude of the pressure. For these cases, a pressure at the entrance and exit were specified. For the power law viscosity parameters employed the velocity profiles and pressures found by the numerical simulation were of the shapes and magnitudes expected. The velocity profiles along the length of the extruder as seen in Figure 84 demonstrate the velocity changing from drag flow with pressure backflow to drag flow plus a positive pressure flow due to the converging channel configuration. Based on calculations for flowrate through a die, the pressure generated at the entrance to the die is of sufficient magnitude to provide the flowrates achieved in the extrusion experiments. As these results appeared to be correct, the next step was to move on to three-dimensional modeling.

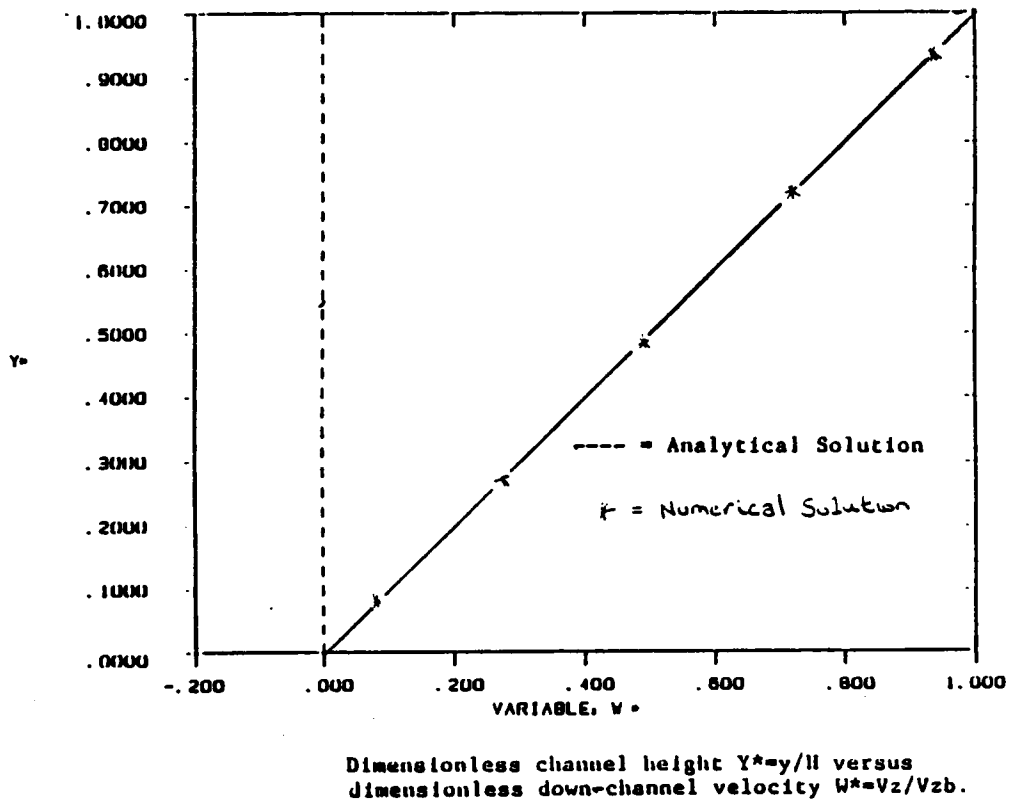

Dimensionless channel height Y*=y/H versus
dimensionless down-channel velocity W*=Vz/Vzb.

Figure 81. Numerical vs. Analytical Solution for Two-Dimension Drag Flow for Soy Dough at 85°C

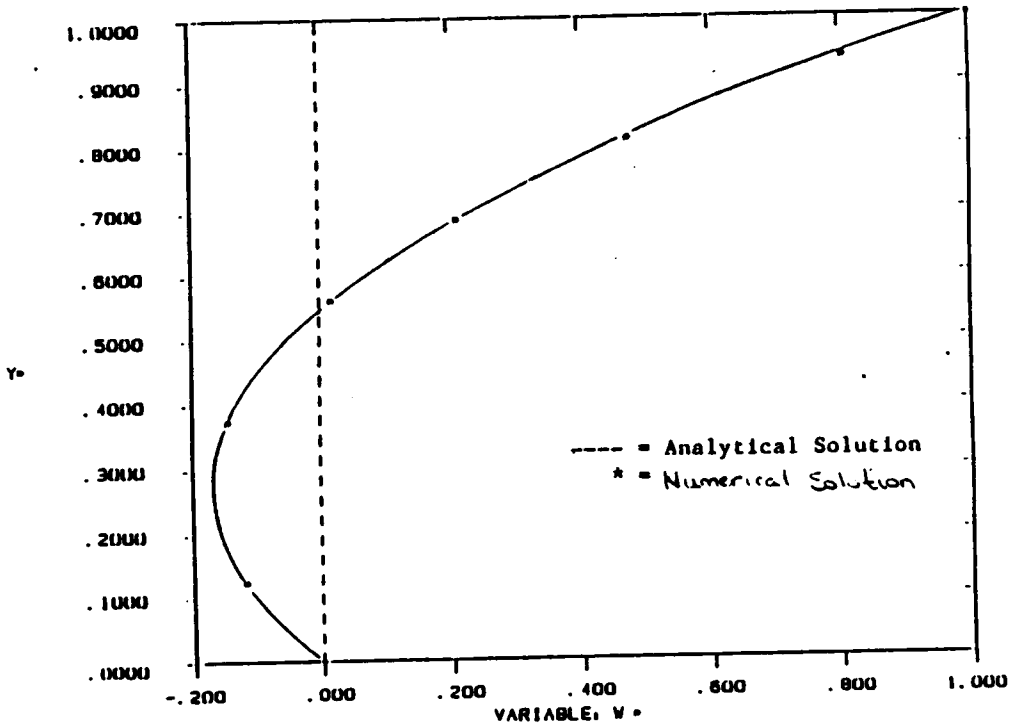

Dimensionless channel height Y*=y/H versus dimensionless down-channel velocity W*=Vz/Vzb. Newtonian fluid.

Figure 82. Numerical vs. Analytical Solution for Two-Dimension Drag and Pressure Flow for Newtonian Fluid

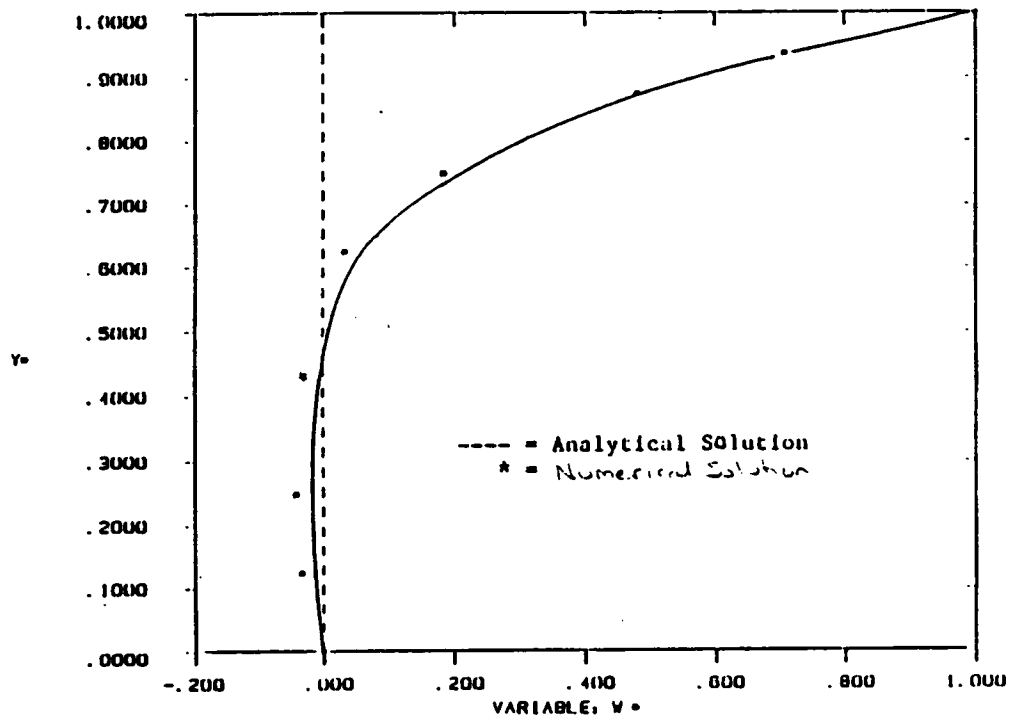

Dimensionless channel height Y*=y/H versus
dimensionless down-channel velocity W*=Vz/Vzb.
Power-law fluid, N=0.4

Figure 83. Numerical vs. Analytical Solution for Two-Dimension Drag and Pressure Flow for Soy Dough at 85°C

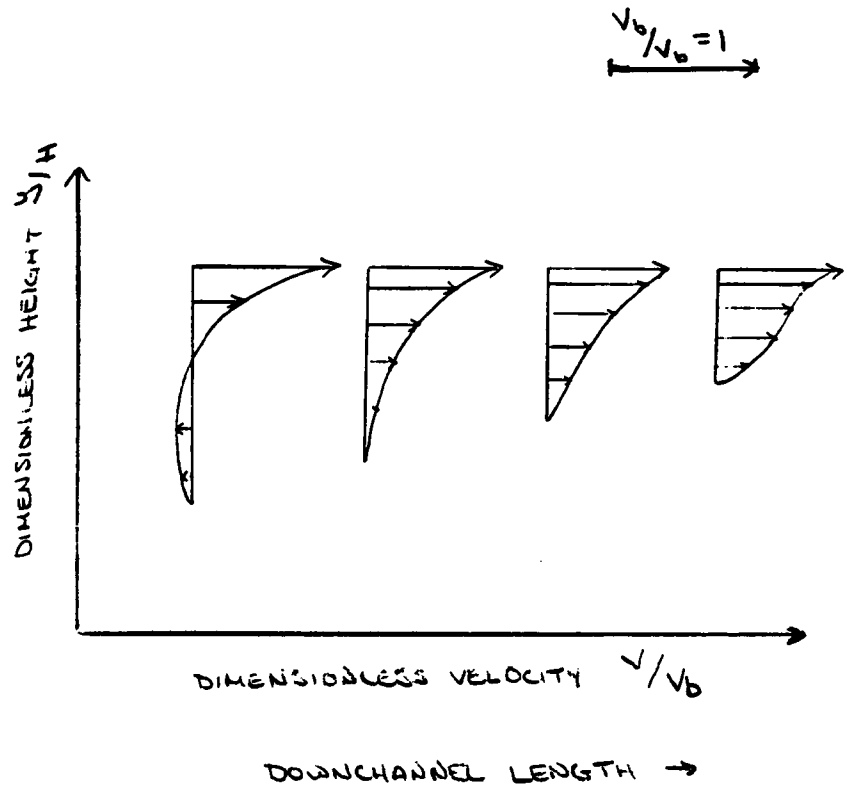

Figure 84. Velocity Profiles in the Extruder found in Two Dimensional Modeling of the Extruder and Die: Power law parameters of dough at 85°C, 40rpm extruder speed

Before the actual three dimensional modeling of the extruder and die assembly was performed, three dimensional modeling of a channel was attempted as for a Newtonian fluid an analytical solution existed which could be compared to the numerical results. The analytical solution used was that extended by Tadmor and Gogos [123] for the metering zone of a single screw extruder. The geometric conditions used in these simulations were a square pitched screw with dimensions similar to the laboraotry extruder. The width and height of the channel corresponded to the width and height at the entrance of the laboratory extruder screw and the length was that of the laboratory screw. The cross-channel flow in the extruder as predicted by the numerical simulation and the analytical solution are plotted in Figure 85. In Figure 86, the downchannel cross-section velocity profiles are plotted for both the numerical and analytical solutions. Once again, in both cases, excellent agreement between the calculated and analytical velocities is found.

Next, the actual modeling of the extruder and die assembly was performed. As mentioned, the three dimensional mesh used for these computer trials was determined by testing two dimensional meshes then adding the third dimension. Even with minimizing mesh size by this method, 2180 elements with 3096 nodes were determined as the minimum mesh which would provide adequate results. This mesh was used in all computer trials. From this point on, only boundary conditions or physical properties and conditions were changed from trial to trial.

In terms of the physical properties and conditions used in the computer trials, one set of values was used first to determine if the boundary conditions specified would indeed yield convergence of the pro-

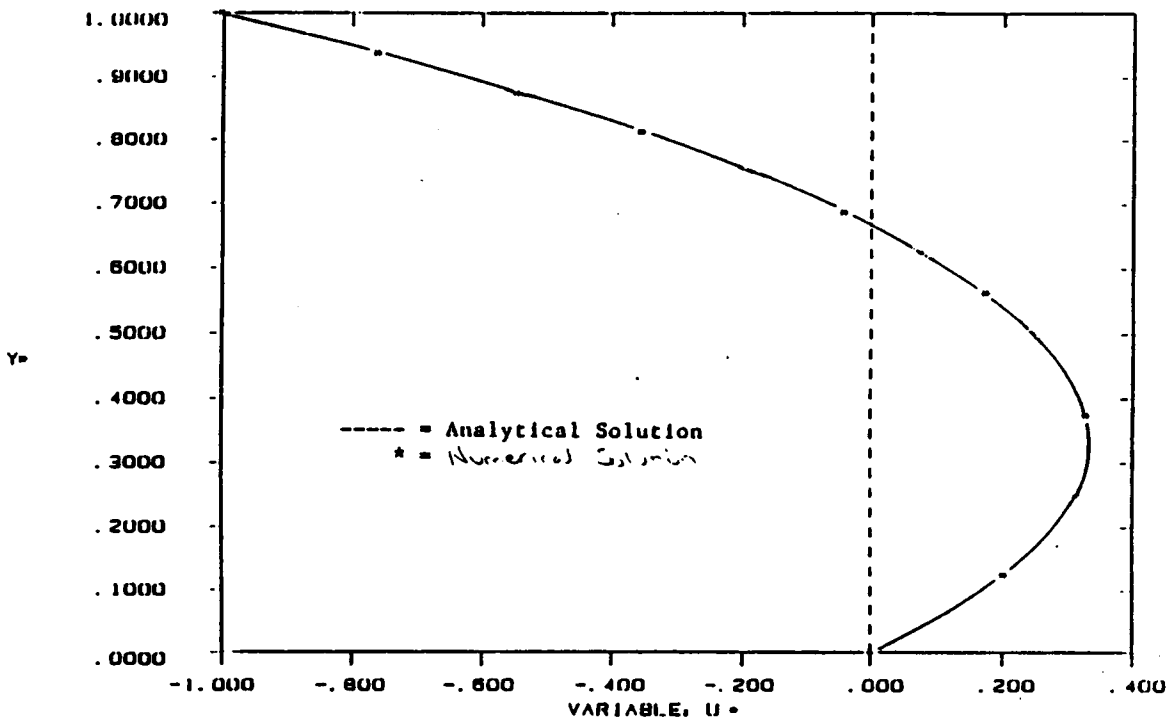

Dimensionless channel height Y*=y/H versus dimensionless cross-channel velocity U*=Vx/Vxb. Newtonian fluid.

Figure 85. Calculated vs. Analytical Cross-Channel Velocity Profiles

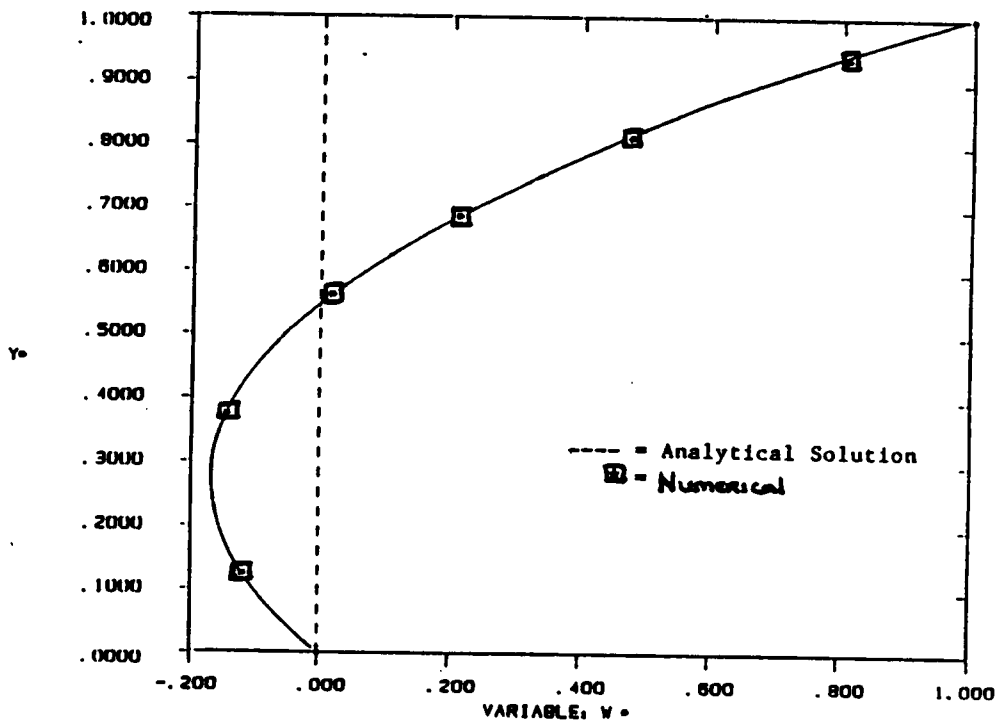

Figure 86. Calculated vs. Analytical Down-Channel Velocity Profiles

gram with realistic results. Realistic results were determined by performing a mass balance on the system, checking for flow in to equal flow out, and reasonable magnitudes of values on velocity and pressure. These physical properties were the viscosity values, power law index and viscosity coefficient, for the soy dough at 25°C and an extruder speed of 40 rpm. The viscosity values for the soy dough at 25°C were chosen for two reasons. The power law index was 0.29, the second largest of all those determined at the experimental temperatures. Employing this power law index should give a better chance for convergence as it was one of the larger values determined for power law indices. Secondly, the viscosity values at 25°C were used because the error associated with using an isothermal viscosity condition would not be a factor. The extruder speed of 40 rpm was chosen so that comparison of computer predictions could be made with the other experimental temperature viscosity values. As mentioned, the higher experimental temperature conditions only produced consistent flow from the laboratory extruder at higher rpm. At 40 rpm, consistent results from laboratory experiments were found for all experimental temperatures. Hence, once boundary conditions which provided convergence of the program with realistic values were found the other viscosity values could be employed in the program. These results could then be compared against one another to determine the effect of the varying viscosity values on the results as well as comparing the computer results to the laboratory experimental results.

Now that the physical properties and conditions have been specified, the boundary conditions to be used must be examined. The specification and explanation of the majority of boundary conditions to be employed has

been previously discussed. Most were specified due to no slip conditions at the walls and were not changed throughout the trials. For the three dimensional case discussed here for modelling of the actual extruder flow, the conditions were assumed to be isothermal for the reasons previously mentioned and hence no temperature boundary conditions were used.

The specification of the boundary conditions at nodes which fall at the corner of two walls having different boundary conditions must be done with care. For example, the edge nodes of the moving top plate and the walls of the channel must be specified in the correct manner. The nodes at the edge at which the plate has a cross-channel velocity toward the center of the channel are specified with both cross-channel and down-channel velocities. However, at the other edge of the top plate where the plate is moving away from the channel, the nodes at the corner must have a zero cross-channel velocity specified with simply a down-channel velocity given. Otherwise material would be allowed to flow out of the channel at that point in the computer program. Similar consideration at all other meetings of boundaries had to be taken to prevent this type of error from occurring.

Of interest is the specification of the entry region of the extruder. As mentioned, a pressure or velocity boundary condition could be used at this face of the mesh. A pressure boundary condition is preferred as using a velocity boundary condition then makes the problem a contrived one. When a velocity boundary condition is used, a velocity profile is input at the inlet face. This in essence sets a flowrate. Hence pressure can then be the only variable which is not set and can be compared for accordance with experimental results. In addition, if the experimental flowrate upon

which the inlet velocity is based is incorrect for any number of reasons, slippage,incomplete packing of the flights, etc., the inlet velocity would be wrong and convergence could not be expected. When a pressure boundary condition is used both velocity and pressure through the extruder is calculated and can be compared to experimental results.

Hence the pressure boundary condition was employed first. The value was set at 15 psi over atmospheric as discussed in the conditions section due to the pressure feed system. Although the program converged to a solution, the results for these conditions were not good. As discussed, a mass balance was calculated using the predicted velocities at the inlet and outlet. The velocities at the inlet however were found to all be negative. This is an immediate sign that a realistic solution was not reached. Velocity and pressure profiles were examined to see if the cause of the error in solution could be determined.

The velocity profiles at various sections along the extruder are displayed in Figure 87. The top and bottom velocities are specified by the boundary conditions. Hence, the calculated velocities are totally negative for 90% of the extruder length as can be seen in the velocity profiles displayed. Only the last 10% of the extruder has some of the calculated velocities as positive numbers. The die section, however, has all positive calculated velocities with parabolic profiles when plotted as in Figure 88. This indicates that the mass that did reach the die did in fact develop a realistic flow profile through the die. The downfall of the program then comes from the flow development in the extruder itself.

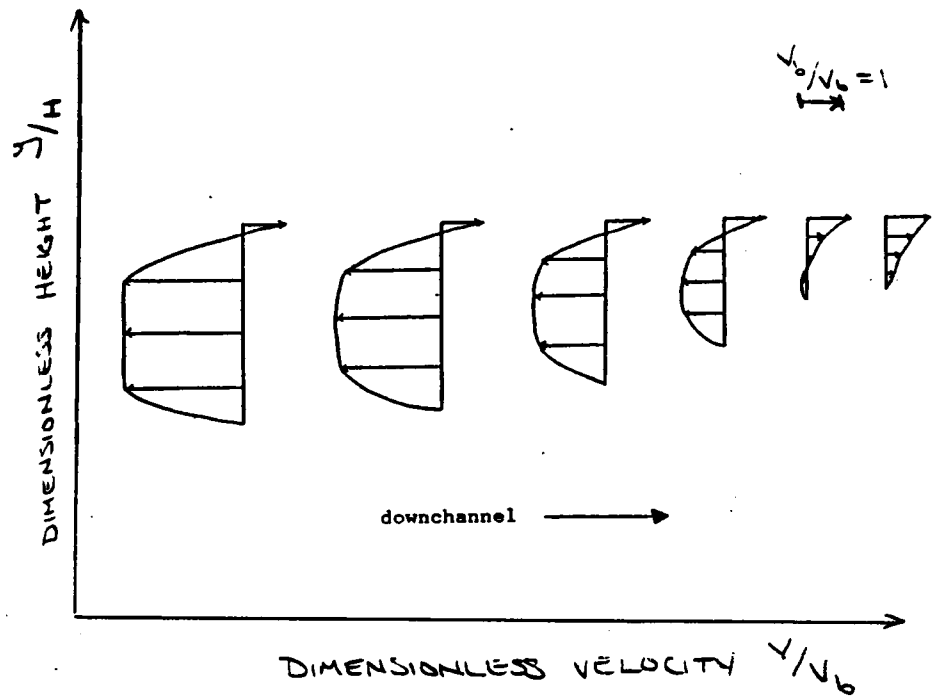

Figure 87. Velocity Profiles in the Extruder for Pressure Entrance Boundary Conditions: Conditions: Press. inlet = 15psi, 85°C, 40rpm

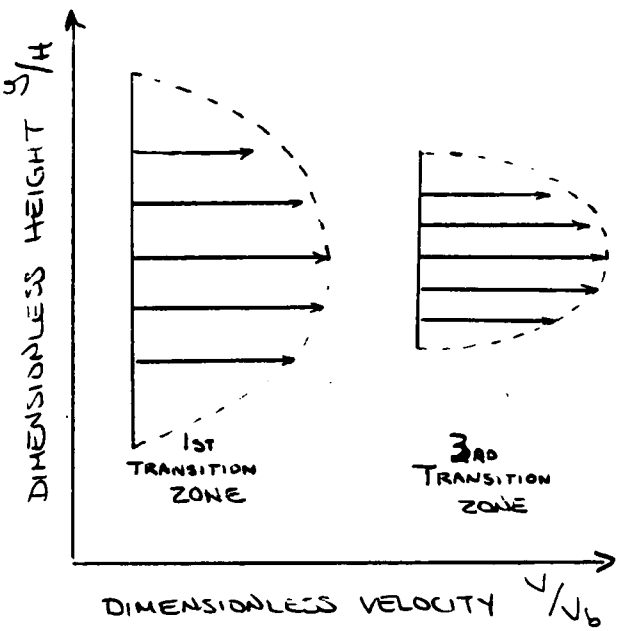

Figure 88. Velocity Profiles in the Die for Pressure Entrance Boundary Conditions: Conditions: Press. inlet = 15psi, 85°C, 40rpm

The pressure profile along the channel was examined next. The "checkerboard oscillation" on pressure was found. When this occurs, the pressure alternates from positive to negative from node to node along the mesh. This is an artifact of the type of element that is used in the mesh and has been documented in other finite element problems. The accepted treatment is to use the average of the pressure over the element as the representative pressure. By using this procedure, the pressure profile was plotted along the length of the extruder. Pressure was seen to build along the length up until the exit of the extruder into the die. As this behavior is expected in extruder flow, at this point it appears to be the velocity calculation which is in error. Although the error may in part be due to the "checkerboard" pressure, the type of element used in the problem could not be changed due to limitations in mesh size. Hence, unless another mesh is used the actual cause of the error can not be determined.

As it appeared for the initial trial with pressure specified at the entrance boundary that the pressure at the inlet of the extruder was not sufficient to prevent backflow of the material out the extruder entrance in the computer program, the pressure specified for the inlet was doubled. Although these were not the conditions the experimental trials were performed at, additional experimental trials could be performed at these conditions with the use of the pressure feed system. The results of the computer trial could then be compared to the laboratory experimental results if the numerical model converged with the higher pressure specification. However, even the increased pressure could not prevent the backflow from occurring. The velocity and pressure profiles resulting

from this trial were very similar to those of the previous trial with negative flow at the entry of the extruder still occurring.

Since a specification of pressure at the entrance boundary did not provide good results, the velocity at the entrance boundary was used. As discussed, this involved calculating a flat velocity profile from the experimentally determined flowrate for the physical conditions being specified to use at the entrance of the extruder. For the 25°C and 40 rpm experimental conditions, this calculation yielded an inlet velocity of 0.317 cm/s. Using this velocity, the computer program was run and the mass balance over the system was checked. For these conditions, the volumetric flowrate at the exit of the extruder was calculated within 5% of the inlet volumetric flowrate. It is possible that the 5% error is introduced in the numerical integration of the velocity profile at the exit rather than by the program itself. But in either case, the agreement found is quite good. A preliminary examination of the pressures showed a realistic magnitude with pressure building along the length of the extruder.

With the results of this trial appearing so reasonable, the decision to perform additional computer trials at other physical conditions was made. Four additional trials were performed. The conditions for these trials were as follows: viscosity constants for soy dough at 25°C with extruder speed at 12 rpm, viscosity constants for soy dough at 75°C with extruder speed at 12 and 40 rpm, and viscosity constants for soy dough at 85°C with extruder speed at 40 rpm. While the results for these four trials varied, all the results were bad. Two of the computer trials did not even converge. These two trials involved the conditions with viscosity

constants for the 75°C soy dough at extruder speeds of 12 and 40 rpm. The power law index used was most likely the cause of the non convergence in these cases. The power law index for the 75°C soy dough was 0.21, the lowest of all power law indices determined at the various experimental temperatures. As mentioned previously, the lower the power law index, the more problems that arise in the computer simulation of flow and hence, the more difficult for convergence to be met. The other two trials converged but mass balances over the systems did not correlate. The pressure and velocity profiles for each case were examined to determine if the cause of the error could be found.

For the inlet velocity specification for physical conditions of viscosity constants of 25°C soy dough at an extruder speed of 12 rpm, the exit flowrate was calculated to be over 15 times less than the specified entrance flowrate. The pressure profile through the extruder had some abnormalities. The pressure in the first third of the extruder exhibits the "checkerboard" syndrome. By using the average pressure over the element and plotting pressure as a function of distance along the extruder, pressure is seen to rise along the length. At the very exit of the die pressure again exhibits the "checkerboard" instability. The velocity profile at various points along the length of the extruder was also examined. As can be seen in Figure 89, the velocity profiles in the first 10% of the extruder show a large backflow occurring. In fact, when a mass balance is performed over the first axial set of elements, only a small amount of mass is allowed to continue to flow downchannel. Hence, it is in the first section of the extruder that the error seems to arise as indicated by both pressure and velocity values. This may be caused by an

incorrect specification of the entrance boundary condition velocity profile. As the viscosity values employed are the same as for the computer trial which gave good results, it is difficult to attribute the error to the physical constants used. However, the extruder speed did change which in turn would change the shear gradients in the calculations and could produce the error.

Of the four additional trials which were performed, this trial was the one which was expected to converge to realistic results. As the only thing that was changed between the two trials was the speed of the extruder, as long as the inlet boundary condition velocity profile was correct the program should have worked. As mentioned, since the experimental results were used to calculate the velocity profile at the inlet, it is possible that this was the cause of the error. However, if drag flow predominates in food dough extrusion as postulated and discussed in the literature, the inlet flowrate was in proportion to the ratio of the speeds and hence should have yielded good results. If all this is accepted as truth, there may be more than one factor contributing to the error in calculation used in the computer trial.

The other trial which failed was the computer run using conditions of viscosity values for the soy dough at 85°C and an extruder speed of 40 rpm. Similar results were found when the pressure and velocity profiles were examined as compared to those of the previously discussed trial. As mentioned, pressure was seen to exhibit the "checkerboard" effect again for the first third of the extruder. Also, negative velocities were again calculated in the program for the first 10% of the extruder. The only major difference seen between the programs is now the mass flowrate at

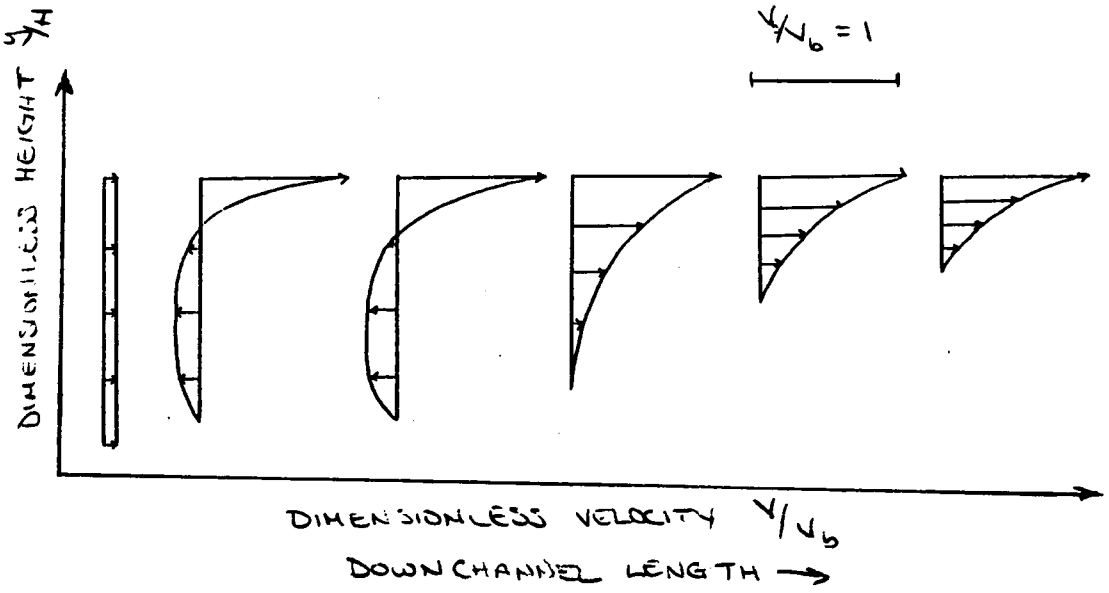

Figure 89. Velocity Profiles along the Extruder with Velocity Entrance Boundary Conditions: Conditions: Vel. inlet = 0.1105 cm/s, 12 rpm, 25 °C

the exit was approximately seven times greater than at the inlet. Whereas the previous program converged to a loss in mass situation, this trial converged to a gain in mass over the system. This change may in part be due to the change in power law index. the power law index for these conditions is in fact greater than for the trial which produced good results so it may be concluded that more than the value of the power law index enters into the cause of the error and the determination of the program converging to a realistic solution. This error may be attributed to the input velocity profile at the inlet boundary condition. As discussed, this velocity profile was calculated based on the flowrate achieved in the laboratory extruder. However, it may be recalled that at the elevated temperature flow instabilities arose. Although the flow at 40 rpm may have appeared stable, it may not have been a true flowrate. The vaporization of the water in the extruder may have still occurred decreasing the friction in the extruder and changing the flowrate of the soy dough. If this is true, an incorrect flowrate condition was entered and there could be little hope of convergence to a correct solution.

With no other explanations as to why the results of the additional programs did not converge realistically and with no other alternatives to try that would, with any degree of certainity, converge, additional computer trials could not be justified in light of the cost. In addition, as none of the additional computer trials which were performed produced good results, no comparative analyses can be made as to the effect of varying physical conditions. The comparative work which can be performed is in fact limited to the results of the one computer trial which did produce good results compared to the results of the laboratory experiment.

Therefore, in addition to the one comparison of computer to laboratory results, in depth examination of the velocity and pressure profiles calculated by the computer program can be performed to determine if the generated data is similar to the behavior of an extruder as described in the literature.

To begin, the pressure profile along the length of the extruder was examined. As shown in Figure 90, pressure continuously built along the length of the extruder up until the last eighth of the extruder. At this point, the pressure is seen to level off. This is due to the change in flow experienced in the extruder, pressure flow contributing positively to the flow plus drag flow instead of purely drag flow or a negative pressure flow contribution. At the entrance to the die, a large drop in pressure was calculated. Pressure continued to drop throughout the die to a value of atmospheric at the exit of the die. When the pressure calculated in the numerical model was compared to that found during the laboratory experimentation good correlation was not observed. Although the down channel pressure measured in the laboratory experiments was less than the pressure at the entrance to the extruder and hence the general shape of the pressure curve is similar, the calculated pressure values are considerably higher than those measured in the laboratory experiments. The values for pressure that were calculated by the numerical method appear more realistic for the flowrates measured. When the pressure drop needed simply forthe flow through the last section of the die was calculated, a larger pressure drop was required than that observed during the laboratory experiments. Hence, the error in pressure seems to arise from the physical experiment rather than the numerical calculation. It

is not known as to why the readings of the pressure during experimentation were so low. It can only be postulated that an incorrect reading was measured from the pressure transducer or an incorrect recording was obtained. No physical reason besides the plugging of the transducer port could be the cause of the pressure readinga error and still obtain the flowrate from the extruder.

Now that the numerical model of the pressure has been examined and the results compared to those obtained in the laboratory experiments, the velocity profiles calculated in the computer simulation were examined. It is recalled that as the laboratory results for flowrate were used for the boundary condition at the inlet to the extruder in the numerical simulation. Hence, the problem is a contrived one and velocities will compare if convergence is met with mass balance. Figure 91 displays the downchannel velocity as a function of distance along the extruder. The velocity plotted is that calculated at the center of the channel. Two significant points are noted. First, the velocity at the entrance of the extruder is posititve and then drops to a negative value. This is due to the specification of the initial velocity in the boundary conditions. The velocity drops to a negative value because of the recirculating or back flow which occurs in an extruder. Secondly, the velocity is seen to continuously build along the extruder length until the entry to the die. The velocity increases smoothly because of the screw geometry. The root diameter continuously increases over the length of the screw, decreasing the channel area. With a constant mass, the velocity of the material must increase as it is moved through a smaller area. At the exit of the extruder and the entrance to the first transition zone of the die, the

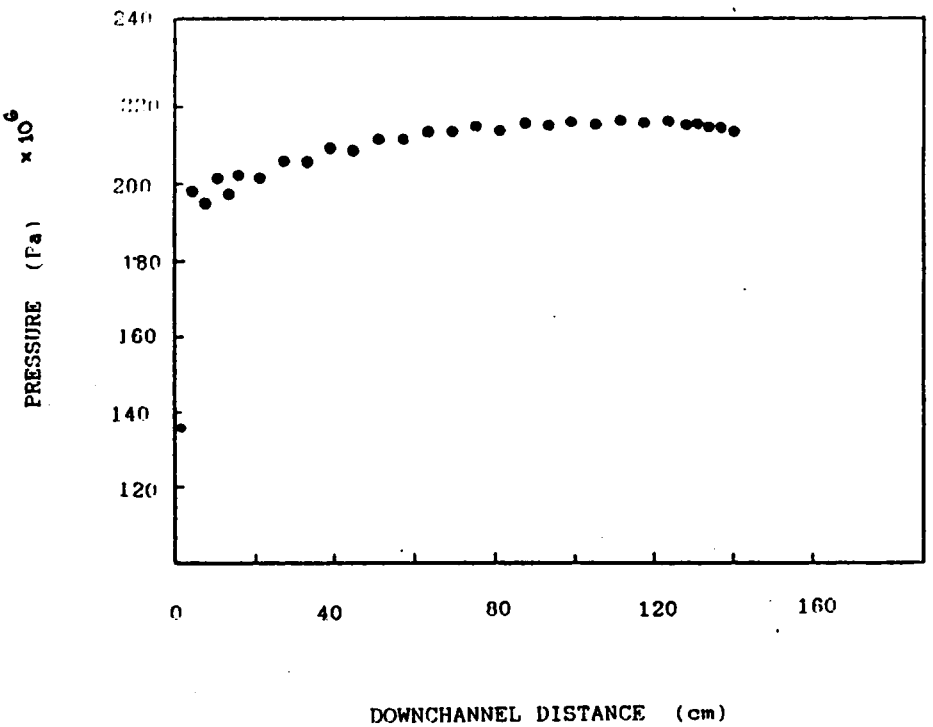

Figure 90. Pressure Build-Up along the Length of the Extruder: Conditions: Vel. inlet=0.317 cm/s, 25°C, 40rpm

velocity is seen to decrease. The velocity decrease is due to the sudden increase in cross sectional area of the first transition zone. As the material moves along the zone, the velocity increases as the first zone is shaped as an inverted cone and hence the cross sectional area is continually decreasing. The velocity then levels off in the second transition zone of the die as this region has constant cross sectional area. At the third transition zone the velocity again continually increases due once more to an inverted cone shape with continuously decreasing cross section. Finally, through the die a constant velocity is maintained.

Next the velocity profile of an downchannel cross section at specific distances along the extruder corresponding to one-fifth of the total length are plotted in Figure 92. The first profile is that of the inlet boundary condition. As discussed, a flat velocity profile as shown was employed. At the next profile, a small backflow pressure velocity is exhibited in the lower portion of the channel with the top half of the channel displaying drag flow. In the next three profiles, only positive velocities are seen which are attributed to the drag flow predominating in the extruder. Finally, the last profile exhibits both drag flow and pressure flow. Unlike the second profile, now the pressure flow is a positive contribution to the net flow. The upper portion of the profile displays the concave shape associated with drag flow with the lower protion of the curve exhibiting the convex shape associated with pressure flow. The last velocity profile does not exhibit the normal extruder flow. the pressure flow in normal extruder operation is a negative contribution throughout the extruder with pressure building continuously until the entry region of the die. However, due to the configuration of the screw

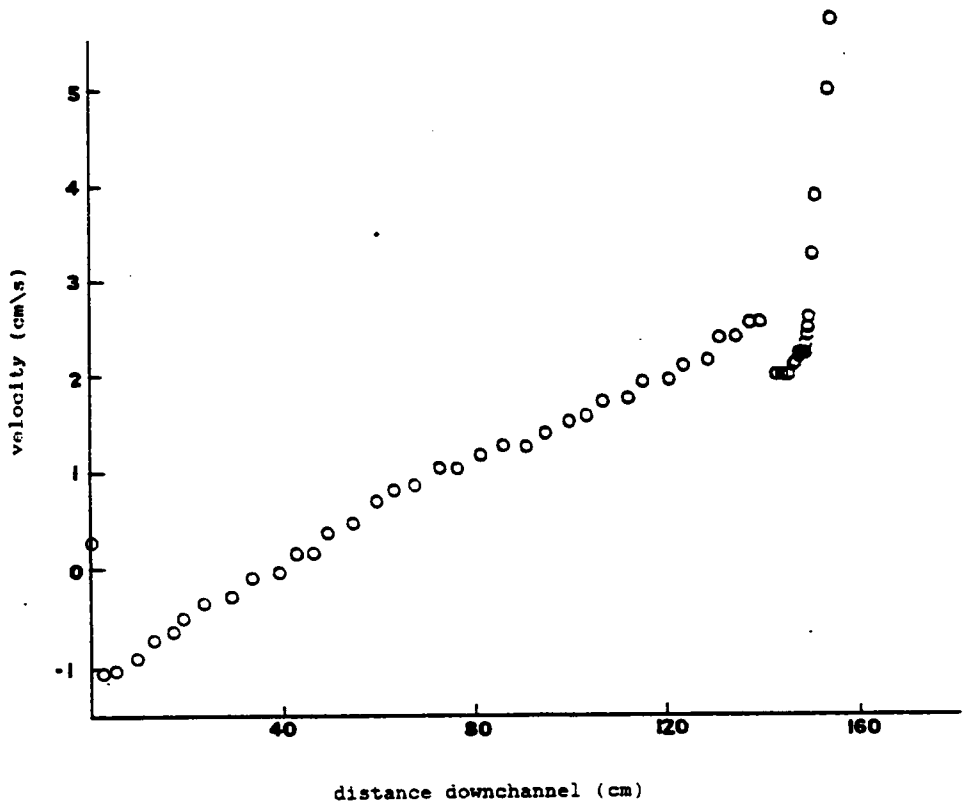

Figure 91. Velocity as a function of Downchannel Distance: Conditions: Vel. inlet=0.317 cm/s, 25°C, 40rpm

in these trials, the channel converges to the degree that more material must move forward than can be made to flow by drag flow alone. Hence, the pressure begins to become a positive force to aid in pushing the material through the converging channel.

In Figure 93 is shown the velocity profiles in an axial cross section at each of the four regions of the die assembly. In the initial transition region of the die, the normal parabolic velocity profile associated with pressure flow is observed. However, the maximum velocity is shifted somewhat from center due to the point of entry into the die assembly of the exit of the extruder. By the time the flow reaches the second transition region this shift has disappeared and the flow is symmetric. As the material travels along the die assembly, the velocities are seen to increase due to the continual decreased cross section of each region. Notice that the profile becomes increasingly elongated as the velocities increase. The changing shape is because of the increased shear associated with the increased velocities. As the shear gradient increases the shape of the velocity profile will change because of the power law index of the fluid. The shapes of the last two profiles are not exactly as expected. The power law index employed in this simulation was 0.29. The closer the index is to zero, the more the flow approaches plug flow which is depicted by a flat profile such as used at the inlet boundary condition. Thus, one would expect the velocity profile to appear more like that of the second region of the die. It is possible that the gradients over the last two section of the die are severe because of the high material velocity. This may lead to incorrect velocity values because of the size of the elements used in the region not being adequate to handle the severity of the gra-

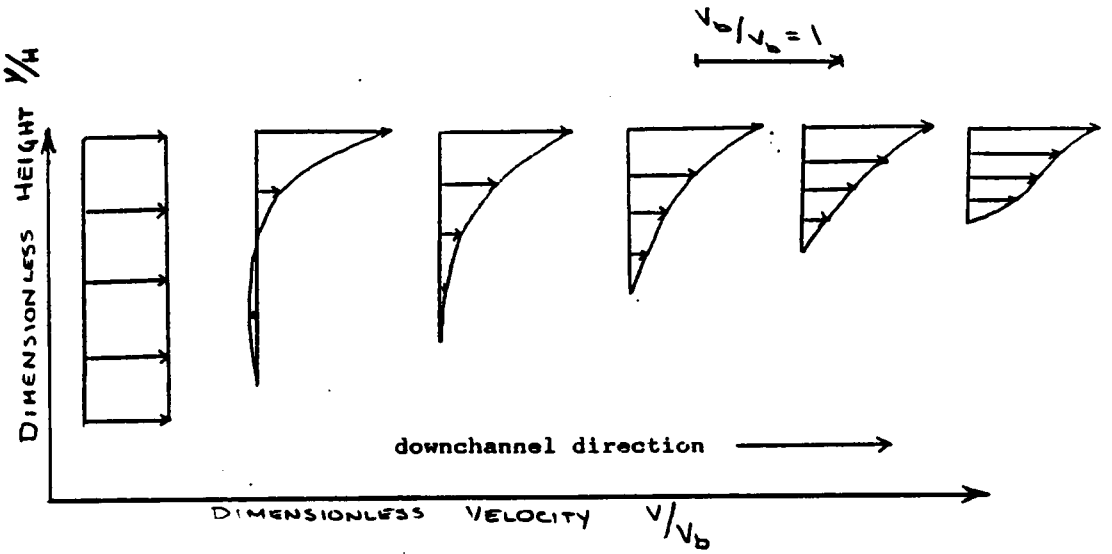

Figure 92. Velocity Profiles Along the Length of the Extruder: Conditions: Vel. inlet=0.317 cm/s, 25°C, 40rpm

dient. For comparison, a calculated profile for flow through a circular die with power law index of 0.29 is shown by the dotted line in Figure 94. The calculated profile is seen to have a much more blunt appearance approaching plug flow as postulated because of the power law index. Hence, the computer generated values may be in error due to an insufficient number of elements to handle the shear gradients present in the die region.

Finally, a cross section of the flow in the extruder is shown in Figure 95. This figure displays the magnitude and direction of flow in the cross section of the extruder. As discussed in the literature [123], a circulatory flow is found due to the diagonally moving top plate of the channel. The same circulating flow is seen in the die. Hence, the fluid follows the same type of flow pattern in the die which was set up in the extruder. Even though there is no external movement which continues the circulatory flow, circulatory flow continues throughout the die.

One last point must be made regarding the numerical work performed. All along, minimizing computational time has been mentioned as a significant factor in consideration of the computer trials performed. This is due to the large costs which are involved in running the numerical program. To give an example of the costs involved, a short comparison the type of computer simulations which were performed throughout this work is given. The costs cited here are purely the costs of the calculations. Additional charges for set-up and print out for each of the runs are essentially constant. For the initial computer trials which tested the performance of the program and the necessary mesh size requirements, computational costs averaged a little less than $50 per trial. These

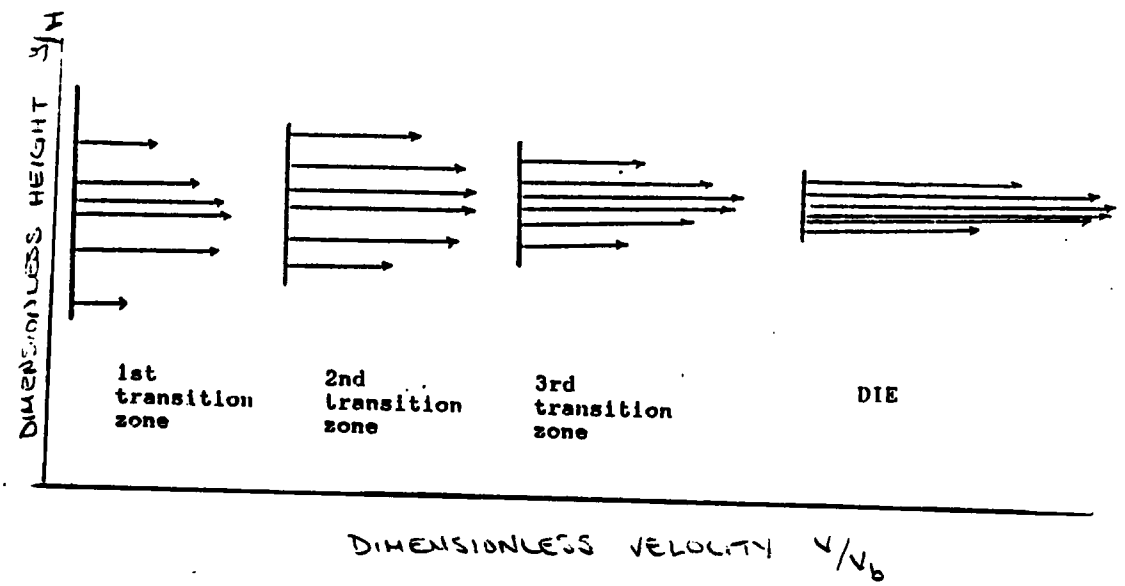

Figure 93. Velocity Profiles in the Four Sections of the Die: Conditions: Vel. inlet=0.317 cm/s, 25°C, 40rpm

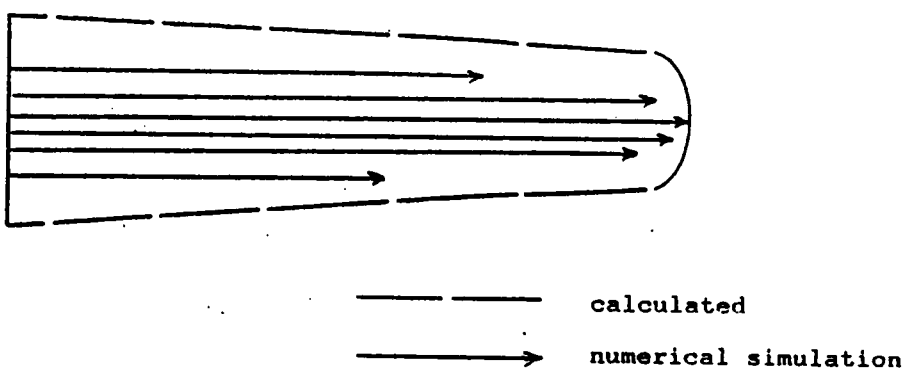

Figure 94. Comparison of Numerical vs. Calculated Velocity Profile in the Die

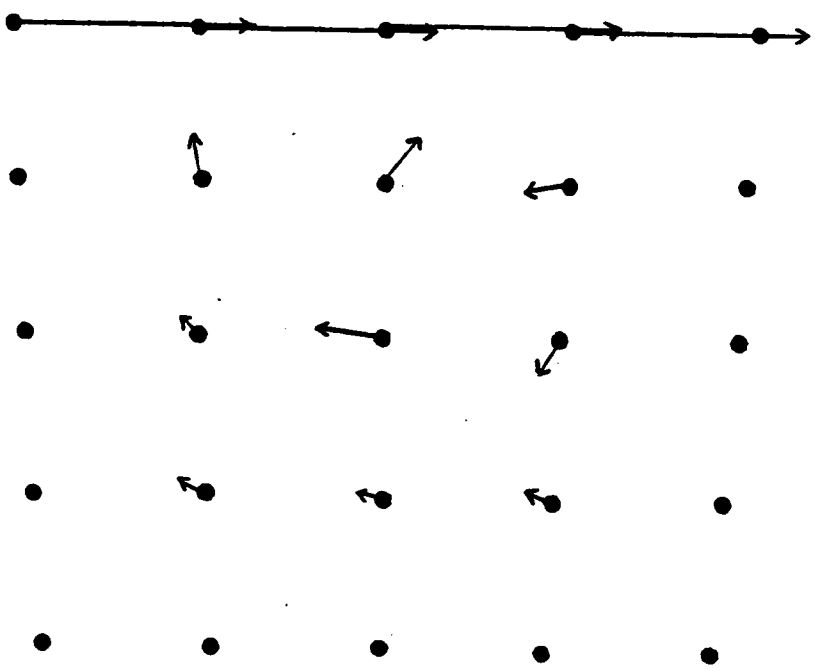

Figure 95. Magnitude and Direction of Flow in Cross Section of Extruder

trials were performed with two-dimensional, isothermal conditions of the extruder section only. When the same conditions were run changing only from isothermal to non-isothermal mode which was used to establish the distance down the extruder to reach experimental set temperature, the computational cost increased to an average cost of around $200. The addition of the die section to the extruder in the two dimensional isothermal conditions also raised the average run cost to $200. No runs were performed with the extruder and die together under non-isothermal conditions in two dimensions so no relative cost increase can be cited. Finally, when the three dimensional isothermal extruder and die computer trials were performed, computational costs rose to approximately $750. In addition, one must remember that any trial attempted that did not converge also used computer time to the maximum allotted time specified in its search for convergence. Hence, these trials increased the overall cost for the whole numerical investigation. From these approximate costs, one can see why computational time enters into consideration for the numerical trials performed.

In summary, the numerical simulations performed did not yield good results. Of the various trials performed employing different boundary conditions and physical conditions, only one trial converged to realistic results. This trial involved the use of a specified flow at the inlet boundary condition with physical conditions of viscosity values for the soy dough at 25°C and an extruder speed of 40 rpm. The results of the numerical simulation were compared to the laboratory experimental results as well as theoretical results. The calculated pressure did not correlate well with the experimental pressure. However, the experimental pressure

was found to appear in error rather than the computer calculated pressure. The shape of the pressure profile did match what had physically happened in the laboratory experiment. In addition, the velocity profiles within the extruder and die matched that which occurred in the laboratory experiment. Some problems were incountered in the die section with the calculated velocity profiles but these were attributed to the mesh used in the numerical simulation.

6.0 CHAPTER SIX: CONCLUSIONS AND RECOMMENDATIONS

6.1 INTRODUCTION

The goal of this work has been to numerically model the cooking extrusion of a soy dough. Many areas of research were covered in obtaining this goal. To begin, the physical properties for the material of study had to be obtained. These properties included viscosity, heat capacity, and thermal conductivity. In addition, the cooking mechanism was explored to determine if a reaction occurred during the cooking process. The heat of reaction, then, was another physical property which needed to be incorporated into the model. Next, experimental extruder runs were performed so that the results of the numerical model could be compared to physical data. Finally, the numerical simulation was performed. This numerical work involved determining the physical geometry of the system, optimizing mesh discretization, determining boundary conditions, and finally, interpreting the computer results. With respect to the results and discussion presented on the work performed throughout this study, the following conclusions and recommendations are made.

6.2 CONCLUSIONS

1. In this study, it was concluded that the limited success of the three-dimensional finite element method employed in the modeling of the cooking extrusion of the 50% added moisture soy dough resulted from the following factors. These factors included complex geometry of the system,

extreme power law index, difficult boundary condition specification, and limitations in mesh size due to computational time.

2. For the purpose of the numerical simulation, the viscosity behavior of the 50% added moisture soy dough was modeled using the Power Law Model of Ostwald de Waele. The viscosity was found to vary with temperature. Consequently, the power law constants, power law index and consistency values, were determined at the temperatures of investigation as follows:

Temperature	n	m
°C		$Pa \cdot s^{-n}$
25	0.29	7115.3
50	0.28	2392.3
75	0.21	2100.7
85	0.40	1326.1

These values were established as the values to use in the numerical simulation of the cooking extrusion at the various experimental temperatures.

3. Heat capacity was determined to be essentially constant at a value of 0.687 cal/g °C over the temperature range of investigation for the 50% added moisture soy dough. This value was established at a value of 0.687 cal/g-°C over the temperature range of investigation for the 50% added moisture soy dough. This value was established as the value to be employed in the non-isothermal numerical simulations.

4. Thermal conductivity was determined directly and found to be essentially constant at a value of 0.211 kg-m/s^3 K. This value was established as the value to be employed in the non-isothermal numerical simulations.

5. It was concluded that an endothermic reaction is produced during cooking of the 50% added moisture soy dough under certain conditions. The specific conditions were not completely defined in this study. However, heat, length of heating time, and shear have been determined to influence the reaction. As the reaction was endothermic it was presumed that cooking does not involve disulfide crosslinking of the proteins but instead consists of a combination of hydrophobic interactions, entanglements, and/or conformational changes.

6. It was determined that a heat of reaction term would not need to be included for in the numerical simulation of the cooking extrusion process. From the DSC experiments which looked at soy dough samples along the length of the screw, it was concluded that no reaction occurred in the sample during the extrusion process at the temperatures investigated.

7. The reaction which occurred in the 50% added moisture soy dough was irreversible in all cases tested. The irreversibility was demonstrated in both DSC and viscosity experiments.

6.3 RECOMMENDATIONS

1. One method of controlled sample preparation was determined and used throughtout experimentation. This method however, does not reflect realistic conditions for industrial purposes. With additional work to be performed, another method for controlled preparation with shorter hold

time needs to be explored. Specifically, the mixing of the water and soy flour should be examined. Possibly a spraying method for addition of the water could be employed to disperse the water more evenly as it is added to the soy flour.

2. Problems were encountered in measuring the viscosity of the soy dough. Two areas which require additional work are high-temperature viscosity measurements and better understanding the entrance pressure correction factor employed in the capillary rheometer experiments. For high temperature measurements, an apparatus which could be attached to the extruder similar to a slit die rheometer may yield better success. To aid in understanding the entrance pressure correction factor not only do more experiments need to be performed but also additional capillary L/D and diameters should be explored.

3. An endothermic reaction could be generated under certain conditions, some which were defined and others which were not. Specifically, exposure to an 85°C environment produced an endothermic reaction when scanned by DSC. Although 85°C seemed to be a key factor, the immediate temperature range was not explored to determine the exact temperature which could trigger this phenomenon. In addition, it was not clearly defined as to what processing conditions would induce this behavior. Therefore, both temperature and processing conditions should be explored in more depth to discover the cause of this endothermic reaction. Also, it appeared that the reactions possessed a kinetics as seen in both the time sweep rheological experiments and the effect of residence time at the elevated temperatures. Hence, the rate of reaction should be explored

once an understanding of the mechanism which produces the reaction is discovered.

4. In conjunction with the determination of the mechanism of the reaction which is generated at elevated temperature, additional exploration of the affect of moisture content on the reactions observed should be performed. Some data has suggested a different reaction mechanism occurring depending on moisture content. In addition, the generation of a larger endothermic peak similar to that observed with the 50% added moisture soy dough was also observed with the lower moisture soy dough at different temperatures. Hence, additional work on the effect of moisture content may give insight to the reaction occurring in the system.

5. Two problems were encountered during use of the thermal conductivity/diffusivity apparatus. First, obtaining the consistent, uniform close packing necessary for accurate measurement was particularly difficult for the higher moisture samples. In addition, the apparatus could only handle temperatures up to 100°C for the higher moisture samples due to the vaporization of water out of the sample. In both cases if experimentation is to continue with low moisture soy doughs no modifications need be performed. However, for higher moisture samples methods to obtain good packing and eliminate the vaporization of water are necessary. Better packing may be obtained if a special plunger to pack the dough is developed or if the dough could be packed tightly with a method to insert the thermocouple and resistance wire at the correct placement developed. A better sealing system for the ends of the tube needs to be designed for

the higher moisture samples for experimentation at temperatures above 100°C or a different method developed.

6. Before additional work in extrusion should proceed changes in the laboratory extruder should be made to simplify the geometry of the extruder for modeling and provide better data for comparison to the numerical simulation. The best method to simplify the geometry of the extruder is simply to replace the current extruder with a different extruder possessing a much shorter screw length with different screw configuration and simplified die assembly. This will greatly decrease the volume to be modelled which will allow a finer mesh without increasing total number of elements as well as possibly simplifying overall geometry. It would also allow use of elements which would eliminate the "checkerboard" pressure observed. Within the limitation of the existing extruder changing the screw configuration might aid in the convergence of the numerical simulation. Screw configuration controls pressure profile in the extruder and hence could simplify calculation. Additional modifications to the current extruder would include incorporating more pressure transducers along the length of the extruder to maintain the pressure profile more closely. This data would provide a better comparison with the numerical results.

7. Many problems were encountered in the numerical modelling of the extrusion of the soy dough. Aside from the problems introduced because of the material of study and financial limitations additional problems were encountered in handling the numerical calculations. The following are suggestions to improve handling of the difficulties and hopefully increase changes of convergence.

a)Many more two dimensional numerical simulations should be performed to look at the flow predictions uner the various physical conditions.

b)If the dimensions of the extruder and die can not be decreased and simplified as recommmended earlier, decoupling the extruder and die may lead to better success for a converging problem.

c)Additional meshes should be examined in which the number, size, and areas of concentration of the elements are varied to aid in convergence.

d)One method to overcome the problems encountered with the low power law index may be to run the problem with an intermediate power law index and use the solution for the initial conditions for the next simulation with the lower power law index.

APPENDIX A. NOTATION USED IN FINITE ELEMENT DISCUSSION

x_i	Cartesian coordinates of a point in the fluid
u_i	Eulerian fluid velocity components in the x_i direction
f_i	body force components per unit volume
g_i	gravitational force components
σ_{ij}	stress tensor
τ_{ij}	deviatoric part of the stress tensor
ε_{ij}	strain-rate (deformation) tensor
p	fluid pressure
δ_{ij}	Kronecker delta
T	temperature
ρ	density
μ	absolute viscosity
ν	kinematic viscosity
λ	second viscosity coefficient
k	thermal conductivity
c_p	heat capacity (specific heat at constant pressure)
β	volume expansion coefficient
T_β	reference temperature for which buoyancy forces are zero
q_s	heat source per unit volume
Φ	viscous dissipation function
h	enthalpy
q_a	applied heat flux
q_c	convective heat flux
q_r	radiative heat flux
q	total heat flux
e	emissivity
σ	Stephan-Boltzman constant
T_c	reference temperature for which convective flux is zero
T_r	reference temperature for which radiative flux is zero
t_i	boundary traction components
ε	penalty parameter

APPENDIX B. CALCULATION OF ERROR BARS ON VISCOSITY DATA

CALCULATION OF ERROR BARS FOR VISCOSITY VALUES

For the error bars included in Figure 32 , simply the mean and standard deviation was calculated for the viscosity data. Two shear rates, one high and one low, were chosen aout of the multiple which were tested on the ICR. The viscosity data from the various experimental runs were then collected.

The mean was calculated by the relationship:

$$\text{Mean} = \frac{\sum_{i=1}^{N} \mu_i}{N}$$

where: μ_i = viscosity data entry

N = number of viscosity experimental data entries

The standard deviation was then computed using the following relationship:

$$\text{Standard Deviation} = \frac{\left[\sum_{i=1}^{N} (\mu_i - \bar{\mu})^2\right]^{1/2}}{N-1}$$

The error bars plotted correspond to the mean +/- two times the standard deviation.

APPENDIX C. FIT OF DATA TO DIFFERENT VISCOSITY MODELS

SAMPLE CALCULATION OF THE FIT OF VISCOSITY DATA TO THE VARIOUS VISCOSITY MODELS

To fit the viscosity data to a viscosity empiricism, the viscosity data was collected for a specific temperature. The viscosity was then fit to the viscosity empiricism using linear regression. The following is an example for the fit of the viscosity data at 75 C for a 50% added moisture dough to a power law viscosity empiricism.

Power Law Equation:

$$\tau_{yx} = -m \left|\dot{\gamma}\right|^{n-1} \dot{\gamma}$$

Rearrangement of the Power Law Equation to a linear form:

$$\ln \tau_{yx} = \ln m + n \ln \dot{\gamma}$$

The mean of the stress at each shear rate is used in the calculation. The power law index, n, is calculated to be 0.53 and ln (power law coefficient) = 7.54 with a correlation coefficient of 0.98.

APPENDIX D. SAMPLE CALCULATION OF THERMAL CONDUCTIVITY

THERMAL CONDUCTIVITY
SAMPLE CALCULATION

For a 0% added moisture sample at room temperature, the temperature of the sample immediately next to the resistance wire at two points in time is required for the conductivity calculation.

at: $\tau_1 = 5.8$ T = 35.0 C
$\tau_2 = 41.3$ T = 45.0 C

using these values:

$$k = \frac{3.413 \ (0.265 \text{ A})^2 \ (16.6 \ \Omega/\text{ft}) \ \ln(41.3/5.8)}{4\pi \ (45.0^\circ\text{C} - 35.0^\circ\text{C}) \ (1.8^\circ\text{F}/^\circ\text{C})}$$

$$k_{25^\circ\text{C}}^{0\%} = 0.0345 \ \text{Btu/(hr ft}^\circ\text{F)}$$

REFERENCES

1. W. J. Morse, In: Soybeans and Soybean Products. K. S. Markley, Ed., Vol. I, p. 3. Interscience Publishers, New York (1950).

2. R. S. Burnett, In: Soybeans and Soybean Products. K. S. Markley, Ed., Vol. II, p. 949. Interscience Publishers, New York (1951).

3. J. V. Ziemba, Food Eng., 38(5): 82 (1966).

4. A. K. Smith, and S. J. Circle, Soyabeans: Chemistry and Technology, AVI Publishing, Westport, CT (1972).

5. O. B. Smith, "Why Use Extrusion?" In: Proceedings from Twelfth Annual Symposium on "Extrusion: Process and Product Development", Central States Section, Amer. Assoc. of Cereal Chemists, St. Louis, MO. (1971).

6. J. L. Shen, and C. V. Morr, J. Am. Oil Chem. Soc. 56: 63A (1979).

7. J. R. Whitaker, and S. R. Tannenbaum, Food Proteins. AVI Publishing Company, Inc. Westport, CT. (1972).

8. I. Koshiyama, J. Sci. Food Agric. 23: 853 (1972).

9. I. Koshiyama, and D. Fukushima, Cereal Chem. 50: 114 (1973).

10. S. Lewin, Displacement of Water and Its Control of Biochemical Reactions. Academic Press, London. (1974).

11. G. M. Mrevlishvili, and P. L. Privalov, "Calorimetric Investigation of Macromolecular Hydration" In Water in Biological Systems, L. P. Kayushin Ed. Consultants Bureau, New York (1969).

12. I. D. Kurtz, T. S. Brassfield, G. D. Law, and G. V. Purcell, Science 163: 1329-1331 (1969).

13. B. German, S. Damodaran, and J. E. Kinsella, J. Agric. Food Chem. 30: 807 , 1982.

14. J. E. Kinsella, CRC Crit. Rev. Food Sci. and Nut. 11: 153 (1978).

15. D. V. Harmann and J. M. Harper, J. Food Sci. 39: 1099 (1974).

16. H. A. Scheraga, Protein Structure, Academic Press, New York, (1961).

17. J. W. S. Hearle and R. H. Peters, eds., Fiber Structure, The Textile Institute, Butterworths, London (1963).

18. R. Farrell, Extrusion Equipment: Types, Functions, and Applications. In Proceedings from Twelfth Annual Symposium on "Extrusion: Process and Product Development." St. Louis, MO.

19. G. C. Mustakas, W. J. Albrecht, G. N. Bookwalter, J. E. McGhee, W. F. Kwolek and E. L. Griffin, Jr., Food Tech. 24: 102, (1970).

20. R. T. Jones, The Structure of Proteins, In Symposium on Foods: Proteins and Their Interactions, H. W. Schultz, and A. F. Anglemeir, Eds. AVI Publishing Co., Westport CT (1964).

21. F. F. Huang and C. Rha, Poly. Eng. Sci. 14(2): 81 (1974).

22. A. L. Fricke, J. P. Clark, and T. F. Mason, AICHE Symp. Ser. 73(163): 134 (1977).

23. P. Melius, Fed. Proc., Fed. Am. Soc. Exp. Biol. 34: 573 (1975).

24. T. F. Tsao, J. M. Harper, and K. M. Repholz, AICHE Symp. Ser. 74(172): 142, (1978).

25. N. Catsimpoolas, FEBS Lett. 4: 259 (1969).

26. N. Catsimpoolas, S. F. Funk, and E. W. Meyer, Cereal Chem. 47: 221 (1970).

27. J. L. Rossen and R. C. Miller, Food Tech. 6: 46 (1973).

28. J. M. Aguilera, F. V. Kosikowski, and L. F. Hood, J. Food Sci., 41: 1209 (1976).

29. A. Tadmor and I. Klein, Engineering Principles of Plasticating Extrusion, Van Nostrand Reinhold Comp., New York, (1970).

30. K. Saio, E. Koyama, and T. Watanabe, Agri. Biol. Chem. Japan 33: 36 (1969).

31. W. J. Wolf, T. E. Babcock, and A. K. Smith, Ultracentrifugal Differences in Soybean Protein Composition. Nature 191: 1395 (1961).

32. W. J. Wolf, J. Agri. Food Chem. 18(6): 969 (1970).

33. A. E. Brown and J. Menkart, in Ultrstructure of Protein Fibers, R. Borasky, ed., Academic Press, New York (1963).

34. A. M. Hermansson, J. Text. Stud. 9: 33 (1978).

35. K. Saio and T. Watanabe, J. Text. Stud. 9: 135 (1969).

36. W. J. Wolf and T. Tamura, Cereal Chem. 46: 331 (1969).

37. D. R. Thompson and J. R. Rosenau, Trans. ASAE 397 (1977).

38. E. B. Bagley, J. Appl. Phys. 28: 624 (1957).

39. J. D. Ferry, Adv. Protein Chem. 3: 1 (1948).

40. Y. C. Jao, A. H. Chen, D. Lewandowski, and W. E. Irwin, J. Food Proc. Eng. 2: 97 (1978).

41. A. C. Beckel, W. C. Bull, and T. H. Hopper, Ind. Eng. Chem. 34: 973 (1942).

42. P. A. Belter, and A. K. Smith, J. Am. Oil Chemist's Soc. 29: 170 (1952).

43. W. J. Wolf, Ph.D. Dissertation, Univ. of Minn. (1956).

44. A. H. Chen, Y. C. Jao, J. W. Larkin, and W. E. Goldstein, J. Food Proc. Eng. 2: 337 (1978).

45. E. V. Jensen, Science 130: 1319 (1959).

46. K. Saio, M. Kajikawa, and T. Watanabe, Agri. Biol. Chem. Japan, 35: 890 (1971).

47. K. Saio, I. Sato, and T. Watanabe, Nippon Shokuhim Kogyo Gakkaishi, Japan, 21: 234 (1974).

48. K. Saio, I. Sato, and T. Watanabe, J. Food Sci. 39: 777 (1974).

49. A. M. Hermansson, J. Food Technol. 12: 177-187 (1977).

50. D. Fukushima, Cereal Chem. 45: 203 (1968).

51. I. Koshiyama, Agri. Biol. Chem. 34: 1815 (1970).

52. A. M. Hermansson, Lebensm.-Wiss. & Technol. 5(1): 24 (1972).

53. P. J. Flory, Faraday Discuss. Chem. Soc. 57: 7 (1974).

54. J. P. C. Chiang and M. Steinberg, Cereal Chem. 43: 195 (1974).

55. J. E. Kinsella, J. Am. Oil Chem. Soc. 56: 242 (1979).

56. Y. Kamata, K. Okubo, and K. Shibasaki, Agri. Biol. Chem.

57. O. B. Smith, Food Eng. 47(7): 48 (1975).

58. M. A. Williams, R. E. Horn, R. P. Rugala, Food Eng. 49(9):99 (1977).

59. M. A. Williams, R. E. Horn, R. P. Rugala, Food Eng. 49(10):87 (1977).

60. D. B. Cumming, D. W. Stanley, and J. M. DeMan, J. of Food Sci., 38 (1973).

61. K. Hashizume, N. Nakurama, and T. Watanabe, Agri. Biol. Chem. 39:1339 (1975).

62. T. Furukawa, S. Ohta, and A Yamamoto, J. Text. Stud. 10:333 (1979).

63. I. Klein and D. Marschall, Computer Programs for Plastics Engineers. Van Nostrand Reinhold, New York (1968).

64. J. A. D. Ewart, The Bakers Digest, 8:22 (1972).

65. D. G. Baird, J. Food Proc. Eng. 5:231 (1982).

66. A. M. Hermansson, J. Text. Stud. 5:425 (1975)

67. S. J. Circle, E. W. Meyer, and R. W. Whitney, Cereal Chem. 41:157 (1964).

68. G. Nenethy, I. Z. Steinberg, and H. A. Scheraga, Biopolymers 1:43 (1963).

69. M. B. Roller, Pol. Eng. and Sci. 15(6):4[illegible] (1975).

70. D. F. Hager, J. Agri. Food Chem. 32:293 (1984).

71. C. H. Remsen and J. P. Clark, J. Food Proc. Eng. 2:39 (1978).

72. J. J. Kelley and R. Pressey, Cereal Chem. 43:195 (1966).

73. T. J. Maurice, and D. W. Stanley, Inst. Can. Sci. Tech., 11(1) (1978).

74. T. J. Maurice, L. D. Burgess, and D. W. Stanley, Inst. Can. Sci. Tech., 9(4) (1976).

75. D. B. Cumming, D. W. Stanley, and J. M. DeMan, Inst. Can. Sci. Tech., 5(3) (1972).

76. American Society for Testing and Materials, ASTM Standards, Vol. 27, Philadelphia, PA (1967).

77. W. H. Darnell, and E. A. J. Mol, SPE J. 12:2029 (1956).

78. Y. C. Jao, A. H. Chen, D. Lewandowski, and W. E. Irwin, Analysis of Soy Dough Rheology in Extrusion, Paper presented at the AICHE meeting, Atlanta, GE (1978).

79. C. I. Chung, in Characterization of Mechanical Properties of Food Materials, Y. Chen Ed., New Jersey, p. 186 (1976).

80. L. D. Burgess, and D. W. Stanley, J. Inst. Can. Sci. Technol. Aliment., 9(4) (1976).

81. R. Cuevas, and M. Cheryan, J. Food Proc. Eng. 2:283 (1979).

82. R. P. Singh, Food Technol. 36(2):87 (1982). (1962a).

83. R. W. Dickerson Jr., Food Technol. 19:198 (1965). (1962b).

84. B. K. Jasberg, G. C. Mustakas, and E. B. Bagley, J. of Rheology 23(4):437 (1979).

85. 1952 Book of ASTM Standards, Part 3, P. 848.

86. J. M. Harper and D. V. Harmann, Trans. ASAE 16(5):941 (1973).

87. J. M. Harper, CRC Crit. Rev. Food Sci. and Nut. 2:155 (1979).

88. L. Levine, "Estimating Operating Parameters in Food Extruders", paper presented at August 1981 AICHE meeting.

89. M. A. Williams, R. E. Horn, and R. P. Rugala, Food Eng. 49(9):99 (1977)

90. J. M. Harper, Crit. Rev. Food Sci. and Nut. J. 11:2 (1978).

91. W. J. Wolf, and J. C. Cowan, Soybeans as Food Source, revised edition, CRC Press, Cleveland, Ohio (1975).

92. J. P. Clark, J. Text. Stud. 9:109 (1978).

93. N. Catsimpoolas, and E. W. Meyer, Cereal Chem. 47:559 (1970).

94. B. Hagerdal, and H. Martens, J. Food Sci. 41:933 (1976).

95. D. J. Muffett, and H. E. Snyder, J. Agri. Food Chem. 28:1303 (1980).

96. D. J. Wright, and P. Wilding, unpublished results.

97. M. Ruegg, U. Moor, and B. Blanc, J. Dairy Res. 44:509 (1977).

98. D. J. Wright, In Developments In Food Proteins-1, B. J. F. Hudson, Ed. Applied Science Publishers, New Jersey.

99. B. H. Vos, Appl. Sci. Research, Hague A5:425 (1955).

100. D. L. Lang, ASTM Bulletin, 9:58 (1956).

101. J. D. Verschoor, and A. Wilber, Heat., Piping. & Air Cond. 7 (1954).

102. S. L. Polley, O. P. Snyder, and P. Kotnour, Food Technol. 11:76 (1980).

103. C. Rauwendaal, ANTEC Conf. Proc., New Orleans, 282 (1984).

104. D. S. C. Fong, Master's thesis, Virginia Tech (1978).

105. R. T. Fenner, Polymer, 18:617 (1977).

106. R. M. Griffith, Ind. Eng. Chem. Fundam. 1:180 (1962).

107. E. E. Agur and J. Vlachopoulas, Poly. Eng. Sci. 22(17): 1084 (1982).

108. E. Zavadsky and J. Karnis, Rheol. Acta 24:556 (1985).

109. Z. Tadmor and E. Broyer, Poly. Eng. Sci. 12:378 (1972).

110. L. Kaeir and Z. Tadmor, Poly. Eng. Sci. 12:387 (1972).

111. Z. Tadmor, D. I. Marshall, and I. Klein, Poly. Eng. Sci. 6:185. (1966).

112. J. Shapiro, A. L. Halmos, and J. R. Pearson, Polymer 17: 905 (1976).

113. R. T. Fenner, Extruder Screw Design, ILIFFE, London (1970)

114. V. I. Yankov, V. I. Boyarchenko, and A. L. Krylov, Inzh Fiz Z. 30:1040 (1976).

115. D. H. Pelletier, VPI-AERO-Report-142, Aerospace and Ocean Engineering Department, Virginia Tech, Balcksburg, VA, (1984).

116. D. H. Pelletier, VPI-AERO-Report-143, Aerospace and Ocean Engineering Department, Virginia Tech, Balcksburg, VA, (1984).

117. J. N. Reddy, An Introduction to the Finite Element Method, McGraw-Hill, (1984).

118. O. C. Zienkiewicz, The Finite Element Method, Third Edition, McGraw-Hill, (1977).

119. D. H. Norrie, and G. de Vries, An Introduction to Finite Element Analysis, Academic Press, New York, (1978).

120. M. S. Engelman, FIDAP: A Fluid Dynamics Analysis Program, Users/Theoretical Manual, Fluid Dynamics International, Evanston, Illinois (1982).

121. M. Viriyayuthakorn and B. Kassahun, ANTEC '84, p. 81-84

122. K. Weissenberrg as cited by B. Rabinowitsch, Z. Physik-Chemie, A145 1(1929).

123. Z. Tadmor and C. Gogos, Principles of Polymer Processing, John Wiley and Sons, New York (1979).

The vita has been removed from the scanned document